



**REFINEMENT OF PROMISING COATING COMPOSITIONS  
FOR DIRECTIONALLY CAST EUTECTICS**

**FINAL REPORT**

by

T. E. Strangman, E. J. Felten and R. S. Benden

UNITED TECHNOLOGIES CORPORATION  
Pratt & Whitney Aircraft Group  
Commercial Products Division

(NASA-CR-135103) REFINEMENT OF PROMISING  
COATING COMPOSITIONS FOR DIRECTIONALLY CAST  
EUTECTICS (Pratt and Whitney Aircraft)  
156 p HC A08/MF A01

N77-11154

CSCL 11C

G3/26

Unclas  
54549

October 1976



prepared for

NATIONAL AERONAUTICS AND SPACE ADMINISTRATION  
NASA-Lewis Research Center  
Contract NAS3-18920

1. Report No. NASA CR-135103		2. Government Accession No.		3. Recipient's Catalog No.	
4. Title and Subtitle REFINEMENT OF PROMISING COATING COMPOSITIONS FOR DIRECTIONALLY CAST EUTECTICS				5. Report Date October 1976	
				6. Performing Organization Code	
7. Author(s) T. E. Strangman, E. J. Felten and R. S. Benden				8. Performing Organization Report No. PWA-5441	
9. Performing Organization Name and Address Pratt & Whitney Aircraft Division United Technologies Corporation East Hartford, Connecticut 06108				10. Work Unit No.	
				11. Contract or Grant No. NAS3-18920	
12. Sponsoring Agency Name and Address National Aeronautics and Space Administration Lewis Research Center Cleveland, Ohio 44135				13. Type of Report and Period Covered Contractor Report	
				14. Sponsoring Agency Code	
15. Supplementary Notes Project Manager, J. P. Merutka, NASA Lewis Research Center, Cleveland, Ohio					
16. Abstract <p>The successful application of high creep strength, directionally solidified <math>\gamma/\gamma' - \delta</math> (Ni-19.7Cb-6Cr-2.5Al) eutectic superalloy turbine blades requires the development of suitable coatings for airfoil, root and internal blade surfaces. In order to improve coatings for the <math>\gamma/\gamma' - \delta</math> alloy, the current investigation had the goals of 1) refining promising coating compositions for directionally solidified eutectics, 2) evaluating the effects of coating/substrate interactions on the mechanical properties of the alloy, and 3) evaluating diffusion aluminate coatings for internal surfaces.</p> <p>Burner rig cyclic oxidation, furnace cyclic hot corrosion, ductility, and thermal fatigue tests indicated that NiCrAlY+Pt (63 to 127<math>\mu</math> Ni-18Cr-12Al-0.3Y + 6<math>\mu</math>Pt) and NiCrAlY (63 to 127<math>\mu</math> Ni-18Cr-12Al-0.3Y) coatings are capable of protecting high temperature gas path surfaces of eutectic alloy airfoils. Burner rig (Mach 0.37) testing indicated that the useful coating life of the 127<math>\mu</math> thick coatings exceeded 1000 hours at 1366 K (2000°F).</p> <p>Isothermal fatigue and furnace hot corrosion tests indicated that 63<math>\mu</math> NiCrAlY, NiCrAlY + Pt and platinum modified diffusion aluminide (Pt + Al) coating systems are capable of protecting the relatively cooler surfaces of the blade root.</p> <p>Finally, a gas phase coating process was evaluated for diffusion aluminizing internal surfaces and cooling holes of air-cooled <math>\gamma/\gamma' - \delta</math> turbine blades.</p>					
17. Key Words (Suggested by Author(s)) Oxidation Resistant Coatings Hot Corrosion Resistant Coatings Directionally Solidified Eutectic Superalloy			18. Distribution Statement  <div style="text-align: center;">Unclassified — Unlimited</div>		
19. Security Classif. (of this report) Unclassified		20. Security Classif. (of this page) Unclassified		22. Price* 3.00	
21. No. of Pages 156					

## **FOREWORD**

**This is the final report of the work performed by the Materials Engineering and Research Laboratory of the Pratt & Whitney Aircraft Division of United Technologies Corporation, East Hartford, Connecticut under NASA-Lewis Research Center contract NAS3-18920, entitled Refinement of Promising Coating Compositions for Directionally Cast Eutectics, and conducted during the period from June 27, 1974 to June 27, 1976.**

**Mr. John Merutka of the NASA-Lewis Research Center served as Project Manager for this program.**

**The Pratt & Whitney Aircraft personnel who contributed to the program are as follows:**

**Mr. L. A. Friedrich, Program Manager  
Mr. N. E. Ulion, Program Manager  
Mr. T. E. Strangman, Principal Investigator  
Dr. E. J. Felten, Senior Research Associate  
Mr. R. S. Benden, Materials Engineer**

## TABLE OF CONTENTS

Section	Title	Page
I.	SUMMARY	1
II.	INTRODUCTION	4
III.	BURNER RIG OXIDATION TESTING	7
	A. Background	7
	B. Specimen Preparation	8
	C. Test Procedures	9
	D. Results and Discussion	10
IV.	FURNACE HOT CORROSION EVALUATION	44
	A. Background	44
	B. Specimen Preparation	44
	C. Test Description	45
	D. Results and Discussion	45
V.	GAS PHASE ALUMINIZING STUDY	60
	A. Background	60
	B. Specimen Preparation	60
	C. Gas Phase Aluminide Optimization	61
VI.	COATING DUCTILITY EVALUATION	69
	A. Background	69
	B. Specimen Preparation	69
	C. Experimental Procedure	69
	D. Test Results	70
	E. Discussion	71
VII.	THERMOMECHANICAL FATIGUE TESTING	79
	A. Background	79
	B. Specimen Preparation	80
	C. Test Procedure	80
	D. Results and Discussion	80
VIII.	ISOTHERMAL FATIGUE TESTING	101
	A. Background	101
	B. Specimen Preparation	101
	C. Experimental Procedure	101
	D. Results and Discussion	102

## **TABLE OF CONTENTS (Cont'd)**

<b>Section</b>	<b>Title</b>	<b>Page</b>
<b>IX.</b>	<b>CONCLUSIONS</b>	<b>123</b>
<b>X.</b>	<b>RECOMMENDATIONS</b>	<b>125</b>
	<b>REFERENCES</b>	<b>126</b>
	<b>DISTRIBUTION</b>	<b>129</b>

## LIST OF ILLUSTRATIONS

Figure	Title	Page
1	Effect of Coating-Substrate Thermal Expansion Mismatch Strain ( $\Delta\epsilon_{\alpha}$ ) on Crack Initiation in NiCoCrAlY Coating During 1366 K Cyclic Oxidation Burner Rig Tests	1
2	578 K Ductility Tests of Coated $\gamma/\gamma' - \delta$ (6 Cr) Show the Influence of the Coating on Fracture Strain of Substrate	2
3	Cycle I (0.3% Strain Range) Thermomechanical Fatigue Life of NiCrAlY and NiCrAlY + Pt Coated $\gamma/\gamma' - \delta$ (6Cr) Alloy	3
4	Effect of NiCrAlY Coating Thickness on 977 K Isothermal Fatigue of $\gamma/\gamma' - \delta$ (6 Cr) Alloy	3
5	Visual Appearance of Coated $\gamma/\gamma' - \delta$ Specimens After 505 Hours of Evaluation in 1366 K (2000°F) Burner Rig Cyclic Oxidation Test (Cycle: 27 Minutes Hot – 3 Minutes Forced Air Cool).	20
6	Visual Appearance of Coatings in Hot Zone Region of $\gamma/\gamma' - \delta$ Specimens After 505 Hours of Evaluation in 1366 K (2000°F) Burner Rig Cyclic Oxidation Test (Cycle: 27 Minutes Hot – 3 Minutes Forced Air Cool).	21
7	Incipient Melting Condition Which Resulted in the Failure of the Pt + Al Coated $\gamma/\gamma' - \delta$ Specimen After 172 Hours of Evaluation in 1366 K (2000°F) Burner Rig Cyclic Oxidation Test (Cycle: 27 Minutes Hot – 3 Minutes Forced Air Cool)	22
8	Pretest and Post-Test Microstructures and Thermal Fatigue Crack Morphology of NiCoCrAlY Coated $\gamma/\gamma' - \delta$ Specimen After 505 Hours of Evaluation in 1366 K (2000°F) Burner Rig Cyclic Oxidation Test (Cycle: 27 Minutes Hot – 3 Minutes Forced Air Cool)	23
9	Pretest and Post-Test Microstructures and Thermal Fatigue Crack Morphology of NiCoCrAlY + Pt Coated $\gamma/\gamma' - \delta$ Specimen After 505 Hours of Evaluation in 1366 K (2000°F) Burner Rig Cyclic Oxidation Test (Cycle: 27 Minutes Hot – 3 Minutes Forced Air Cool)	23

## LIST OF ILLUSTRATIONS (Cont'd)

Figure	Title	Page
10	Small Thermal Fatigue Crack in NiCrAlY Coated $\gamma/\gamma'$ - $\delta$ Specimen Which Initiated At a Coating Defect (Pit) After 505 Hours of Evaluation in Burner Rig Cyclic Oxidation Test. This Defect is Slightly Outside the 1366 K (2000°F) Hot Zone Region of the Specimen.	24
11	Pretest and Post-Test Microstructures of NiCrAlY + Pt Coated $\gamma/\gamma'$ - $\delta$ Specimen After 505 Hours of Evaluation in 1366 K (2000°F) Burner Rig Cyclic Oxidation Test (Cycle: 27 Minutes Hot – 3 Minutes Forced Air Cool).	25
12	Pretest and Post-Test Microstructures of NiCrAlY Coated $\gamma/\gamma'$ - $\delta$ Specimen After 505 Hours of Evaluation in 1366 K (2000°F) Burner Rig Cyclic Oxidation Test (Cycle: 27 Minutes Hot – 3 Minutes Forced Air Cool).	25
13	Microstructure of Coating Cracks in Virgin Low Aluminum NiCrAlY + Diffusion Aluminide (Pack, Inward) Coated $\gamma/\gamma'$ - $\delta$ Burner Rig Specimen.	26
14	Thermal Expansion Data	27
15	Pretest and Post-Test Microstructures and Thermal Fatigue Crack Morphology of NiCrAlY + Diffusion Aluminide Coated $\gamma/\gamma'$ - $\delta$ Specimen After 505 Hours of Evaluation in 1366 K (2000°F) Burner Rig Cyclic Oxidation Test (Cycle: 27 Minutes Hot – 3 Minutes Forced Air Cool).	28
16	Surface and Cross-Section Morphology of Crack in NiCrAlY + Diffusion Aluminide Coated $\gamma/\gamma'$ - $\delta$ Specimen After 505 Hours of Evaluation in 1366 K (2000°F) Burner Rig Cyclic Oxidation Test. This Crack was Detected in the Coating Prior to Testing.	29
17	Effect of Cobalt and Platinum Additions on 1311 K (1900°F) NiCrAl Thermal Expansion	30
18	Visual Appearance of Coated $\gamma/\gamma'$ - $\delta$ Erosion Bars After 516 (Top) and 1005 Hours (Bottom) of Evaluation in 1366 K (2000°F) Burner Rig Cyclic Oxidation Test (Cycle: 55 Minutes Hot – 5 Minutes Forced Air Cool).	31
19	Surface Appearances of Unrepaired and Repaired NiCrAlY + Pt (Top), NiCrAlY (Bottom) and NiCrAlSiY (Bottom) Coated $\gamma/\gamma'$ - $\delta$ Specimens After 1005 Hours of Evaluation in 1366 K (2000°F) Burner Rig Cyclic Oxidation Test.	32

## LIST OF ILLUSTRATIONS (Cont'd)

Figure	Title	Page
20	Surface Condition on NiCrAlSiY Coated $\gamma/\gamma'$ - $\delta$ Specimen (R-7795) After 226 Hours of Evaluation in 1366 K (2000°F) Burner Rig Cyclic Oxidation Test. Incipient Melting Zone (Outlined by Arrows) Developed During the Initial 22 Hours of Testing.	33
21	Contrast in Oxide Scale Adherence on NiCrAlSiY Coated $\gamma/\gamma'$ - $\delta$ Specimens After 246 Hours of 1366 K (2000°F) Burner Rig Cyclic Oxidation Test.	33
22	Relatively Severe Thermal Fatigue Cracks in (A) NiCrAlSiY, (B) Unrepaired NiCrAlY + Pt and (C) NiCrAlY Coated $\gamma/\gamma'$ - $\delta$ Specimens Which Developed During 1366 K (2000°F) Burner Rig Test. Un-oxidized Crack Extension into $\gamma/\gamma'$ - $\delta$ Substrate is Thought to Have Occurred During Post-Test Metallographic Preparation.	34
23	Pretest and Post-Test Microstructures of NiCrAlSiY Coated $\gamma/\gamma'$ - $\delta$ Specimens After 516 and 1005 Hours of Evaluation in 1366 K (2000°F) Burner Rig Cyclic Oxidation Test (Cycle: 55 Minutes Hot – 5 Minutes Forced Air Cool).	35
24	Relative Nickel, Aluminum, Silicon and Columbium X-Radiation Intensities of NiCrAlSiY Coated $\gamma/\gamma'$ - $\delta$ (Ni-19.7Cb-6Cr-2.5Al) Specimen in Pretest Condition.	36
25	Blistered Condition of Platinum Rich Surface Layer of NiCrAlY + Pt Coating Prior to Being Repaired.	37
26	Pretest and Post-Test Microstructures of Repaired NiCrAlY + Pt Coated $\gamma/\gamma'$ - $\delta$ Specimens After 516 and 1005 Hours of Evaluation in 1366 K (2000°F) Burner Rig Cyclic Oxidation Test (Cycle: 55 Minutes Hot – 5 Minutes Forced Air Cool).	38
28	Pretest and Post-Test Microstructures of Unrepaired NiCrAlY + Pt Coated $\gamma/\gamma'$ - $\delta$ Specimens After 516 and 1005 Hours of Evaluation in 1366 K (2000°F) Burner Rig Cyclic Oxidation Test (Cycle: 55 Minutes Hot – 5 Minutes Forced Air Cool).	39
28	Contrast in Visual Appearances of (A) Unrepaired and (B) Repaired NiCrAlY + Pt and (C) NiCrAlY Coated $\gamma/\gamma'$ - $\delta$ Specimens After 1005 Hours of Evaluation in 1366 K (2000°F) Burner Rig Cycle Oxidation Test.	40
29	Relative Nickel, Chromium, Aluminum, Yttrium, Platinum and Columbium X-Radiation Intensities of Unrepaired NiCrAlY + Pt Coated $\gamma/\gamma'$ - $\delta$ (1 Cr) Specimen in Pretest Condition.	41

## LIST OF ILLUSTRATIONS (Cont'd)

Figure	Title	Page
30	Relative Nickel, Chromium, Aluminum, Yttrium, Platinum and Columbium X-Radiation Intensities of Repaired NiCrAlY + Pt Coated $\gamma/\gamma'$ - $\delta$ (6 Cr) Specimen in Pretest Condition.	42
31	Pretest and Post-Test Microstructures of NiCrAlY Coated $\gamma/\gamma'$ - $\delta$ Specimens After 516 and 1005 Hours of Evaluation in 1366 K (2000°F) Burner Rig Cyclic Oxidation Test (Cycle: 55 Minutes Hot – 5 Minutes Forced Air Cool).	43
32	Surface Condition of $\gamma/\gamma'$ - $\delta$ Eutectic Alloy Coupons, Which Were Coated With Approximately 63 $\mu$ of Ni-18Cr-12Al-0.3Y by Electron Beam Vapor Deposition and Then Sputter Coated With Approximately 6 $\mu$ of Platinum, After Hot Corrosion Testing (250 Cycles) at 1172 K (1650°F).	48
33	Visual Appearance of Gas Phase Aluminide Coated $\gamma/\gamma'$ - $\delta$ Simulated Air Cooled Blade Specimen After Hot Corrosion Testing (20 Cycles) at 1172 K (1650°F).	48
34	Surface Condition of $\gamma/\gamma'$ - $\delta$ Eutectic Alloy Coupons, Which Were Coated With Approximately 127 $\mu$ of Ni-18Cr-5Al-0.3Y and Then Pack Aluminized, After Hot Corrosion Testing (140 Cycles) at 1172 K (1650°F).	48
35	(A) Pretest and (B) Post-test Microstructures of $\gamma/\gamma'$ - $\delta$ Eutectic Alloy Coupons Coated With Approximately 63 $\mu$ of Ni-23Co-18Cr-12.5Al-0.3Y by Electron Beam Vapor Deposition. The Coated $\gamma/\gamma'$ - $\delta$ Coupon was Evaluated for 250 Cycles In the 1172 K (1650°F) Cyclic Hot Corrosion Test.	49
36	(A) Pretest and (B) Post-test Microstructures of $\gamma/\gamma'$ - $\delta$ Eutectic Alloy Coupons Coated With Approximately 63 $\mu$ of Ni-23Co-18Cr-12.5Al-0.3Y By Electron Beam Vapor Deposition and Then Sputter Coated With Approximately 6 $\mu$ of Platinum. The Coated $\gamma/\gamma'$ - $\delta$ Coupon Was Evaluated for 250 Cycles In the 1172 K (1650°F) Cyclic Hot Corrosion Test.	50
37	(A) Pretest and (B) Post-test Microstructures of $\gamma/\gamma'$ - $\delta$ Eutectic Alloy Coupons Coated With Approximately 63 $\mu$ of Ni-18Cr-12Al-0.3Y by Electron Beam Vapor Deposition and Then Sputter Coated With Approximately 6 $\mu$ (0.25 mil) of Platinum. The Coated $\gamma/\gamma'$ - $\delta$ Coupon Was Evaluated for 250 Cycles In the 1172 K (1650°F) Cyclic Hot Corrosion Test.	51

## LIST OF ILLUSTRATIONS (Cont'd)

Figure	Title	Page
38	Relative Aluminum, Platinum and Chromium X-Radiation Intensities for As-Coated D.S. $\gamma/\gamma'$ - $\delta$ Eutectic Alloy. The Coating Consists of 63 $\mu$ of Electron Beam Vapor Deposited Ni-18Cr-12Al-0.3Y Plus 6 $\mu$ Sputtered Platinum.	52
39	(A) Pretest and (B) Post-Test Microstructures of $\gamma/\gamma'$ - $\delta$ Eutectic Alloy Coupons Sputter Coated With Approximately 6 $\mu$ of Platinum and Then Pack Aluminized. The Coated $\gamma/\gamma'$ - $\delta$ Coupon Was Evaluated for 250 Cycles In the 1172 K (1650°F) Cyclic Hot Corrosion Test.	53
40	Relative Aluminum, Platinum and Chromium X-Radiation Intensities for As-Coated D.S. $\gamma/\gamma'$ - $\delta$ Eutectic Alloy. The Coating Consists of 6 $\mu$ Sputtered Platinum Plus 25 to 76 $\mu$ Diffusion Aluminide.	54
41	Relative Aluminum, Platinum and Chromium X-Radiation Intensities of Coated D.S. $\gamma/\gamma'$ - $\delta$ Eutectic Alloy After a 1172 K (1650°F) Laboratory Hot Corrosion Test. The Coating Consists of 6 $\mu$ Sputtered Platinum Plus 25 to 76 $\mu$ Diffusion Aluminide.	55
42	(A) Pretest and (B) Post-test Microstructures of $\gamma/\gamma'$ - $\delta$ Eutectic Alloy Coupons Coated With Approximately 127 $\mu$ of Ni-18Cr-5Al-0.3Y and Then Diffusion Aluminized (Pack, Inward). The Coated $\gamma/\gamma'$ - $\delta$ Coupon Was Evaluated for 110 Cycles In the 1172 K (1650°F) Cyclic Hot Corrosion Test.	56
43	(A) Pretest and (B, C) Post-test Microstructures of $\gamma/\gamma'$ - $\delta$ Eutectic Alloy Coupons Coated With Approximately 127 $\mu$ of Ni-18Cr-5Al-0.3Y and Then Diffusion Aluminized (Pack, Outward). The Coated $\gamma/\gamma'$ - $\delta$ Coupon Was Evaluated for 140 Cycles In the 1172 K (1650°F) Cyclic Hot Corrosion Test.	57
44	(A) Pretest and (B) Post-Test Microstructures of $\gamma/\gamma'$ - $\delta$ Eutectic Alloy Coupons Coated With Approximately 127 $\mu$ of Ni-18Cr-5Al-0.3Y. The Coated $\gamma/\gamma'$ - $\delta$ Coupon Was Evaluated for 250 Cycles In The 1172 K (1650°F) Cyclic Hot Corrosion Test.	58
45	Post-test Microstructure of Gas Phase Aluminide Coated $\gamma/\gamma'$ - $\delta$ Simulated Air Cooled Blade Specimen After 20 Hours of Cyclic Hot Corrosion Testing At 1172 K (1650°F). (A) Typical Coating Microstructure In Unfailed Regions. (B) Localized Pitting Attack of the Coating. (C) Oxide Blister and Associated Substrate Attack.	59
46	Simulated $\gamma/\gamma'$ - $\delta$ Air Cooled Blade Specimen	65
47	PWA 275 Coating Chamber Design	65

## LIST OF ILLUSTRATIONS (Cont'd)

Figure	Title	Page
48	Variation of Diffusion Aluminide Coating Thickness With $\delta$ Phase Platelet Thickness	66
49	Typical PWA 275 Coating Microstructure at Junction of ECM Cooling Hole and Internal and External Surfaces of $\gamma/\gamma' - \delta$ Simulated Air Cooled Blade Specimen (Run 6).	67
50	Thickness of PWA 275 Coating On Internal and External Surfaces of $\gamma/\gamma' - \delta$ Eutectic Alloy Specimen As a Function of Coating Time At 1366 K (2000°F).	67
51	Dependence of PWA 275 Coating Thickness On Coating Time At 1366 K (2000°F) and Phases Being Aluminized In ECM Cooling Holes of $\gamma/\gamma' - \delta$ Eutectic Alloy Specimen.	68
52	Post-test Microstructure of Pt + Al Coated $\gamma/\gamma' - \delta$ Tensile Ductility Specimen Showing Secondary Cracking. Coating Fracture Strain, 0.5 to 0.7%; Specimen Failure Strain, 4.2%; Test Temperature, 578 K.	76
53	Post-test Microstructure of NiCrAlY + Pt Coated $\gamma/\gamma' - \delta$ Tensile Ductility Specimen Showing Secondary Cracking. Coating Fracture Strain, 0.5 to 0.7%; Specimen Failure Strain, 4.5%; Test Temperature, 578 K.	76
54	Post-test Microstructure of NiCoCrAlY + Pt Coated $\gamma/\gamma' - \delta$ Tensile Ductility Specimen Showing Secondary Cracking. Coating Fracture Strain, 0.5 to 0.7%; Specimen Failure Strain, 3.1%; Test Temperature, 578 K.	77
55	Post-test Microstructure of NiCoCrAlY Coated $\gamma/\gamma' - \delta$ Tensile, Ductility Specimen; Note Secondary Cracking In Diffusion Affected Substrate. Coating Fracture Strain, > 2.0%; Substrate Failure Strain, 2.7%; Test Temperature, 578 K.	77
56	Post-test Microstructure of Low Aluminum NiCrAlY + Diffusion Aluminide (Pack, Inward) Coated $\gamma/\gamma' - \delta$ Tensile Ductility Specimen Showing Secondary Cracking. Coating Fracture Strain, 0.2 to 0.4%; Specimen Failure Strain, 3.2%; Test Temperature, 578 K.	78

## LIST OF ILLUSTRATIONS (Cont'd)

Figure	Title	Page
57	Post-test Microstructure of NiCrAlSiY Coated $\gamma/\gamma' - \delta$ Tensile Ductility Specimen Showing Secondary Cracking. Coating Fracture Strain, 1.3 to 1.6%; Specimen Failure Strain, 1.6%; Test Temperature, 578 K.	78
58	Schematic Relationship Between Thermomechanical Fatigue Cycles In Substrate and Coating. The Zero-Strain Condition of the Coating Is Set At the Maximum Temperature of the Thermomechanical Fatigue Cycle.	88
59	Thermal Fatigue Lives of NiCrAlY and NiCrAlY + Pt Coated $\gamma/\gamma' - \delta$ and D.S. MAR-M 200 + Hf Specimens.	89
60	Microstructure of NiCrAlY Coated $\gamma/\gamma' - \delta$ (6 Cr) Specimen (E 300) Which Was Evaluated for 2678 Cycles In a Cycle I (700 to 1311 K; $\Delta\epsilon_{TM} = 0.30\%$ ) Thermomechanical Fatigue Test.	90
61	Longitudinal Microstructure and Secondary Crack Morphology in NiCrAlY Coated $\gamma/\gamma' - \delta$ (6Cr) Specimen (E 300) Which was Evaluated for 2678 Cycles in a Cycle I (700 to 1311 K; $\Delta\epsilon_{TM} = 0.30\%$ ) Thermomechanical Fatigue Test. Oxide Inclusions and Substrate Porosity May Have Contributed to Crack Initiation.	91
62	Scanning Electron Microscope (SEM) Fracture Surface Photograph of Secondary Thermal Fatigue Crack (B) In NiCrAlY Coated $\gamma/\gamma' - \delta$ Specimen (E 300) Which Was Evaluated for 2678 Cycles In a Cycle I (700 to 1311 K; $\Delta\epsilon_{TM} = 0.30\%$ ) Thermomechanical Fatigue Test. Coating Crack Initiation Was Detected After Approximately 1550 Cycles.	92
63	Surface Propagation of Thermal Fatigue Cracks in NiCrAlY Coated $\gamma/\gamma' - \delta$ Specimen E 300 ( $\Delta\epsilon_{TM} = 0.30\%$ ).	93
64	Transverse (Left) and Longitudinal (Right) Cross-section Microstructures of NiCrAlY Coated $\gamma/\gamma' - \delta$ (6Cr) Specimen (E 487) Which Was Evaluated for 7286 Cycles in a Cycle I (755 to 1200 K; $\Delta\epsilon_{TM} = 0.30\%$ ) Thermomechanical Fatigue Test. The Longitudinal Microstructure Shows a Small Thermal Fatigue Crack Which has Propagated a Short Distance into the Eutectic Alloy Substrate.	94
65	Microstructure of NiCrAlY + Pt Coated $\gamma/\gamma' - \delta$ (6Cr) Specimen (E 290) which was Evaluated for 4486 Cycles in a Cycle I (700 to 1311 K; $\Delta\epsilon_{TM} = 0.30\%$ ) Thermomechanical Fatigue Test.	95

## LIST OF ILLUSTRATIONS (Cont'd)

Figure	Title	Page
66	Surface Propagation of Thermal Fatigue Cracks in NiCrAlY + Pt Coated $\gamma/\gamma' - \delta$ Specimen E 290 ( $\Delta\epsilon_{TM} = 0.30\%$ ).	96
67	Optical Fracture Surface Photographs of Secondary Thermal Fatigue Cracks D (top) and E (bottom) in NiCrAlY + Pt Coated $\gamma/\gamma' - \delta$ Specimen (E 290) which was Evaluated for 4486 Cycles in a Cycle I (700 to 1311 K; $\Delta\epsilon_{TM} = 0.30\%$ ) Thermomechanical Fatigue Test. Initiation of Both Coating Cracks was Detected After Approximately 450 Cycles.	97
68	Microstructures of Pit Initiated Thermal Fatigue Cracks in NiCrAlY + Pt Coated $\gamma/\gamma' - \delta$ (6Cr) Specimen (E 290) which was Evaluated for 4486 Cycles in a Cycle I (700 to 1311 K; $\Delta\epsilon_{TM} = 0.30\%$ ) Thermomechanical Fatigue Test. An Oxidation Affected Zone Envelopes both Cracks. In Addition, for the Longer Crack (bottom), the $\delta$ Phase has Started to Rupture Ahead of the Crack Tip.	98
69	Microstructure of NiCrAlY + Pt Coated $\gamma/\gamma' - \delta$ (6Cr) Specimen (E 488) which was Evaluated for 5270 Cycles in a Cycle I (755 to 1200 K; $\Delta\epsilon_{TM} = 0.30\%$ ) Thermomechanical Fatigue Test.	99
70	Average Cycle I Thermomechanical Fatigue Crack Propagation Rates in $\gamma/\gamma' - \delta$ Eutectic Superalloy Obtained with NiCrAlY (E 300, 487) and NiCrAlY + Pt (E 204, 279, 288, 290) Coated Specimens are Shown with Initial and Final Values of the Strain Intensity Factor Range, $\Delta K_e$ . Data from Uncoated Specimens (E 173, 295) are Provided for Comparison.	100
71	Isothermal Reversed Bending (Krouse) Fatigue Specimen.	110
72	977 K(1300 F) Isothermal Fatigue Data for Directionally Solidified $\gamma/\gamma' - \delta$ (6Cr) Alloy.	111
73	977 K(1300 F) Isothermal Fatigue Data for Directionally Solidified MAR-M 200 + Hf Alloy.	112
74	977 K(1300 F) Isothermal Fatigue Data for Coated and Uncoated Longitudinal Grain Orientation $\gamma/\gamma' - \delta$ (6Cr) Alloy.	113

## LIST OF ILLUSTRATIONS (Cont'd)

Figure	Title	Page
75	Fracture Surfaces of Pit (Left) and Flake (Right) Initiated Fatigue Cracks in NiCrAlY Coated $\gamma/\gamma' - \delta$ Specimen (No. 10) which was Evaluated in 977 K(1300°F) LCF Test. Cracking was Confined to the Coating During the First $10^4$ Cycle Increment at a Strain Range of 0.5 Percent. Significant Crack Penetration Into the $\gamma/\gamma' - \delta$ Substrate Occurred During the Next $10^4$ Cycle Increment at a Strain Range of 0.55 Percent.	114
76	Estimated Effect of NiCrAlY Coating Thickness on 977 K(1300°F) Fatigue Strength of $\gamma/\gamma' - \delta$ (6Cr) Alloy.	115
77	Coating Crack Propagation Rate Versus Strain Range Data for Several Cracks in NiCrAlY Coated $\gamma/\gamma' - \delta$ and D.S. MAR-M 200 + Hf Specimens which were Fatigue Tested at 977 K(1300°F). Note That the Strain Range Required to Achieve a Given Propagation Rate is Greater for the Thinner Coating.	116
78	Coating Crack Propagation Rate Data as a Function of the Strain Range ( $\Delta\epsilon$ ) Times the Square Root of the Coating Thickness ( $\sqrt{t}$ ) for NiCrAlY Coated $\gamma/\gamma' - \delta$ and D.S. MAR-M 200 + Hf Specimens Which were Fatigue Tested at 977 K (1300°F).	117
79	977 K(1300°F) Isothermal Fatigue Data for NiCrAlY Coated Longitudinal Grain Orientation $\gamma/\gamma' - \delta$ (6Cr) Directionally Solidified Eutectic Alloy Systems.	118
80	Morphology of Pit Initiated Fatigue Crack in Plane of NiCrAlY Coating on $\gamma/\gamma' - \delta$ Specimen (No. 11) Which was Evaluated in 977 K(1300°F) LCF Test.	119
81	Morphology of Pit Initiated Fatigue Crack in Plane of NiCrAlY Coating on D.S. MAR-M 200 + Hf Specimen (No. 15) Which was Evaluated in 977 K(1300°F) LCF Test.	120
82	Secondary Crack Microstructures in NiCrAlY + Pt and NiCrAlY Coated Longitudinal and Transverse Grain Orientation $\gamma/\gamma' - \delta$ Specimens Which Formed During $10^4$ Cycle LCF Tests at 977 K (1300°F).	121
83	Secondary Crack Microstructures in Pt + Al Coated Longitudinal and Transverse Grain Orientation $\gamma/\gamma' - \delta$ Specimens Which Were Formed During 977 K(1300°F) $10^6$ Cycle HCF and $10^4$ Cycle LCF Tests, Respectively.	122

## LIST OF TABLES

Table	Title	Page
I	Coating Systems Evaluated in 1366 K (2000°F) Cyclic Oxidation Burner Rig Tests	8
II	PWA 275 Process Parameters	63
III	PWA 275 Coated Test Specimens	64
IV	PWA 275 Coated + Four Hours at 1352 K	64
V	578 K(600°F) Coating Fracture and Specimen Failure Strains	73
VI	578 K(600°F) Coating Fracture and $\gamma/\gamma' - \delta$ Failure Strains (NASA Contract NAS3-16792)	74
VII	578 K(600°F) Coating and $\gamma/\gamma' - \delta$ Substrate Fracture Strains (Air Force Contract F33657-71-C-0789)	75
VIII	Thermomechanical Fatigue Test Conditions	87
IX	977 K(1300°F) $10^4$ Cycle Strain-Stepped LCF Tests of Longitudinal Grain Orientation $\gamma/\gamma' - \delta$ (6Cr) and MAR-M 200 + Hf Directionally Solidified Superalloys.	107
X	977 K(1300°F) $10^4$ Cycle Strain-Stepped LCF Tests of Transverse Grain Orientation $\gamma/\gamma' - \delta$ (6Cr) and MAR-M 200 + Hf Directionally Solidified Superalloys.	108
XI	977 K(1300°F) $10^6$ Cycle Strain-Stepped HCF Tests of Longitudinal Grain Orientation $\gamma/\gamma' - \delta$ (6Cr) and MAR-M 200 + Hf Directionally Solidified Superalloys.	109

## I. SUMMARY

The successful application of high creep strength, directionally solidified  $\gamma/\gamma' - \delta$  (Ni-19.7Cb-6Cr-2.5 Al) eutectic superalloy turbine blades requires the development of suitable coatings for airfoil, root and internal blade surfaces. Coating development and evaluation efforts under NASA Contract NAS3-16792 identified coating systems which demonstrated significant potential for protecting the  $\gamma/\gamma' - \delta$  alloy in a high temperature turbine environment and, at the same time, indicated some areas which required additional investigation. In order to further improve coatings for the  $\gamma/\gamma' - \delta$  alloy, the current investigation had the goals of 1) refining promising coating compositions for directionally solidified eutectics, 2) evaluating the effects of coating/substrate interactions on the mechanical properties of the alloy, and 3) evaluating diffusion aluminide coatings for internal surfaces. Electron beam vapor deposition, sputtering, and diffusion aluminizing coating techniques, singly or in selected combinations, were employed to fabricate seven candidate coating systems for protecting the  $\gamma/\gamma' - \delta$  directionally solidified (D.S.) eutectic alloy.

Burner rig cyclic oxidation, furnace cyclic hot corrosion, ductility, and thermal fatigue tests indicated that NiCrAlY+Pt (63 to 127 $\mu$  Ni-18Cr-12Al-0.3Y + 6 $\mu$  Pt) and NiCrAlY (63 to 127 $\mu$  Ni-18Cr-12Al-0.3Y) coatings are capable of protecting high temperature gas path surfaces of eutectic alloy airfoils. Burner rig (Mach 0.37) testing indicated that the useful coating life of the 127 $\mu$  thick coatings exceeded 1000 hours at 1366 K (2000°F).

Comparative burner rig testing of the candidate coating systems on the  $\gamma/\gamma' - \delta$  and D.S. MAR-M 200 + Hf alloys indicated that the thermal fatigue resistance of a given coating system was dependent on the coating-substrate thermal expansion mismatch strain ( $\Delta\epsilon_\alpha$ ) as shown in Figure 1 for NiCoCrAlY coatings. Minimizing  $\Delta\epsilon_\alpha$  in the coating enhances the thermal fatigue resistance of the coating-substrate system.

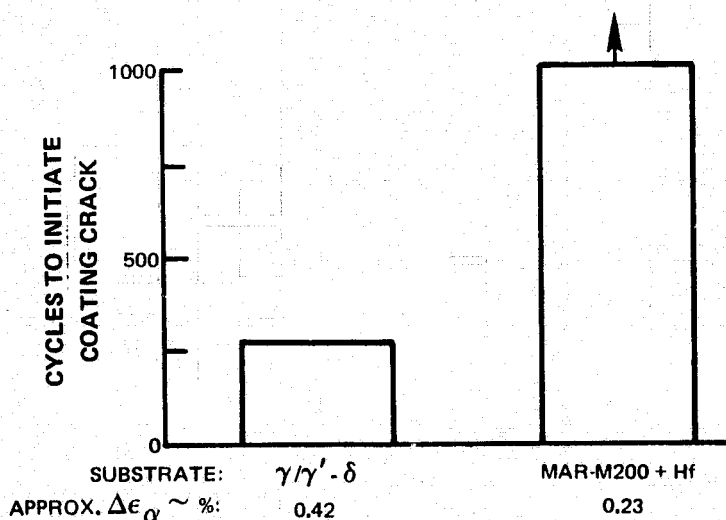


Figure 1

Effect of Coating-Substrate Thermal Expansion Mismatch Strain ( $\Delta\epsilon_\alpha$ ) on Crack Initiation in NiCoCrAlY Coating During 1366 K Cyclic Oxidation Burner Rig Tests.

Cyclic furnace hot corrosion testing (1172 K for 250 hours) indicated that NiCrAlY, NiCrAlY + Pt, NiCoCrAlY, NiCoCrAlY + Pt and Pt + Al coatings provide a significant amount of protection in a Na<sub>2</sub>SO<sub>4</sub> contaminated environment. Hot corrosion failures were observed in low aluminum NiCrAlY + diffusion aluminide and gas phase aluminide coated  $\gamma/\gamma'$ - $\delta$  specimens during the course of these tests.

Analysis of ductility tests conducted at 578 K indicated that the mechanical properties of the coating could affect the fracture strain of the eutectic alloy substrate as indicated in Figure 2. In order to put these results into perspective, it should be noted that the purpose of this tensile ductility test is to verify that the fracture strains of the coatings exceed values (0.15 to 0.35 percent strain) which are expected in a typical gas turbine airfoil. These results indicate that the fracture strains of all the coating systems which have been evaluated on the  $\gamma/\gamma'$ - $\delta$  alloys exceed the magnitude of anticipated thermal strains with the possible exception of the NiCrAlY + Al system.

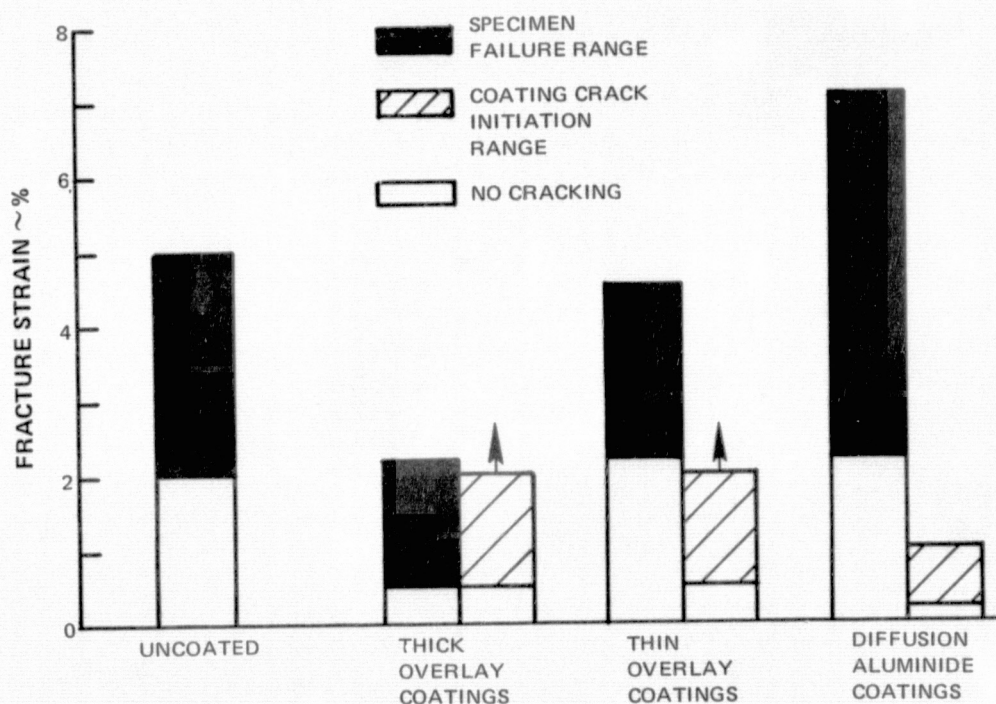


Figure 2 578 K Ductility Tests of Coated  $\gamma/\gamma'$ - $\delta$  (6Cr) show the Influence of the Coating on Fracture Strain of the Substrate.

Thermomechanical fatigue tests indicated that, for a given strain range, the maximum temperature and/or temperature range significantly affect specimen life as shown in Figure 3.

Isothermal fatigue and furnace hot corrosion tests indicated that 63 $\mu$  NiCrAlY, NiCrAlY + Pt and platinum modified diffusion aluminide (Pt + Al) coating systems are capable of protecting the relatively cooler surfaces of the blade root. Test data and a fracture mechanics analysis showed that coating thickness has a significant effect on both coating crack initiation and specimen failure. Fatigue data for 66 and 127 $\mu$  NiCrAlY coated  $\gamma/\gamma'$ - $\delta$  specimens illustrates this behavior in Figure 4.

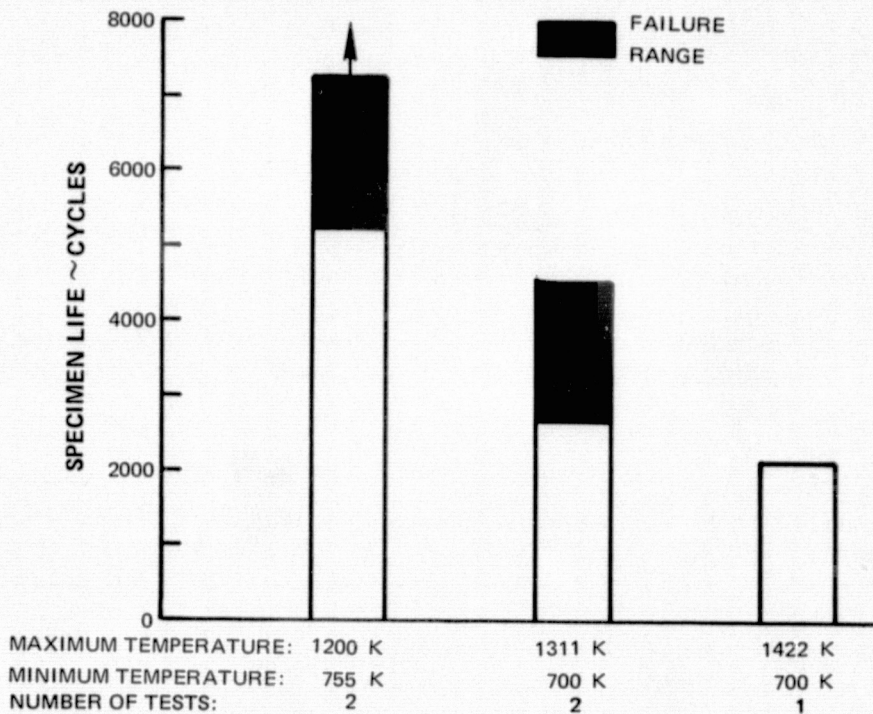


Figure 3 Cycle I (0.3% Strain Range) Thermomechanical Fatigue Life of NiCrAlY and NiCrAlY + Pt Coated  $\gamma/\gamma' - \delta$  (6Cr) Alloy.

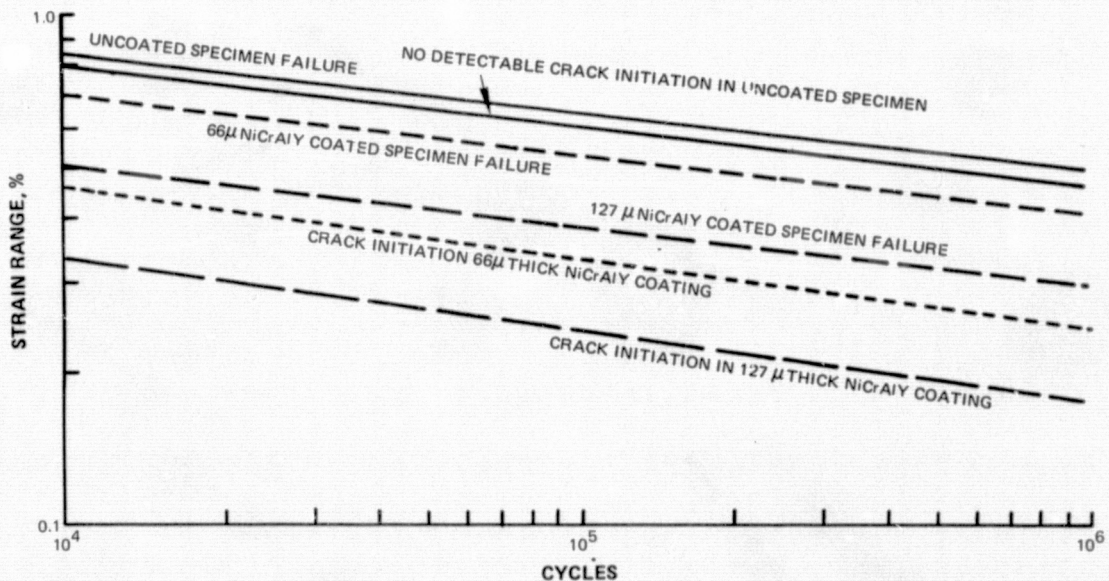


Figure 4 Effect of NiCrAlY Coating Thickness on 977 K Isothermal Fatigue of  $\gamma/\gamma' - \delta$  (6Cr) Alloy.

Evaluation of a gas phase coating process for diffusion aluminizing internal surfaces and cooling holes of air-cooled  $\gamma/\gamma' - \delta$  blades indicated that the  $\gamma/\gamma'$  phase regions in the substrate microstructure were aluminized to about twice the depth of the  $\delta$  phase platelets.

## II. INTRODUCTION

Increased turbine inlet temperatures and/or increased rotor speeds (resulting in higher blade stresses) in advanced gas turbine engine designs require turbine materials with strength and temperature capabilities beyond those of current generation nickel-base superalloys. Directionally solidified eutectic superalloys containing  $\text{Ni}_3\text{Cb}$  ( $\delta$  phase) reinforcing platelets in a  $\text{Ni}_3\text{Al}$  ( $\gamma'$ ) strengthened nickel-chromium solid solution ( $\gamma$ ) matrix have a potential temperature advantage of 56 to 83 K (100 to 150°F) at a given stress (or 40 to 60 percent increase in load carrying capability at a given temperature) over current nickel-base superalloys and represent a class of alloys that is a candidate to meet the challenge of advanced turbine material requirements.

Oxidation characteristics of this Ni-19.7Cb-6 Cr-2.5Al alloy, which will subsequently be referred to as  $\gamma/\gamma'-\delta$ , are such that protective coatings are required over a wide range of temperatures (refs. 1, 2 and 3). Depending upon the exposure temperature, two types of behavior are possible. At relatively low temperatures (below  $\sim 1073$  K), selective oxidation of the  $\delta$  phase occurs, while at higher temperatures, diffusion in the eutectic alloy promotes a more uniform mode of oxidation. Between approximately 1073 and 1373 K, a continuous  $\gamma$  layer forms adjacent to a relatively planar scale. At higher temperatures (above about 1423 K), the  $\delta$  phase becomes continuous between the eutectic alloy and the oxide scale. In both cases, the rate at which oxidation proceeds is unacceptable, and development of suitable coatings is therefore an important factor for the successful utilization of eutectic alloy turbine components.

A preliminary evaluation of the compatibility and oxidation resistance of selected diffusion and overlay coatings on eutectic alloys was performed at Pratt & Whitney Aircraft (P&WA). The 1366 K (2000°F) cyclic oxidation burner rig test indicated that the diffusion coatings examined did not provide any significant protection for the  $\gamma/\gamma'-\delta$  alloy at this temperature. One specimen failed after nine hours due to melting while the remaining specimens were severely oxidized after 140 hours of exposure, or less. In contrast to the diffusion coatings, a NiCrAlY overlay coating on  $\gamma/\gamma'-\delta$  experienced only moderate degradation after exposure for 700 hours in this test. A CoCrAlY overlay coating on a  $\gamma'-\delta$  (Ni-23Cb-4.4Al) alloy exhibited cracking in the as-coated (fully processed) condition. Such cracking was attributed to formation of a brittle phase at the coating-alloy interface and/or thermal expansion mismatch strains between the alloy and coating.

These initial P&WA evaluations with the coated  $\gamma/\gamma'-\delta$  alloy in conjunction with extensive experience, including detailed oxidation, hot corrosion, and mechanical property data on conventional nickel-base superalloys, provided the basis for 1) selecting currently available coating systems and processes for protecting the  $\gamma/\gamma'-\delta$  eutectic superalloy in an Air Force program (ref. 4) and 2) formulating additional candidate developmental coating systems which were evaluated under a NASA sponsored program (NAS3-16792) (ref. 5).

The above NASA program, "Coatings for Directional Eutectics", identified the NiCrAlY + Pt coating system as having the best combination of oxidation, hot corrosion, diffusional stability, and mechanical properties on the  $\gamma/\gamma'-\delta$  alloy. Based on the data obtained in the

NASA program, the NiCrAlY + Pt coating system was selected for evaluation in the design data portion of the Air Force program (ref. 4).

Thus, considerable prior experience, including detailed oxidation, hot corrosion and mechanical property data with coated conventional and eutectic nickel-base superalloys, was available to facilitate the selection of the candidate coating systems for this program. A brief review of the reasons for including specific elements into the candidate coating compositions is provided in the following paragraphs.

Overlay coating compositions were based on the knowledge that aluminum is required for protective  $\text{Al}_2\text{O}_3$  scale formation, yttrium for scale adherence (refs. 6 through 9), and chromium for both promotion of  $\text{Al}_2\text{O}_3$  formation (ref. 10) and enhancement of hot corrosion (sulfidation) resistance. NiCrAlY compositions offer superior elevated temperature oxidation resistance and diffusional stability on nickel-base superalloys. Additions of cobalt to NiCrAlY enhance hot corrosion resistance and improve coating ductility.

Since it was assumed that total surface protection of the  $\gamma/\gamma'$ - $\delta$  alloy would be required, a diffusion aluminide type coating is necessary for lower operating temperature surfaces, particularly internal cooling cavities and possibly the blade root. Therefore, subsequent aluminizing of a previously deposited low aluminum overlay coating appeared to offer a unique processing advantage in that all surfaces could be coated while simultaneously increasing the protectivity of the airfoil overlay coating to a more desirable level. Indeed, results (ref. 11) reported in the literature have shown that this approach can be an effective method to increase coating life.

It has been shown (refs. 12 and 13) that additions of precious metals such as platinum to aluminide coatings on nickel-base superalloys have significantly increased the useful lives of these coatings in high temperature oxidation. Experiments with platinum-aluminum alloys, which form  $\text{Al}_2\text{O}_3$  scales, indicate that the spalling resistance of the oxide scale is enhanced by the presence of platinum (ref. 14). Laboratory evaluations conducted at P&WA have shown that additions of 5 to 10 w/o of platinum to NiCrAl(Y) alloys provide improved oxidation and hot corrosion resistance. Extensive testing under a previous NASA contract (ref. 5) indicated that platinum may enhance the mechanical and physical characteristics of overlay coatings in addition to improving the oxidation resistance.

Silicon additions to NiCrAl (refs. 11, 15 and 16) have been reported to improve oxidation performance. This effect was not demonstrated in a previous evaluation of a NiCrAlSiY coating applied with a plasma spray process (ref. 5). Since that program, it was found that NiCrAlSiY compositions can be deposited with the electron beam physical vapor deposition process. Therefore, NiCrAlSiY coatings were re-evaluated in this program.

The electron beam physical vapor deposition process (refs. 17 and 18) was used to apply the multielement overlay coatings. In particular instances, sputtering and pack coating techniques were employed in conjunction with the electron beam process to achieve the desired coating composition and microstructure. In one instance, sputtering and pack cementation techniques were used to apply a platinum modified diffusion aluminide coating.

Because of the line-of-sight restrictions of overlay type coatings, internal surfaces and cooling holes must be coated with a diffusion aluminide. An evaluation of conventional pack aluminide type coating in a previous program (ref. 4) indicated that small diameter cooling holes in the  $\gamma/\gamma'-\delta$  alloy were difficult to coat satisfactorily. Limited testing under that program indicated that better coverage could be obtained with the gas phase aluminizing process. This coating process was optimized for the  $\gamma/\gamma'-\delta$  alloy in this program.

While previous development and evaluation efforts demonstrated significant potential for protecting the  $\gamma/\gamma'-\delta$  alloy in a high temperature turbine environment, several areas which required additional evaluation were identified.

Burner rig 1366 K (2000°F) cyclic oxidation testing of coated  $\gamma/\gamma'-\delta$  and directionally solidified (D.S.) MAR-M200+Hf superalloy specimens indicated that thermal fatigue and oxidation resistance of a coating system were dependent on the substrate (ref. 5). Therefore, additional burner rig testing was conducted in this program to evaluate six candidate coating systems on these alloys in order to obtain a better understanding of the coating-substrate interaction phenomenon. Thermal expansion data were also obtained in this program as well as in a P&WA funded program which facilitated interpretation of the burner rig results.

A parallel effort to optimize the structure and composition of the  $\gamma/\gamma'-\delta$  eutectic alloy was also being conducted (ref. 19). In particular, the solidification characteristics of the  $\gamma/\gamma'-\delta$  (1 Cr) alloy resulted in microstructure improvements. The effect of this eutectic alloy modification on coated system performance was also assessed in a 1366 K burner rig test.

Increasing the burner rig data base for the NiCrAlY + Pt and NiCrAlY coating systems, which exhibited excellent performance during previous furnace and burner rig tests (refs. 4 and 5), and evaluating a silicon modified NiCrAlY coating applied by the electron beam physical vapor deposition process were also goals of this program.

In addition to high temperature oxidation, the  $\gamma/\gamma'-\delta$  alloy requires protective coatings to inhibit intermediate temperature hot corrosion (accelerated oxidation in the presence of  $\text{Na}_2\text{SO}_4$ ). Therefore, the candidate coating systems (with the exception of the NiCrAlSiY composition) were evaluated in a furnace hot corrosion test at 1172 K (1650°F).

Another objective of this program was to assess the effects of the candidate coating systems on mechanical properties of the coated eutectic alloy. Ductility tests at 578 K (600°F) were used to evaluate the low temperature strain capability of the coating-substrate systems. Three candidate coating systems for the blade root (NiCrAlY, NiCrAlY + Pt and Pt + Al) were evaluated for fatigue resistance at 977 K (1300°F). Thermomechanical fatigue tests were used to quantitatively assess the thermal fatigue resistance of two candidate airfoil coatings (NiCrAlY + Pt and NiCrAlY) on the eutectic alloy.

### III. BURNER RIG OXIDATION TESTING

#### A. BACKGROUND

Previous high temperature furnace and burner rig tests have indicated that both NiCrAlY and NiCrAlY + Pt coating systems can provide oxidation resistance for the  $\gamma/\gamma'$ - $\delta$  alloy for extended exposures at 1366 and 1422 K (2000 and 2100°F) (refs. 4 and 5). In addition, furnace testing of these coating-alloy systems indicated that they are protective (for shorter periods of time) at temperatures up to 1478 to 1505 K (2200 to 2250°F).

Burner rig testing of NiCoCrAlY, NiCrAlY + Al and NiCrAlY + Pt coating systems at 1366 K for 1016 hours of cyclic oxidation also indicated, however, that thermal fatigue cracks formed in these coating systems on the  $\gamma/\gamma'$ - $\delta$  alloy (ref. 5); of these coating systems, the NiCrAlY + Pt coating exhibited the best resistance to thermal fatigue crack initiation and propagation. Similar cyclic oxidation burner rig testing at 1422 K for 498 hours indicated that NiCrAlY coated  $\gamma/\gamma'$ - $\delta$  specimens also exhibited only minor thermal fatigue cracking (ref. 4). It was also noted that the tendency of these coating systems to form thermal fatigue cracks was dependent on the substrate (ref. 5); coating initiated thermal fatigue cracking was not observed in these coating systems on D.S. MAR-M 200 + Hf specimens which were evaluated concurrently with the coated eutectic alloy specimens.

Thermal expansion data indicated that coating-substrate thermal expansion strains would be larger in coatings on the  $\gamma/\gamma'$ - $\delta$  alloy than on D.S. MAR-M 200 + Hf and may provide a partial explanation for the thermal fatigue cracking which was observed (ref. 5). In addition, the depth of thermal fatigue crack penetration into the  $\gamma/\gamma'$ - $\delta$  substrate also appeared to be a function of the coating which was present. It was proposed that the thermal expansion mismatch strain in the coating, the elastic modulus of the coating, coating thickness, the density of cracks, and the oxidation characteristics of a coating crack may be factors contributing to the observed behavior.

Two 1366 K cyclic oxidation burner rig tests have been conducted in this program. The first of these tests was for 505 hours and had the objectives of 1) further defining the role of platinum in terms of coating performance, 2) qualitatively evaluating the thermal fatigue resistance of thinner overlay coatings with and without platinum, 3) evaluating the NiCrAlY + Al system with the diffusion aluminide layer being formed by an "inward" process (ref. 20), and 4) assessing the possibility of using the Pt + Al diffusion aluminide coating system (a candidate system for blade root applications) for protecting the gas path surfaces of the airfoil. For comparison, additional D.S. MAR-M 200 + Hf specimens were also coated with the candidate systems and evaluated. (The evaluation of the  $\gamma/\gamma'$ - $\delta$  specimen coated with NiCrAlY and the coated D.S. MAR-M 200 + Hf specimens was not part of this contractual program; however, the results of the evaluation are included for comparison purposes.)

The second cyclic oxidation test was for 1005 hours and had the objectives of 1) obtaining additional burner rig data for the NiCrAlY and NiCrAlY + Pt coatings, with the latter coating being additionally evaluated on a low chromium  $\gamma/\gamma'$ - $\delta$  (1Cr) alloy, and 2) burner rig evaluation of a silicon modified NiCrAlY coating applied by the electron beam physical vapor deposition process. Nominal coating thicknesses and chemistries of the coating systems

which were evaluated in these tests are provided in Table I.

TABLE I  
COATING SYSTEMS EVALUATED IN 1366 K (2000°F)  
CYCLIC OXIDATION BURNER RIG TESTS

#### TEST 1

Total Test Time: 505 Hours

Oxidation Cycle: 27 minutes hot - 3 minutes forced air cool

Coating Systems:

- (1) 63 $\mu$  Ni-18Cr-12Al-0.3Y (eb)
- (2) 63 $\mu$  Ni-18Cr-12Al-0.3Y (eb) + 6 $\mu$  Pt (s)
- (3) 63 $\mu$  Ni-23Co-18Cr-12Al-0.3Y (eb)
- (4) 63 $\mu$  Ni-23Co-18Cr-12Al-0.3Y (eb) + 6 $\mu$  Pt (s)
- (5) 127 $\mu$  Ni-18Cr-5Al-0.3Y (eb) + diffusion aluminide (p)
- (6) 6 $\mu$  Pt(s) + 25-76 $\mu$  diffusion aluminide (p)

#### TEST 2

Total Test Time: 1005 hours

Oxidation Cycle: 55 minutes hot - 5 minutes forced air cool

Coating Systems:

- (1) 127 $\mu$  Ni-18Cr-12Al-0.3Y (eb)
- (2) 127 $\mu$  Ni-18Cr-12Al-0.3Y (eb) + 6 $\mu$  Pt (s)
- (3) 127 $\mu$  Ni-18Cr-12Al-4Si - 0.3Y (eb)

#### Coating Processes:

- eb - electron beam vapor deposition
- p - pack cementation
- s - sputter deposition

In addition, thermal expansion data were obtained for three coating compositions (Ni-17.8Cr-4.8 Al, Ni-17.7Cr-9.1Al, and Ni-18.1Cr-10.2Al-5Pt). These data and the results of a larger P&WA program (not related to this contract) were used to facilitate interpretation of thermal fatigue behavior.

#### B. SPECIMEN PREPARATION

Eutectic alloy burner rig specimens (refs. 4 and 5) were directionally solidified by the Casting Development Section of the Materials Engineering and Research Laboratory using a multiple cavity shell mold. The bars were solidified at the rate of 1.27 cm (0.5 inch)/hour in a modified Bridgman furnace. Since the erosion bar configuration is cast to size, the only precoating surface preparation employed was a light abrasive belting to radius edges and improve surface finish. The coating systems which were applied to these specimens are indicated in Table I.

Coating procedures were identical to those used previously (ref. 4 and 5).

Briefly, (Ni,Co,Si) CrAlY overlay coatings applied by the electron beam physical vapor deposition process (refs. 17 and 18) are deposited in vacuum on superalloy components which are rotated in the vapor of an evaporating coating ingot source. This technique depends upon a continuous feeding of ingot stock at a rate consistent with the evaporation rate of the liquid in order to control thickness and composition. An alloy ingot of the desired composition is fed upward through a water-cooled crucible. As the ingot emerges at the top of the crucible, a high-powered, focused electron beam is played on the emerging end causing local melting and forming a liquid pool contained by the walls of the crucible and solid ingot below. Due to differences in the vapor pressures of the elements in the overlay coating composition, the liquid vapor source is necessarily maintained at different composition than the vapor phase which is to be deposited. In order to maintain a constant vapor phase (coating) composition, an ingot of the coating composition is fed into the molten pool precisely at the same rate as the vapors evaporate. Control of the cast ingot feed stock was the primary method for control of the coating composition.

Conventional sputtering and pack techniques were used to apply Pt layers and diffusion aluminide coatings, respectively.

Coating alloy thermal expansion specimens (5 cm x 0.63 cm dia.) were drop cast in copper molds and machined to the indicated dimensions. In order to minimize microsegregation, these specimens were given a 1352 K/4 hour/H<sub>2</sub> heat treatment prior to machining. (Differences between the drop cast and coating microstructures are not considered significant from a thermal expansion standpoint since the phases in the coating compositions are cubic; thermal expansion is isotropic for cubic phase materials.)

### C. TEST PROCEDURES

The candidate coating systems were evaluated in two 1366 K (2000°F) cyclic oxidation burner rig tests (Table I), which simulate a gas turbine engine environment, for times of 505 and 1005 hours. A maximum of 12 specimens were simultaneously exposed to the exhaust gases (combustion products of Jet A fuel and air) of the burner which had a gas velocity of Mach 0.37. The specimens were rotated at 1750 rpm in the burner exhaust gases to provide as uniform temperature conditions from specimen to specimen as possible. Specimen temperature was continuously monitored with an optical pyrometer and the fuel pressure automatically regulated to maintain the designated temperature. Cycling was accomplished by automatically moving the burner away from the specimens at designated intervals. During the cooling portion of the cycle, a compressed air blast was directed on the rotating specimens. Testing was interrupted every 16 to 20 hours to permit visual examination and weighing of each specimen.

Thermal expansion measurements were performed by Dynatech Corporation with a Netzsch electronic automatic recording dilatometer.

## D. RESULTS AND DISCUSSION

### 1. Test 1 (505 hours at 1366 K)

Five of the six coated  $\gamma/\gamma' - \delta$  specimens and all of the coated D.S.MAR-M200+Hf specimens completed the 505 hour burner rig test. The visual condition of the coated  $\gamma/\gamma' - \delta$  specimens at the conclusion of testing is shown in Figure 5. Figure 6 shows the hot zone region of these specimens at higher magnification. Individual performance of the candidate coating systems are discussed below.

#### a. Pt + Al

The Pt + Al coated  $\gamma/\gamma' - \delta$  specimen failed after 172 hours due to incipient melting (Figure 7). Since the diffusion zone microstructure of the Pt + Al coating on the  $\gamma/\gamma' - \delta$  alloy is similar to that of the diffusion aluminide coating, which has an incipient melting temperature of approximately 1394 K (2050°F) (ref. 4), and since the  $\gamma'$  phase of the substrate did not dissolve, it is thought that the overtemperature condition was relatively mild. Insufficient overtemperature capability is therefore a factor which limits use of the Pt + Al coating to cooler regions of  $\gamma/\gamma' - \delta$  turbine blades, i.e., the root. The other coating-substrate systems including the Pt + Al coated D.S. MAR-M 200 + Hf specimen, were visually unaffected by the overtemperature.

#### b. NiCoCrAlY and NiCoCrAlY + Pt

It can be seen in Figure 6 that the  $\gamma/\gamma' - \delta$  specimens coated with the NiCoCrAlY and NiCoCrAlY + Pt coatings developed numerous thermal fatigue cracks which tend to be preferentially oriented parallel to the solidification direction of the substrate; crack initiation in the NiCoCrAlY and NiCoCrAlY + Pt coatings was first detected after 136 and 56 hours, respectively. Post-test metallography indicated that thermal fatigue cracks had propagated through the coating and into the diffusion affected substrate zone (Figures 8 and 9).

The cracking behavior of the NiCoCrAlY coated  $\gamma/\gamma' - \delta$  specimen is visually similar to that previously observed for thicker (127 $\mu$ ) NiCoCrAlY coated  $\gamma/\gamma' - \delta$  specimens which were evaluated in a similar 1366 K cyclic oxidation burner rig test (ref. 5). Relatively large tensile strains (approximately 0.38 percent strain) can develop in the coating during cooling (1366 K  $\rightarrow$  room temperature) as a consequence of NiCoCrAlY -  $\gamma/\gamma' - \delta$  thermal expansion mismatch and are contributory to the formation of these cracks. It is presently thought that the general orientation of these cracks parallel to the solidification direction of the  $\gamma/\gamma' - \delta$  substrate may be a result of elastic anisotropy in the substrate. The thermal fatigue cracks initiated in areas which were apparently free of coating defects. In addition, the  $\gamma/\gamma' - \delta$  erosion bars were visually examined before coating and were relatively free of surface defects.

It was noted that the thermal fatigue cracks which formed in the thinner ( $\sim 63\mu$ ) NiCoCrAlY coatings, which were evaluated in this test, did not penetrate into the  $\gamma/\gamma' - \delta$  substrate as much as cracks in the previously tested  $\gamma/\gamma' - \delta$  specimens with thicker ( $\sim 127\mu$ ) NiCoCrAlY coatings (ref. 5). To a first approximation, this coating thickness effect on substrate crack propagation is consistent with a fracture mechanics model (ref. 21).

While thermal fatigue cracking has been the primary degradation mechanism for the NiCoCrAlY and NiCoCrAlY + Pt coated  $\gamma/\gamma' - \delta$  specimens, alumina scale spallation was also significant. For the NiCoCrAlY coated  $\gamma/\gamma' - \delta$  specimen, alumina spallation was observed after 126 hours of testing. Alumina scale adherence was slightly better for the NiCoCrAlY + Pt coated specimen.

Pretest and post-test hot zone microstructures of the NiCoCrAlY and NiCoCrAlY + Pt coatings on the  $\gamma/\gamma' - \delta$  specimens (Figures 8 and 9) was  $\gamma$ (Ni solid solution) phase; the aluminum rich  $\beta$ (NiAl) phase was consumed by oxidation. In addition, an approximately  $60\mu$  thick band of  $\gamma$  phase was present in the diffusion affected substrate adjacent to the coating. The total thickness of the diffusion affected  $\gamma/\gamma' - \delta$  zone was approximately  $140\mu$ ; the balance of the diffusion affected substrate layer consisted of a  $\gamma + \delta$  zone which had been depleted of the  $\gamma'$  phase.

#### c. NiCrAlY and NiCrAlY + Pt

$\gamma/\gamma' - \delta$  specimens coated with the NiCrAlY and NiCrAlY + Pt coatings were visually free of thermal fatigue cracks (Figure 6). However, metallographic examination of the NiCrAlY coated  $\gamma/\gamma' - \delta$  specimen revealed the presence of a very small crack which initiated at a pit defect in the coating (Figure 10). The length of this crack in the plane of the coating was only  $180\mu$ .

Adherence of the protective alumina scale was best on the NiCrAlY + Pt coated  $\gamma/\gamma' - \delta$  specimen with no scale spallation being observed during the first 194 hours of testing. For comparison, alumina scale spallation initiated significantly earlier (after 126 hours of testing) on the  $\gamma/\gamma' - \delta$  specimen which was coated with NiCrAlY. Once scale spallation was initiated, the amount of alumina spallation gradually increased during the test. From the standpoint of oxidation resistance, the effect of the platinum surface layer was to prolong the adherence of the original alumina scale by approximately 50%.

Pretest and post-test microstructures of both the NiCrAlY + Pt and NiCrAlY coated specimens are provided in Figure 11 and 12, respectively. These figures indicate that the post-test coating microstructures were similar after the 505 hours exposure in the 1366 K burner rig. In both cases, the coating was  $\gamma$  phase at the end of testing. A continuous approximately 40 to  $50\mu$  thick band of  $\gamma'$ (Ni<sub>3</sub>Al) phase was present in the diffusion affected substrate zone of the NiCrAlY + Pt coated specimen. The total thickness of the diffusion affected substrate zone was approximately 60 to  $70\mu$ ; the balance of the interdiffusion zone thickness consisted of a thin  $\gamma + \gamma'$  layer adjacent to the unaffected  $\gamma/\gamma' - \delta$  substrate. The interdiffusion zone of the NiCrAlY coated specimen was similar with the exception that the  $\gamma'$  band was thinner and, in some areas, semi-continuous in the hot zone as a result of aluminum loss by oxidation; the  $\gamma'$  band was continuous in a slightly cooler region of the erosion bar.

#### d. NiCrAlY + Al

A few cracks formed in the NiCrAlY + diffusion aluminide coated  $\gamma/\gamma' - \delta$  erosion bars during the coating process. The spare specimen was metallographically examined to characterize the morphology of the coating cracks. Examples of these cracks are provided in Figure 13. Most

of the coating cracks were confined to the high aluminum content layer; one crack, however, had propagated through the thickness of the coating to the coating-substrate interface. Similar cracks were also observed in the NiCrAlY + Al coated furnace hot corrosion coupons (see Section IV); cracks in the noneutectic composition furnace coupons propagated a significant distance into the substrate.

It is thought that initiation of cracks in the NiCrAlY + diffusion aluminide (pack, inward) coating is associated with both the brittle, high aluminum content layers, which are formed during pack aluminizing of the NiCrAlY, and the relatively low thermal expansion characteristics of the  $\gamma/\gamma' - \delta$  substrate. Pack aluminizing of the Ni-18Cr-5Al-0.3Y coating was done at 1033 K to produce an inward diffusion, high aluminum content layer of  $\text{Ni}_2\text{Al}_3$ .  $\text{Ni}_2\text{Al}_3$  layers formed by pack aluminizing nickel-base superalloys with higher thermal expansion coefficients are very brittle; for example, the room temperature fracture strain of a diffusion aluminized layer is only 0.1 percent on a Waspaloy® substrate (ref. 22). Since the  $\gamma/\gamma' - \delta$  alloy has a significantly lower expansion coefficient than Waspaloy®, it is thought that cracks formed in the  $\text{Ni}_2\text{Al}_3$  layer during cooling to room temperature as a result of tensile coating-substrate thermal expansion mismatch strains. After forming the  $\text{Ni}_2\text{Al}_3$  layer, the specimens were heat treated (1352 K/4 hours/argon) to diffuse the  $\text{Ni}_2\text{Al}_3$  to the  $\beta(\text{NiAl})$  phase. While the  $\beta$  phase coatings are also brittle at low temperatures (refs. 23 and 24),  $\beta$  phase coatings do have slightly greater fracture strains at low temperatures on conventional nickel-base superalloys, i.e., greater than approximately 0.2 percent at room temperature. (The higher fracture strain of  $\beta$  phase type coatings on conventional superalloys may be partially due to compressive coating-substrate thermal expansion mismatch strains developing in the coating during cooling.)

In order to understand the propagation of the coating cracks (after diffusion heat treatment at 1352 K) through the relatively ductile, low aluminum content Ni-18Cr-5Al-0.3Y layer, which separates the high aluminum content zone from the substrate, it is useful to consider thermal expansion data which were obtained in this program to facilitate the analysis of thermal fatigue cracking. Data for the following drop cast coating compositions are provided in Figure 14:

- Ni-17.8Cr-4.8Al
- Ni-17.7Cr-9.1Al
- Ni-18.1Cr-10.2Al-5Pt

Also included in this figure are data for Ni-20.2Co-20.1Cr-12.1Al,  $\gamma/\gamma' - \delta$ ,  $\gamma' - \delta$  and  $\delta$  alloys which were obtained during previous P&WA, Air Force (ref.4) and NASA (ref. 25) programs. These data indicate that large tensile thermal expansion mismatch strains form in the low aluminum NiCrAlY layer during cooling (1352 K to room temperature); these mismatch strains are approximately 0.5 percent and 1 percent in the Ni-18Cr-5Al-0.3Y layer on the  $\gamma/\gamma' - \delta$  and  $\delta$ -rich off-eutectic alloys, respectively. The excessively large tensile strains provide a reasonable explanation for the coating crack propagation into the off-eutectic furnace coupons (Section IV).

With the exception of the initial cracks in the virgin coating, the NiCrAlY + diffusion aluminide coated  $\gamma/\gamma' - \delta$  specimen was visually uncracked during the first half of this test. Eventually,

however, thermal fatigue cracks initiated in the hot zone of the coating. Like the cracks in the NiCoCrAlY and NiCoCrAlY + Pt coated  $\gamma/\gamma' - \delta$  specimens, the thermal fatigue cracks were oriented parallel to the solidification direction (Figure 6). Post-test metallographic examination indicated that both the thermal fatigue cracks (Figure 15) and the pretest cracks (Figure 16) had propagated a short distance into the  $\gamma/\gamma' - \delta$  substrate.

Post-test metallographic examination of the NiCrAlY + diffusion aluminide coated  $\gamma/\gamma' - \delta$  specimen (Figure 15) indicated that the hot zone coating was depleted of the aluminum rich  $\beta$  and  $\gamma'$  phases and was  $\gamma$  phase at the completion of testing. A band of  $\gamma'$  was present in the diffusion affected substrate zone was approximately 60 to 70  $\mu$ . The amount of aluminum depletion from the coating is associated with repeated spallation of the protective alumina scale; scale spallation was first observed after 56 hours of testing.

#### e. Coated D.S. MAR-M 200 + Hf

These coatings were also evaluated on directionally solidified MAR-M 200 + Hf for comparative purposes. Visual examination indicated that, in general, thermal fatigue cracks did not form in the coatings during testing. One small crack was observed in the NiCrAlY + diffusion aluminide coated D.S. MAR-M 200 + Hf specimen after 243 hours of testing; this crack was similar in appearance to the pretest cracks in this coating on the  $\gamma/\gamma' - \delta$  alloy. It is probable that, due to its size (less than 1mm in length), the crack went undetected during the first part of that test.

In addition, alumina scale adherence was generally better for these coatings on the D.S. MAR-M 200 + Hf alloy. A pitting mode of coating attack was initiating localized coating failures at the end of the test in the NiCoCrAlY, NiCoCrAlY + Pt and NiCrAlY coated D.S. MAR-M 200 + Hf specimens. Small amounts of alumina spallation preceded the formation of the oxidation pits; the distribution of the oxide pits also indicated that the microsegregation pattern in the directionally solidified substrate may be associated with this mode of coating degradation.

Oxide pitting was not observed in thicker (127  $\mu$ ) NiCoCrAlY coated D.S. MAR-M 200 + Hf specimens which were previously evaluated in a 1366 K cyclic oxidation burner rig test for 1016 hours (ref. 5). Consequently, it is thought that the thinner NiCoCrAlY coatings evaluated during the current burner rig test may have permitted coating-substrate interdiffusion to affect the outer portion of the coating faster and accelerate the oxide pitting mode of coating failure.

The oxide pitting mode of coating degradation was also observed during the previous burner rig test in 127  $\mu$  thick NiCrAlY + Al and NiCrAlY + Pt coated D.S. MAR-M 200 + Hf specimens which were exposed for 523 hours (ref. 5). It should also be noted, however, that a companion NiCrAlY + Pt coated D.S. MAR-M 200 + Hf specimen exhibited no pitting after 1016 hours of evaluation.

#### f. Thermal Fatigue Analysis

To summarize the thermal fatigue results, this test and the previous 1366 K cyclic oxidation burner rig test under contact NAS 3-16792 demonstrated that coated  $\gamma/\gamma' - \delta$  specimens exhibited the following relative thermal fatigue trends:

<u>Coating</u>	<u>Thermal Fatigue Cracking</u>
NiCrAlY	Minor
NiCrAlY + Pt	Minor
NiCrAlY + Al	Moderate to Severe
NiCoCrAlY	Severe
NiCoCrAlY + Pt	Severe

In comparison, none of the above coating systems exhibited any coating initiated thermal fatigue cracks on the D.S. MAR-M 200 + Hf alloy.

Thermal expansion data for coating alloys obtained in this program and similar data from a P&WA internal program were used to facilitate the interpretation of thermal fatigue trends which were observed during burner rig testing. Thermal expansion data at 1311 K (1900°F) for NiCrAlPt and NiCoCrAl and NiCoCrAlPt compositions are indicated in Figure 17; the scatter band for the NiCrAl compositions is provided for comparative purposes. It can be seen that cobalt additions tend to increase the thermal expansion coefficient of the NiCrAl coating alloys while the platinum additions tend to decrease the thermal expansion coefficient. Platinum additions to the NiCoCrAl alloy tended to give thermal expansion values which were slightly greater than the "typical" NiCoCrAl data. These trends were also observed at 1089, 1200 and 1366 K. Thermal expansion coefficients of  $\gamma/\gamma' - \delta$  and MAR-M 200 + Hf have also been included in this figure for comparative purposes.

Due to rapid stress relaxation in these oxidation resistant coatings at high temperatures, it is convenient to define the zero elastic strain condition of the coating at the maximum temperature. Figure 17 indicates that the coating-substrate thermal expansion mismatch strain ( $\Delta\epsilon_\alpha$ ) which develops in a coating on cooling from the maximum temperature will be tensile and that the magnitude of  $\Delta\epsilon_\alpha$  will be greater for a coating on the  $\gamma/\gamma' - \delta$  alloy. This figure also indicated that  $\Delta\epsilon_\alpha$  is greater for NiCoCrAl and NiCoCrAlPt than for NiCrAl and NiCrAlPt coating composition applied to the  $\gamma/\gamma' - \delta$  alloy. It should also be noted that  $\Delta\epsilon_\alpha$  probably increases for a given coating-substrate system as the aluminum content of the coating is depleted by oxidation and interdiffusion with the substrate.

To a first approximation, the thermal fatigue cracking trend which developed during burner rig testing of ductile overlay coatings on the  $\gamma/\gamma' - \delta$  and MAR-M 200 + Hf is directly related to  $\Delta\epsilon_\alpha$ , the thermal expansion mismatch strain.

As a consequence of low coating ductility below about 978 K (1200°F), diffusion aluminide type coatings (e.g., the aluminum rich outer layer of the NiCrAlY + Al coating system) are dependent on compressive coating-substrate thermal expansion mismatch strains, which develop during cooling, to counteract tensile thermal strains which peak below 978 K. Diffusion aluminide coatings on conventional superalloys (e.g., MAR-M 200 + Hf) initially develop relatively large compressive mismatch strains in the coating which are in the order of 0.2 percent strain when the coated superalloy is cooled from 1366 K to room temperature. Due to the lower expansion coefficient of the  $\gamma/\gamma' - \delta$  alloy, diffusion aluminide coatings on the  $\gamma/\gamma' - \delta$  alloy do not develop the relatively large compressive thermal expansion mismatch strains and are consequently more prone to initiate thermal fatigue cracks than diffusion aluminide coatings on conventional superalloys. As diffusion aluminide coatings become degraded (aluminum content diminishes) during service exposures at high temperatures, the thermal expansion coefficient of the coating will increase; thus, diffusion aluminide coatings can become more susceptible to thermal fatigue cracking as they become degraded.

## 2. Test 2 (1005 Hours at 1366 K)

Of the initial complement of ten specimens in this 1005-hour burner rig 1366 K (2000°F) cyclic oxidation test, eight were of the  $\gamma/\gamma'$ - $\delta$  (6Cr) and two were of the  $\gamma/\gamma'$ - $\delta$  (1Cr) eutectic alloy compositions. The  $\gamma/\gamma'$ - $\delta$  (6Cr) erosion bars were coated with the following nominal compositions:

- 127 $\mu$  (5 mils) Ni-18Cr-12Al-0.3Y (3 specimens);
- 127 $\mu$  (5 mils) Ni-18Cr-12Al-0.3Y + 6 $\mu$  (0.25 mil) platinum (3 specimens);
- 127 $\mu$  (5 mils) Ni-18Cr-12Al-4Si-0.3Y (2 specimens)

The two  $\gamma/\gamma'$ - $\delta$  (1Cr) specimens were coated with the NiCrAlSiY + Pt system.

Four specimens, one of each coating-substrate system, were removed for metallographic examination after 516 hours of testing. The other six burner rig specimens were tested for 1005 hours.

The visual conditions of the coated  $\gamma/\gamma'$ - $\delta$  burner rig specimens after 516 and 1005 hours of testing is provided in Figure 18. Surface photographs of the hot zone region of the specimens which were evaluated for 1005 hours are shown at higher magnification in Figure 19. The performance of these coating systems are discussed below.

### a. NiCrAlSiY

A small amount of incipient melting was visually observed in the NiCrAlSiY coated specimens during the initial 22 hour exposure increment. Since the surface of the coating remained intact, it was decided to continue running the specimens. No additional increase in incipient melting was observed during the course of the 1005 hour test. The surface appearance of the incipient melting zone after 226 hours of testing is shown in Figure 20.

The two NiCrAlSiY coated specimens exhibited differences in initial oxide scale adhesion. One specimen (R-7795) initially exhibited excellent adherence with scale spallation not being observed until 258 hours. In contrast, the duplicate specimen (R-7796) exhibited scale spallation after only 55 hours of testing. The contrast in visual appearance of these specimens after 246 hours of testing is shown in Figure 21. After oxide scale spalling initiated on specimen R-7795, the spalling pattern developed in a similar manner (i.e., craze cracking of oxide followed by spallation) to the pattern which was observed earlier on specimen R-7796.

Thermal fatigue cracks were also detected in the NiCrAlSiY coated specimens after 189 (R-7795) and 357 (R-7796) hours; an example is provided in Figure 22A. Crack propagation was confined to the coating and diffusion affected substrate zone.

Pretest and post-test microstructures of the NiCrAlSiY coated  $\gamma/\gamma'$ - $\delta$  specimens are provided in Figure 23. The pretest microstructures of the NiCrAlSiY coated specimens indicate that a small amount of incipient melting may have occurred in the coating during the 1352 K (1975°F)/4 hour/H<sub>2</sub> diffusion heat treatment. Examination of the post-test microstructures revealed that coating-substrate interdiffusion was extensive and that the coating was

predominantly  $\gamma$  (Ni solid solution) phase with a minor amount of  $\gamma'$  ( $\text{Ni}_3\text{Al}$ ) phase near the original coating-substrate interface. A semicontinuous band of  $\gamma'$  was present in the diffusion affected substrate zone. The  $\delta$  phase appeared to be transformed (possibly to  $(\text{Ni}, \text{Si})_3\text{Cb}$ ) in the diffusion affected substrate zone in the pretest and post-test microstructures.

Only minor remnants of the incipient melting condition, which was visually observed in the hot zones of the NiCrAlSiY coated specimens after the initial 22 hours of testing, remained by the time the specimens were metallographically examined. It is thought that extensive coating-substrate interdiffusion diluted the silicon content and raised the incipient melting temperature of the interdiffusion zone. Previous furnace testing of a  $\gamma/\gamma'$ - $\delta$  coupon coated with a 2 percent silicon content plasma sprayed NiCrAlSiY composition did not experience incipient melting at 1478 K (ref. 5). Phase coarsening reactions and depletion of the coating (by oxidation) are thought to have eliminated most of the microstructural features (i.e., dendrites) which would normally be associated with an incipient melting condition.

Electron beam microprobe analysis of the pretest microstructure of the NiCrAlSiY coated specimen (Figure 24) indicated that the silicon was uniformly distributed through the coating at a level of about 4.2 (weight) percent. The diffusion affected substrate zone exhibited higher silicon concentrations (about 8.5 to 11 percent). The  $\delta$  ( $\text{Ni}_3\text{Cb}$ ) phase in the diffusion affected substrate layer adjacent to the coating was altered by silicon substitution for some of the nickel.

As indicated above, the pretest microstructure indicated that the NiCrAlSiY coating was partially fused during the postcoating heat treatment at 1352 K. The primary phase which coarsened during the heat treatment was  $\gamma$  (Ni solid solution) with the approximate composition of Ni-19Cr-7Al-4Si. Microprobe analysis of the eutectic between the  $\gamma$  phase regions indicated that the approximate composition was Ni-10Cr-17Al-4Si. The bulk chemistry for the coating was Ni-16.2Cr-10.7Al-4.5Si-0.1Y.

#### **b. NiCrAlY + Pt**

During the pretest metallographic inspection of the NiCrAlY + Pt coated specimens, it was observed that the platinum-rich surface layer on three of the five specimens (R-7787, R-7790 and R-7791) exhibited microscopic blisters in portions of the platinum-rich surface layer (Figure 25). The coatings on these specimens were repaired by abrasively removing (vapor honing) the defective platinum-rich surface layer and sputter cleaning the NiCrAlY surface prior to deposition of a new platinum-rich surface layer. The NiCrAlY + Pt coatings on specimens R-7788 and R-7789 did not exhibit any blistering of the surface layer and did not receive any repair. Pretest microstructures of the two variations of the NiCrAlY + Pt coating which were evaluated are provided in Figures 26 and 27.

Visual inspection indicated that the repaired NiCrAlY + Pt coatings exhibited excellent oxide scale adhesion compared with the other coating systems which were evaluated; oxide scale spallation on NiCrAlY + Pt coated Specimen R-7787, R-7790 and R-7791 was first observed after 276, 610 and 276 cycles, respectively. In fact, visual examination of the hot zones of these specimens revealed relatively large areas where the oxide scale did not spall

during the 1005 hour exposure (Figure 28B). Metallographic examination of specimen R-7787 after 516 hours and specimen R-7791 after 1005 hours of evaluation in the 1366°K cyclic oxidation burner rig test indicated that the outer portion of the coating was  $\gamma$  phase. A relatively thick band of  $\gamma'$  was present in the inner portion of these coatings and the diffusion affected substrate zone (Figure 26). The post-test condition of the repaired NiCrAlY + Pt coatings is similar to that which has been observed previously (ref. 5).

In contrast, the two NiCrAlY + Pt coatings, which were tested in the unrepaired condition, exhibited initial oxide scale adhesion which was intermediate between the NiCrAlY and repaired NiCrAlY + Pt coatings. Oxide scale spallation was first observed after 149 hours on the two unrepaired NiCrAlY + Pt coatings (specimens R-7788 and R-7789). Periodic visual examination indicated that the rate of oxide spallation from these two specimens increased during the test and exceeded the rate of oxide scale spallation from the NiCrAlY coated specimens.

Post-test examination of the unrepaired NiCrAlY + Pt specimens indicated that the outer portion of the coating was  $\gamma$  phase (Figure 27). The  $\gamma'$  layer in the diffusion affected substrate zone was thinner than in the repaired coatings. This observation reflects accelerated consumption of aluminum from the coating due to the repeated spallation of the oxide scale during the test.

Thermal fatigue cracks were detected in the NiCrAlY + Pt coated  $\gamma/\gamma'-\delta$  specimens (R-7787, R-7788, R-7789, R-7790 and R-7791) after 347, 610, 471, 181 and 357 hours, respectively. Post-test examination of specimens R-7787 and R-7789, which were tested for 516 hours, indicated that all of the thermal fatigue cracks were confined to the coating and the adjacent diffusion affected substrate zone. Most of the cracks were contained in the outer  $\gamma$  phase layer. While visual examination indicated that thermal fatigue cracking did not initiate in NiCrAlY + Pt (unrepaired) coated specimen R-7788 until 610 hours, the cracks propagated rapidly after initiation; after 1005 hours of testing, this specimen exhibited relatively severe thermal fatigue cracking (Figures 19 and 28A). Post-test examination of this specimen indicated that some of the thermal fatigue cracks propagated a short distance into the  $\gamma/\gamma'-\delta$  (1Cr) alloy (Figure 22B).

It can be seen from Figures 19 and 28 that thermal fatigue cracking in the repaired NiCrAlY + Pt coatings was less severe than the cracking in the unrepaired coatings. Those cracks which formed were generally confined to the coating and diffusion affected substrate. The relatively good thermal fatigue behavior for the repaired NiCrAlY + Pt coatings was consistent with previous results (ref. 5).

The NiCrAlY + Pt coatings on the 1Cr (specimens R-7787 and R-7788) and the 6Cr (specimens R-7789, R-7790 and R-7791)  $\gamma/\gamma'-\delta$  alloy did not exhibit any significant differences in coated system performances which could be attributed to the chromium content of the substrate.

Electron beam microprobe analysis of the pretest microstructures of the two NiCrAlY + Pt coating system variations (Figures 29 and 30) and the NiCrAlY coating system were undertaken. The results of the analysis indicated that the coating constituents were present in their expected concentrations.

It was noted that the unrepaired NiCrAlY + Pt and NiCrAlY coatings were enriched in yttrium to a depth of about  $10\mu$  below the coating surface. The yttrium was probably in the form of  $Y_2O_3$  and is thought to have formed by internal oxidation during the postcoating heat treatment at 1352 K. The microprobe analysis also indicated that yttrium content was apparently reduced below this enrichment zone for a considerable depth (about 50 to  $70\mu$ ); it is speculated that this result is produced by yttrium diffusion toward the higher oxygen activity at the surface. This yttrium distribution is considered typical of heat treated NiCrAlY + Pt and NiCrAlY coatings. Previous post-test microprobe analysis of a NiCrAlY + Pt coated  $\gamma/\gamma' - \delta$  specimen, which was evaluated for 1016 hours in a 1366 K cyclic oxidation test (ref. 5), indicated that similar yttrium distributions were present in coatings which exhibited excellent oxidation and thermal fatigue performance.

Abrasive removal of the porous Pt-rich surface layer from the repaired specimens also removed the yttrium-rich zone. Electron beam microprobe analysis of the repaired coating confirmed that the yttrium content at the surface was minimal in the repaired coating. Thus, the excellent oxide scale adhesion which was observed in these specimens may be primarily a result of the platinum addition to the coating.

### c. NiCrAlY

NiCrAlY coatings also provided excellent oxidation protection for the  $\gamma/\gamma' - \delta$  alloy in the 1366 K cyclic oxidation burner rig test. Figures 19 and 28 indicate that the visual condition of the NiCrAlY coated  $\gamma/\gamma' - \delta$  specimens was intermediate to the two variations of the NiCrAlY + Pt system. The three NiCrAlY coated specimens first exhibited oxide spallation between 22 and 37 hours. Minor accounts of scale spallation were observed during the 1005 hours of the test.

Specimen R-7793 was removed for metallographic examination after 516 hours of testing. The other two NiCrAlY coated specimens completed the 1005 hours burner rig test without exhibiting visual evidence of coating failure.

Post-test metallographic examination of the NiCrAlY coated specimen (R-7793) after 516 hours indicated that the coating contained a significant amount of  $\gamma'$  phase dispersed in a  $\gamma$  matrix (Figure 31). Examination of specimen (R-7794) after the 1005 hours of burner rig testing indicated that the coating was  $\gamma$  phase at the completion of testing. A relatively thick (approximately  $50\mu$ ) layer of  $\gamma'$  was present in the diffusion affected substrate zones of both specimens.

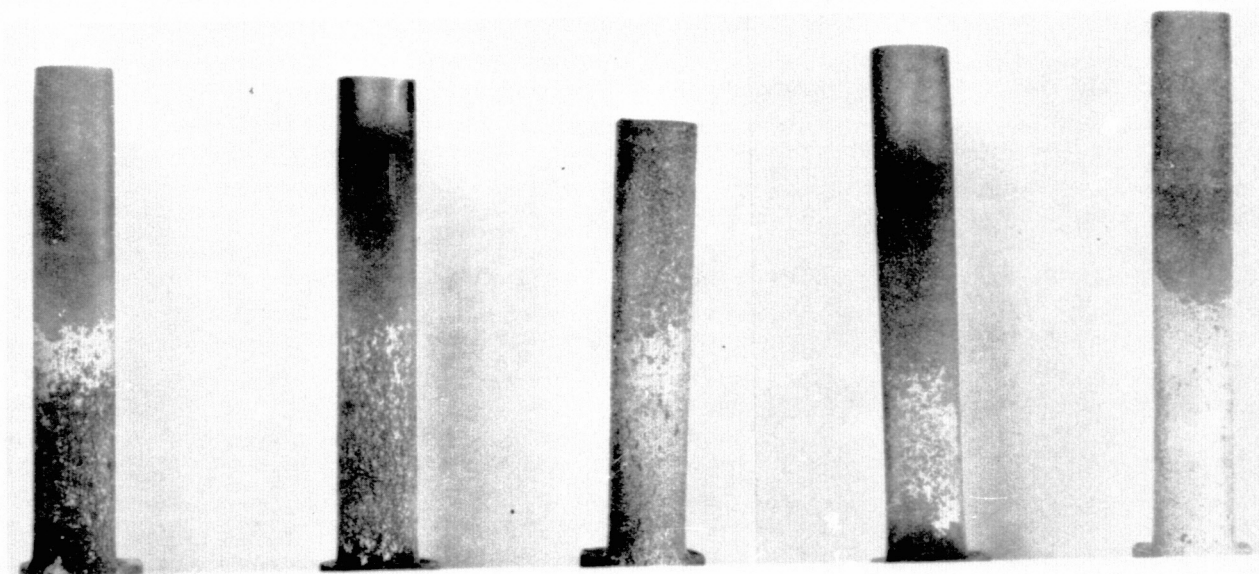
Small thermal fatigue cracks were detected in NiCrAlY coated  $\gamma/\gamma' - \delta$  specimens R-7792, R-7793 and R-7794 after 189, 375 and 435 hours, respectively. Cracking was generally confined to the coating and diffusion affected substrate zones. One crack in specimen R-7792 propagated a short distance (approximately  $50\mu$ ) beyond the diffusion affected substrate zone (Figure 22C).

### 3. Summary

In summary, 1366 K burner rig testing of coated  $\gamma/\gamma' - \delta$  specimens has yielded the following conclusions:

- NiCrAlY + Pt and NiCrAlY coatings provided excellent oxidation protection for the  $\gamma/\gamma' - \delta$  in 1366 K (2000°F) burner rig tests.
- Of the coating systems which have been evaluated on the  $\gamma/\gamma' - \delta$  alloy, NiCrAlY and NiCrAlY + Pt coatings have exhibited the best resistance to thermal fatigue.
- The thermal fatigue resistance of a given coating system is dependent on the coating-substrate thermal expansion mismatch strains.
- None of the candidate coating systems exhibited thermal fatigue cracking on the D.S. MAR-M 200 + Hf alloy.
- NiCrAlSiY and Pt + Al coated  $\gamma/\gamma' - \delta$  specimens are limited by incipient melting to use below 1366 K.
- The oxidation resistance of NiCrAlY + Pt coated  $\gamma/\gamma' - \delta$  specimens was not significantly affected by reducing the substrate chromium content from 6 to 1 percent.

ORIGINAL PAGE IS  
OF POOR QUALITY



	NiCoCrAlY	NiCoCrAlY + Pt	NiCrAlY + Al	NiCrAlY + Pt	NiCrAlY
VISUAL DETECTION OF THERMAL FATIGUE CRACKING:	136 HOURS	56 HOURS	297 HOURS	NOT DETECTED	NOT DETECTED
INITIAL DETECTION OF OXIDE SCALE SPALLATION:	126 HOURS	126 HOURS	56 HOURS	194 HOURS	126 HOURS

Figure 5

Visual Appearance of Coated  $\gamma/\gamma'$  -  $\delta$  Specimens After 505 Hours of Evaluation in 1366 K (2000°F) Burner Rig Cyclic Oxidation Test (Cycle: 27 Minutes Hot - 3 Minutes Forced Air Cool). (K-15096)

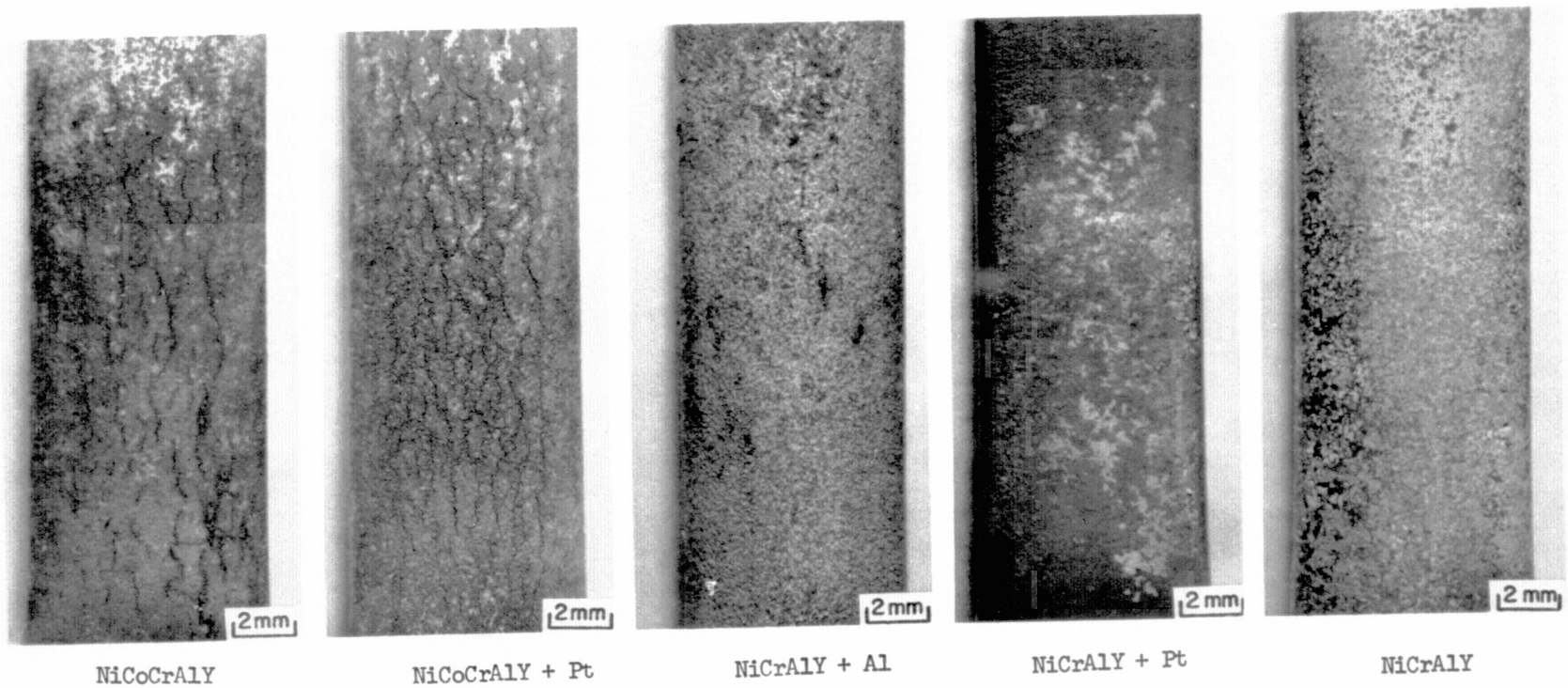
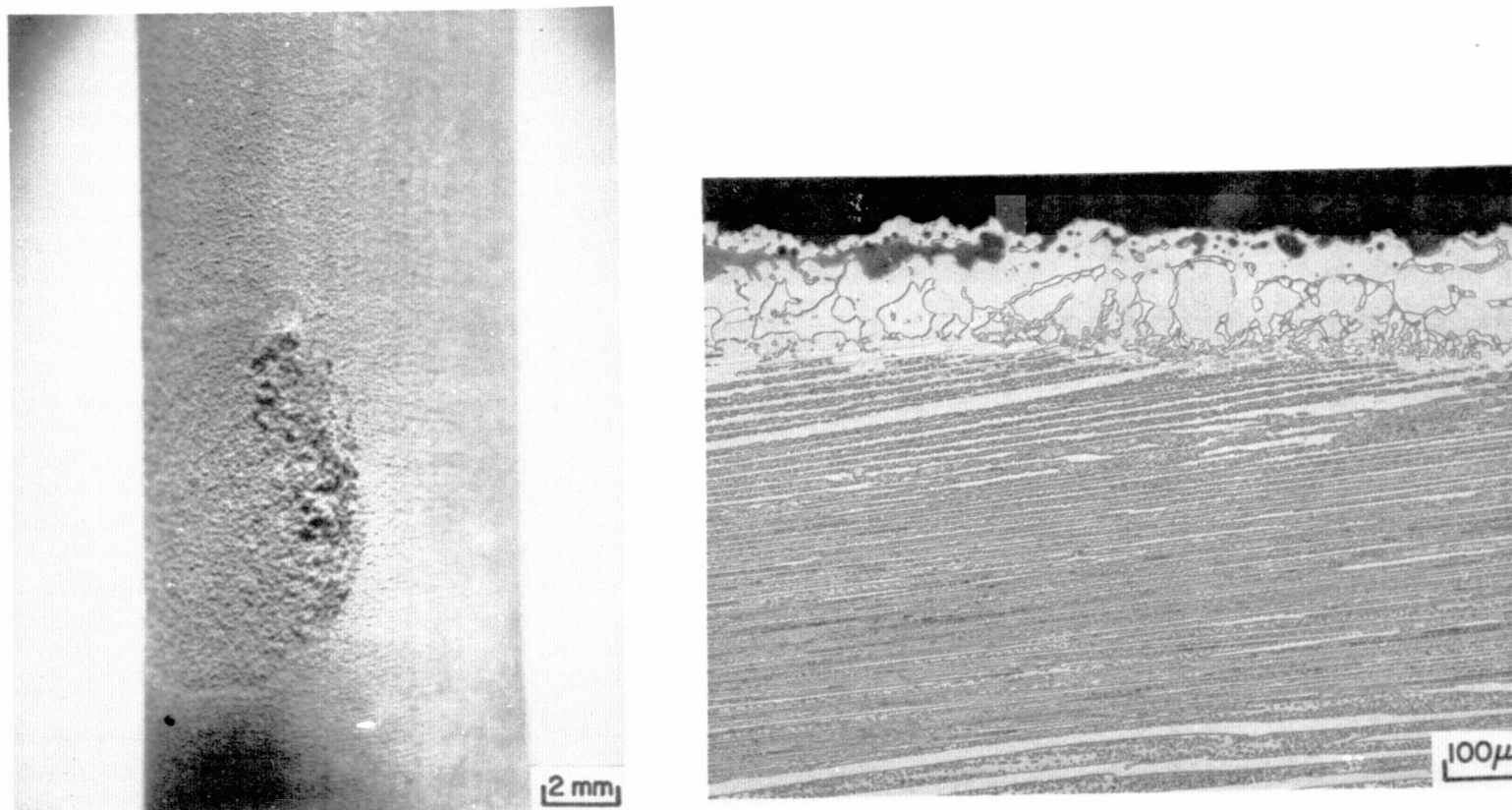
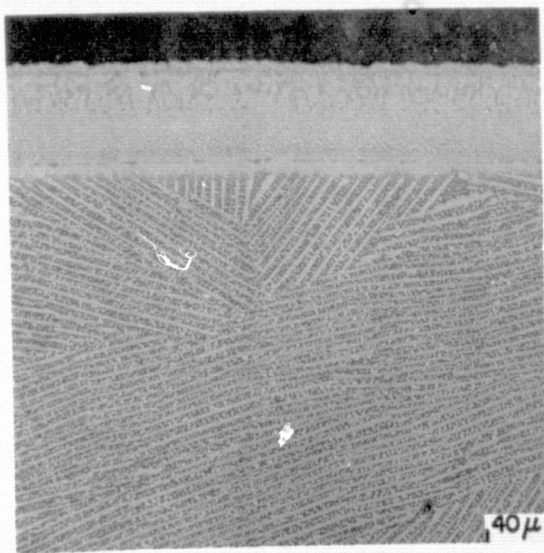


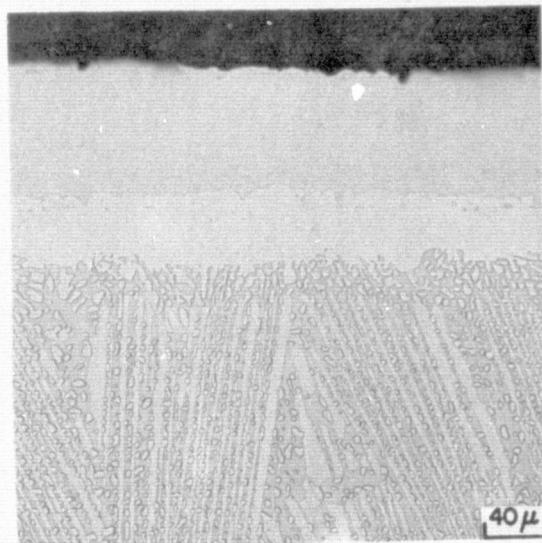
Figure 6 Visual Appearance of Coatings in Hot Zone Region of  $\gamma/\gamma'$  -  $\delta$  Specimens After 505 Hours of Evaluation in 1366 K (2000°F) Burner Rig Cyclic Oxidation Test (Cycle: 27 Minutes Hot - 3 Minutes Forced Air Cool). (K-15098)



*Figure 7 Incipient Melting Condition Which Resulted in the Failure of the Pt + Al Coated  $\gamma/\gamma'$ - $\delta$  Specimen After 172 Hours of Evaluation in 1366 K (2000°F) Burner Rig Cyclic Oxidation Test (Cycle: 27 Minutes Hot – 3 Minutes Forced Air Cool) (K-13335)*

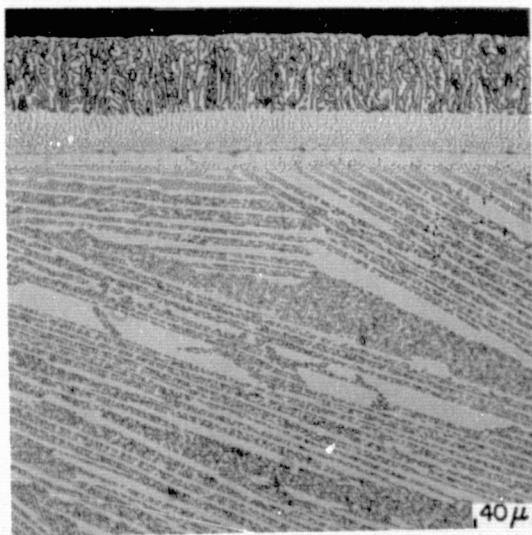


PRETEST

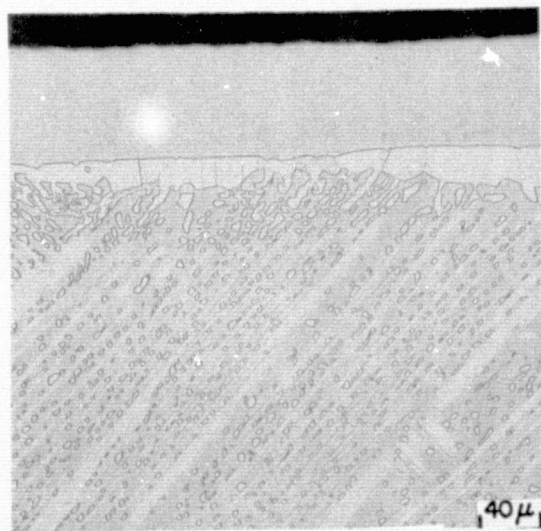


POST-TEST

*Figure 8 Pretest and Post-Test Microstructures and Thermal Fatigue Crack Morphology of NiCoCrAlY Coated  $\gamma/\gamma'$ - $\delta$  Specimen After 505 Hours of Evaluation in 1366 K (2000°F) Burner Rig Cyclic Oxidation Test (Cycle: 27 Minutes Hot – 3 Minutes Forced Air Cool).*

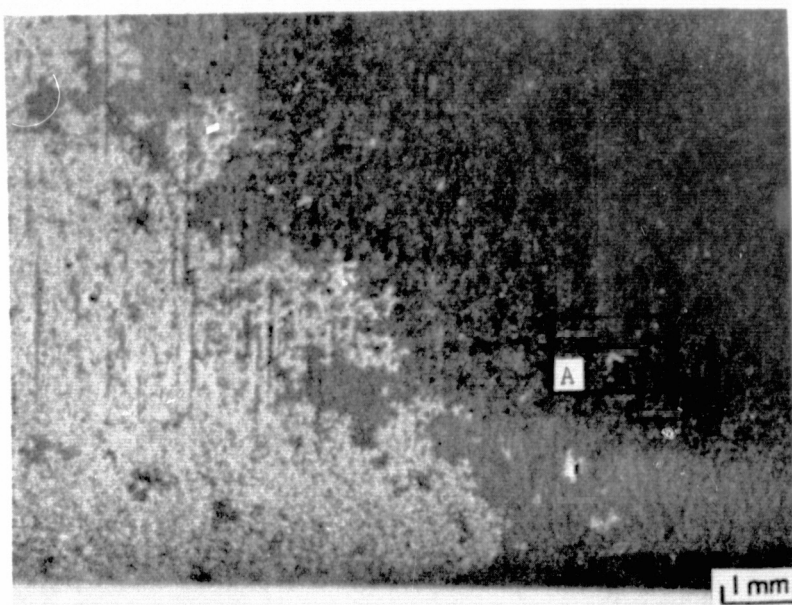


PRETEST

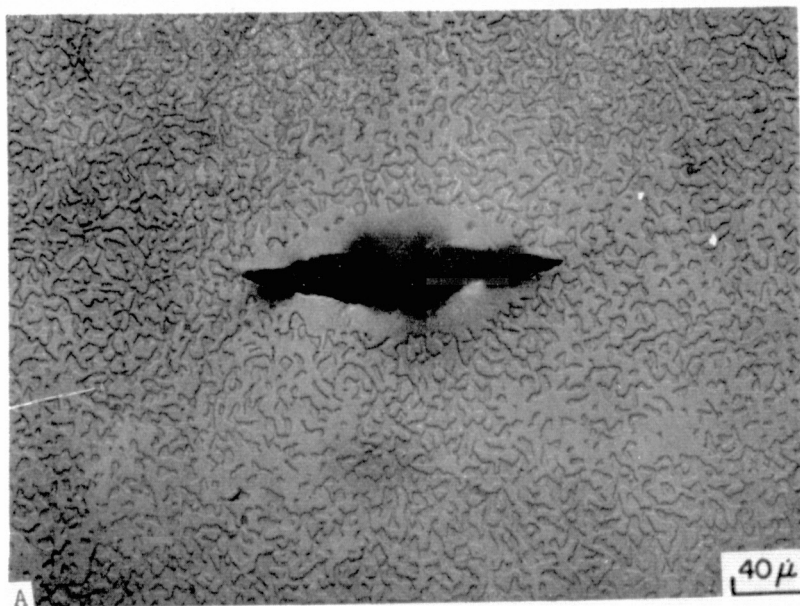


POST-TEST

*Figure 9 Pretest and Post-Test Microstructures and Thermal Fatigue Crack Morphology of NiCoCrAlY + Pt Coated  $\gamma/\gamma'$ - $\delta$  Specimen After 505 Hours of Evaluation in 1366 K (2000°F) Burner Rig Cyclic Oxidation Test (Cycle: 27 Minutes Hot – 3 Minutes Forced Air Cool).*



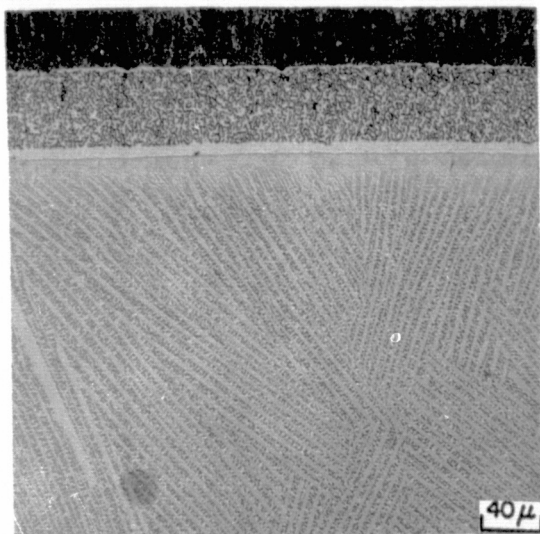
SPECIMEN SURFACE



COATING MICROSTRUCTURE (IN PLANE OF COATING)

Figure 10 Small Thermal Fatigue Crack in NiCrAlY Coated  $\gamma/\gamma'$ - $\delta$  Specimen Which Initiated At a Coating Defect (Pit) After 505 Hours of Evaluation in Burner Rig Cyclic Oxidation Test. This defect is slightly outside the 1366 K (2000°F) hot zone region of the specimen.

(K-15103)

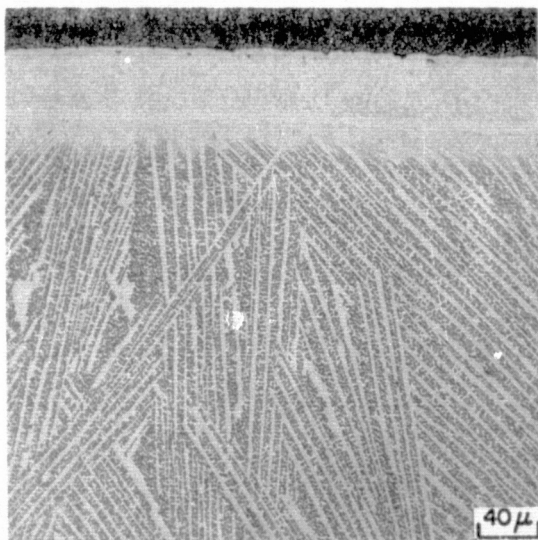


PRETEST



POST-TEST

**Figure 11** Pretest and Post-Test Microstructures of NiCrAlY + Pt Coated  $\gamma/\gamma'$ - $\delta$  Specimen After 505 Hours of Evaluation in 1366 K (2000°F) Burner Rig Cyclic Oxidation Test (Cycle: 27 Minutes Hot – 3 Minutes Forced Air Cool).



PRETEST



POST-TEST

**Figure 12** Pretest and Post-Test Microstructures of NiCrAlY Coated  $\gamma/\gamma'$ - $\delta$  Specimen After 505 Hours of Evaluation in 1366 K (2000°F) Burner Rig Cyclic Oxidation Test (Cycle: 27 Minutes Hot – 3 Minutes Forced Air Cool).

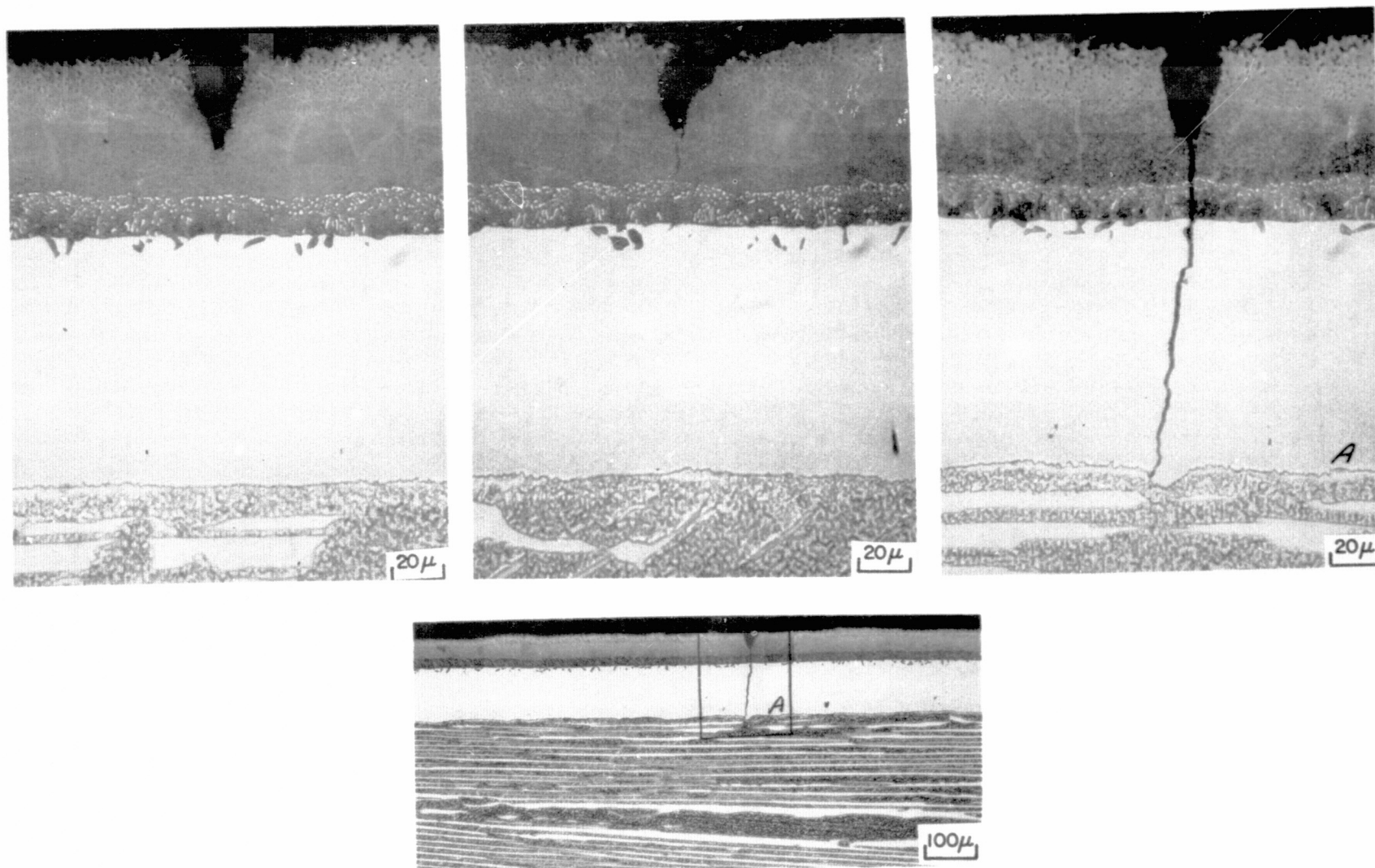


Figure 13 Microstructure of Coating Cracks in Virgin Low Aluminum NiCrAlY + Diffusion Aluminide (Pack, Inward) Coated  $\gamma/\gamma'$  -  $\delta$  Burner Rig Specimen. (K-13337)

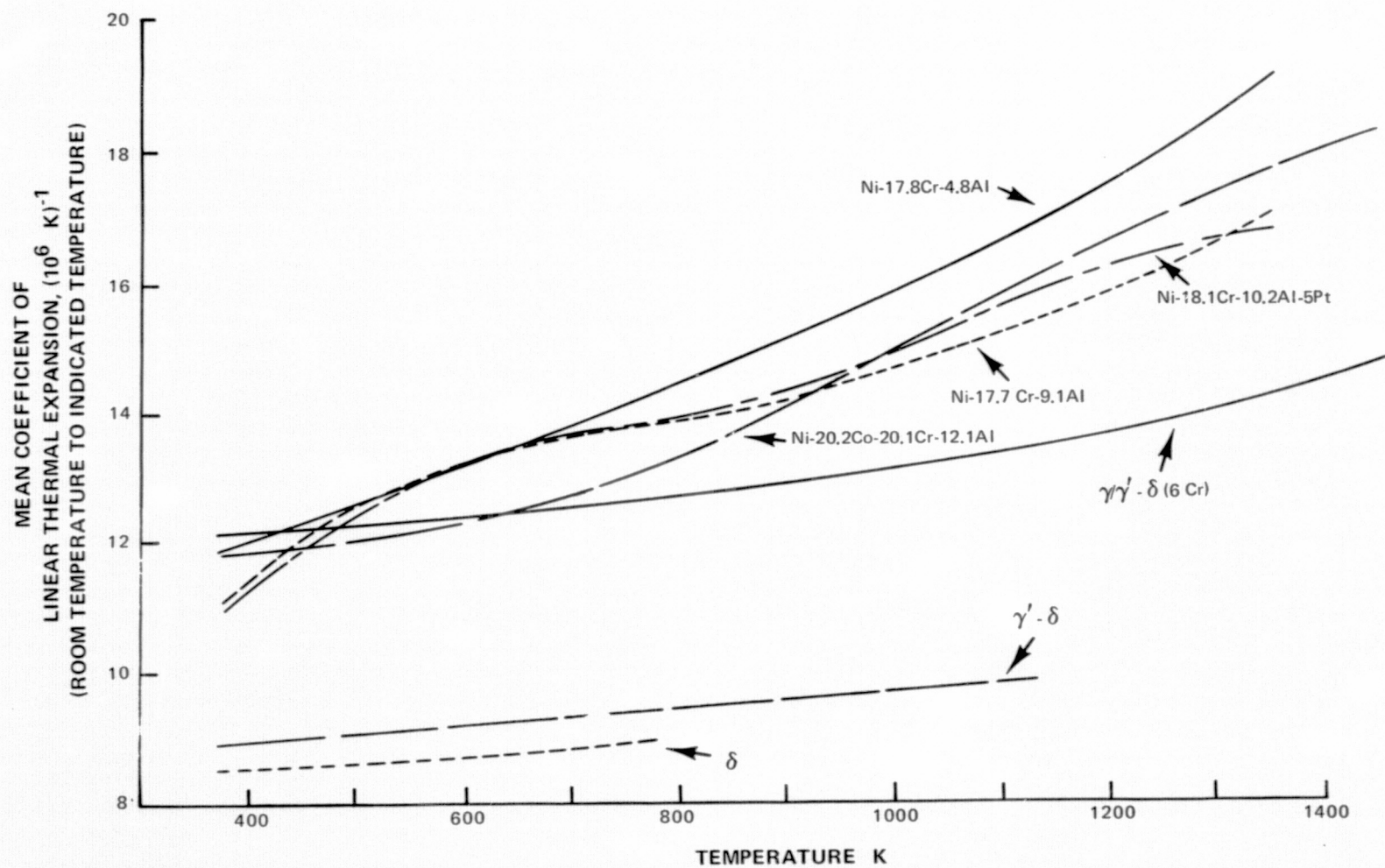
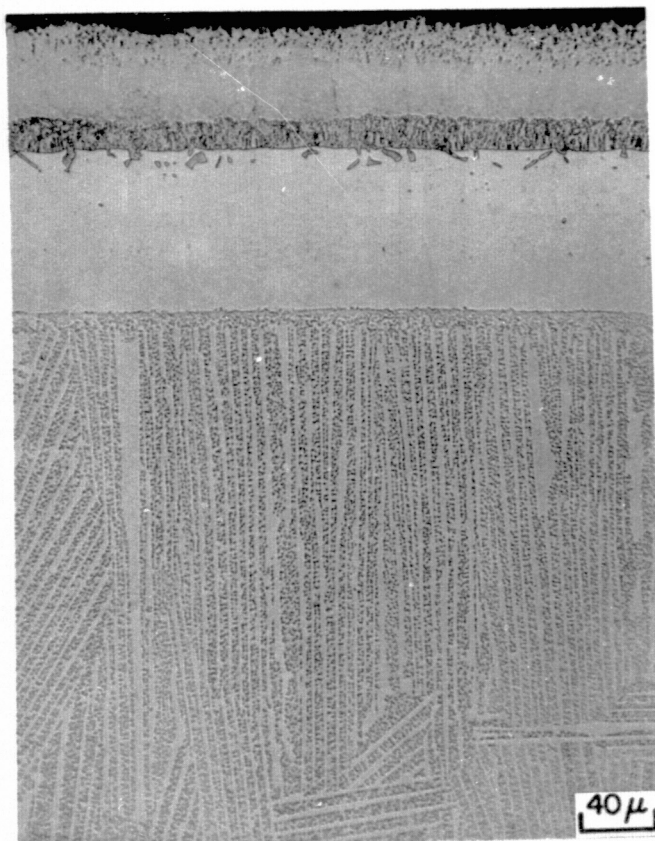


Figure 14 Thermal Expansion Data



PRETEST



POST-TEST

*Figure 15 Pretest and Post-Test Microstructures and Thermal Fatigue Crack Morphology of NiCrAlY + Diffusion Aluminide Coated  $\gamma/\gamma'$ - $\delta$  Specimen After 505 Hours of Evaluation in 1366 K (2000°F) Burner Rig Cyclic Oxidation Test (Cycle: 27 Minutes Hot – 3 Minutes Forced Air Cool).*

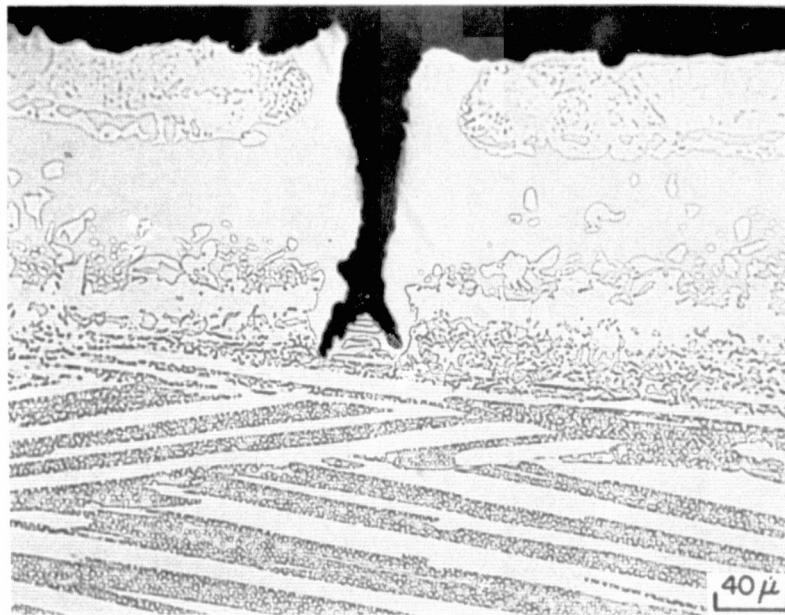
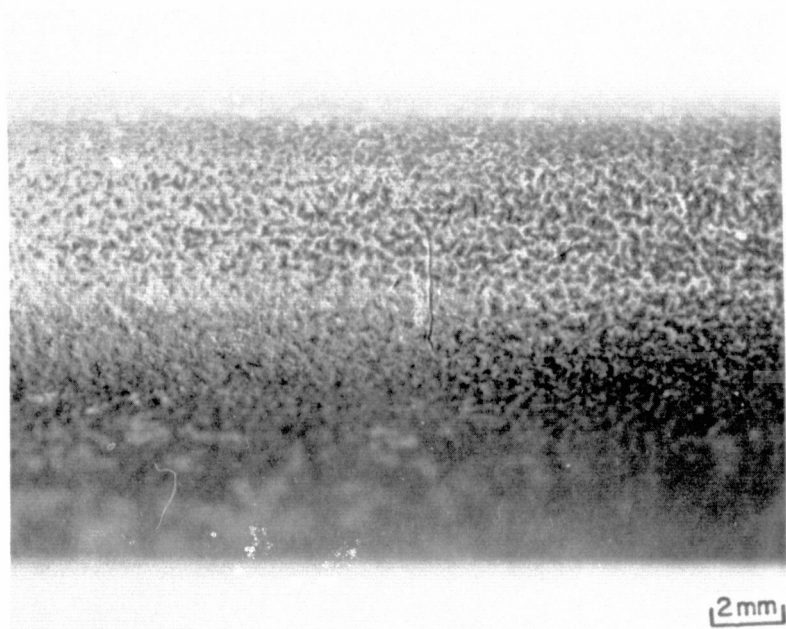


Figure 16 Surface and Cross-Section Morphology of Crack in NiCrAlY + Diffusion Aluminide Coated  $\gamma/\gamma'$ - $\delta$  Specimen After 505 Hours of Evaluation in 1366 K (2000°F) Burner Rig Cyclic Oxidation Test. This crack was detected in the coating prior to testing. (K-15102)

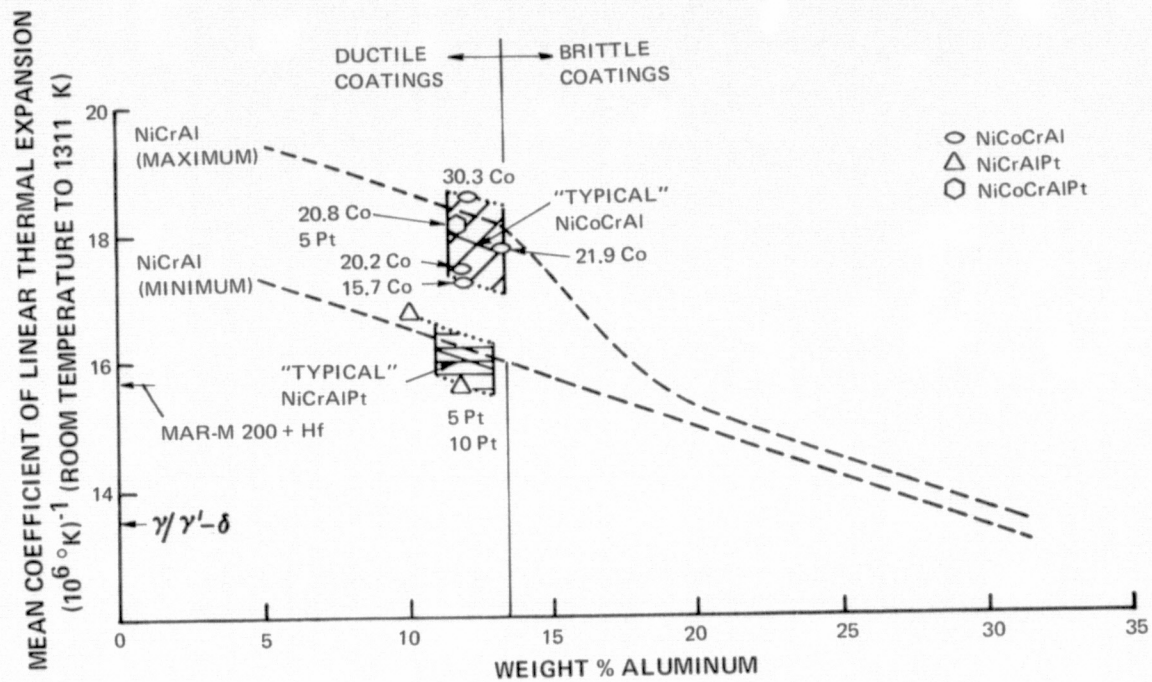
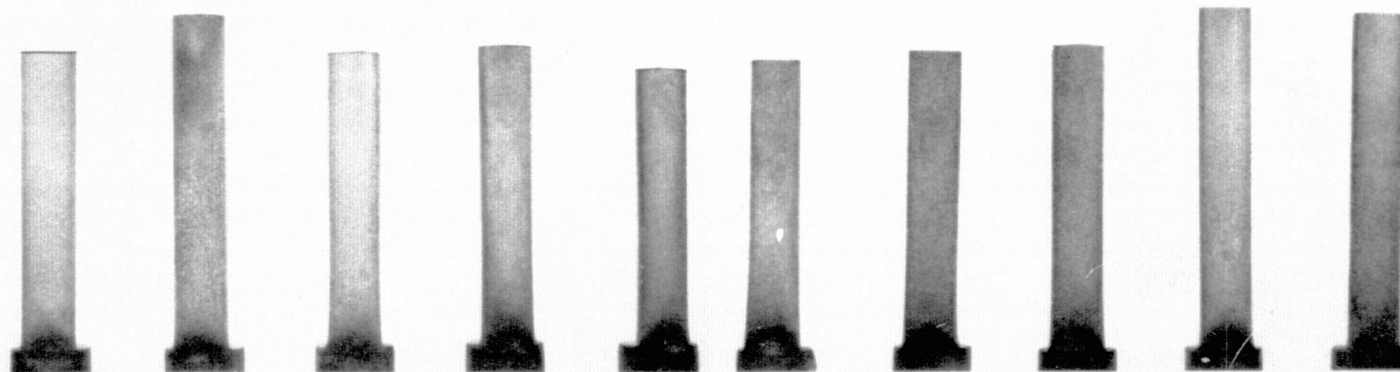


Figure 17 Effect of Cobalt and Platinum Additions on 1311 K (1900°F) NiCrAl Thermal Expansion

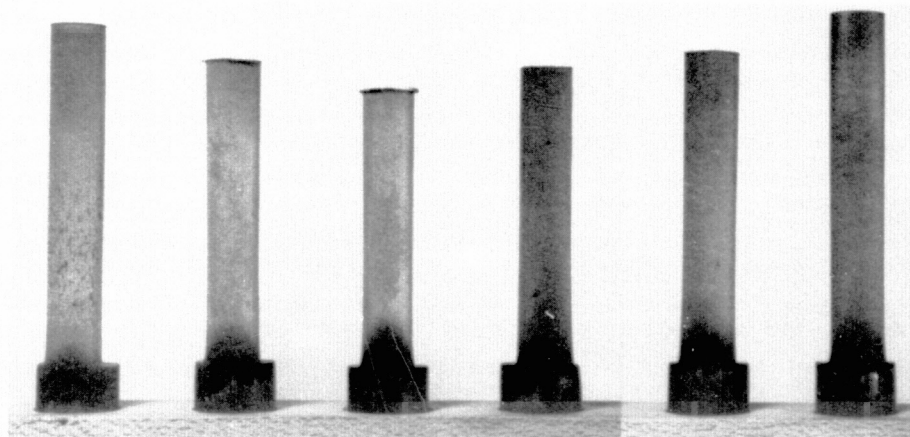
516 Hours



Identification:  
Coating:  
Substrate:

R-7787      R-7788      R-7789      R-7790      R-7791      R-7792      R-7793      R-7794      R-7795      R-7796  
 ← NiCrAlY + Pt →      ← NiCrAlY →      ← NiCrAlSiY →  
 ←  $\gamma/\gamma'$ - $\delta$  (1Cr) →      ←  $\gamma/\gamma'$ - $\delta$  (6 Cr) →

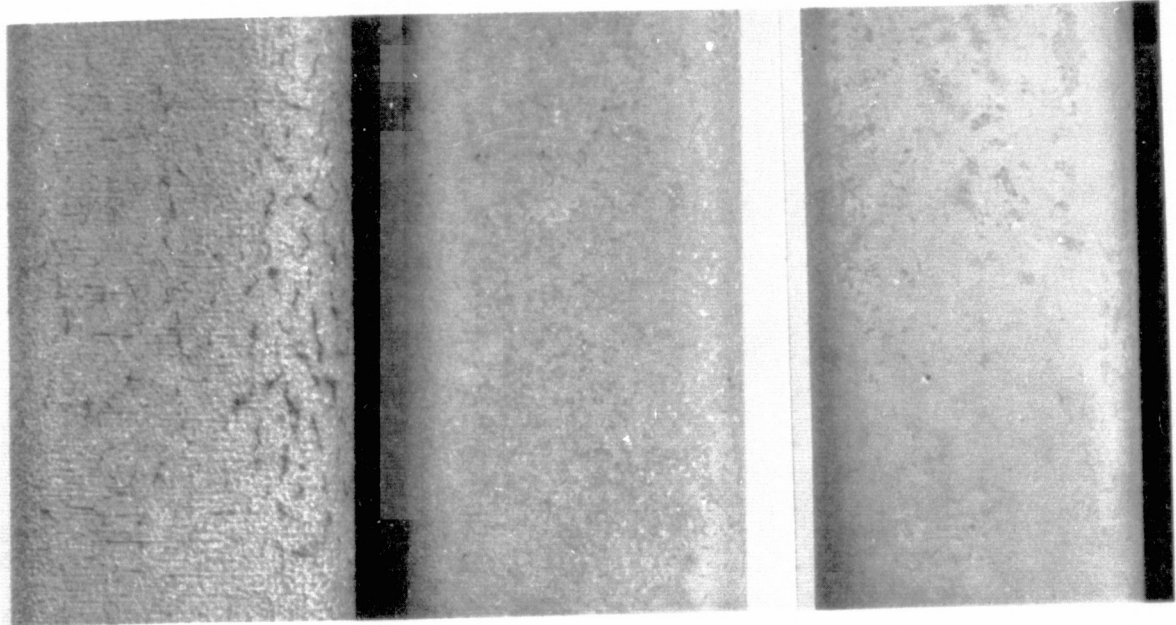
1005 Hours



Identification:  
Coating:  
Substrate:

R-7788      R-7790      R-7791      R-7792      R-7794      R-7795  
 ← NiCrAlY + Pt →      ← NiCrAlY →      ← NiCrAlSiY →  
 ←  $\gamma/\gamma'$ - $\delta$  (1 Cr) →      ←  $\gamma/\gamma'$ - $\delta$  (6 Cr) →

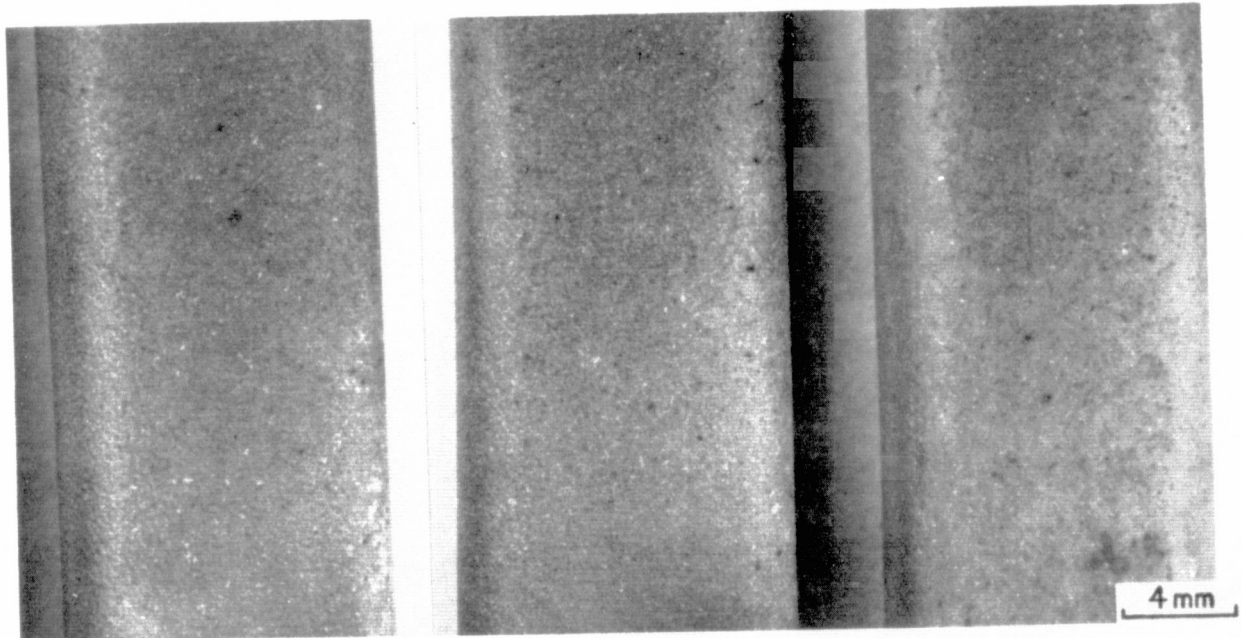
Figure 18 Visual Appearance of Coated  $\gamma/\gamma'$ - $\delta$  Erosion Bars After 516 (Top) and 1005 Hours (Bottom) Of Evaluation in 1366 K (2000°F) Burner Rig Cyclic Oxidation Test (Cycle: 55 Minutes Hot – 5 Minutes Forced Air Cool). (K-20917)



R-7788  
UNREPAIRED NiCrAlY + Pt

R-7790  
REPAIRED NiCrAlY + Pt

R-7791  
REPAIRED NiCrAlY + Pt



R-7792  
NiCrAlY

R-7794  
NiCrAlY

R-7795  
NiCrAlSiY

Figure 19 Surface Appearances of Unrepaired and Repaired NiCrAlY + Pt (Top), NiCrAlY (Bottom) And NiCrAlSiY (Bottom) Coated  $\gamma/\gamma'$  -  $\delta$  Specimens After 1005 Hours of Evaluation in 1366 K (2000°F) Burner Rig Cyclic Oxidation Test. (K-20918)

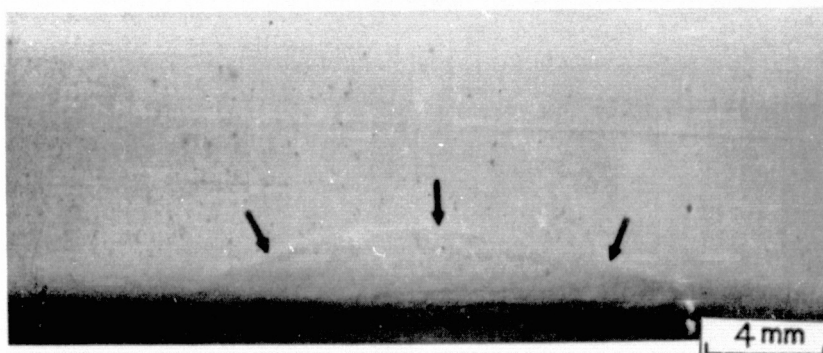
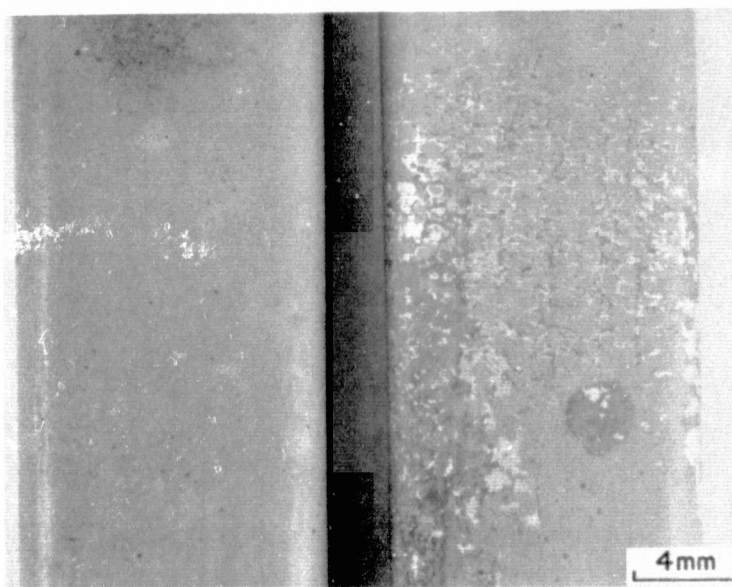


Figure 20 Surface Condition of NiCrAlSiY Coated  $\gamma/\gamma'$ - $\delta$  Specimen (R-7795) After 226 Hours of Evaluation in 1366 K (2000°F) Burner Rig Cyclic Oxidation Test. Incipient melting zone (outlined by arrows) developed during the initial 22 hours of testing. (K-19037)



R-7795

R-7796

Figure 21 Contrast in Oxide Scale Adherence on NiCrAlSiY Coated  $\gamma/\gamma'$ - $\delta$  Specimens After 246 Hours of 1366 K (2000°F) Burner Rig Cyclic Oxidation Test. (K-19038)

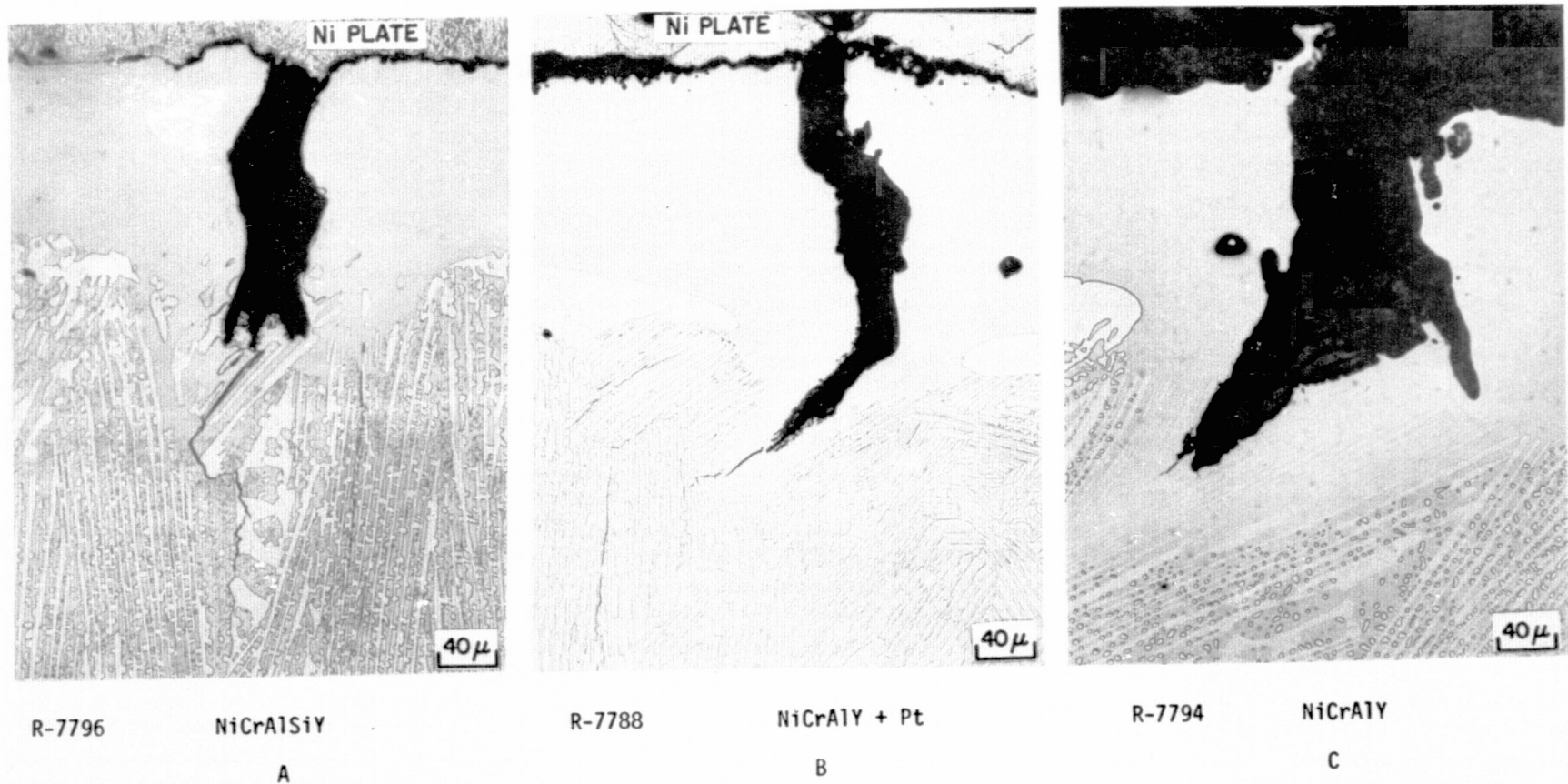


Figure 22 Relatively Severe Thermal Fatigue Cracks in (A) NiCrAlSiY, (B) Unrepaired NiCrAlY + Pt And (C) NiCrAlY Coated  $\gamma/\gamma'$ - $\delta$  Specimens Which Developed During 1366 K (2000°F) Burner Rig Test. Unoxidized crack extension into the  $\gamma/\gamma'$ - $\delta$  substrate is thought to have occurred during post-test metallographic preparation. (K-20919)

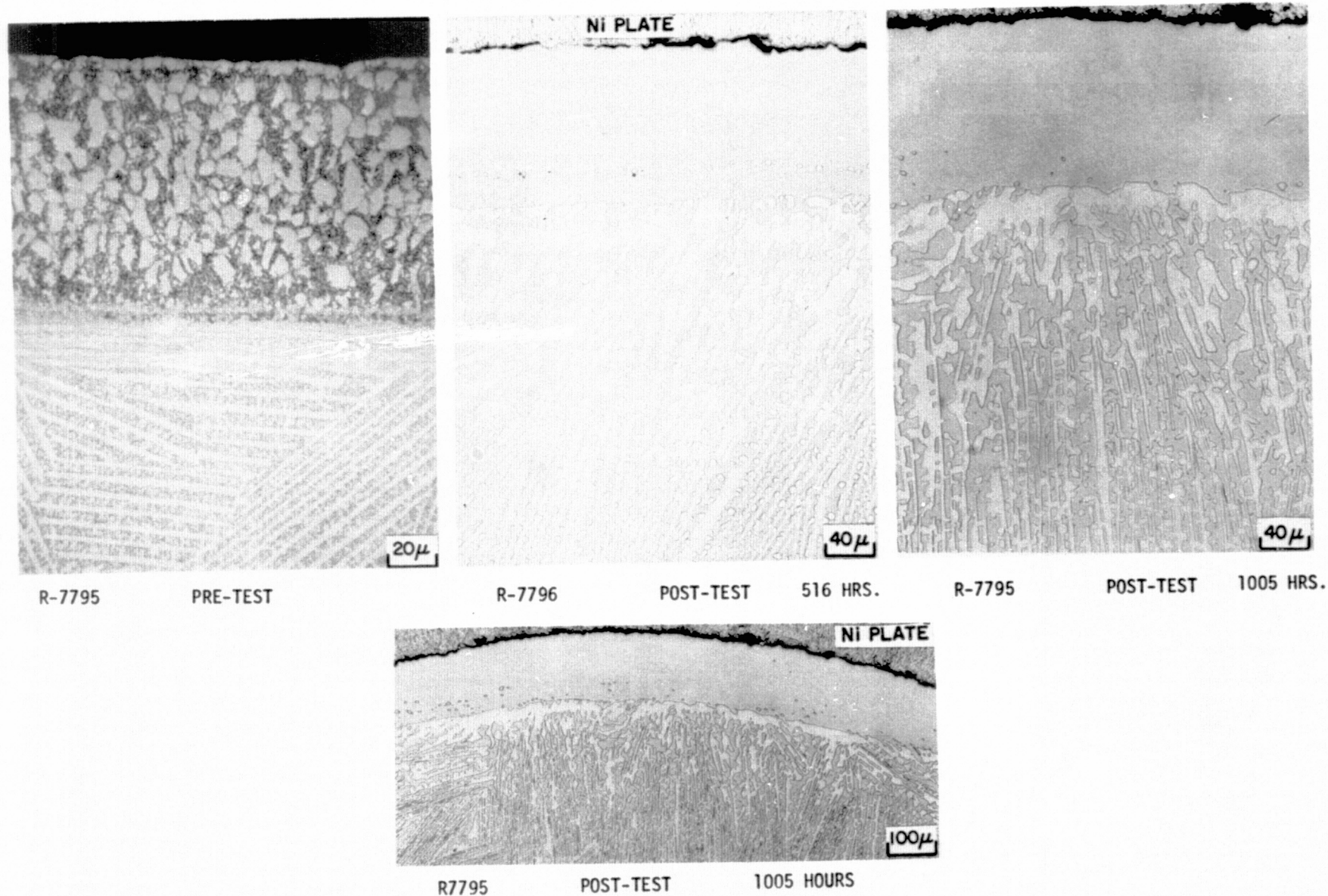


Figure 23 Pretest and Post-Test Microstructures of NiCrAlSiY Coated  $\gamma/\gamma'$ - $\delta$  Specimens After 516 And 1005 Hours of Evaluation in 1366 K (2000°F) Burner Rig Cyclic Oxidation Test (Cycle: 55 Minutes Hot – 5 Minutes Forced Air Cool). (K-20920)

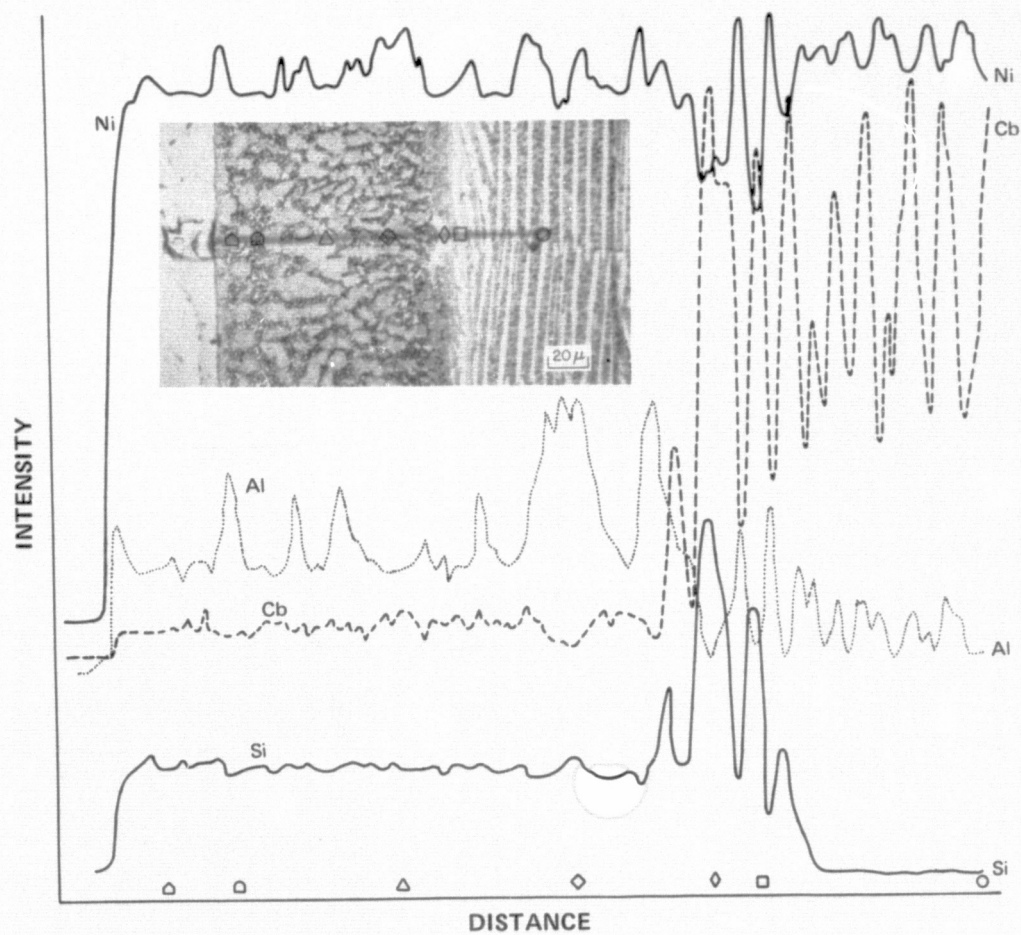
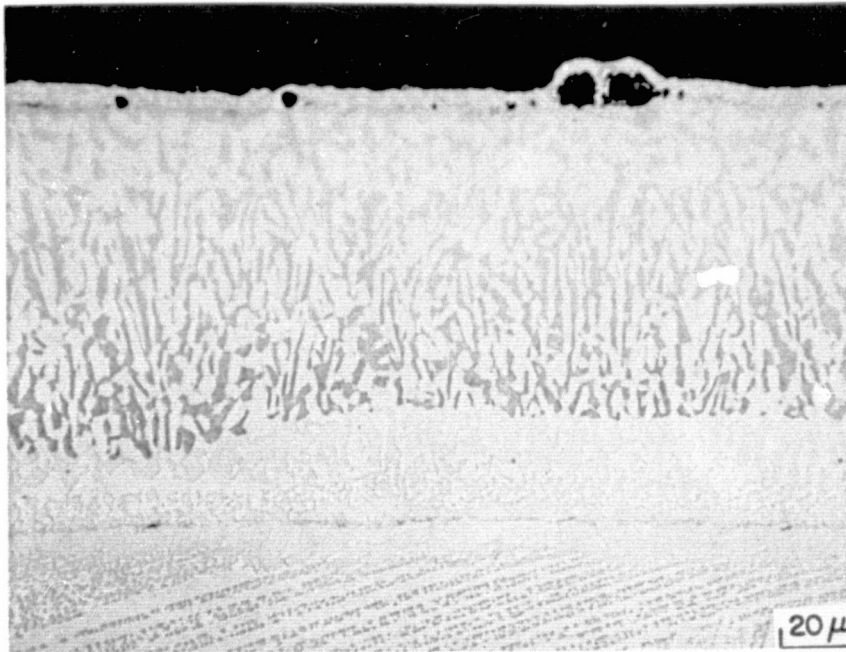


Figure 24 Relative Nickel, Aluminum, Silicon and Columbium X-Radiation Intensities of NiCrAlSiY Coated  $\gamma/\gamma'$ - $\delta$  (Ni-19.7Cb-6Cr-2.5Al) Specimen in Pretest Condition.



R-7791

*Figure 25 Blistered Condition of Platinum Rich Surface Layer of NiCrAlY + Pt Coating Prior to Being Repaired. (K-19040)*

ORIGINAL PAGE IS  
OF POOR QUALITY

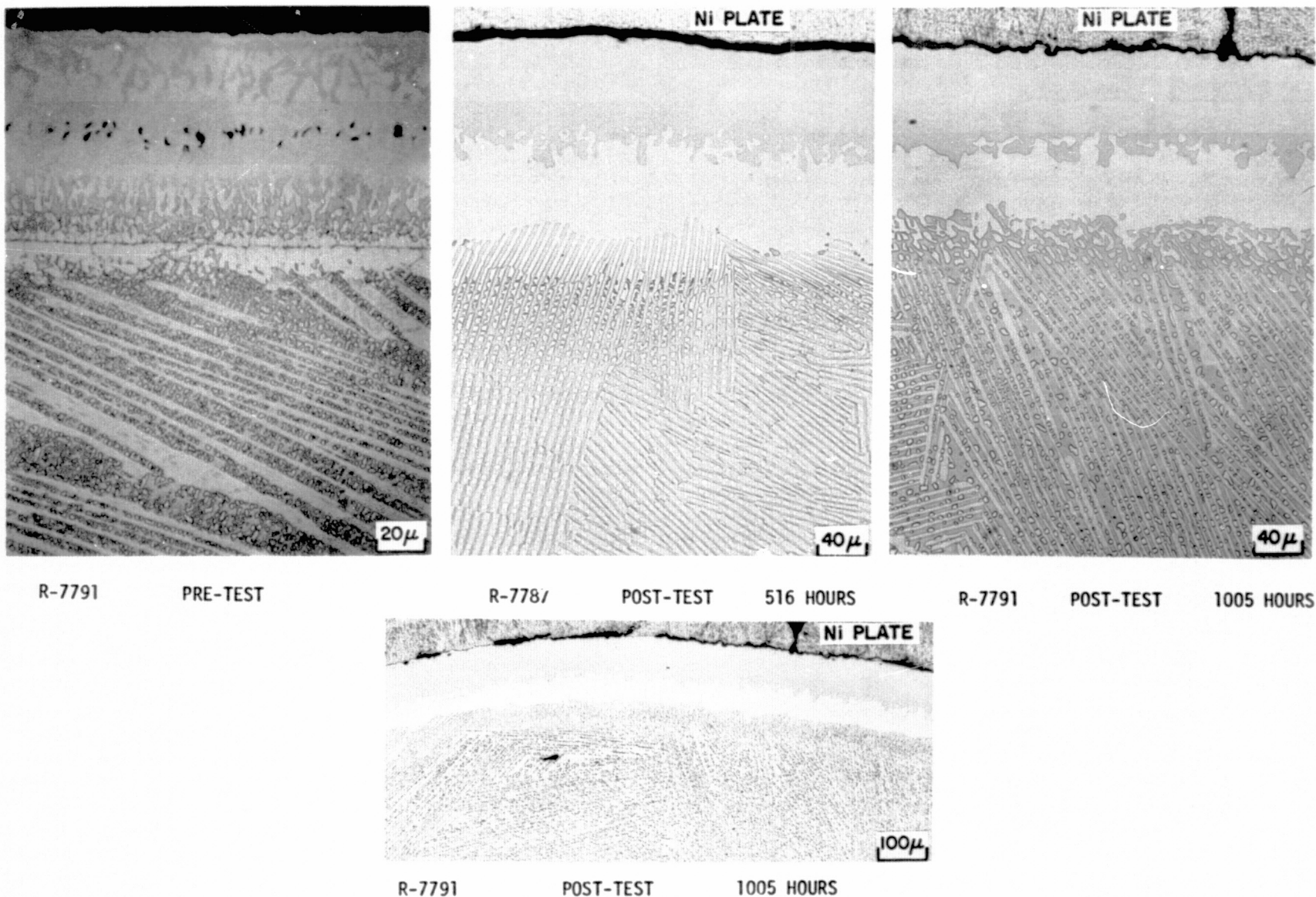
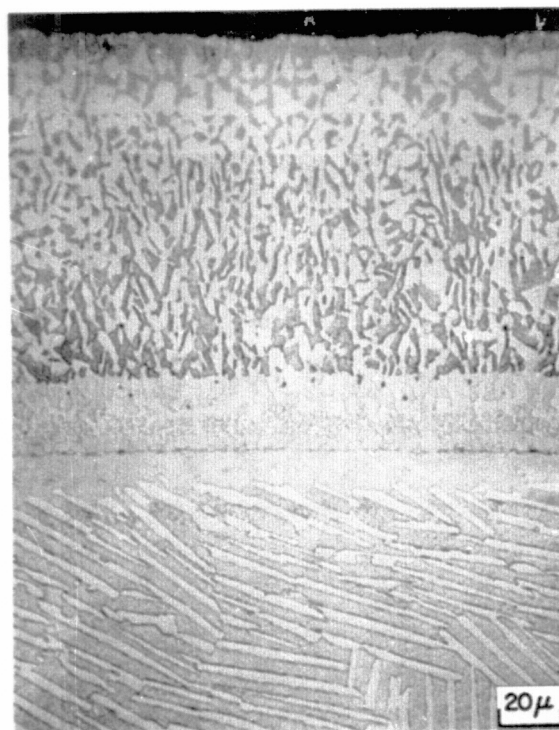
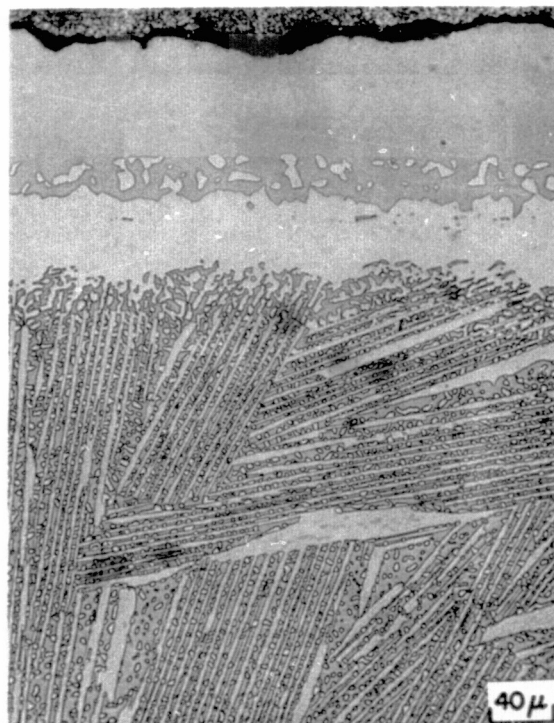


Figure 26 Pretest and Post-Test Microstructures of Repaired NiCrAlY + Pt Coated  $\gamma/\gamma' - \delta$  Specimens After 516 and 1005 Hours of Evaluation in 1366 K (2000°F) Burner Rig Cyclic Oxidation Test (Cycle: 55 Minutes Hot – 5 Minutes Forced Air Cool). (K-20922)



R-7788

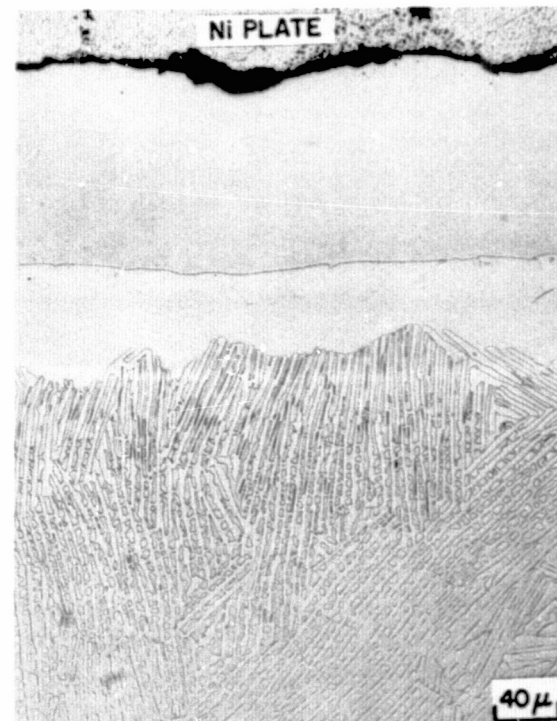
PRE-TEST



R-7789

POST-TEST

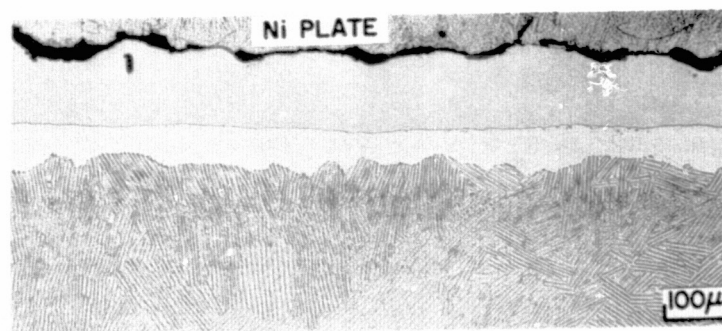
516 HOURS



R-7788

POST-TEST

1005 HOURS



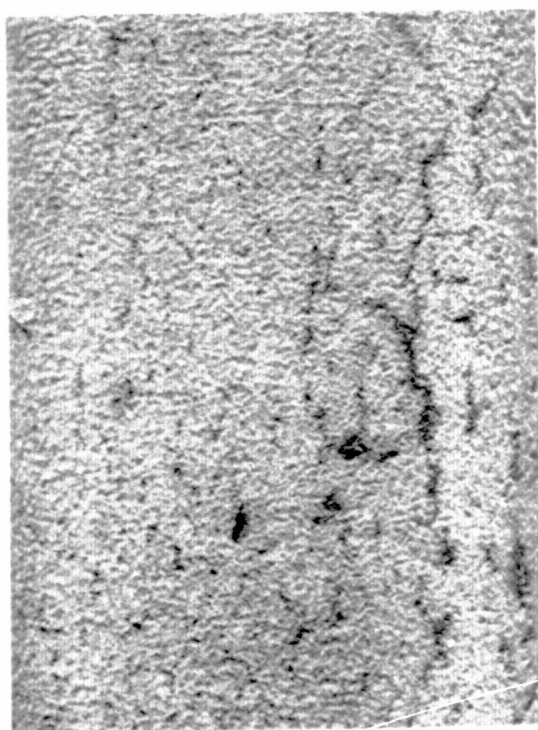
R-7788

POST-TEST

1005 HOURS

ORIGINAL PAGE IS  
OF POOR QUALITY

Figure 27 Pretest and Post-Test Microstructures of Unrepaired NiCrAlY + Pt Coated  $\gamma/\gamma'$ - $\delta$  Specimens After 516 and 1005 Hours of Evaluation in 1366 K (2000°F) Burner Rig Cyclic Oxidation Test (Cycle: 55 Minutes Hot – 5 Minutes Forced Air Cool). (K-20923)



R-7788

UNREPAIRED NiCrAlY + Pt

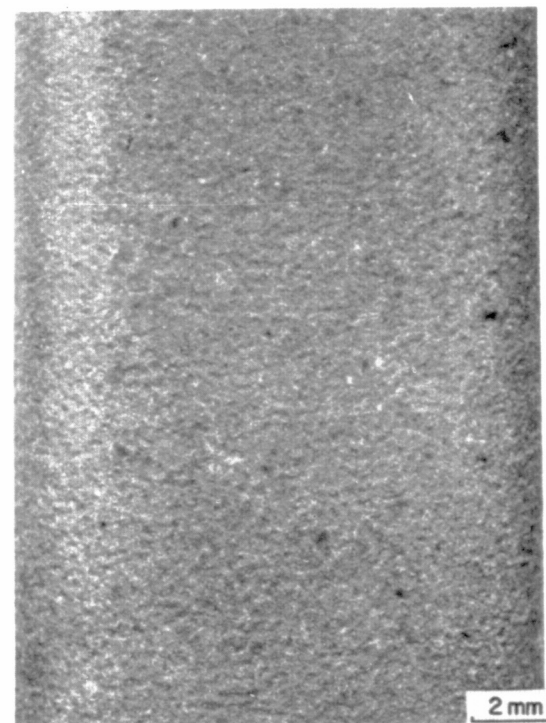
A



R-7791

REPAIRED NiCrAlY + Pt

B



R-7794

NiCrAlY

C

*Figure 28 Contrast in Visual Appearances of (A) Unrepaired and (B) Repaired NiCrAlY + Pt and (C) NiCrAlY Coated  $\gamma/\gamma'$ - $\delta$  Specimens After 1005 Hours of Evaluation in 1366 K (2000°F) Burner Rig Cyclic Oxidation Test. (K-20921)*

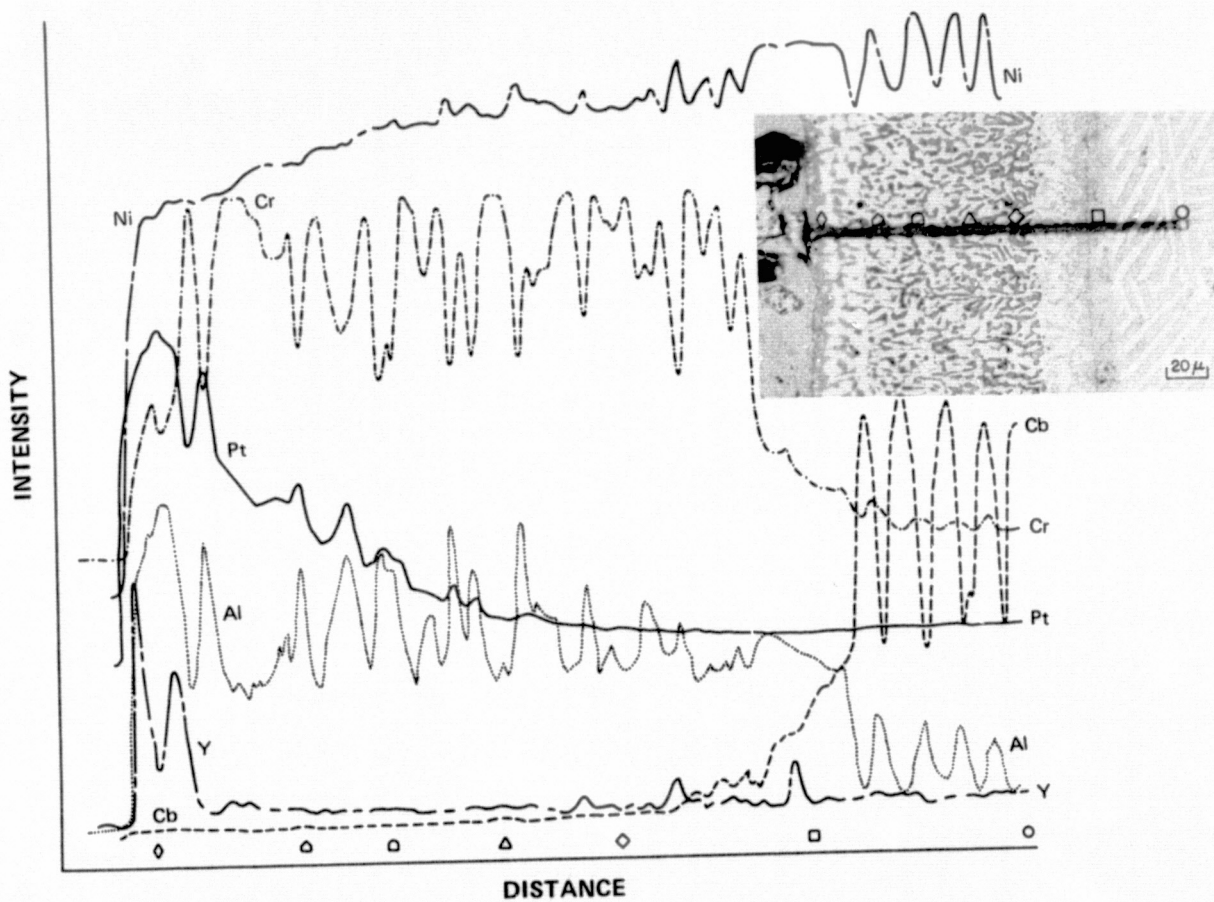


Figure 29 Relative Nickel, Chromium, Aluminum, Yttrium, Platinum and Columbium X-Radiation Intensities of Unrepaired NiCrAlY + Pt Coated  $\gamma/\gamma'$ - $\delta$  (1Cr) Specimen in Pretest Condition.

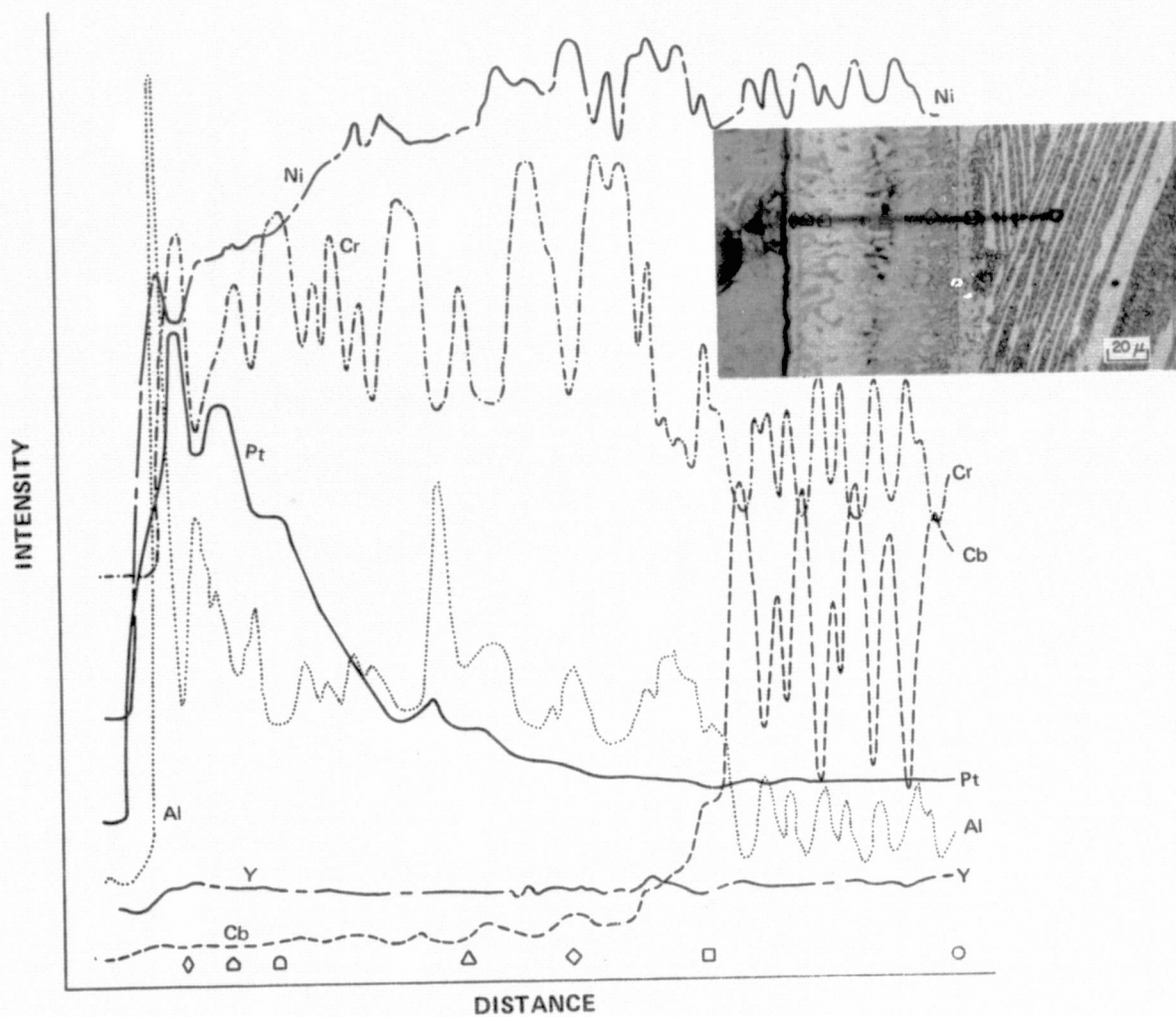


Figure 30 Relative Nickel, Chromium, Aluminum, Yttrium, Platinum and Columbium X-Radiation Intensities of Repaired NiCrAlY + Pt Coated  $\gamma/\gamma'$ - $\delta$  (6Cr) Specimen in Pretest Condition.

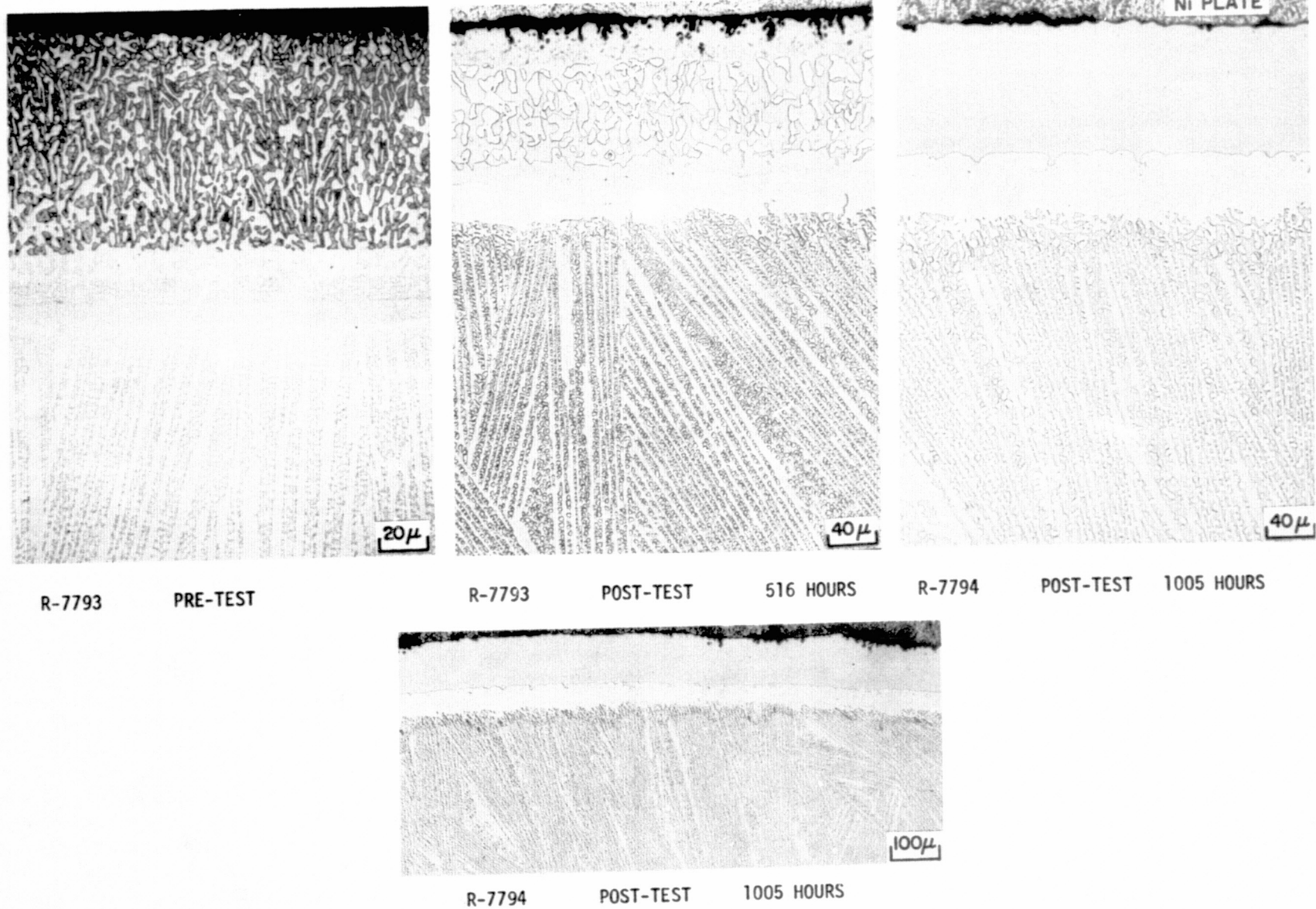


Figure 31 Pretest and Post-Test Microstructures of NiCrAlY Coated  $\gamma/\gamma'$ - $\delta$  Specimens After 516 and 1005 Hours of Evaluation in 1366 K (2000°F) Burner Rig Cyclic Oxidation Test (Cycle: 55 Minutes Hot – 5 Minutes Forced Air Cool). (K-20924)

## IV. FURNACE HOT CORROSION EVALUATION

### A. BACKGROUND

Intermediate temperature hot corrosion resistance is a primary requirement for airfoil and blade root coatings. Since blade roots operate at temperatures significantly below the airfoil levels, diffusion aluminide type coatings are not limited by overtemperature capability considerations for this application. Alternatively, applying the airfoil coatings to the root surfaces may provide an acceptable solution to root coating requirements and be economically desirable by reducing the number of processing operations.

Therefore, laboratory hot corrosion testing of  $\gamma/\gamma'$ - $\delta$  coupons coated with the following candidate coating compositions was conducted in order to evaluate their potential for providing protection for the root:

- $63\mu$  (2.5 mils) Ni-23Co-18Cr-12.5Al-0.3Y;
- $63\mu$  (2.5 mils) Ni-23Co-18Cr-12.5Al-0.3Y +  $6\mu$  (0.25 mil) platinum;
- $63\mu$  (2.5 mils) Ni-18Cr-12Al-0.3Y +  $6\mu$  (0.25 mil) platinum;
- $6\mu$  (0.25 mil) platinum + 25-76 $\mu$  (1 to 3 mils) diffusion aluminide;
- 127 $\mu$  (5 mils) Ni-18Cr-5Al-0.3Y +  $63\mu$  (2.5 mils) diffusion aluminide (pack, inward and outward);
- 127 $\mu$  (5 mils) Ni-18Cr-5Al-0.3Y.

In addition, the gas phase diffusion aluminide coating, which was optimized for internal surfaces and cooling holes (Section V) was also evaluated in furnace hot corrosion.

### B. SPECIMEN PREPARATION

Furnace coupons (2.2 x 2.2 x 0.15 cm) were machined from directionally solidified  $\gamma/\gamma' - \delta$  (Ni-19.7Cb-6Cr-2.5Al) sheet investment castings (solidification rate: 1.25 cm/hour). TD nickel support rods, which are required for fixturing during the coating operation, were attached to corners of these coupons. These coupons were then coated with the candidate coating compositions.

(Ni,Co) CrAlY compositions were applied with the electron beam physical vapor deposition process. Platinum layers were applied by sputtering. Outward diffusion aluminide coating layers were applied to platinum and low aluminum NiCrAlY coated  $\gamma/\gamma' - \delta$  specimens by a 1297 K (1875°F) pack in 12.5 and 9 hours, respectively. Inward diffusion aluminide coatings were applied to low aluminum NiCrAlY coated  $\gamma/\gamma' - \delta$  specimens by a 1033 K (1400°F) pack in 1.25 hours; the coating was then heat treated (1352 K/4 hours/argon) to convert the  $\text{Ni}_2\text{Al}_3$  surface layer to NiAl. Visual examination of these specimens after coating indicated the presence of craze cracks in the coating. In addition, the NiCrAlY, NiCrAlY + Pt, NiCoCrAlY and NiCoCrAlY + Pt coated specimens also received a diffusion heat treatment (1352 K/4 hours/ $\text{H}_2$ ).

Tubular  $\gamma/\gamma' - \delta$  specimens containing small diameter (0.5 and 0.75 mm) cooling holes were coated with the five and eleven hour gas phase aluminizing cycles at 1366 K which were

recommended at the conclusion of the optimization study (Section V). Additional specimen preparation details are provided in that section.

### C. TEST DESCRIPTION

Duplicate specimens representative of each coating system were evaluated for up to 250 hours in this 1172 K (1650°F) cyclic (50 minutes hot — 10 minutes cool) furnace hot corrosion test. Before every 20 cycles of testing, 0.5 mg cm<sup>-2</sup> of Na<sub>2</sub>SO<sub>4</sub> was applied to each specimen. After each 20 cycles, the specimens were washed, weighed and examined visually.

During the test, it was observed that the support tab region on the furnace coupons corroded extensively resulting in abnormally large weight gains (see Figure 32). For this reason, the weight changes observed could not be used to accurately evaluate coating performance. Post-test coating microstructures and the physical appearances of the coatings away from the tabs were used to rank coating performance during this evaluation.

### D. RESULTS AND DISCUSSION

With the exception of the support tab region at specimen corners, the quality of the surface oxide formed on the coated specimens was excellent in most instances (see Figure 32). Only the gas phase aluminide and the low aluminum NiCrAlY + diffusion aluminide (pack, outward) coated  $\gamma/\gamma' - \delta$  specimens showed evidence of excessive attack, as shown in Figures 33 and 34, respectively. Random oxide blisters were observed on the surfaces of these specimens when testing was terminated.

Metallographic examination of the NiCoCrAlY (Figure 35) and NiCoCrAlY + Pt (Figure 36) coated  $\gamma/\gamma' - \delta$  specimens confirmed impressions obtained by visual examination. The coating microstructures were not significantly affected by reaction with the hot salt.

Alterations in the pretest NiCrAlY + Pt coating microstructure, which are associated with phase transformation in the Ni-Cr-Al system, were produced as a result of the 1172°K test temperature (see Figure 37). (In addition, it was noted that the off-eutectic substrate condition was present only in the pretest coupon. The substrate of the NiCrAlY + Pt coated  $\gamma/\gamma' - \delta$  specimens which were tested had the desired  $\gamma/\gamma' - \delta$  eutectic microstructure.) Little degradation resulting from interaction with the molten Na<sub>2</sub>SO<sub>4</sub> was observed. Furthermore, comparison of Figure 37B with Figure 35B and 36B once again shows the greater diffusional stability of NiCrAlY-type coatings. Replacement of some of the nickel with cobalt increases the amount of interaction with the substrate.

Electron microprobe scans for aluminum, platinum and chromium in the pretest microstructure of the NiCrAlY + Pt coating indicated that the platinum in the overlay coating was clearly associated with the aluminum-rich  $\beta$ -NiAl phase (Figure 38). In this coating, the chromium is associated with the  $\gamma$ -nickel solid solution phase. Thus, the chromium peaks are out of phase with those of aluminum and platinum. The electron microprobe scan of the tested specimen showed no significant change in elemental concentrations.

Representative sections of the Pt + diffusion aluminide coating are shown in Figure 39. Except for some slightly thicker segments of oxide scale, the coating has not been severely degraded during the course of the test. In addition, the diffusional stability of the coating at 1172 K appears to be excellent.

Electron microprobe analysis of the Pt + Al coating indicated that the platinum was concentrated near the external surface even though it had been sputtered on the specimen prior to the aluminizing step. In addition, the tested specimen was examined for the presence of sulfur, since the formation of sulfides is deleterious to the life of a coating (ref. 26). A small amount of sulfur was found in the diffusion aluminide coating, none in the overlay coating. It was judged, from the amount of sulfur present in the coating, that degradation of the diffusion aluminide coating was minimal. Scans of pretest and post-test Pt + Al coating microstructures for Al, Pt and Cr are provided in Figures 40 and 41.

Further examination of the post-test electron microprobe scan of the Pt + Al coating indicated the following:

- The oxide scale formed on the specimen during the laboratory hot corrosion test is aluminum-rich and is presumably  $\text{Al}_2\text{O}_3$ . This oxide scale is also relatively thick.
- The platinum in the coating is still concentrated at the coating-gas interface, although some diffusion has taken place (compare with Figure 40).
- There is a chromium-rich peak just below the surface which may be due to the presence of a CrS particle.

Hot corrosion testing of specimens with the low aluminum NiCrAlY + diffusion aluminide (pack, inward) coating was initiated before the extent of the cracking in the coating was known. These cracks, which extend entirely through the coating and into off-eutectic substrate in the as-coated condition (Figure 42A), facilitated entry of the  $\text{Na}_2\text{SO}_4$  into the specimen and led to extensive hot corrosion attack during the 110 cycles to which the specimen was subjected (Figure 42B). In addition to attack of the substrate, undercutting of the coating at the substrate interface was observed. As seen in Figure 42B, the coating is also preferentially attacked beginning at the crack wall and extending laterally at a depth of about  $40\mu$  from the external surface. (A more detailed discussion of the cracking is provided in Section III.)

Low aluminum NiCrAlY + diffusion aluminide (pack, outward) coatings also failed prematurely after 140 cycles as a result of the formation of oxide blisters (see Figure 34). At sites where the blisters were observed, the coating was locally penetrated and the substrate extensively attacked (Figure 43). However, no evidence of cracking in the coating was observed and a different failure mode appears to be operative. At sites where there is no local failure, modest degradation in the form of intergranular attack was observed.

The low aluminum NiCrAlY coated specimen was attacked to a moderate extent during the laboratory hot corrosion testing (Figure 44). The oxide scale formed on this specimen, while adherent, was thicker than that formed on the NiCrAlY + Pt, NiCoCrAlY and NiCoCrAlY + Pt coatings. The diffusional stability of this coating was good.

Visual examination of the gas phase aluminide coated  $\gamma/\gamma' - \delta$  specimens indicated that local coating failures were initiated during the first 20 cycles (Figure 33). Testing of the duplicate specimens for each of the two process variations was continued to 40 cycles; at that point, the test was terminated. Metallographic examination of the specimens showed that the coating had failed in localized areas with up to  $125\mu$  of base metal attack. Figure 45 shows the formation of an oxide blister which occurred when hot corrosion attack reached the  $\gamma/\gamma' - \delta$  substrate. The coating microstructure representative of unfailed regions is also provided in this figure.

The short hot corrosion life of the gas phase deposited diffusion aluminide coating is consistent with the behavior of a pack aluminide coating which was evaluated in a 1145 K (1600°F) isothermal burner rig test in another program (ref. 4). That program indicated that the hot corrosion resistance of the pack aluminide coating had a strong substrate dependence with the same coating being unfailed on the D.S. MAR-M 200 + Hf alloy after 300 hours when the test was terminated.

Previous testing also indicated that the pack aluminized  $\gamma/\gamma' - \delta$  alloy exhibited negligible oxidation degradation during a 1200 K (1700°F) cyclic oxidation burner rig test (ref. 4). It is therefore expected that the gas phase aluminide coatings will be adequate for internal surfaces and cooling holes of eutectic alloy components where only an oxidation environment is anticipated. For the external surfaces such as the blade root, a hot corrosion environment is possible, and the gas phase aluminide coating would probably not provide the desired protection.

In summary, the furnace hot corrosion test results indicate that, except for the gas phase aluminide and low aluminum NiCrAlY + diffusion aluminide coatings, all of the remaining coatings provided a significant amount of protection during the course of the hot corrosion test. Based on metallographic examination, the NiCrAlY + Pt coating affords the greatest degree of protection to the eutectic alloy in the corrosion test.

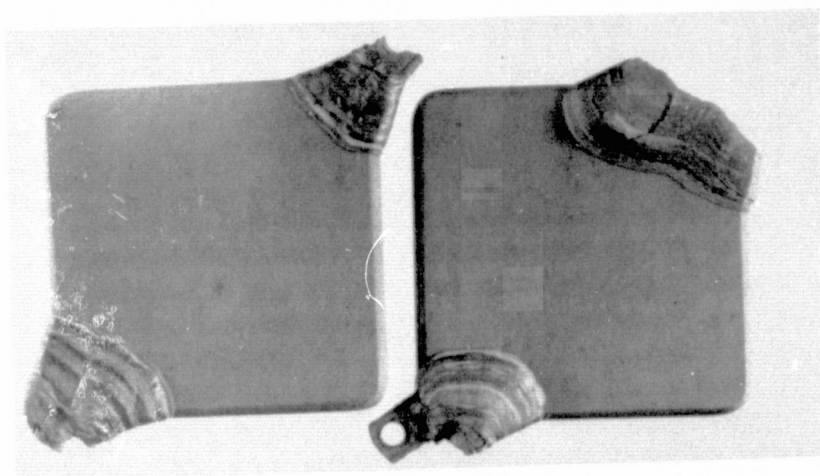


Figure 32

Surface Condition of  $\gamma/\gamma'$ - $\delta$  Eutectic Alloy Coupons, Which Were Coated with Approximately  $63\mu$  of Ni-18Cr-12Al-0.3Y by Electron Beam Vapor Deposition and Then Sputter Coated with Approximately  $6\mu$  of Platinum, After Hot Corrosion Testing (250 Cycles) at 1172 K (1650°F). (K-13226)

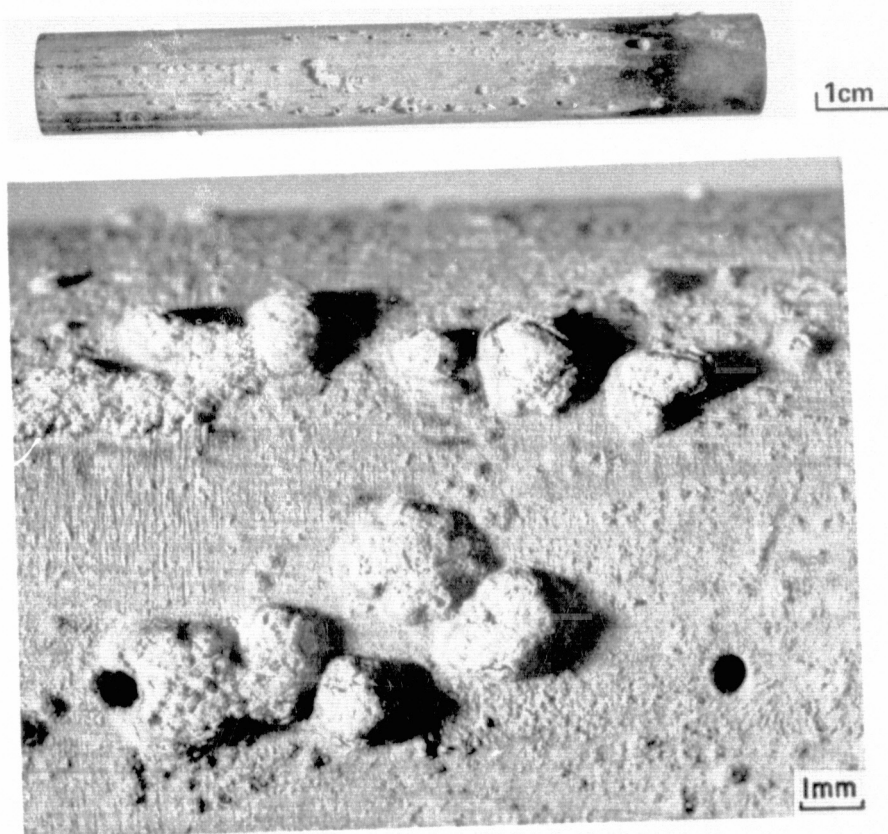


Figure 33

Visual Appearance of Gas Phase Aluminide Coated  $\gamma/\gamma'$ - $\delta$  Simulated Air Cooled Blade Specimen After Hot Corrosion Testing (20 Cycles) at 1172 K (1650°F).

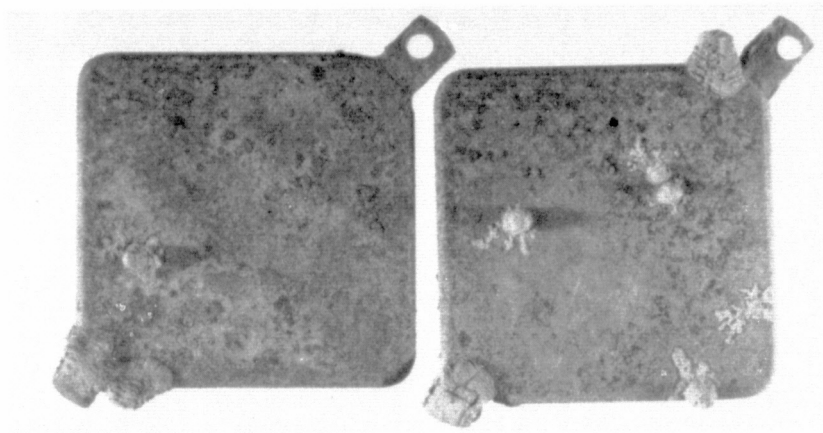
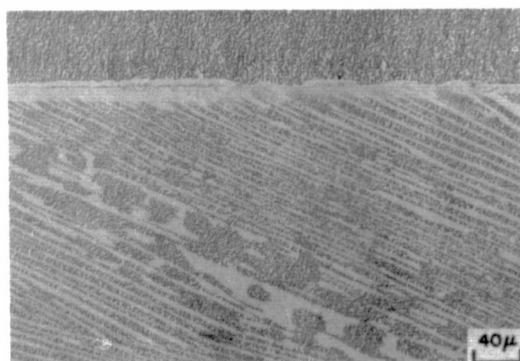
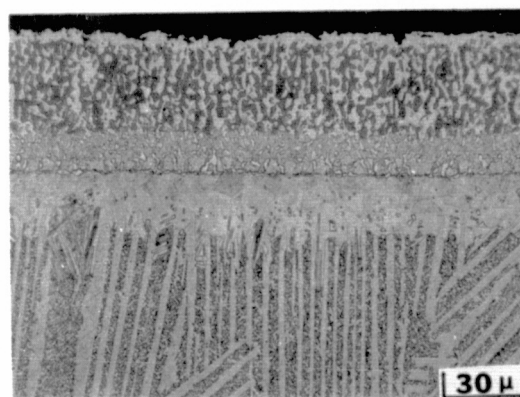


Figure 34 Surface Condition of  $\gamma/\gamma'$ - $\delta$  Eutectic Alloy Coupons, Which Were Coated with Approximately  $127\mu$  of Ni-18Cr-5Al-0.3Y and Then Pack Aluminized, After Hot Corrosion Testing (140 Cycles) at 1172 K (1650°F). (K-13226)

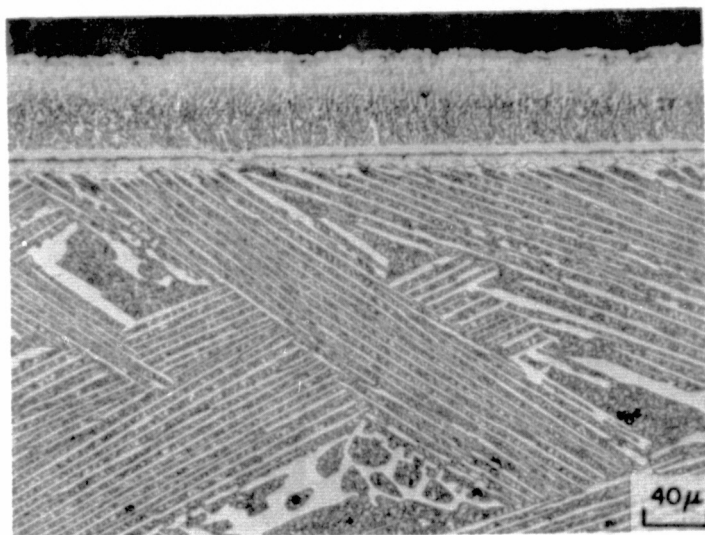


A

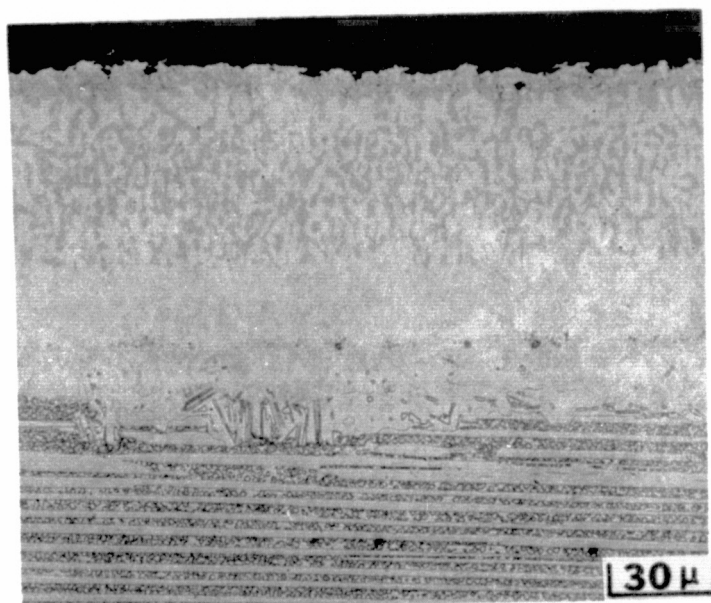


B

Figure 35 (A) Pretest and (B) Post-test Microstructures of  $\gamma/\gamma'$ - $\delta$  Eutectic Alloy Coupons Coated with Approximately  $63\mu$  of Ni-23Co-18Cr-12.5Al-0.3Y by Electron Beam Vapor Deposition. The Coated  $\gamma/\gamma'$ - $\delta$  Coupon was Evaluated for 250 Cycles In The 1172 K (1650°F) Cyclic Hot Corrosion Test. (K-13327)



A

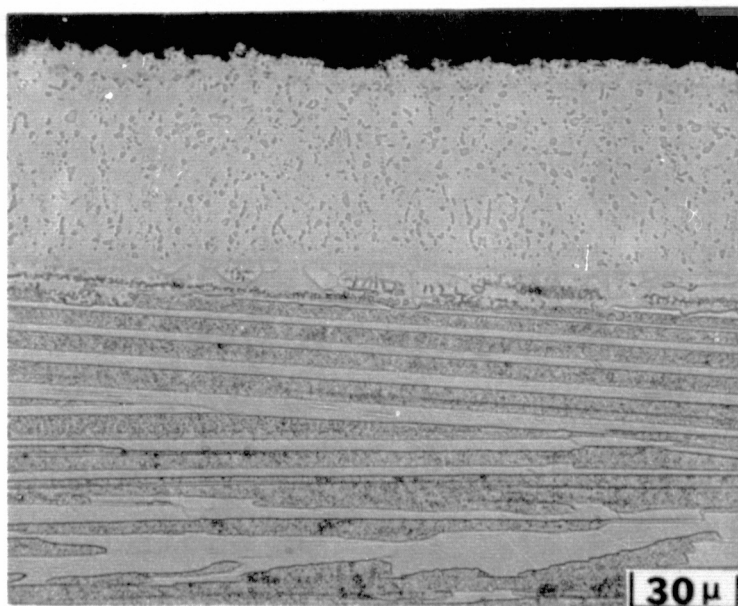


B

*Figure 36 (A) Pretest and (B) Post-test Microstructures of  $\gamma/\gamma'$ - $\delta$  Eutectic Alloy Coupons Coated with Approximately 63  $\mu$  of Ni-23Co-18Cr-12.5Al-0.3Y By Electron Beam Vapor Deposition and Then Sputter Coated with Approximately 6  $\mu$  of Platinum. The Coated  $\gamma/\gamma'$ - $\delta$  Coupon Was Evaluated for 250 Cycles in the 1172 K (1650°F) Cyclic Hot Corrosion Test. (K-13328)*



A



B

Figure 37 (A) Pretest and (B) Post-test Microstructures of  $\gamma/\gamma'$ - $\delta$  Eutectic Alloy Coupons Coated with Approximately  $63\mu$  of Ni-18Cr-12Al-0.3Y by Electron Beam Vapor Deposition And Then Sputter Coated with Approximately  $6\mu$  (0.25 mil) of Platinum. The Coated  $\gamma/\gamma'$ - $\delta$  Coupon Was Evaluated for 250 Cycles In The 1172 K (1650°F) Cyclic Hot Corrosion Test. (K-13329)

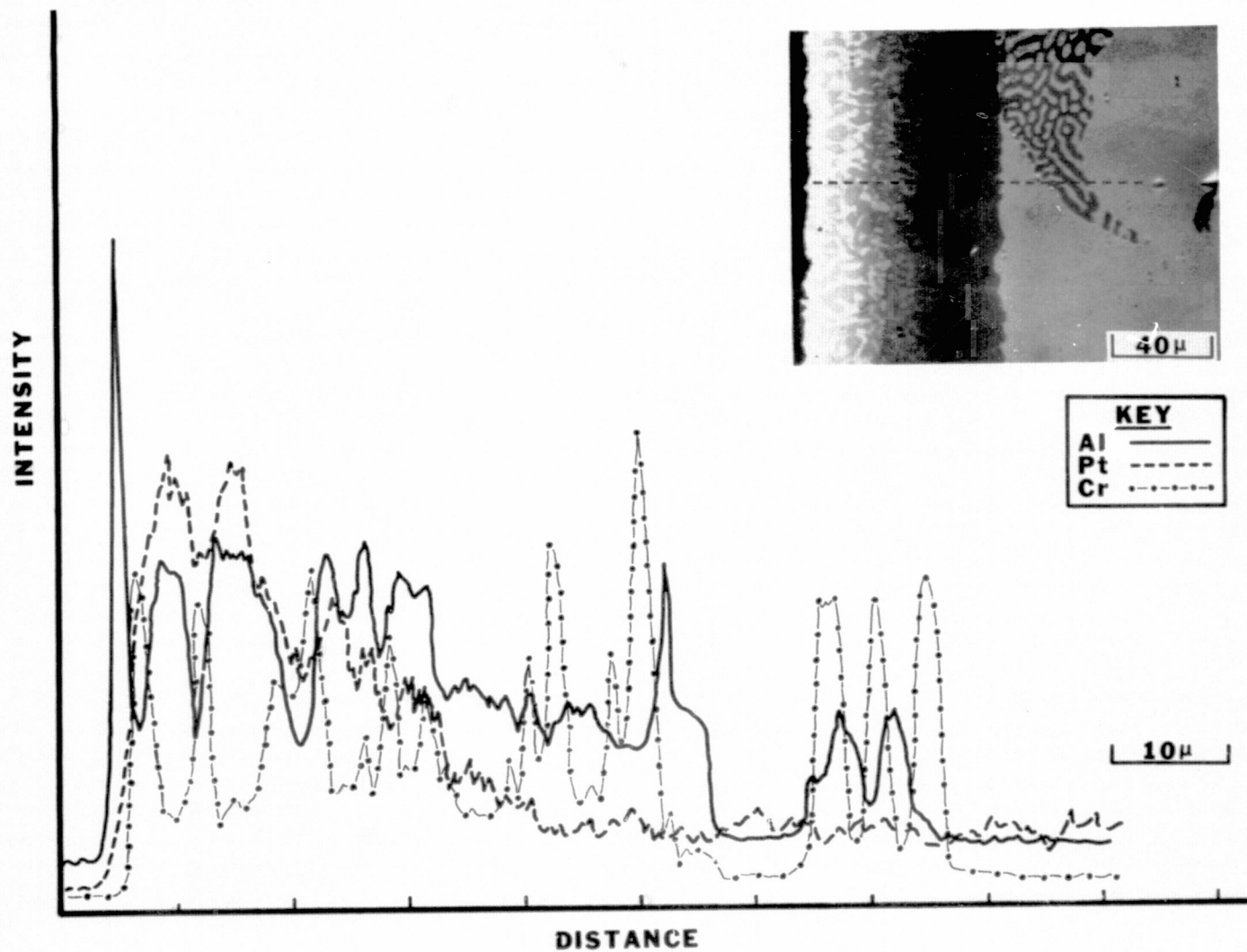
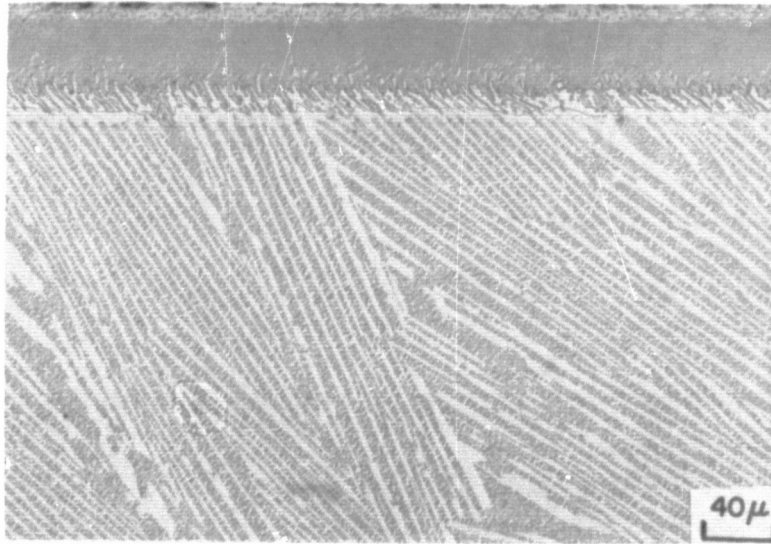
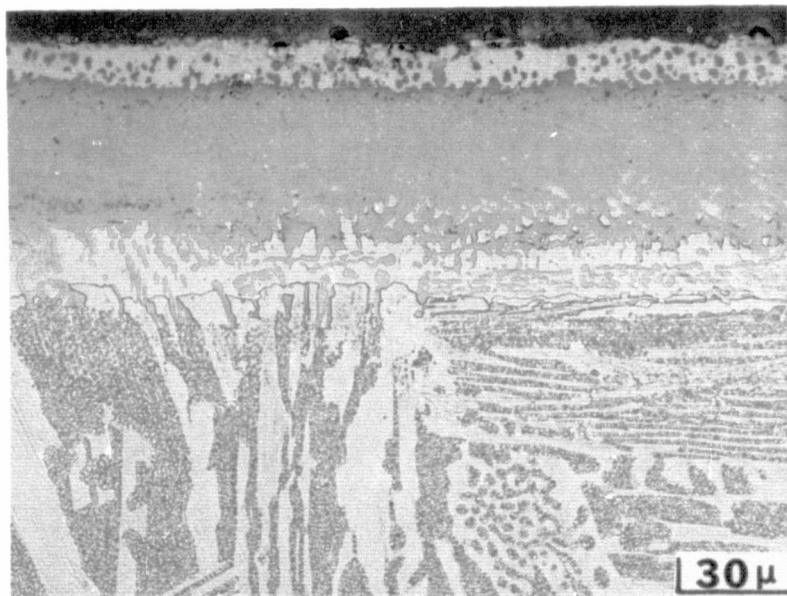


Figure 38 Relative Aluminum, Platinum and Chromium X-Radiation Intensities for As-Coated D.S.  $\gamma/\gamma'$ - $\delta$  Eutectic Alloy. The Coating Consists of 63  $\mu$  of Electron Beam Vapor Deposited Ni-18Cr-12Al-0.3Y Plus 6  $\mu$  Sputtered Platinum. (K-15106)



A



B

Figure 39 (A) Pretest and (B) Post-test Microstructures of  $\gamma/\gamma'$ - $\delta$  Eutectic Alloy Coupons Sputter Coated with Approximately  $6\mu$  of Platinum and Then Pack Aluminized. The Coated  $\gamma/\gamma'$ - $\delta$  Coupon Was Evaluated for 250 Cycles In The 1172 K (1650°F) Cyclic Hot Corrosion Test. (K-13330)

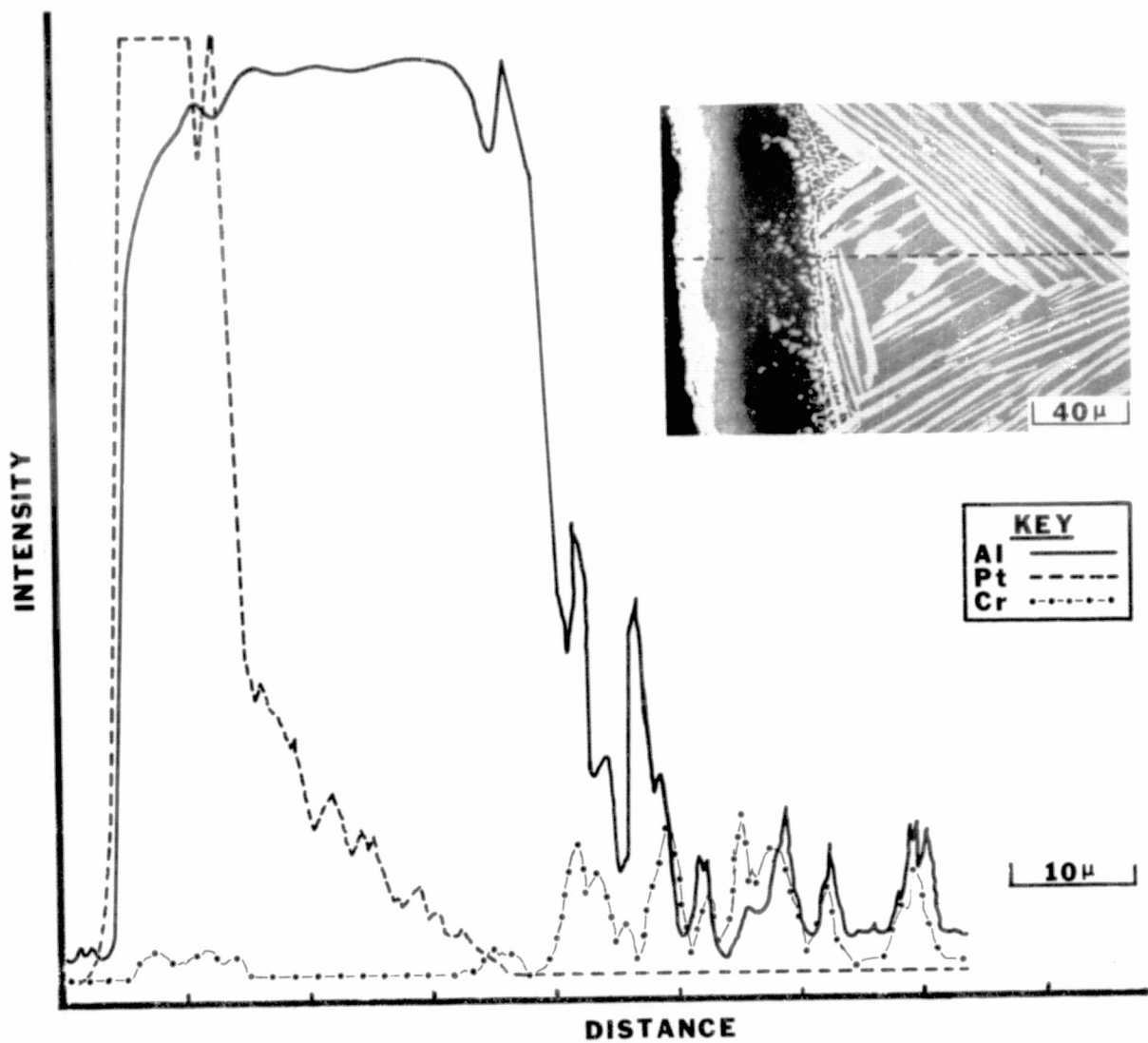


Figure 40 Relative Aluminum, Platinum and Chromium X-Radiation Intensities for As-Coated D.S.  $\gamma/\gamma'$ - $\delta$  Eutectic Alloy. The Coating Consists of 6  $\mu$  Sputtered Platinum Plus 25 to 76  $\mu$  Diffusion Aluminide. (K-15105)

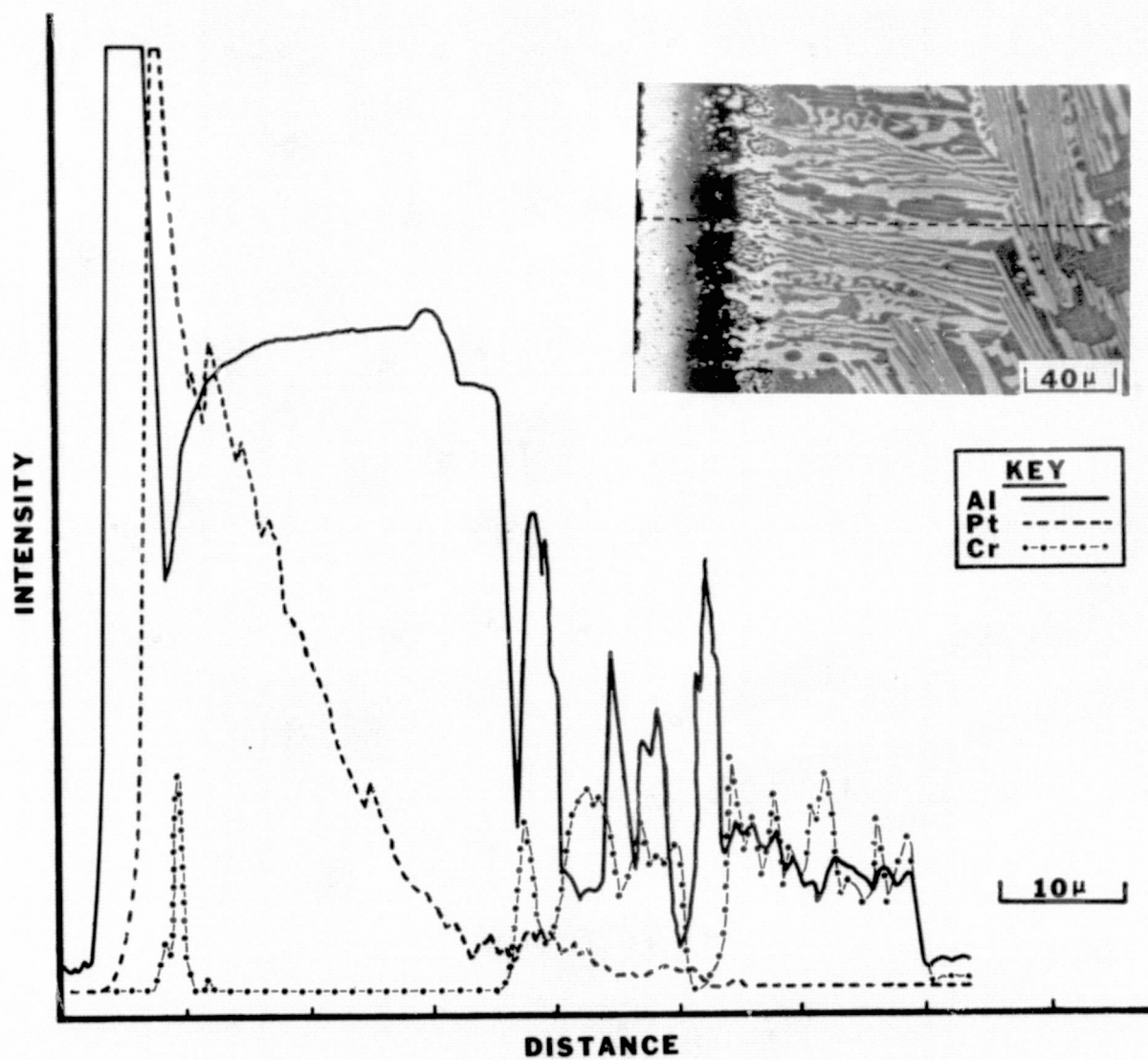
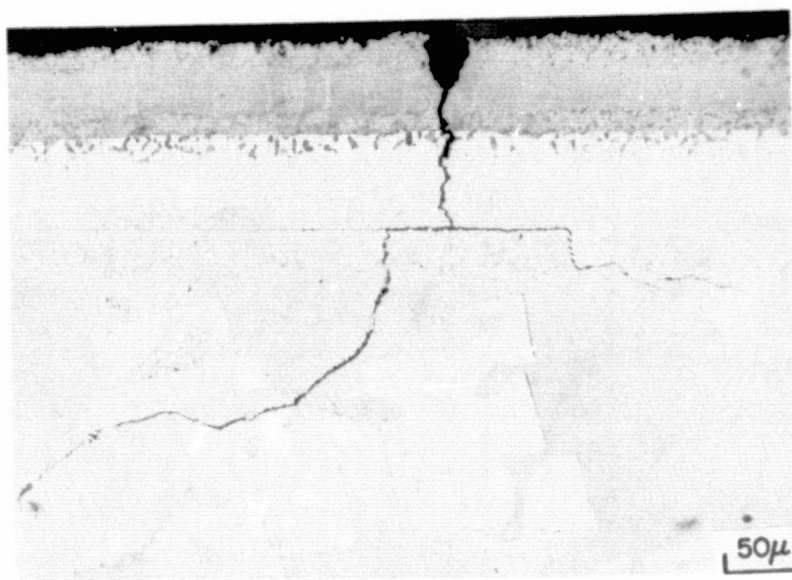
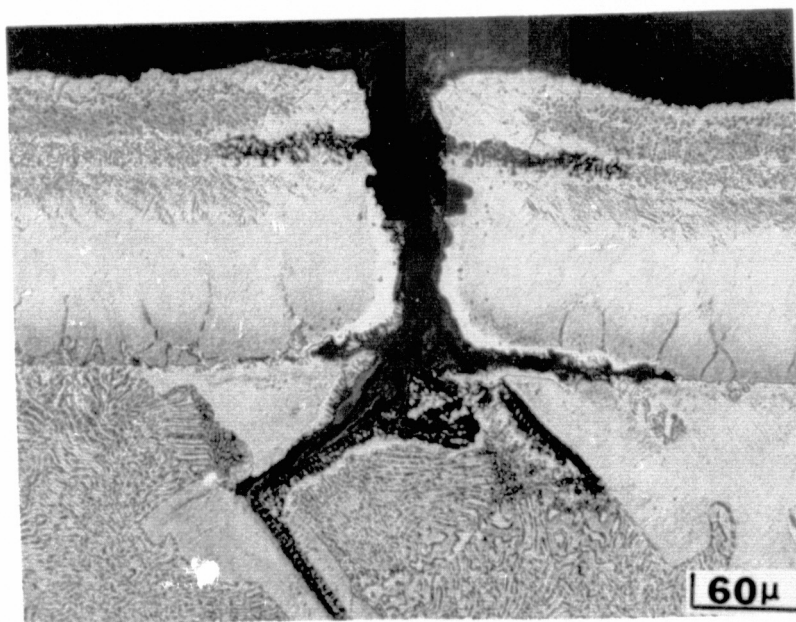


Figure 41 Relative Aluminum, Platinum and Chromium X-Radiation Intensities of Coated D.S.  $\gamma/\gamma'$ - $\delta$  Eutectic Alloy After a 1172 K (1650°F) Laboratory Hot Corrosion Test. The Coating Consists of 6μ Sputtered Platinum Plus 25 to 76μ Diffusion Aluminide. (K-15107)



A



B

Figure 42 (A) Pretest and (B) Post-test Microstructures of  $\gamma/\gamma'$ - $\delta$  Eutectic Alloy Coupons Coated with Approximately  $127\mu$  of Ni-18Cr-5Al-0.3Y and Then Diffusion Aluminized (Pack, Inward). The Coated  $\gamma/\gamma'$ - $\delta$  Coupon Was Evaluated for 110 Cycles In The  $1172K$  ( $1650^{\circ}F$ ) Cyclic Hot Corrosion Test. (K-13331)

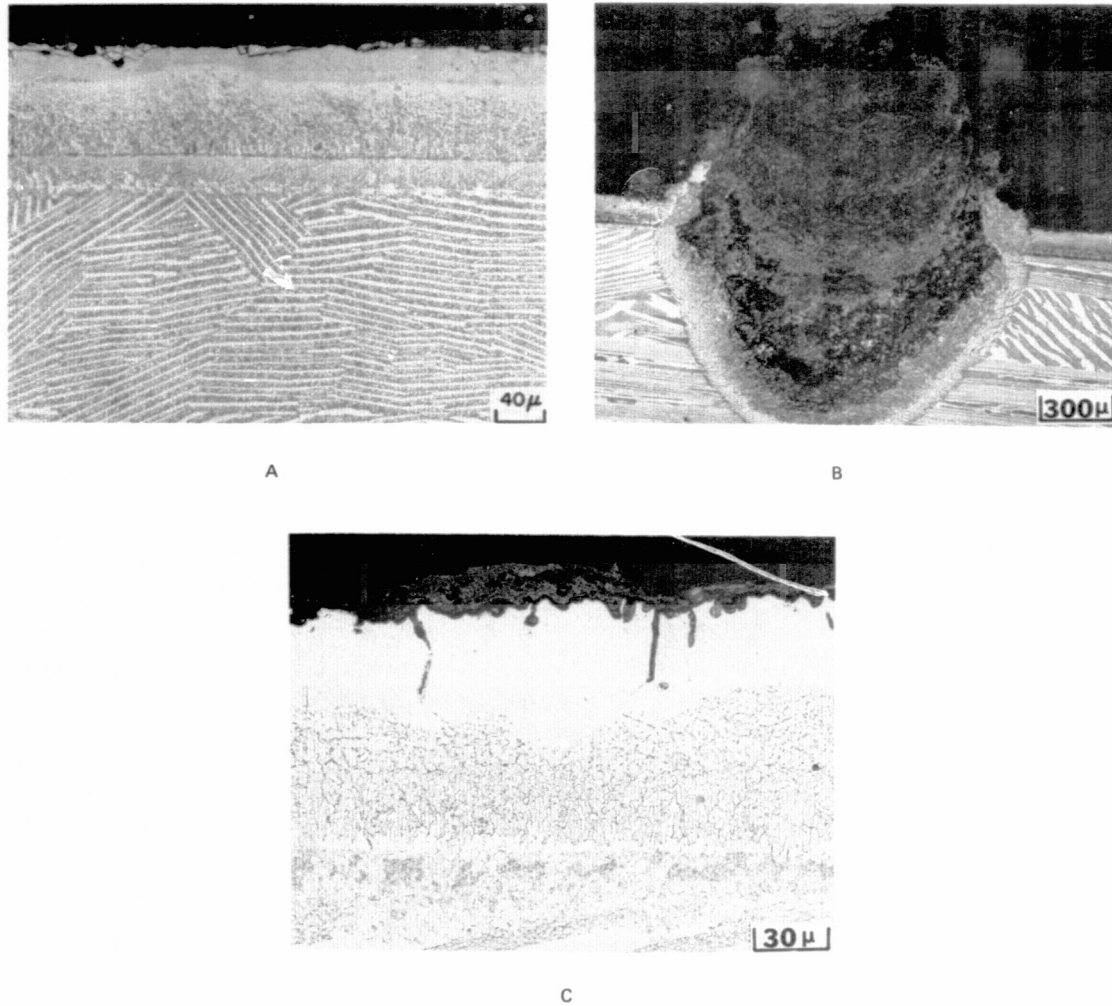
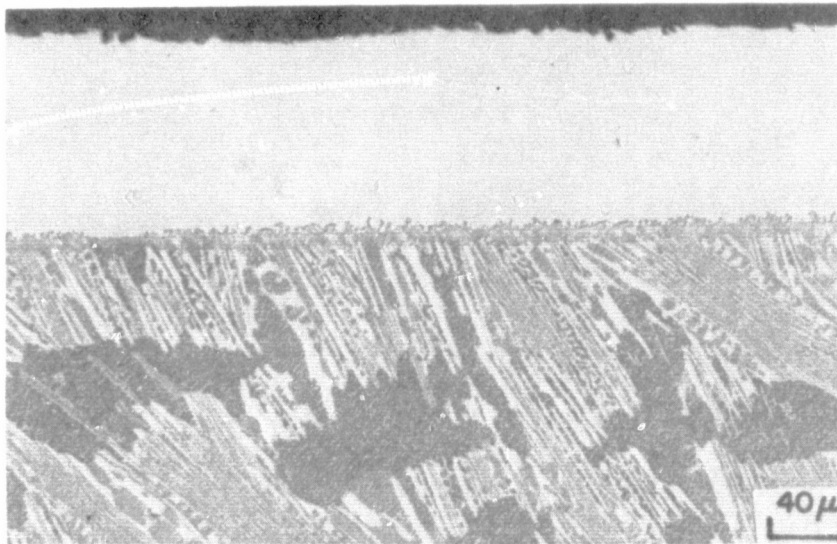
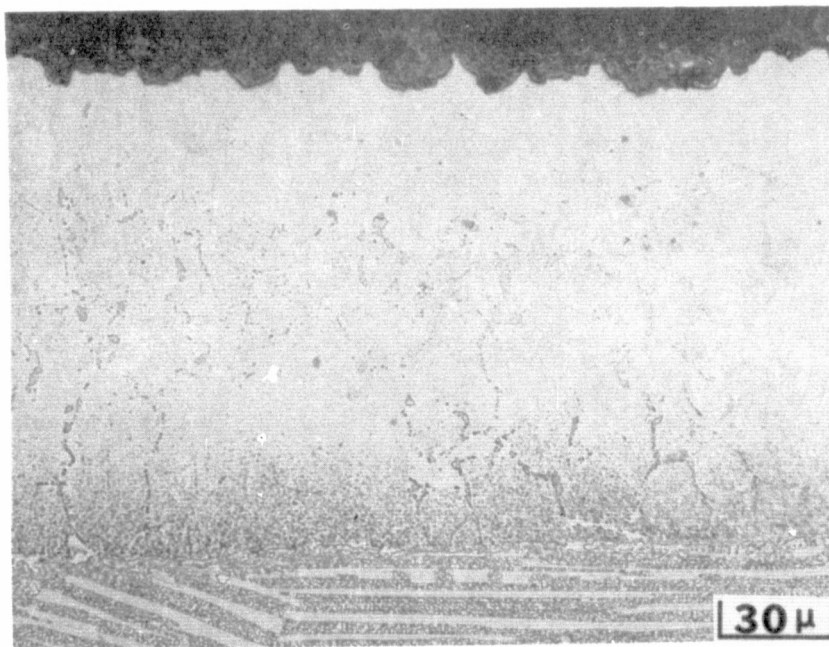


**Figure 43** (A) Pretest and (B, C) Post-test Microstructures of  $\gamma/\gamma'$ - $\delta$  Eutectic Alloy Coupons Coated with Approximately 127 μ of Ni-18Cr-5Al-0.3Y And Then Diffusion Aluminized (Pack, Outward). The Coated  $\gamma/\gamma'$ - $\delta$  Coupon Was Evaluated for 140 Cycles In The 1172 K (1650°F) Cyclic Hot Corrosion Test. (K-13333 and K-13332)



A

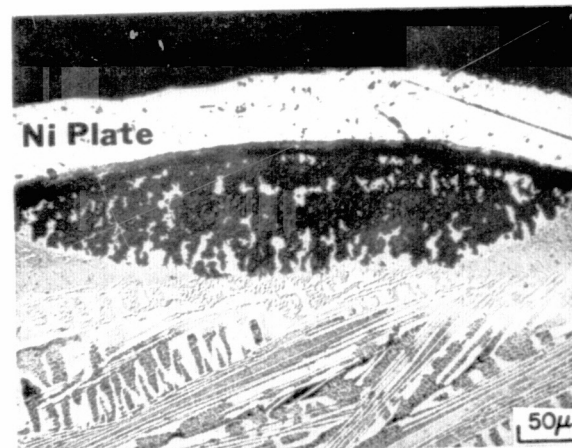


B

**Figure 44** (A) Pretest and (B) Post-test Microstructures of  $\gamma/\gamma'$ - $\delta$  Eutectic Alloy Coupons Coated with Approximately 127 $\mu$  of Ni-18Cr-5Al-0.3Y. The Coated  $\gamma/\gamma'$ - $\delta$  Coupon Was Evaluated for 250 Cycles In The 1172 K (1650°F) Cyclic Hot Corrosion Test. (K-13334)



**A**



**B**



**C**

**Figure 45** *Post-test Microstructure of Gas Phase Aluminide Coated  $\gamma/\gamma'$ - $\delta$  Simulated Air Cooled Blade Specimen After 20 Hours of Cyclic Hot Corrosion Testing At 1172 K (1650°F). (A) Typical Coating Microstructure in Unfailed Regions. (B) Localized Pitting Attack of The Coating. (C) Oxide Blister and Associated Substrate Attack.*

## V. GAS PHASE ALUMINIZING STUDY

### A. BACKGROUND

The  $\gamma/\gamma' - \delta$  alloy requires oxidation resistant coatings on both internal and external surfaces of an air cooled turbine blade. Due to the line-of-sight restrictions of overlay type coatings, internal surfaces and cooling holes must be coated with a diffusion aluminide coating.

An evaluation of conventional pack aluminide type coatings in a previous program (ref. 4) indicated that small diameter cooling holes in the  $\gamma/\gamma' - \delta$  alloy were difficult to coat satisfactorily. Limited testing under that program indicated that better coverage could be obtained with the gas phase aluminizing process. For that program,  $\gamma/\gamma' - \delta$  coupons with nominal 0.25, 0.45 and 0.625-mm diameter electrical discharge machined (EDM) holes were fully aluminized to a depth of  $50\mu$ .

Available techniques for producing small diameter holes in  $\gamma/\gamma' - \delta$  specimens were also evaluated in the above program. The results of that program indicated that the EDM technique frequently introduced small surface-connected microcracks into the eutectic alloy adjacent to the hole wall. In addition, a thin remelt layer lined the EDM holes; this layer was occasionally observed to be contaminated with tungsten (the electrode material). Examination of laser drilled holes indicated that a variable thickness remelt layer was present which had a tendency to delaminate. Holes produced by electrochemical machining (ECM) were observed to have surface irregularities due to the  $\gamma/\gamma'$  phase regions being chemically attacked to a slightly greater degree than the  $\delta$  phase regions.

The objective of this phase of the program was to optimize the gas phase diffusion aluminide coating (PWA 275) process for coating internal surfaces and ECM cooling holes in a simulated eutectic alloy airfoil specimen.

### B. SPECIMEN PREPARATION

Twelve simulated airfoil specimens were machined from 1.6-cm diameter investment cast  $\gamma/\gamma' - \delta$  (6 Cr) rods which were directionally solidified at a rate of 1.25 cm/hour in alumina shell molds. The simulated air cooled blade configuration was made to represent the internal cavity and current cooling holes (diameter and length) anticipated for an air cooled  $\gamma/\gamma' - \delta$  blade. The simulated  $\gamma/\gamma' - \delta$  blade specimens are hollow cylindrical tubes [7.6 mm (0.3 inch) ID and 12.7 mm (0.5 inch) OD]. Four sets of eight ECM drilled holes were spaced 90 degrees apart. The series of eight holes consisted of two holes of 0.5 mm (0.020 inch) and 0.75 mm (0.030 inch) in diameter drilled at 90 degrees and 45 degrees to the surface (Figure 46).

During the development of the gas phase process to coat conventionally cast and directionally solidified superalloys, it was determined that a two-chambered coating boat improved the internal coating uniformity on the more complex blade configurations. The two-chambered boat being used in this program is shown schematically in Figure 47. Basically, the aluminizing vapors for the internal coating are generated from a powder mixture contained in the lower chamber. These vapors are mixed with an inert gas which provides a

positive flow, allowing the vapor mixture to pass through a tube and through the internal surface of the test specimen. The upper chamber contains the test specimen to be coated which is supported on a tube above a second powder mixture which generates vapor to coat the external surfaces.

### C. GAS PHASE ALUMINIDE OPTIMIZATION

This gas phase deposition process (PWA 275) requires a definition of process parameters for each superalloy component to accommodate the individuality of its substrate composition and configuration. It was determined that eight  $\gamma/\gamma' - \delta$  simulated air cooled blade test specimens were required to adequately define all process parameters. Four test specimens were used to determine the process temperature, flow rate and powder mixture parameters. The basis for Run 1 was the current basic parameter set for the PWA 275 process. The test specimen for Run 2 was sealed at one end and the conditions of Run 1 were repeated. Run 2 was used to determine whether an advantage would be gained by forcing the gas generated in the lower chamber to pass through the cooling holes into the upper chamber. Run 3 evaluated the use of a lower process temperature. Run 4 determined the effect of an increase in the activator content. The remaining four test specimens were used in determining a time at temperature versus thickness curve for optimum coating conditions. Test conditions for the gas phase aluminizing process study are provided in Table II.

After each of the first four runs, the PWA 275 coated  $\gamma/\gamma' - \delta$  specimens were metallographically examined in the as-coated and heat treated conditions. The post-coating heat treatment consisted of four hours at 1352 K in an argon atmosphere.

Metallographic examination of these specimens showed that the  $\gamma/\gamma'$  phase regions in the substrate were aluminized to a greater depth than the  $\delta$  phase platelets. This effect was especially pronounced in the ECM cooling air holes where both phases were exposed at 90 and 45 degree angles to the surface of the specimen. Figure 48 illustrates these localized variations in coating thickness; this figure also indicates that coating thickness variations were dependent on the thickness of the  $\delta$  phase platelets. Figure 49 shows the contrast in coating microstructure which was observed in ECM cooling holes and internal and external surfaces. Tables III and IV illustrate the optically measured coating thickness. The results are tabulated for the internal coating thickness (coating on the ID), the external coating thickness (coating on the OD), and the cooling hole coating thickness. The coating thicknesses measured throughout the cooling holes were further tabulated to include the phase dependent coating thickness variations for both hole diameters and orientations. In general, the coating thickness obtained by aluminizing the  $\gamma/\gamma'$  phase regions was found to be about twice that obtained by aluminizing the  $\delta$  phase platelets for both the 1311 K (1900°F) and 1366 K (2000°F) coating runs.

The sealed test specimen of Run 2 showed no significant thickness increase in the cooling holes. Therefore, the test specimens were left open for subsequent coating trials.

Increasing the activator content resulted in a slight increase in coating thickness. The aluminide coating thickness over  $\delta$  phase regions increased by about  $5\mu$  while the coating thickness over  $\gamma/\gamma'$  phase areas increased by about  $20\mu$ . Therefore, increasing the activator content slightly increased the magnitude of the local coating thickness variations.

For a constant activator content (5 weight percent), the coatings produced at 1366 K (2000°F) were about twice as thick as the coating formed at 1311 K (1900°F). Increasing the activator content from 5 to 10 weight percent produced coating thicknesses which were closer to those obtained at 1366 K.

Based on the results of the parameter study, the remaining four  $\gamma/\gamma' - \delta$  specimens were used to establish the relationship between coating time and coating thickness for the higher temperature (1366 K) process conditions. The times selected were 2, 5, 8 and 11 hours. The five hour coating trial duplicated Run 1 and illustrated the reproducibility of the process (Table IV, Run 6). After each time cycle, the test specimen was heat treated four hours at 1352 K in argon and examined metallographically.

Coating thickness results are tabulated in Table IV for Runs 5 through 8. Figure 50 shows the variation of internal and external coating thickness as a function of time at temperature. Figure 51 shows the variation of cooling hole coating thicknesses as a function of time at temperature and substrate phases. Comparison of Figures 50 and 51 shows that the minimum coating thickness measured on the internal and the external surfaces is equivalent to the minimum coating thickness obtained over  $\delta$  phase regions in the cooling holes. The maximum coating thickness on the internal and external surfaces (Figure 50) was within the scatter band of coating thickness obtained over  $\gamma/\gamma'$  phase regions in the cooling holes.

Coatings produced with the five hour (Runs 1, 6) and 11 hour (Run 8) gas phase aluminizing cycles at 1366 K (2000°F) were selected for further evaluation in the 1172 K (1650°F) hot corrosion test. Duplicate  $\gamma/\gamma' - \delta$  specimens were coated with these two cycles and evaluated as indicated previously in Section IV.

TABLE II

## PWA 275 PROCESS PARAMETERS

Run No.	External Pack Composition			Internal Pack Composition			Flow Rate (liters/hour)	Time at Temperature (hours)	Temperature ( K)
	Co <sub>2</sub> Al <sub>5</sub>	Activator	Al <sub>2</sub> O <sub>3</sub>	Co <sub>2</sub> Al <sub>5</sub>	Activator	Al <sub>2</sub> O <sub>3</sub>			
1	10 w/o	10 w/o	80 w/o	10 w/o	5 w/o	85 w/o	170	5	1366
2*	10 w/o	10 w/o	80 w/o	10 w/o	5 w/o	85 w/o	170	5	1366
3	10 w/o	10 w/o	80 w/o	10 w/o	5 w/o	85 w/o	170	5	1311
4	10 w/o	20 w/o	70 w/o	10 w/o	10 w/o	80 w/o	170	5	1311
5	10 w/o	10 w/o	80 w/o	10 w/o	5 w/o	85 w/o	170	2	1366
6	10 w/o	10 w/o	80 w/o	10 w/o	5 w/o	85 w/o	170	5	1366
7	10 w/o	10 w/o	80 w/o	10 w/o	5 w/o	85 w/o	170	8	1366
8	10 w/o	10 w/o	80 w/o	10 w/o	5 w/o	85 w/o	170	11	1366

\*During Run 2, the tube was sealed at the top such that all of the coating vapors would pass through the cooling air holes.

TABLE III

## PWA 275 COATED TEST SPECIMENS

Run	External Coating Thickness (microns)	Internal Coating Thickness (microns)	0.50 mm Holes Coating Thickness (microns)				0.75 mm Holes Coating Thickness (microns)			
			90°		45°		90°		45°	
			$\gamma/\gamma'$ -Phases	$\delta$ -Phase	$\gamma/\gamma'$ -Phases	$\delta$ -Phase	$\gamma/\gamma'$ -Phases	$\delta$ -Phase	$\gamma/\gamma'$ -Phases	$\delta$ -Phase
1	31 - 71	28 - 76	71 - 84	25 - 31	76 - 89	25 - 42	76 - 89	25 - 42	76 - 84	25 - 31
2	31 - 71	30 - 71	64 - 84	36 - 43	76 - 84	36 - 41	68 - 84	25 - 43	76 - 84	30 - 42
3	20 - 41	15 - 46	36 - 41	15 - 20	38 - 41	13 - 18	36 - 46	15 - 25	38 - 41	15 - 20
4	25 - 43	28 - 64	51 - 61	15 - 20	71 - 76	23 - 25	53 - 61	20 - 25	51 - 64	18 - 25

TABLE IV

## PWA 275 COATED + FOUR HOURS AT 1352 K

Run	External Coating Thickness (microns)	Internal Coating Thickness (microns)	0.50 mm Holes Coating Thickness (microns)				0.75 mm Holes Coating Thickness (microns)			
			90°		45°		90°		45°	
			$\gamma/\gamma'$ -Phases	$\delta$ -Phase	$\gamma/\gamma'$ -Phases	$\delta$ -Phase	$\gamma/\gamma'$ -Phases	$\delta$ -Phase	$\gamma/\gamma'$ -Phases	$\delta$ -Phase
1	31 - 69	28 - 71	64 - 76	28 - 31	64 - 84	25 - 33	76 - 84	25 - 42	64 - 76	25 - 33
2	42 - 84	42 - 67	64 - 76	31 - 42	64 - 76	36 - 46	67 - 76	36 - 41	64 - 76	36 - 46
3	20 - 64	20 - 46	56 - 64	18 - 23	46 - 53	23 - 25	53 - 57	20 - 25	46 - 51	20 - 25
4	30 - 61	25 - 71	53 - 69	28 - 30	46 - 51	28 - 36	66 - 76	28 - 33	56 - 64	25 - 30
5	20 - 42	20 - 46	53 - 64	20 - 32	48 - 64	20 - 32	42 - 56	25 - 28	51 - 64	25 - 32
6	30 - 71	31 - 64	56 - 71	25 - 38	57 - 64	28 - 42	64 - 84	32 - 42	71 - 84	25 - 32
7	42 - 84	36 - 84	64 - 80	32 - 42	60 - 76	30 - 39	60 - 81	39 - 48	60 - 76	25 - 39
8	42 - 93	46 - 93	64 - 84	42 - 51	71 - 84	42 - 53	76 - 93	42 - 46	76 - 93	46 - 55

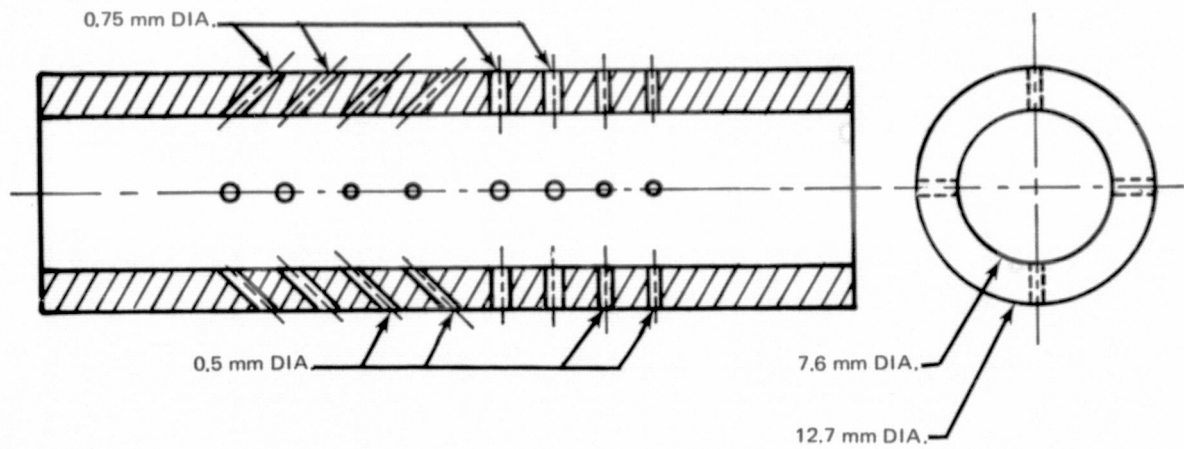


Figure 46 Simulated  $\gamma/\gamma'$  -  $\delta$  Air Cooled Blade Specimen

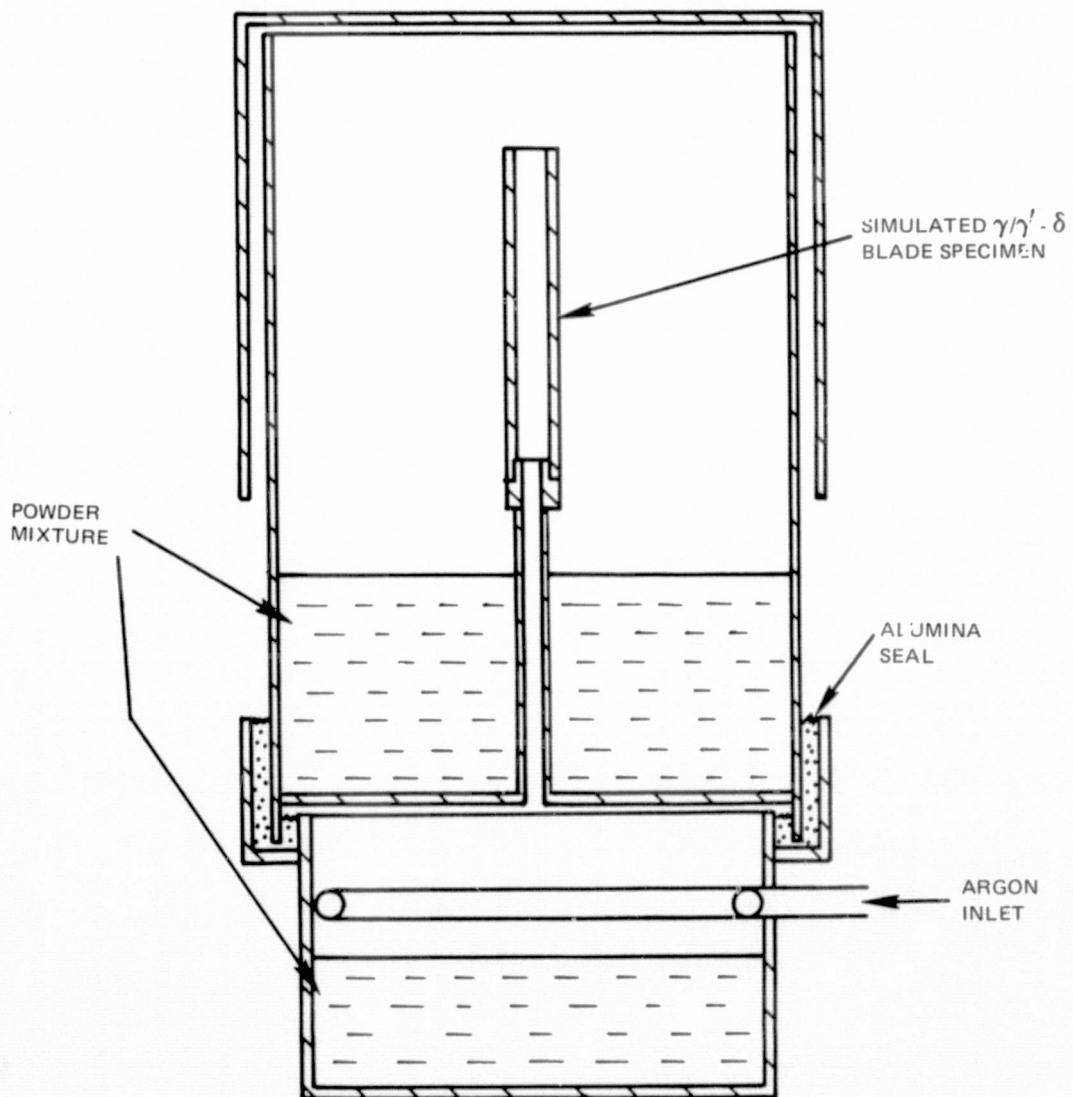
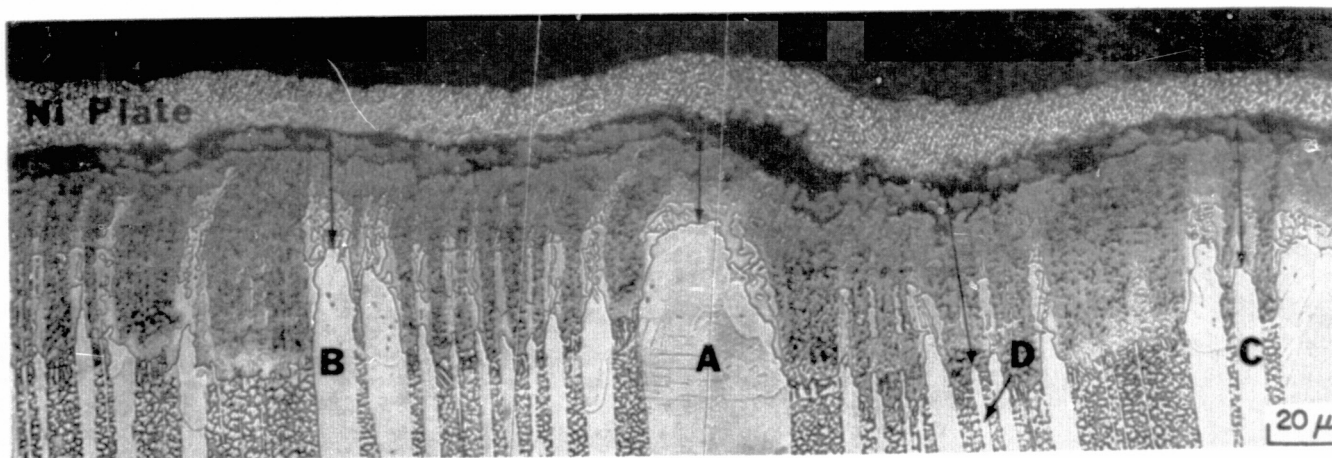


Figure 47 PWA 275 Coating Chamber Design



	$\delta$ PLATELET THICKNESS	COATING THICKNESS
A	41 $\mu$	25 $\mu$
B	10 $\mu$	32 $\mu$
C	6 $\mu$	38 $\mu$
D	2 $\mu$	48 $\mu$
$\gamma/\gamma'$ -PHASE REGION	-	57 - 64 $\mu$

Figure 48 Variation of Diffusion Aluminide Coating Thickness With  $\delta$  Phase Platelet Thickness  
(K-20925)

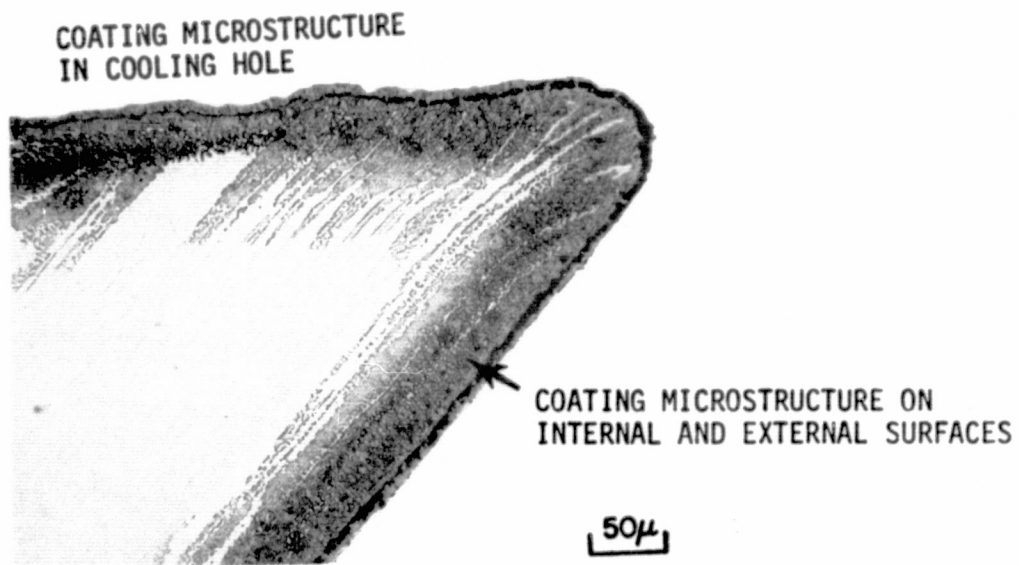


Figure 49 Typical PWA 275 Coating Microstructure at Junction of ECM Cooling Hole and Internal and External Surfaces of  $\gamma/\gamma'$ - $\delta$  Simulated Air Cooled Blade Specimen (Run 6). (K-20926)

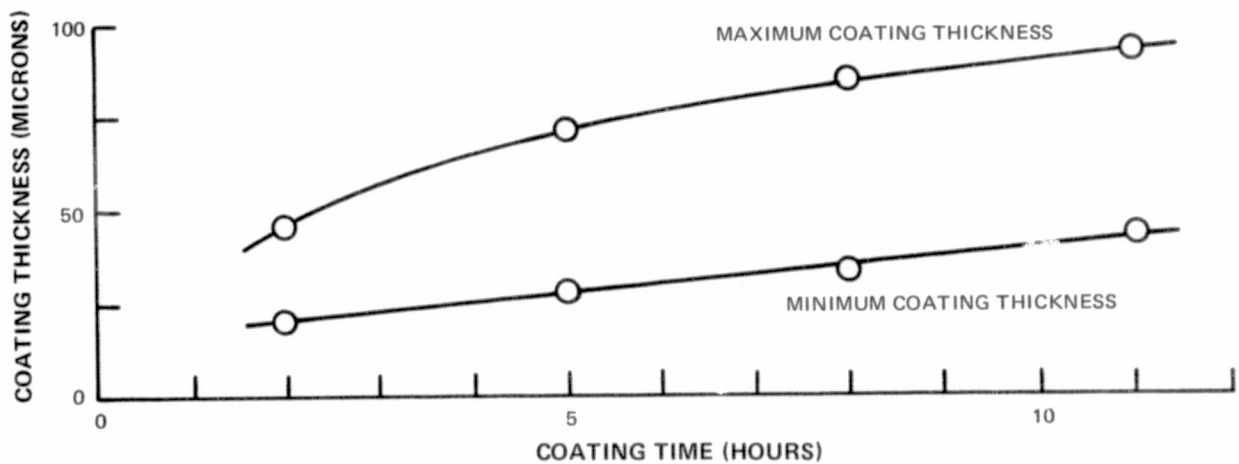
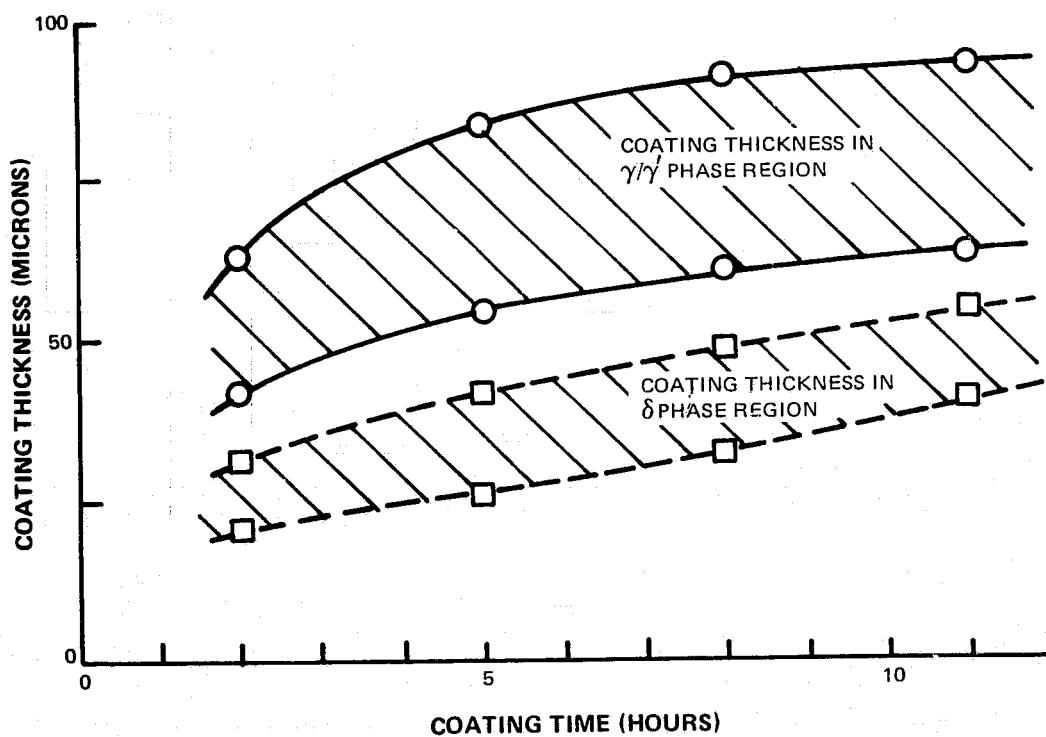


Figure 50 Thickness of PWA 275 Coating on Internal and External Surfaces of  $\gamma/\gamma'$ - $\delta$  Eutectic Alloy Specimen as a Function of Coating Time at 1366 K (2000°F)



**Figure 51** Dependence of PWA 275 Coating Thickness on Coating Time at 1366 K (2000°F) and Phases Being Aluminized in ECM Cooling Holes of  $\gamma/\gamma'$ - $\delta$  Eutectic Alloy Specimen

## VI. COATING DUCTILITY EVALUATION

### A. BACKGROUND

Ductility tests at 578 K (600°F) are used to screen coating-substrate systems and verify that they can withstand a few relatively severe thermal strains with peak tension at low temperatures where many coatings are relatively brittle. The thermal strain ranges present in typical gas turbine airfoils are expected to be in the order of 0.15 to 0.35 percent strain.

Previous ductility evaluations of coated  $\gamma/\gamma'-\delta$  eutectic at 578 K indicated that substrate failure strains were influenced by the particular coating system present (refs. 4, 5). In general, aluminized specimens exhibited substrate failure strains which were similar to those for the uncoated alloy ( $> 2$  percent), while those for the overlay coated specimens varied from less than 1 percent to 2 percent depending upon the particular system.

Reducing the thickness of the overlay coating from about  $127\mu$  (5 mils) to  $63.5\mu$  (2.5 mils) was thought to provide a solution for alleviating low temperature, low strain failures. This hypothesis was evaluated in this program with three of the six candidate overlay coating systems (NiCrAlY + Pt, NiCoCrAlY + Pt and NiCoCrAlY). NiCrAlY + Al and NiCrAlSiY coating systems were evaluated at nominal  $127\mu$  thicknesses. In addition, the  $\sim 70\mu$  thick Pt + Al coating was evaluated for coating ductility.

### B. SPECIMEN PREPARATION

Twelve tensile specimens were machined from 11-cm length x 1.6-cm diameter rods which were directionally solidified in alumina investment casting shell molds at a rate of 1.25 cm/hour. The specimen geometry is identical to that used previously (refs. 4 and 5).

Duplicate specimens were then coated with the following six candidate coating systems:

- Pt + Al
- NiCrAlY + Pt
- NiCoCrAlY + Pt
- NiCoCrAlY
- NiCrAlY + Al
- NiCrAlSiY

In addition, two directionally solidified (D.S.) MAR-M 200 + Hf specimens were prepared and coated with the NiCrAlY + Pt coating system.

### C. EXPERIMENTAL PROCEDURE

Coating ductility determinations were made by running an interrupted tensile test. The coated specimen was heated to the specified temperature and then loaded in tension to a predetermined level of strain. The specimen was then unloaded and cooled to room temperature so that plastic surface replicas could be taken. Testing was continued in an incremental fashion, with replicas being taken after each strain increase, until cracking of the

coating was detected. Surface replicas were examined at a minimum magnification of 100X to detect cracking. In addition, failure strains for all the coated specimens were determined.

#### D. TEST RESULTS

Coating cracks were initiated in the Pt + Al coating between 0.5 and 0.7 percent strain; failure strains for the duplicate specimens were 3.3 and 4.2 percent strain. Post-test examination of the specimen indicated that the coating cracked extensively; typical secondary cracks in the Pt + Al coating are shown in Figure 52.

Cracking in the NiCrAlY + Pt coating was initiated between 0.5 and 0.7 percent strain. Post-test examination of secondary cracks indicated that coating cracks were predominately confined to the thin Pt-rich surface layer as shown in Figure 53. Specimen failure strains for these specimens varied from 3.4 to 4.5 percent strain.

For comparison, the duplicate NiCrAlY + Pt coated D.S. MAR-M200 + Hf specimens exhibited coating fracture strains between 1.0 and 1.4 percent strain and specimen failure strains of 7.4 and 8.9 percent. Metallographic examination of secondary coating cracks indicated that the morphology of the cracks was similar to the cracks in the same coating on the  $\gamma/\gamma' - \delta$  alloy; coating cracking was predominantly confined to the thin Pt-rich surface layer.

Secondary cracking in the Pt-rich surface layer of the NiCoCrAlY + Pt coating (Figure 54) also initiated between 0.5 and 0.7 percent strain. In addition, post-test metallography indicated that some secondary cracks also were present in the diffusion affected substrate. Specimen failure strains varied from 2.2 to 3.1 percent strain.

Replica examination of the NiCoCrAlY coated  $\gamma/\gamma' - \delta$  specimens indicated that the NiCoCrAlY coating was uncracked after 1.9 to 2.0 percent strain. Post-test metallographic examination of the NiCoCrAlY coated  $\gamma/\gamma' - \delta$  specimen revealed the presence of short cracks in the diffusion affected substrate zone, however (see Figure 55). Specimen failures occurred at strains of 2.4 and 2.7 percent.

Fracture of the NiCrAlY + Al (pack, inward) coating was detected between 0.2 and 0.4 percent strain. In addition, it should be recalled that this coating was cracked in the virgin condition on the  $\gamma/\gamma' - \delta$  erosion bars (See Section III). The microstructure of typical secondary cracks is shown in Figure 56. Specimen failure strains varied between 3.2 and 6.5 percent for this system.

Failure of the  $127\mu$  thick NiCrAlSiY coated  $\gamma/\gamma' - \delta$  specimens occurred at 1.4 and 1.6 percent total (elastic and plastic) strain. Examination of the surface replicas for each specimen failed to reveal any indication of coating cracking prior to the final strain increments. Therefore, coating crack initiation occurred just prior or concurrent with specimen failure, i.e., in the ranges of 1.05 to 1.4 percent and 1.3 to 1.6 percent strain, respectively. The microstructure of a secondary crack in the NiCrAlSiY coated specimen is shown in Figure 57. Metallographic examination also indicated that the substrate contained  $\gamma$  phase

dendrites which indicate that the columbium content was somewhat low. Fracture strain data obtained for the coated eutectic alloy in this program is summarized in Table V. Ductility data obtained in previous NASA (ref. 5) and Air Force (ref. 4) programs are provided in Tables VI and VII for comparison.

## E. DISCUSSION

The data obtained during the current investigation is consistent with ductility data obtained previously in other programs (refs. 4, 5).

$\gamma/\gamma' - \delta$  specimens coated with diffusion aluminide type coatings (e.g., Pt + Al and NiCrAlY + Al) exhibited similar coating fracture strains as other diffusion aluminide-type coatings (Al, Cr + Al, Ni + Cr + Al and NiCrAlY + Al) which were previously evaluated. Briefly, coating crack initiation occurs between 0.2 and 1.0 percent strain for diffusion aluminide-type coatings. Numerous additional closely spaced coating cracks form as the coated  $\gamma/\gamma' - \delta$  specimens are pulled to failure. Failure strains of diffusion aluminide coatings vary between 2.2 and 7.1 percent strain; these strain levels are consistent with those of uncoated  $\gamma/\gamma' - \delta$  specimens at 578 K.

The brittle behavior of the diffusion aluminide-type coatings is due to the  $\beta$  (NiAl) inter-metallic matrix phase which is characteristic of practical diffusion aluminide coating systems (refs. 23, 24). In contrast, practical (Ni,Co) CrAlY overlay coating microstructures are not restricted to  $\beta$  phase matrix compositions. When required, increased coating ductility can be obtained by dispersing the aluminum-rich  $\beta$  phase in a metallic  $\gamma$  (Ni, Co solid solution) phase matrix. The aluminum content of overlay coatings has the largest single effect upon coating ductility, with the lower aluminum compositions exhibiting the higher ductility (ref. 24). However, decreasing the aluminum content also decreases the oxidation/hot corrosion life of (Ni, Co) CrAlY coatings. Thus, unlike the diffusion aluminides, the overlay coatings can be adjusted through chemistry selection to provide the best trade-off of oxidation/hot corrosion life and ductility to meet the needs of a given application.

Referring to Table V, it can be observed that the fracture strain of the NiCoCrAlY coating was  $> 2$  percent strain. Fracture strains of the NiCrAlY + Pt and NiCoCrAlY + Pt coatings were between 0.5 and 0.7 percent strain. Metallographic examination indicated, however, that this decreased ductility was associated with the thin Pt-rich surface layer which etches similar to the  $\beta$  phase (See Figures 53 and 54); the adjacent coating exhibited excellent coating ductility.

In previous investigations (refs. 4, 5), it was noted that  $\gamma/\gamma' - \delta$  specimens coated with relatively thick ( $\sim 125\mu$ ) (Ni, Co) CrAlY coatings tended to exhibit specimen failure strains in the range of 0.5 to 2.2 percent which were below the typical 2 to 5 percent failure strains of the uncoated  $\gamma/\gamma' - \delta$  alloy at 578 K. The specimen failure strains (1.4 and 1.6 percent) of the NiCrAlSiY coated specimens are consistent with this behavior.

Prior testing also indicated that the relatively low strain failures of (Ni, Co) CrAlY coated  $\gamma/\gamma' - \delta$  specimens were probably the result of a mechanical interaction between the relatively thick ( $\sim 125\mu$ ) coating and the substrate (refs. 4, 5).

In the case of the higher aluminum content NiCrAlY and NiCoCrAlY overlay coatings, which are relatively brittle at 578 K, evidence is available to indicate that crack initiation usually occurred in the coating. Low strain specimen failures frequently occurred almost concurrently with coating crack formation. Some  $\gamma/\gamma' - \delta$  specimens coated with ductile NiCoCrAlY and NiCrAlY (5 Al) + NiCoCrAlY coatings also exhibited low strain specimen failures. Metallographic examination of these specimens revealed the presence of cracked substrate porosity adjacent to the coating in some instances. Once microcracks have been initiated in either the coating, the diffusion affected substrate zone, or the adjacent substrate (which has not been affected by coating-substrate interdiffusion), it is speculated that these microcracks could then propagate into the coating and/or continue propagating into the substrate in order to produce a critical crack size.

Fracture mechanics concepts indicated that, if the coating is cracked to the substrate, the elastic modulus and the thickness of the coating will affect the magnitude of the crack's stress intensity factor, i.e. a crack in a strong, thick coating should be more deleterious than a crack in a strong, thin coating. Therefore, it was thought that reducing the thickness of the strong coating layer may provide a solution to the low strain failure phenomenon. The results obtained in this program tend to substantiate this hypothesis. Failure strains of  $\gamma/\gamma' - \delta$  specimens coated with thin ( $\sim 60\mu$ ) overlay coatings were between 2.2 and 4.5 percent strain; these values are similar to the ductility of uncoated  $\gamma/\gamma' - \delta$  at this temperature.

A possible explanation for the good ductility of diffusion aluminide coated  $\gamma/\gamma' - \delta$  specimens with cracks through the coating thickness is that, due to the very high density of coating cracks, the effective elastic modulus of the cracked coatings was very low. If this hypothesis is correct, an individual crack in a highly cracked coating would not represent a large stress raiser. Thin coating thicknesses of diffusion aluminide type coatings are also beneficial from a stress raiser standpoint.

Finally, in order to put these results into perspective, it should be recalled that the purpose of this tensile ductility test is to verify that the fracture strains of the coatings exceed values in the order of 0.15 to 0.35 percent strain which are expected in a typical gas turbine airfoil.

The results of this and previous investigations indicate that the fracture strains of all the coating systems which have been evaluated on the  $\gamma/\gamma' - \delta$  alloys exceed the magnitude of anticipated thermal strains with the possible exception of the NiCrAlY + Al system. In addition, it has been demonstrated that somewhat higher specimen failure strains can be obtained by decreasing the coating thickness. However, since the magnitude of the thermal strains is low, there is probably minimal benefit in reducing coating thickness on the airfoil; thermal fatigue testing (Section VII) has demonstrated that acceptable fatigue lives for  $\gamma/\gamma' - \delta$  specimens can be obtained with NiCrAlY and NiCrAlY + Pt coatings applied to a thickness of  $\sim 125\mu$ . Furthermore, reducing coating thickness would also adversely affect the oxidation life.

TABLE V

## 578 K (600°F) COATING FRACTURE AND SPECIMEN FAILURE STRAINS

Coating System	Coating Fracture Strain (%)	Specimen Failure Strain (%)	Nominal Coating Thickness (microns)
Pt (sputter) + Al (pack)	0.5-0.7	4.2	70
Pt (sputter) + Al (pack)	0.5-0.7	3.3	70
Ni-15.8Cr-12.5Al-0.2Y (e.b.) + Pt (sputter)	0.5-0.7	4.5	62.5
Ni-15.8Cr-12.5Al-0.2Y (e.b.) + Pt (sputter)	< 1.4	3.4	62.5
Ni-24.0Co-18.8Cr-12.1Al-0.2Y (e.b.) + Pt (sputter)	0.5-0.7	3.1	62.5
Ni-24.0Co-18.8Cr-12.1Al-0.2Y (e.b.) + Pt (sputter)	0.9-1.1*	2.2	62.5
Ni-24.1Co-18.8Cr-12.0Al-0.2Y (e.b.)	> 1.9*	2.4	62.5
Ni-24.1Co-18.8Cr-12.0Al-0.2Y (e.b.)	> 2.0	2.7	62.5
Ni-16.4Cr-6.4Al-0.04Y (e.b.) + diffusion aluminide (pack-inward)	0.2-0.4	6.5	127
Ni-16.4Cr-6.4Al-0.04Y (e.b.) + diffusion aluminide (pack-inward)	0.2-0.4	3.2	127
Ni-17.0Cr-10.7Al-3.5Si-0.1Y (e.b.)	1.05-1.4	1.4	127
Ni-17.0Cr-10.7Al-3.5Si-0.1Y (e.b.)	1.3-1.6	1.6	127

\*NiCoCrAlY layer was very thin; possible abrasion of coating occurred during glass bead peening operation.

TABLE VI

578 K (600°F) COATING FRACTURE AND  $\gamma/\gamma' - \delta$  FAILURE STRAINS  
(NASA CONTRACT NAS3-16792)

Coating System	Nominal Coating Thickness (microns)	Coating Fracture Strain (%)	Specimen Fracture Strain (%)
Ni-15.2Cr-12.8Al-0.31Y	125	0.60-0.70	0.70
Ni-17.8Cr-12.6Al-0.31Y	125	0.40-0.49	0.74
Ni-29.4Co-19.1Cr-15.6Al-0.35Y	125	0.40-0.47	0.47
Ni-29.4Co-19.1Cr-15.6Al-0.35Y	125	0.40-0.48	0.48
Ni-15.2Cr-12.8Al-0.31Y + Pt	125	0.61-0.81	1.97
Ni-15.3Cr-7.1Al-0.34Y + Pack Aluminide	125	0.41-0.51	>7.15
Ni-15.3Cr-7.1Al-0.34Y + Pack Aluminide	125	0.40-0.52	6.1
Ductile Aluminide	30	0.51-0.67	4.04
Ductile Aluminide	30	0.79-1.02	2.28
Nickel/Chromize/Aluminize	100	0.40-0.50	6.04
Nickel/Chromize/Aluminize	100	0.41-0.51	4.83
Uncoated	—		3.56
Uncoated	—		3.40

TABLE VII

578 K (600°F) COATING AND  $\gamma/\gamma'$  -  $\delta$  SUBSTRATE FRACTURE STRAINS  
(AF CONTRACT F33657-71-C-0789)

Coating System	Nominal Coating Thickness (microns)	Coating Fracture Strain (%)	Specimen Fracture Strain (%)
PWA 270	60	>2.0	2.47
PWA 270	60	>2.0	2.58
PWA 270	40	>2.0	2.40
PWA 270	40	>2.0	2.70
PWA 270	125	1.10-1.18	1.18
PWA 270	125	>2.0	2.21
NiCrAlY + PWA 270	25 + 100	0.5-0.67	0.67
NiCrAlY + PWA 270	25 + 100	0-0.49	0.50
NiCrAlY + PWA 270	60 + 60	2.01	2.64
NiCrAlY + PWA 270	60 + 60	1.36-1.68	2.68
PWA 28	25	0.5-0.6	3.97
PWA 28	25	0.6-0.8	2.37
PWA 28	75	0.40	2.60
PWA 28	75	0.45	2.20
NiCrAlY + PWA 28	25 + 100	0.3-0.4	3.70
NiCrAlY + PWA 28	25 + 100	0.3-0.4	3.20
Uncoated	—	—	2.0-5.0

PWA 270: Ni-23Co-18Cr-12.5Al-0.3Y

NiCrAlY: Ni-18Cr-6Al-0.3Y

PWA 28: Diffusion Aluminide (outward)

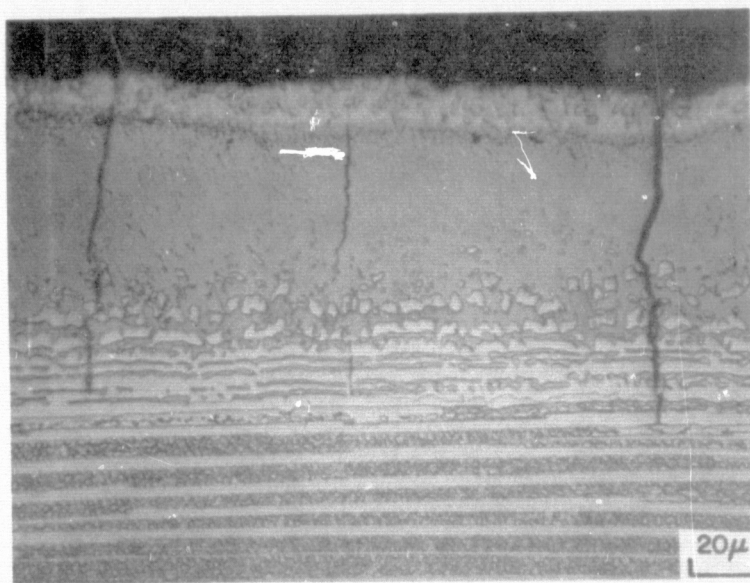


Figure 52 Post-Test Microstructure of Pt + Al Coated  $\gamma/\gamma' - \delta$  Tensile Ductility Specimen Showing Secondary Cracking. Coating Fracture Strain, 0.5 to 0.7%; Specimen Failure Strain, 4.2%; Test Temperature, 578 K. (K-13338)

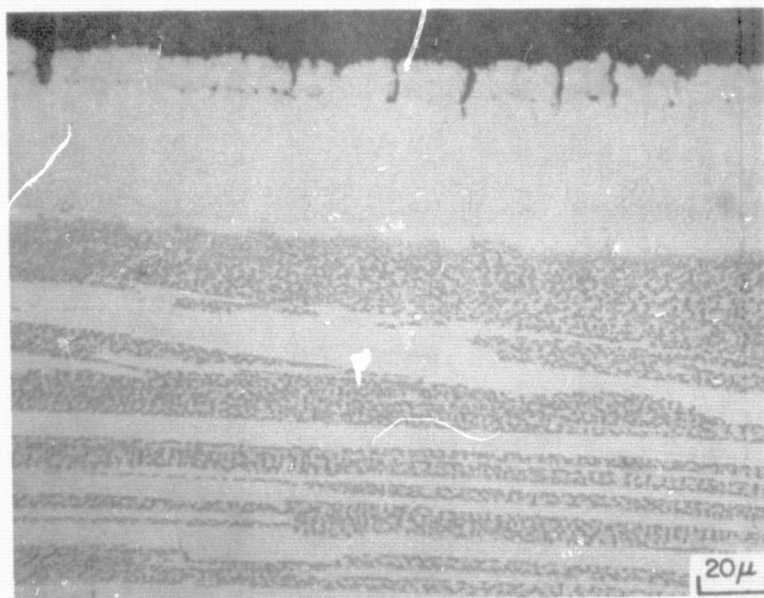


Figure 53 Post-Test Microstructure of NiCrAlY + Pt Coated  $\gamma/\gamma' - \delta$  Tensile Ductility Specimen Showing Secondary Cracking. Coating Fracture Strain, 0.5 to 0.7%; Specimen Failure Strain, 4.5%; Test Temperature, 578 K. (K-13338)

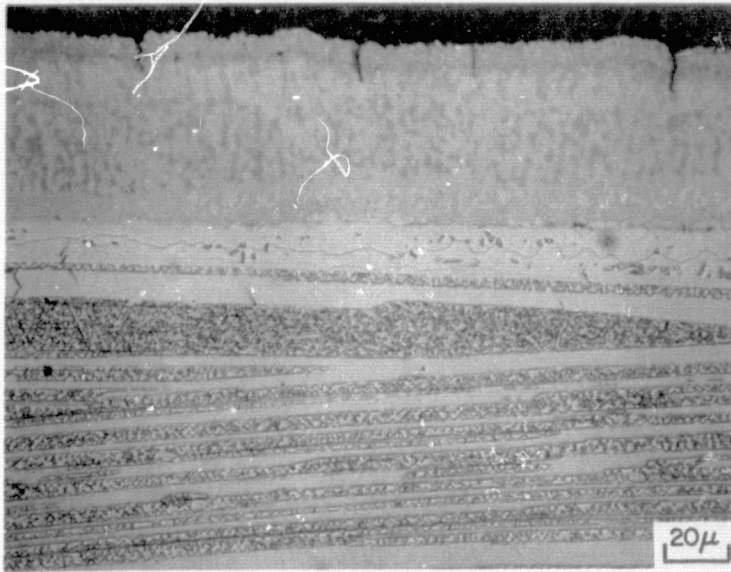


Figure 54 Post-Test Microstructure of NiCoCrAlY + Pt Coated  $\gamma/\gamma'$ - $\delta$  Tensile Ductility Specimen Showing Secondary Cracking. Coating Fracture Strain, 0.5 to 0.7%; Specimen Failure Strain, 3.1%; Test Temperature, 578 K. (K-13339)

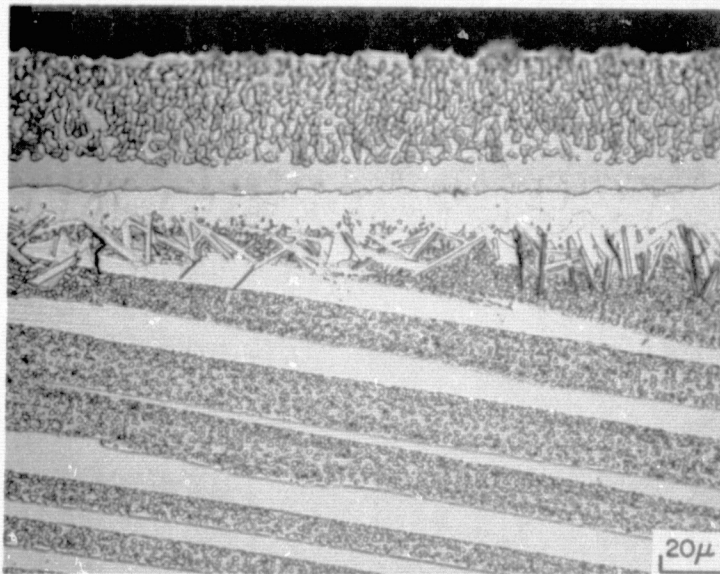
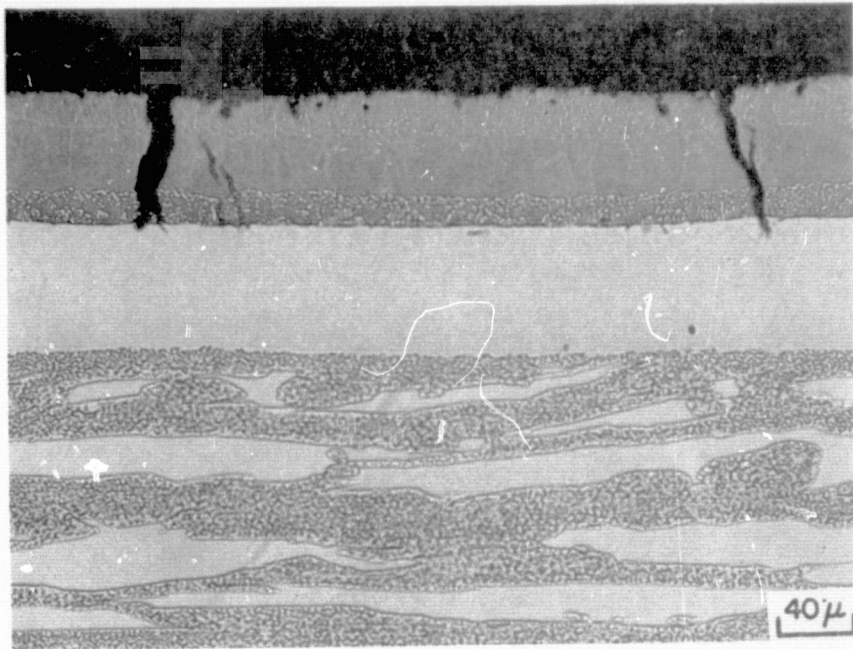
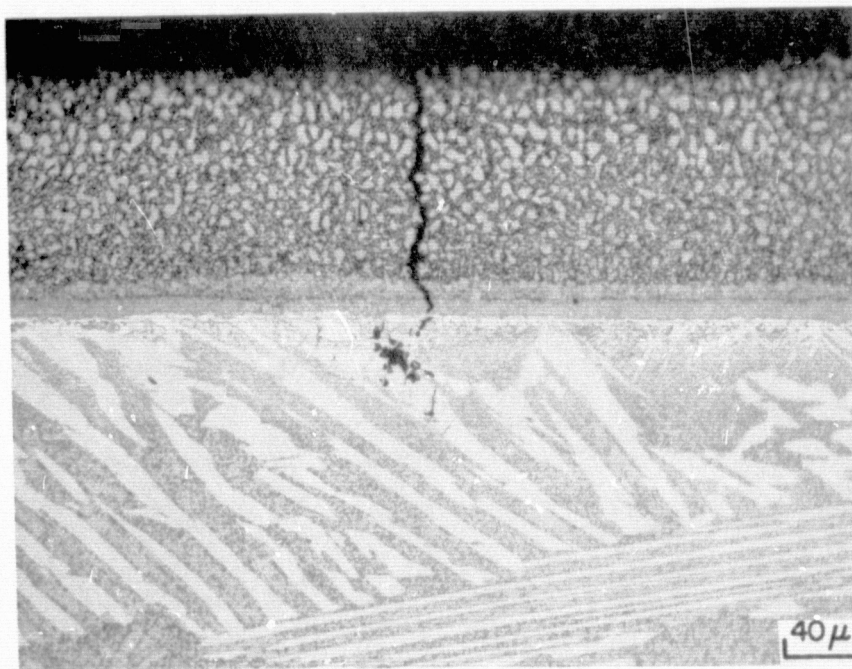


Figure 55 Post-Test Microstructure of NiCoCrAlY Coated  $\gamma/\gamma'$ - $\delta$  Tensile Ductility Specimen; Note Secondary Cracking in Diffusion Affected Substrate. Coating Fracture Strain, >2.0%; Substrate Failure Strain, 2.7%; Test Temperature, 578 K. (K-13339)



*Figure 56 Post-Test Microstructure of Low Aluminum NiCrAlY + Diffusion-Aluminide (Pack, Inward) Coated  $\gamma/\gamma'$  -  $\delta$  Tensile Ductility Specimen Showing Secondary Cracking Coating Fracture Strain, 0.2 to 0.4%; Specimen Failure Strain, 3.2%; Test Temperature, 578 K (K-13240)*



*Figure 57 Post-Test Microstructure of NiCrAlSiY Coated  $\gamma/\gamma'$  -  $\delta$  Tensile Ductility Specimen Showing Secondary Cracking. Coating Fracture Strain, 1.3 to 1.6%; Specimen Failure Strain, 1.6%; Test Temperature, 578 K.*

## VII. THERMOMECHANICAL FATIGUE TESTING

### A. BACKGROUND

Airfoil cracking due to the strain-temperature cycling, which occurs on acceleration and deceleration of a gas turbine engine, is one of the major factors limiting the life of high-pressure turbine blades. This fatigue cracking is caused by cyclic strains induced by temperature gradients in the airfoil, usually in the vicinity of the leading or trailing edge. In addition, it has been observed that the thermal fatigue life of a given superalloy can be significantly altered by application of oxidation resistant coatings (ref. 24). Consequently, it is important to evaluate the thermal fatigue properties of all candidate materials for turbine blade applications.

Advanced hollow airfoil designs employ complex internal air cooling schemes which are necessary to maintain the structural superalloy at acceptable temperature levels. Depending on the specific component, thin-walled sections can experience widely different thermal fatigue cycles wherein the maximum tensile strain may occur at low, intermediate or high temperatures. Laboratory thermomechanical fatigue tests are designed to simulate the important aspects of these engine thermal cycles. Thermomechanical fatigue (TMF) Cycle I peaks tensile and compressive strains at the low and high temperature, respectively; Cycle II peaks the tensile and compressive strains at high and low temperatures, respectively (see Figure 54).

An investigation of the mechanical properties of NiCoCrAlY coatings indicated that, at high temperatures, the flow stress (creep resistance) of ductile NiCoCrAlY coatings is low, and significant creep can occur at low strain rates (ref. 22). As a result, stress relaxation occurs in the coating at high temperatures during cruise conditions, and equilibration of the coating to a zero elastic strain condition occurs. It is therefore convenient to define the zero strain condition of the coating at the maximum temperature of the TMF cycle, as shown in Figure 58. While this type of data has not been obtained for NiCrAlY and NiCrAlY + Pt coatings, similar behavior is expected for these coating systems.

Because the coating and superalloy substrate will, in general, have different coefficients of thermal expansion,  $\alpha$ , significant thermal expansion mismatch strains can develop in a coating during thermal cycling. These tensile or compressive thermal expansion mismatch strains can, respectively, increase or decrease the magnitude of the coating strain as shown in Figure 58.

When significant Cycle I (maximum tension at minimum temperature) type thermomechanical strain conditions are present on an airfoil, it is of particular concern from a coating standpoint since many coatings have limited ductility at relatively low temperatures (refs. 24, 27). Cycle II, which peaks the tensile strain at relatively high temperatures, is generally of less concern from a coating viewpoint. Since coating-substrate interactions were of primary interest in these investigations, NiCrAlY and NiCrAlY + Pt coated thermomechanical fatigue specimens were evaluated under Cycle I conditions. A NiCrAlY + Pt coated  $\gamma/\gamma' - \delta$  specimen was evaluated under Cycle II conditions for comparative purposes, however, in an Air Force program (ref. 4).

A fracture mechanics model (ref. 21) has recently been developed for analysis of the propagation of coating initiated thermal fatigue cracks into superalloy substrates under Cycle I thermal strain conditions (maximum tension at minimum temperature). This model indicated that, in addition to the magnitude of the thermomechanical strain range ( $\Delta\epsilon_{TM}$ ), coating-substrate thermal expansion mismatch strain ( $\Delta\epsilon_{\alpha}$ ), coating thickness ( $t$ ), and the coating-substrate elastic modulus ratio ( $E_c/E_s$ ) significantly affect the rate of crack propagation into the substrate.

Based on the burner rig and hot corrosion test results obtained in this program, as well as previous data obtained under NASA (ref. 5) and Air Force (ref. 4) contracts, the NiCrAlY + Pt and NiCrAlY coating systems were selected for coating the  $\gamma/\gamma' - \delta$  (6 Cr) specimens.

## B. SPECIMEN PREPARATION

Four  $\gamma/\gamma' - \delta$  (6 Cr) thermomechanical fatigue castings were directionally solidified in contoured alumina investment casting shell molds and machined to the required specimen geometry as described elsewhere (refs. 4, 5). These specimens were then coated with  $127\mu$  (0.005 inch) of Ni-18Cr-12Al-0.3Y by the electron beam vapor deposition process. Two of these specimens also received a sputtered  $6\mu$  (0.00025 inch) thick surface layer of Pt which was subsequently diffused into the NiCrAlY layer during the postcoating diffusion heat treatment at 1352 K.

## C. TEST PROCEDURE

Thermomechanical strain cycling tests were performed in a closed loop servo hydraulic fatigue machine which provided synchronized, independently programmable thermal and mechanical cycling. Cycle I temperature and strain conditions were programmed so that the specimen would be in tension (+0.15 percent strain) at the minimum temperature and in compression (-0.15 percent strain) at the maximum temperature. An induction coil surrounding the specimen was used for heating, and forced air directed on the outer surface of the specimen was used for cooling. The cycle period was 135 seconds.

The Cycle I temperature range (755 to 1200 K) which was used for specimens E487 and E488 was based on a thermal strain analysis for an air cooled  $\gamma/\gamma' - \delta$  eutectic alloy turbine blade (ref. 28). The 0.3 percent strain range, which was used in these tests, permits a direct comparison with the data obtained (prior to the thermal strain analysis) with Cycle I (700 to 1311 K) conditions; it should be noted, however, that the calculated thermal strain range for an air-cooled eutectic alloy turbine blade is lower (0.16 percent strain).

Plastic replicas of the coating surface were taken periodically to facilitate detection of coating cracks. Post-test analysis included visual examination of fracture surfaces of selected coating-initiated thermal fatigue cracks and metallographic examination of the coating and substrate microstructures.

## D. RESULTS AND DISCUSSION

Respective thermomechanical fatigue lives of NiCrAlY and NiCrAlY + Pt coated  $\gamma/\gamma' - \delta$  (6 Cr) specimens which were tested under this contract and previous NASA (ref. 5) and

Air Force (ref. 4) contracts are provided in Table VIII and Figure 59; in addition, Cycle I data from an internal P&WA program for D.S. MAR-M 200 + Hf specimens coated with these coating systems is included for comparison. It can be seen from this figure that the data generated in this contract represents the longest Cycle I thermal fatigue lives which have been thus far obtained with the  $\gamma/\gamma' - \delta$  alloy.

Further inspection of Figure 59 indicates that decreasing the maximum temperature from 1422 K (2100°F) to 1200 K (1700°F) appears to significantly improve the Cycle I thermal fatigue life.

As previously indicated, the shape of the strain-temperature cycle is a significant factor. The NiCrAlY + Pt coated  $\gamma/\gamma' - \delta$  specimen which was tested under Cycle II (700 to 1311 K;  $\Delta\epsilon_{TM} = 0.43$  percent) was unfailed after 4386 cycles; post-test examination of this specimen indicated that the cracking was confined to the oxide scale.

In addition, it should be noted that, for a given strain range, the coated D.S. MAR-M 200 + Hf specimens exhibited better Cycle I thermal fatigue lives than the coated  $\gamma/\gamma' - \delta$  specimens.

Post-test metallographic examination of NiCrAlY coated  $\gamma/\gamma' - \delta$  specimen E300, which was tested for 2678 cycles under Cycle I (700 to 1311 K;  $\Delta\epsilon_{TM} = 0.3$  percent) conditions, indicated that oxide inclusions were present in the substrate microstructure adjacent to the primary crack and probably contributed to crack initiation (Figures 60 and 61). Inspection of Table VIII indicates that oxide casting inclusions in the substrate contributed to initiation of the primary crack in six of the twelve  $\gamma/\gamma' - \delta$  specimens conditions. In general, the shortest Cycle I failure lives at a given strain range in Figure 59 are associated with initiation of the primary crack at this type of defect.

Figure 60 shows the cross-section microstructure of the NiCrAlY coated  $\gamma/\gamma' - \delta$  specimen (E300) adjacent to the primary crack and indicates that, in addition to the oxide inclusions, the  $\gamma/\gamma' - \delta$  microstructure was cellular and contained  $\delta$  "dendrites" which indicate that the columbium content of the alloy was slightly excessive. Figure 57 shows a longitudinal view of the specimen microstructure. A secondary crack which initiated at or near the uncoated internal surface is shown in this figure; it is probable that oxide inclusions or casting porosity may have contributed to the initiation of this crack.

The NiCrAlY coating microstructure which developed during the 2678-cycle thermal fatigue test is more complex than the microstructure of the virgin coating. Briefly, the virgin NiCrAlY coating has a predominantly  $\gamma$  (Ni solid solution) +  $\beta$  (NiAl) microstructure after a diffusion heat treatment at 1352 K. At lower temperatures, the  $\gamma + \beta$  microstructure becomes unstable and  $\alpha$  (chromium) and  $\gamma'$  ( $\text{Ni}_3\text{Al}$ ) phases precipitate. Specifically, the Ni-Cr-Al phase diagram (ref. 29) indicates that at 1273 K the Ni-18Cr-12Al composition should exist as a four phase,  $\gamma + \gamma' + \beta + \alpha$ , microstructure. At a lower temperature 1123 K, the stable coating phases would be predominantly  $\gamma'$  and  $\alpha$ . The outer portion of the NiCrAlY coating reflects the cyclic precipitation and solutioning reactions which occur during thermal cycling (700 to 1311 K); all four of the above phases appear to be present in this part of the coating (Figures 60 and 61). In contrast, the coating adjacent to the  $\gamma/\gamma' - \delta$  substrate is affected by columbium diffusion from the substrate and aluminum loss to the substrate; the phases present in the coating at this location appear to be  $\gamma$ ,  $\gamma'$  and  $\alpha$ .

Some secondary cracks were also initiated by pit defects in the NiCrAlY coating. Some of these cracks were broken open for analysis of the fracture surface with the scanning electron microscope (Figure 62). It is interesting to note that the thermal fatigue crack appeared to be propagating faster in the substrate than in the coating. Surface crack growth data (Figure 63) for three of these cracks in specimen E300 was obtained from plastic replicas of the specimen surface which were taken periodically during the test. Crack growth rates in the NiCrAlY coating were initially constant for a particular crack; the range of initial coating crack propagation rates was approximately 0.12 to 0.20  $\mu$ /cycle ( $4.6 \times 10^{-6}$  to  $7.8 \times 10^{-6}$  inch/cycle) for the three secondary cracks which were measured.

The longer specimen life of the second NiCrAlY coated  $\gamma/\gamma' - \delta$  specimen E487, which was unfailed after 7286 cycles of testing under Cycle I (755 to 1200 K;  $\Delta\epsilon_{TM} = 0.3$  percent) conditions, is attributed to the lower maximum temperature and/or reduced temperature range as well as improved specimen quality. Unlike the previous specimen, oxide inclusions appeared to be absent in the  $\gamma/\gamma' - \delta$  substrate. In addition, examination of the series of surface replicas, which were taken periodically during the test, indicated that the delay period for crack initiation at pit and flake defects in the coating was approximately 4800 to 5600 cycles. A fracture mechanics analysis of thermal fatigue crack penetration into the  $\gamma/\gamma' - \delta$  substrate indicated that the rate of crack propagation into the substrate was also reduced. (This analysis is discussed in greater detail later in this section.) Surface measurements of crack lengths in specimen E487 indicated that the rate of propagation,  $d(2b)/dN$ , of thermal fatigue cracks in the NiCrAlY coating were about 0.22 to 0.27  $\mu$ /cycle; these coating crack propagation rates are similar to those obtained from specimen E300 (0.12 to 0.20  $\mu$ /cycle).

Post-test metallographic examination of the NiCrAlY coated  $\gamma/\gamma' - \delta$  specimen E487 indicated that the coating microstructure was predominately  $\gamma$ ,  $\gamma'$  and  $\alpha$  (See Figure 60); this microstructure is thought to be the result of the lower maximum temperature (1200 K) of the thermomechanical fatigue test. Figure 64 also indicates that the eutectic alloy microstructure was basically lamellar with a small fraction of primary  $\delta$  phase "dendrites".

A small thermal fatigue crack is also shown in Figure 64. This crack propagated to a depth of  $\sim 55\mu$  into the eutectic alloy and was filled with oxide in the substrate. An oxidation affected zone was observed adjacent to the substrate crack. Two thermal fatigue cracks were broken open at the conclusion of the test in order to examine the thermal fatigue fracture surface. These cracks had an approximately semielliptical crack surface geometry. The maximum depth of coating crack propagation into the eutectic alloy substrate was 81  $\mu$ . The average penetration rate of this crack into the substrate (substrate crack depth/cycle increment between coating crack initiation and end of test) was approximately  $4 \times 10^{-2} \mu$ /cycle.

The substrate microstructure of the NiCrAlY + Pt coated  $\gamma/\gamma' - \delta$  specimen E290, which was tested under Cycle I (700 to 1311 K;  $\Delta\epsilon_{TM} = 0.3$  percent) conditions, had a lamellar structure which contained fewer  $\delta$  "dendrites" (Figure 65); this specimen also contained significantly fewer oxide inclusions. It is thought that the relatively long life, 4486 cycles to a 50 percent load drop (a specimen failure criterion), was partly a result of the improved microstructure. Examination of surface replicas which were taken during this test indicated that most of the thermal fatigue cracks, including the one that eventually resulted in specimen

failure, were initiated at coating pits. (One secondary thermal fatigue crack was initiated by substrate inclusions.)

Inspection of Table VIII shows that specimen failures in three of the twelve coated  $\gamma/\gamma' - \delta$  specimens, which have been tested under Cycle I conditions, had the primary crack initiated at a defect in the overlay coating; in addition, four of the other specimens had exhibited coating defect initiated thermal fatigue cracks. Therefore, when significant defects in the  $\gamma/\gamma' - \delta$  substrate are absent, thermal fatigue cracks may be expected to initiate at defects in the coating. (The formation of pit and flake defects in overlay coatings has been discussed previously (ref. 30.))

Surface crack growth data were obtained from the replicas for several of these cracks. Crack growth rates in the NiCrAlY + Pt coating were also initially constant for a particular crack; the range of initial coating crack propagation rates was approximately 0.19 to 0.42  $\mu$ /cycle ( $7.5 \times 10^{-6}$  to  $1.65 \times 10^{-5}$  inch/cycle). These crack growth rates are slightly faster than crack growth rates which were obtained for similar cracks in the NiCrAlY coating. Surface crack growth data is shown graphically in Figure 66 for five of these cracks.

At the conclusion of this test, a few of the pit initiated cracks in the NiCrAlY + Pt coated  $\gamma/\gamma' - \delta$  specimen were broken open in order to examine the fracture surfaces; typical cracks (D and E) are shown in Figure 67. It can be seen that the coating initiated thermal fatigue cracks develop an approximately semielliptical geometry. Referring to Figures 66 and 67, it can be seen that crack D was propagating into the substrate during the period of relatively constant growth. (Similar thermomechanical fatigue tests of NiCoCrAlY coated D.S. MAR-M 200 + Hf have indicated that substrate crack initiation is approximately concurrent with crack initiation at through-thickness coating defects (pits and flakes) (ref. 24).

Fracture surface and replica analysis of the largest pit initiated crack (F) indicated that it had propagated to a depth of 1016  $\mu$  (40 mils) (the wall thickness of the specimen) when the crack had a surface length of approximately 3048  $\mu$  (120 mils); this observation indicates that approximately 3200 cycles were involved in propagation of the crack from the coating-substrate interface to a depth of 1016  $\mu$ .

The microstructures of two pit initiated thermal fatigue cracks are shown in Figure 68. These cracks are filled with oxide, and a relatively large oxidation affected zone is present around both cracks in the substrate. (See Figure 64 for a comparison of the crack tip microstructure produced with a lower (1200 K) peak cycle temperature.) In the case of the larger crack, which is almost through the wall thickness, the  $\delta$  phase is cracking a short distance in front of the oxygen affected zone at the crack tip. This difference in crack propagation behavior is thought to be associated with the larger strain intensity factor range of the longer crack.

The post-test microstructure of the NiCrAlY + Pt coating (Figure 65) adjacent to the  $\gamma/\gamma' - \delta$  substrate was similar to that of the NiCrAlY coating. As described in Section III (and ref. 5), the outer portion of the NiCrAlY coating was significantly altered by inter-diffusion with the platinum surface layer.

Post-test examination of the NiCrAlY + Pt coated  $\gamma/\gamma' - \delta$  specimen E488, which had a thermal fatigue life of 5270 cycles under Cycle I (755 to 1200 K;  $\Delta\epsilon_{TM} = 0.3$  percent), indicated that the primary crack in the specimen was initiated at a flake defect in the coating. Examination of the series of surface replicas indicated that the coating crack initiation occurred at the flake defect after  $\sim 1500$  cycles.

Additional inspection of the thermal fatigue crack in the  $\gamma/\gamma' - \delta$  substrate indicated that the fracture surface was relatively smooth to a depth of about  $700\mu$  (0.028 inch); at this depth, the fracture surface became rougher. The surface length (2b) of the crack was approximately  $3000\mu$  when the substrate crack depth was  $700\mu$ . Correlation of the fracture surface measurement with replica crack length measurements indicated that the transition occurred approximately 600 cycles before failure. It is speculated that the roughness transition on the fracture surface may indicate the start of  $\delta$  phase microcracking ahead of the main crack front.

Metallographic examination of this NiCrAlY + Pt coated  $\gamma/\gamma' - \delta$  specimen (Figure 69) indicated that the coating microstructure appeared to be predominantly  $\gamma'$  and  $\alpha$  which is characteristic of NiCrAl-type coatings aged at temperatures below 1200 K. This coating microstructure is also observed in the "cold zones" of NiCrAlY + Pt coated burner rig specimens tested at 1366 K (hot zone temperature) (ref. 5). The eutectic alloy microstructure was basically lamellar with a small fraction of primary  $\delta$  phase "dendrites".

As previously mentioned, a fracture mechanics model has recently been developed to facilitate the analysis of coating crack propagation into superalloy substrates (ref.21). This model was modified by including the appropriate crack geometry correction factor for a semielliptical surface crack (ref. 31), to account for the observed crack shape, and used to estimate initial and final values of the strain intensity factor range ( $\Delta K_e$ ) for the most severe coating initiated cracks in six  $\gamma/\gamma' - \delta$  specimens which were tested under Cycle I conditions. The calculation of the initial value of  $\Delta K_e$  assumed that the coating crack had a semicircular geometry when substrate cracking initiated. Geometry correction factors used in calculating the final values of  $\Delta K_e$  were based on the observed crack length and depth measurements from the fracture surfaces. These estimated strain intensity factor range values and average substrate crack propagation rates are provided in Figure 70. Crack propagation rate (da/dN) vs.  $\Delta K_e$  data for Cycle I (700 to 1311 K) conditions for the  $\gamma/\gamma' - \delta$  alloy (ref. 4) are also provided for comparison.

Further analysis of the data in Figure 70 indicated that, for Cycle I (700 to 1311 K) conditions, a Paris (ref. 32) type crack propagation relationship,

$$da/dN = 71 \Delta K_e^{2.0} \text{ meter/cycle,}$$

could represent both types of data. Integration of this crack propagation relationship from the coating-substrate interface to the final crack depths of the four cracks which were considered resulted in cycle increments for crack propagation which were within  $\pm 32$  percent of the observed cycles; i.e.,

$$N = \int_{a_0}^{a_f} \frac{da}{71 \Delta K_e^{2.0}} = N_{\text{observed}} (\pm 32\%).$$

A similar analysis of the Cycle I (755 to 1200 K) data indicates that crack propagation rates are about a factor of three slower under these conditions if a crack growth rate relationship with the same exponential dependence on  $\Delta K_e$  is assumed.

Finally, the Cycle I (700 to 1311 K) crack growth rate relationship was extrapolated to lower values of  $da/dN$  and  $\Delta K_e$  in order to make lower strain range estimates of the number of cycles required to propagate a crack in a  $100\mu$  thick NiCrAlY + Pt coating from the coating-substrate interface to a depth of  $1000\mu$  (the wall thickness) in the  $\gamma/\gamma' - \delta$  specimen; the estimated propagation cycles are shown in Figure 59. For a given strain range, propagation life estimates would be longer by about a factor of three for Cycle I (755 to 1200 K) conditions.

It should be stressed that these estimates at lower strain ranges should be used only as first order approximations. For example, the actual  $da/dN$  vs.  $\Delta K_e$  relationship for the  $\gamma/\gamma' - \delta$  alloy may extrapolate to lower values of  $da/dN$  with a different (either increased or decreased) dependence on the value of  $\Delta K_e$ . In addition, environmental effects may be more significant at very low crack propagation rates and, therefore, may invalidate the extrapolation of the assumed  $da/dN$  vs.  $\Delta K_e$  relationship.

An additional observation concerning coating crack initiation is that decreasing the Cycle I temperature range from 700 - 1311 K to 755 - 1200 K resulted in a significant improvement in the cycles to initiate coating cracks at pit and flake defects. For example, the cycles to coating crack initiation increased by factors of 3 to 13 for the NiCrAlY + Pt and NiCrAlY coatings, respectively, evaluated under Cycle I (755 to 1200 K;  $\Delta\epsilon_{TM} = 0.3$  percent) conditions. The improvement in crack initiation resistance is thought to be associated with decreasing the magnitude of the coating-substrate thermal expansion mismatch strain range,  $\Delta\epsilon_\alpha$ , in the NiCrAlY ( $\Delta\epsilon_\alpha$  reduced by  $\sim 0.12$  percent strain) and NiCrAlY + Pt ( $\Delta\epsilon_\alpha$  reduced by  $\sim 0.11$  percent strain) coating systems. This trend is consistent with thermomechanical coating crack initiation data for NiCoCrAlY coated superalloys (ref. 24); that work indicated that the cycles to coating crack initiation at coating defects exhibited a Coffin-Manson type elastic strain range versus cycles to coating crack initiation ( $N_I$ ) relationship,

$$(\Delta\epsilon_\alpha + \Delta\epsilon_{TM}) = AN_I^{-0.07}$$

Assuming that a similar relationship applies for the NiCrAlY and NiCrAlY + Pt coating systems, the cycles to coating crack initiation is expected to be a significant contribution (e.g., greater than 5000 cycles) to the fatigue life at the 0.16 percent strain range anticipated for an air cooled eutectic alloy turbine blade (ref. 28).

Thus, the distinction between the total fatigue life (crack initiation and propagation) and the propagation life is important. At relatively low thermal strain range values, which are

characteristic of long life commercial gas turbine blades, the cycles required to initiate a coating crack can be a significant fraction of the total thermal fatigue life. Therefore, actual thermal fatigue lives will be expected to exceed the propagation life estimates in Figure 59.

In summary, thermal fatigue crack initiation and propagation in coated  $\gamma/\gamma' - \delta$  specimens have been evaluated, and the following conclusions were derived:

- The strain-temperature cycle shape has a significant effect on coating crack initiation; Cycle I, which peaks tensile strains at the minimum temperature, is the most severe from a coatings standpoint.
- When significant defects in the  $\gamma/\gamma' - \delta$  substrate are absent, thermal fatigue cracks have a strong tendency to initiate at defects in the NiCrAlY + Pt and NiCrAlY coatings.
- Reducing the Cycle I temperature range from 700 - 1311 K to 755 - 1200 K improves the resistance to crack initiation of NiCrAlY + Pt and NiCrAlY coatings on the  $\gamma/\gamma' - \delta$  alloy.
- For a given value of  $\Delta K_{\text{Ic}}$ , the crack propagation rate in the substrate is decreased by a factor of about three by reducing the Cycle I temperature range from 700 - 1311 K to 755 - 1200 K.
- At relatively low Cycle I thermal strain ranges, the cycles required to initiate a crack in NiCrAlY and NiCrAlY + Pt coatings is expected to be a significant fraction of the total fatigue life.
- For a given strain range, the coated D.S. MAR-M200 + Hf specimens exhibited better Cycle I (700 to 1311 K) thermal fatigue lives than coated  $\gamma/\gamma' - \delta$  specimens.

**TABLE VIII**  
**THERMOMECHANICAL FATIGUE TEST CONDITIONS**

<u>Specimen Identification</u>	<u>Coating Chemistry, w/o</u>	<u>Substrate</u>	<u>Cycle</u>	<u>Number of Cycles</u>	<u><math>\Delta\epsilon_{TM}</math> %</u>	<u>Comments</u>
E300*	Ni-17.7Cr-12.4Al-0.17Y	$\gamma/\gamma' - \delta$	I (700-1311 K) (800-1900°F)	2678	0.30	Coating crack initiation at coating pits was first detected after ~ 409 cycles; primary crack was initiated by substrate inclusions.
E487*	Ni-18.9Cr-11.5Al-0.17Y	$\gamma/\gamma' - \delta$	I (755-1200 K)	7286	0.30	Crack initiation at coating defect occurred after ~ 5300 cycles; specimen had not failed when testing was discontinued.
1422-69**	Ni-16.8Cr-11.8Al-0.45Y	D.S. Mar-M 200 + Hf	I (700-1311 K)	590 591-1083 1084-2224 2225-3277	0.25 0.30 0.35 0.40	Coating crack initiation was first detected after ~ 1455 cycles; specimen was unfailed when testing was discontinued.
E290*	Ni-17.7Cr-12.4Al-0.17Y + Pt	$\gamma/\gamma' - \delta$	I (700-1311 K)	4486	0.30	Coating crack initiation was first detected at pit defects after ~ 450 cycles.
E488*	Ni-18.9Cr-11.5Al-0.17Y + Pt	$\gamma/\gamma' - \delta$	I (755 - 1200 K)	5270	0.30	Primary crack initiated at coating flake after ~ 1500 cycles.
E146***	Ni-18.6Cr-11.4Al-0.16Y + Pt	$\gamma/\gamma' - \delta$	I (700-1311 K)	119	0.50	Failed due to oxide inclusions in substrate.
A-74-124***	Ni-18.6Cr-11.4Al-0.16Y + Pt	$\gamma/\gamma' - \delta$	I (700-1311 K)	593	0.50	Failed in a cellular band in substrate.
E194***	Ni~18Cr~12Al~0.3Y + Pt	$\gamma/\gamma' - \delta$	I (700-1311 K) (800-1900°F)	29	0.51	Failed due to oxide inclusions in substrate.
E279****	Ni~18Cr~12Al~0.3Y + Pt	$\gamma/\gamma' - \delta$	I (700-1311 K)	1157	0.33	Failure initiation at oxide inclusion in substrate; secondary coating crack initiation at pit defects was first detected after 89 cycles.
E204****	Ni~18Cr~12Al~0.3Y + Pt	$\gamma/\gamma' - \delta$	I (700-1311 K)	637	0.46	Primary crack was initiated at a coating pit.
E278****	Ni~18Cr~12Al~0.3Y + Pt	$\gamma/\gamma' - \delta$	I (700-1311 K)	737	0.42	Failure initiated at internal surface.
E179****	Ni~18Cr~12Al~0.3Y + Pt	$\gamma/\gamma' - \delta$	I (700-1311 K)	620	0.43	Failure initiation at oxide inclusion in substrate.
E342****	Ni~18Cr~12Al~0.3Y + Pt	$\gamma/\gamma' - \delta$	II (700-1311 K)	4386	0.43	Unfailed; cracking confined to surface oxide scale.
E301****	Ni~18Cr~12Al~0.3Y + Pt	$\gamma/\gamma' - \delta$	I (700-1422 K) (800-2100°F)	2012	0.30	Coating crack initiation at coating pit occurred after approximately 445 cycles; primary crack was probably associated with oxide inclusions in substrate.
1422-72**	Ni-17.6Cr-12.4Al-0.27Y + Pt	DS Mar-M 200 + Hf	I (700-1311 K)	1000 1001-2296 2297-3139 3140-5165	0.30 0.35 0.40 0.44	Coating cracks initiation associated with surface rumpling; specimen had not failed when testing was discontinued.

$\Delta\epsilon_{TM}$ : Thermomechanical strain range which was applied to specimen.

\* Specimen tested under Contract NAS3-18920.

\*\* Data from an internal P&WA program.

\*\*\* Specimen tested under Contract NAS3-16792.

\*\*\*\* Specimen tested under Contract F33657-71-C-0789.

ORIGINAL PAGE IS  
OF POOR QUALITY

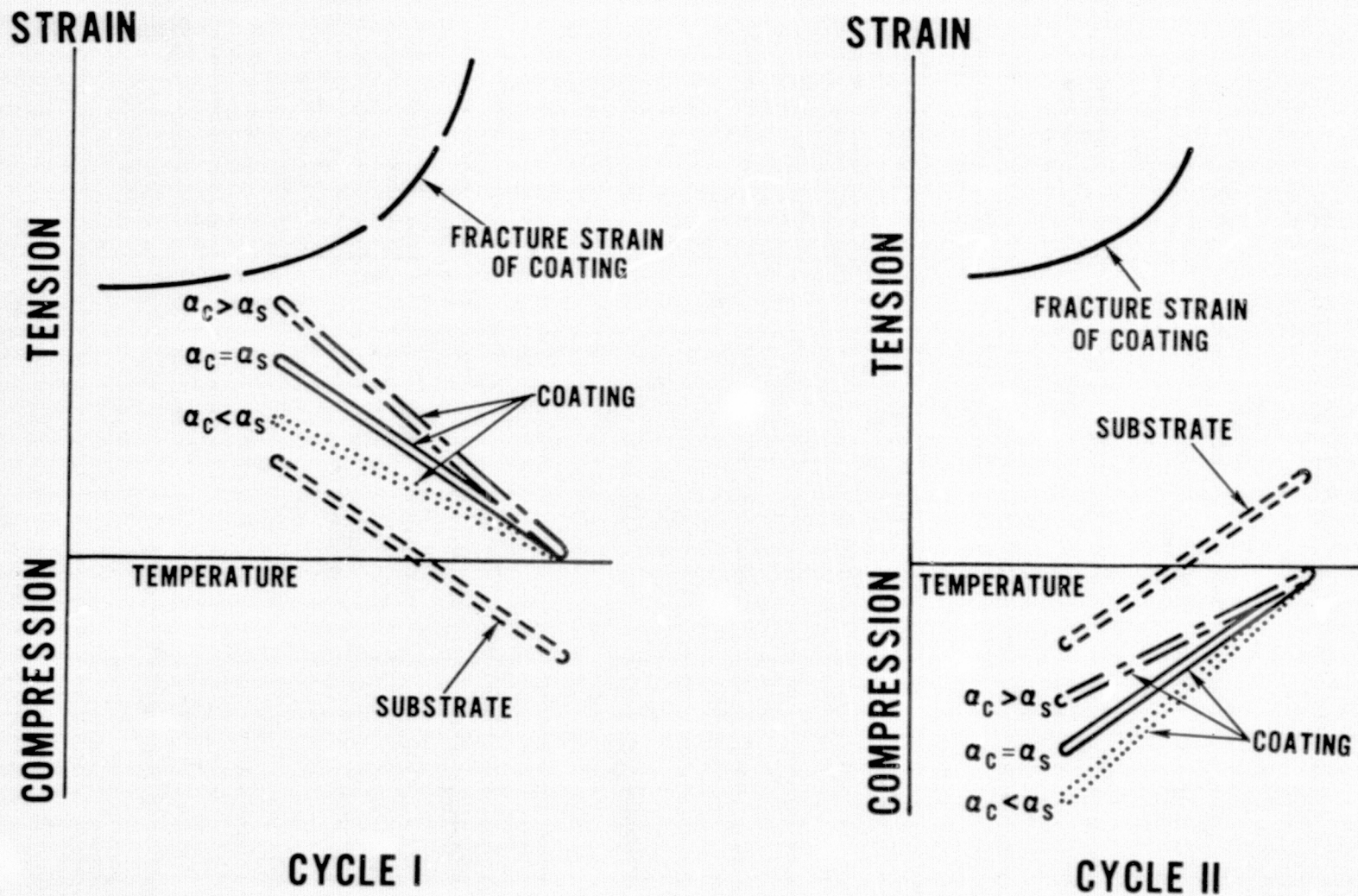


Figure 58 Schematic Relationship between Thermomechanical Fatigue Cycles in Substrate and Coating. The Zero-Strain Condition of the Coating is Set at the Maximum Temperature of the Thermomechanical Fatigue Cycle.

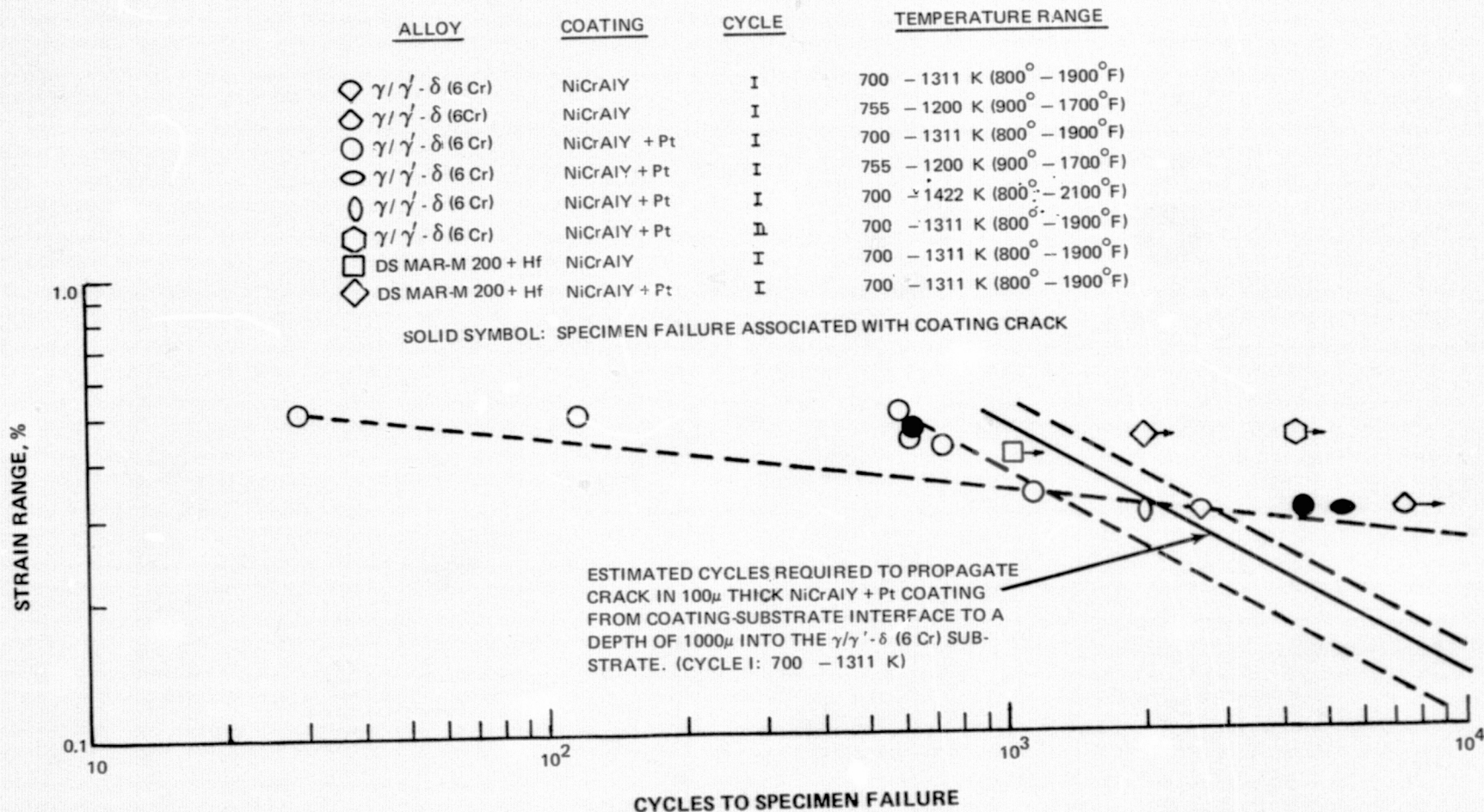


Figure 59 Thermal Fatigue Lives of NiCrAlY and NiCrAlY + Pt Coated  $\gamma/\gamma' - \delta$  and D.S. MAR-M 200 + Hf Specimens.

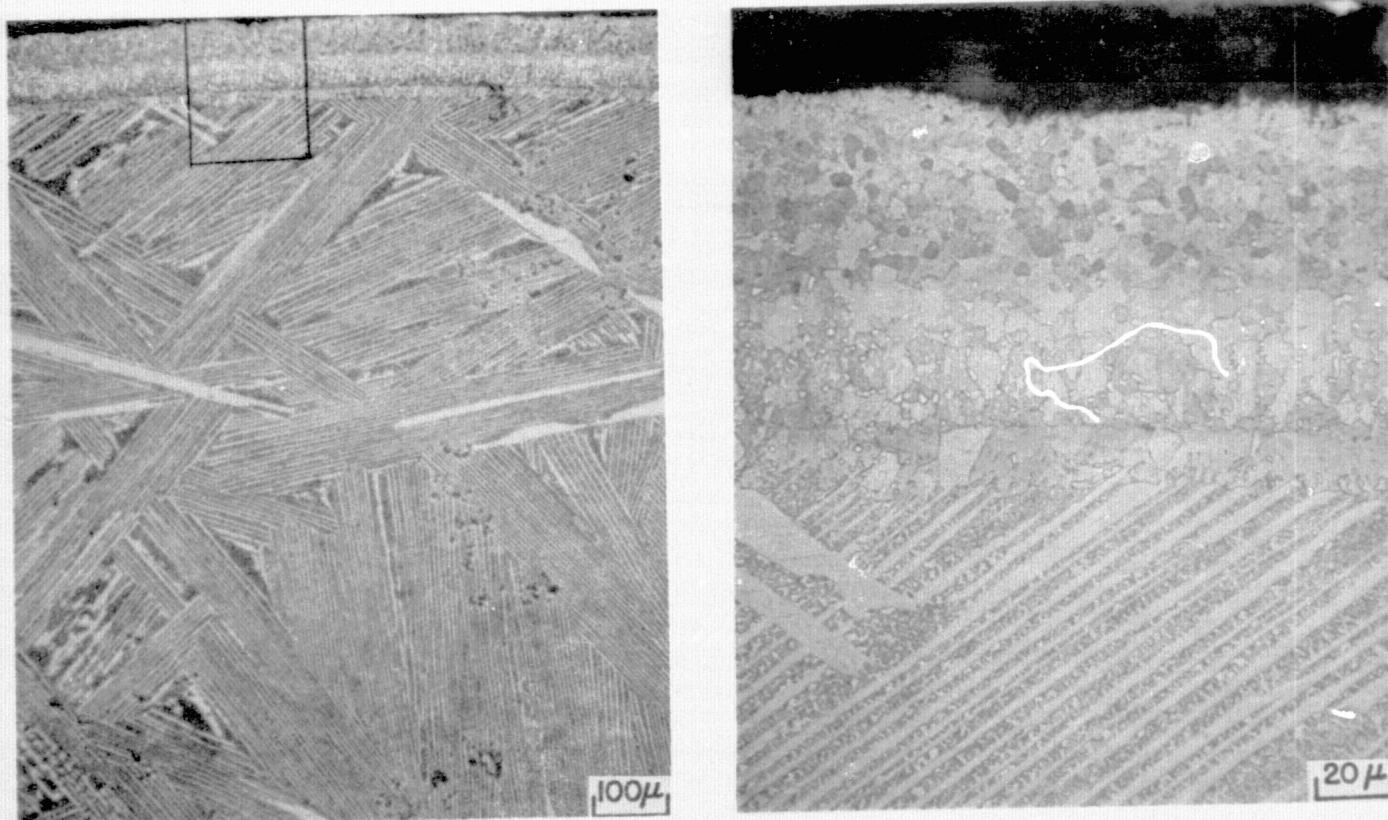


Figure 60 Microstructure of NiCrAlY Coated  $\gamma/\gamma'$  -  $\delta$  (6Cr) Specimen (E 300) which was Evaluated for 2678 Cycles in a Cycle I (700 to 1311 K;  $\Delta\epsilon_{TM} = 0.30\%$ ) Thermomechanical Fatigue Test. (K-16733)

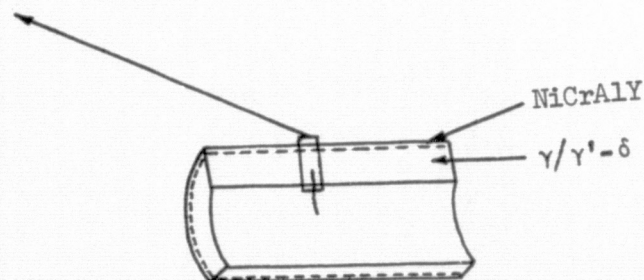
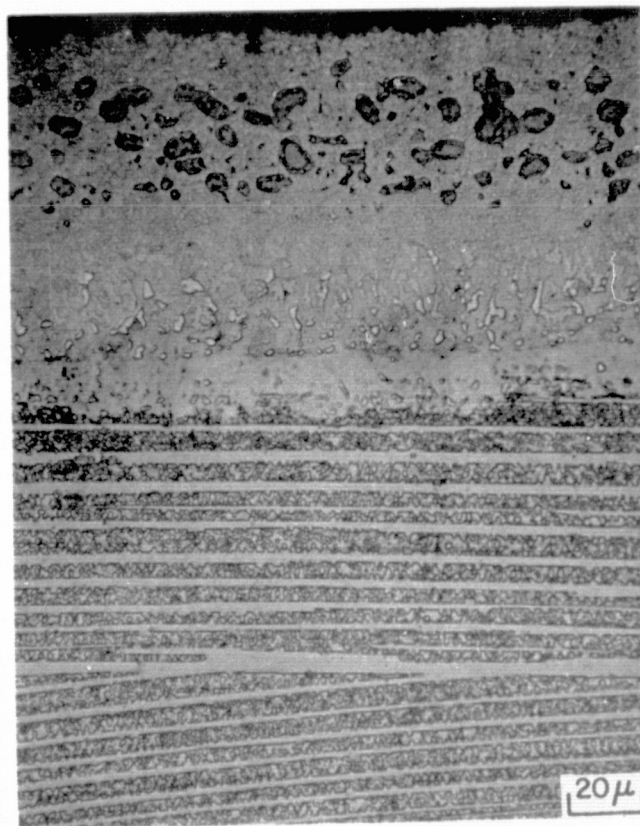


Figure 61 Longitudinal Microstructure and Secondary Crack Morphology in NiCrAlY Coated  $\gamma/\gamma' - \delta$  (6Cr) Specimen (E 300) which was Evaluated for 2678 Cycles in a Cycle I (700 to 1311 K;  $\Delta\epsilon_{TM} = 0.30\%$ ) Thermomechanical Fatigue Test. Oxide Inclusions and Substrate Porosity may have Contributed to Crack Initiation. (K-16734)



*Figure 62 Scanning Electron Microscope (SEM) Fracture Surface Photograph of Secondary Thermal Fatigue Crack in NiCrAlY Coated  $\gamma/\gamma'$  -  $\delta$  Specimen (E 300) which was Evaluated for 2678 Cycles in a Cycle I (700 to 1311 K;  $\Delta\epsilon_{TM} = 0.30\%$ ) Thermomechanical Fatigue Test. Coating Crack Initiation was Detected after Approximately 1550 Cycles. (K-16735)*

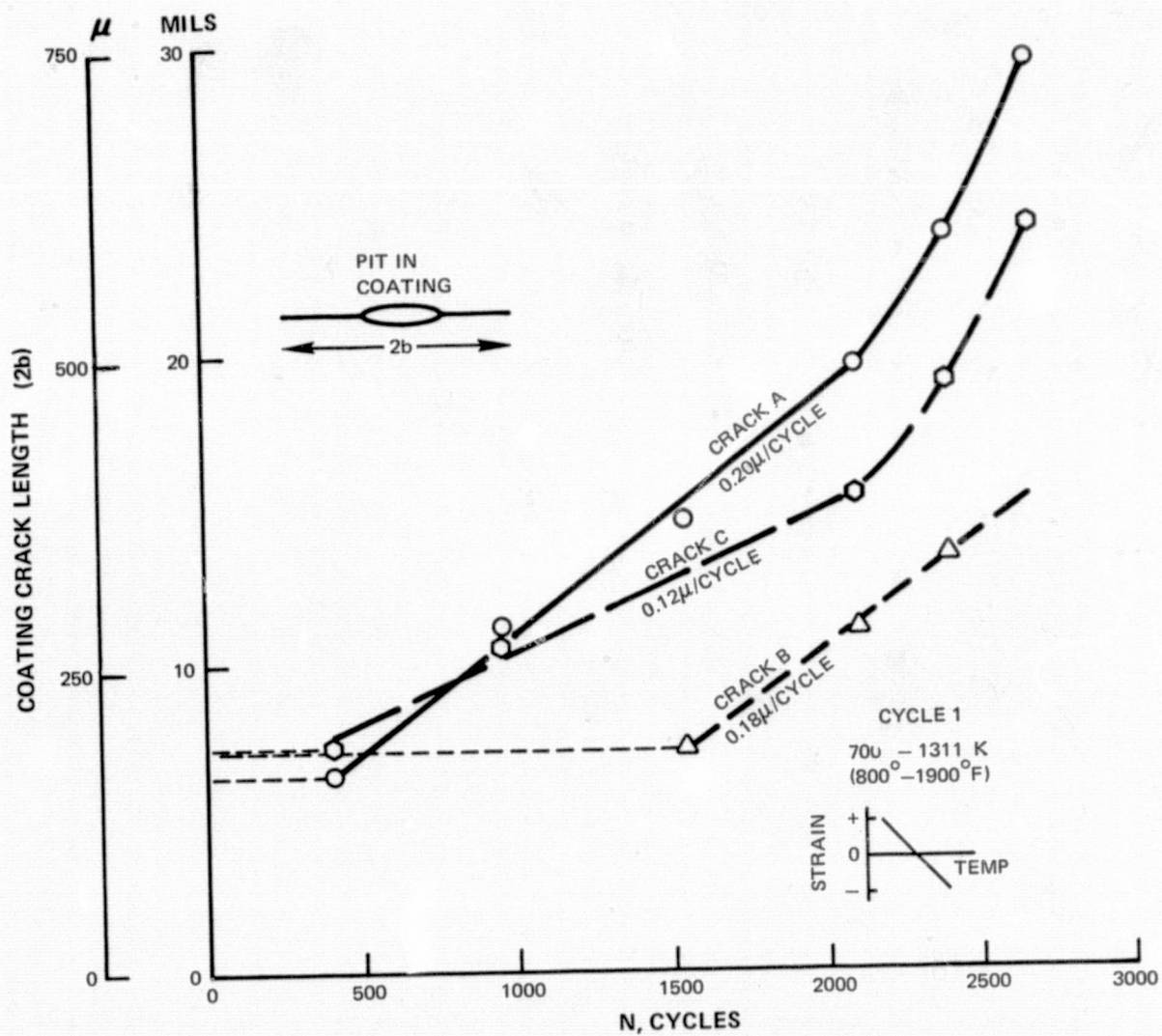
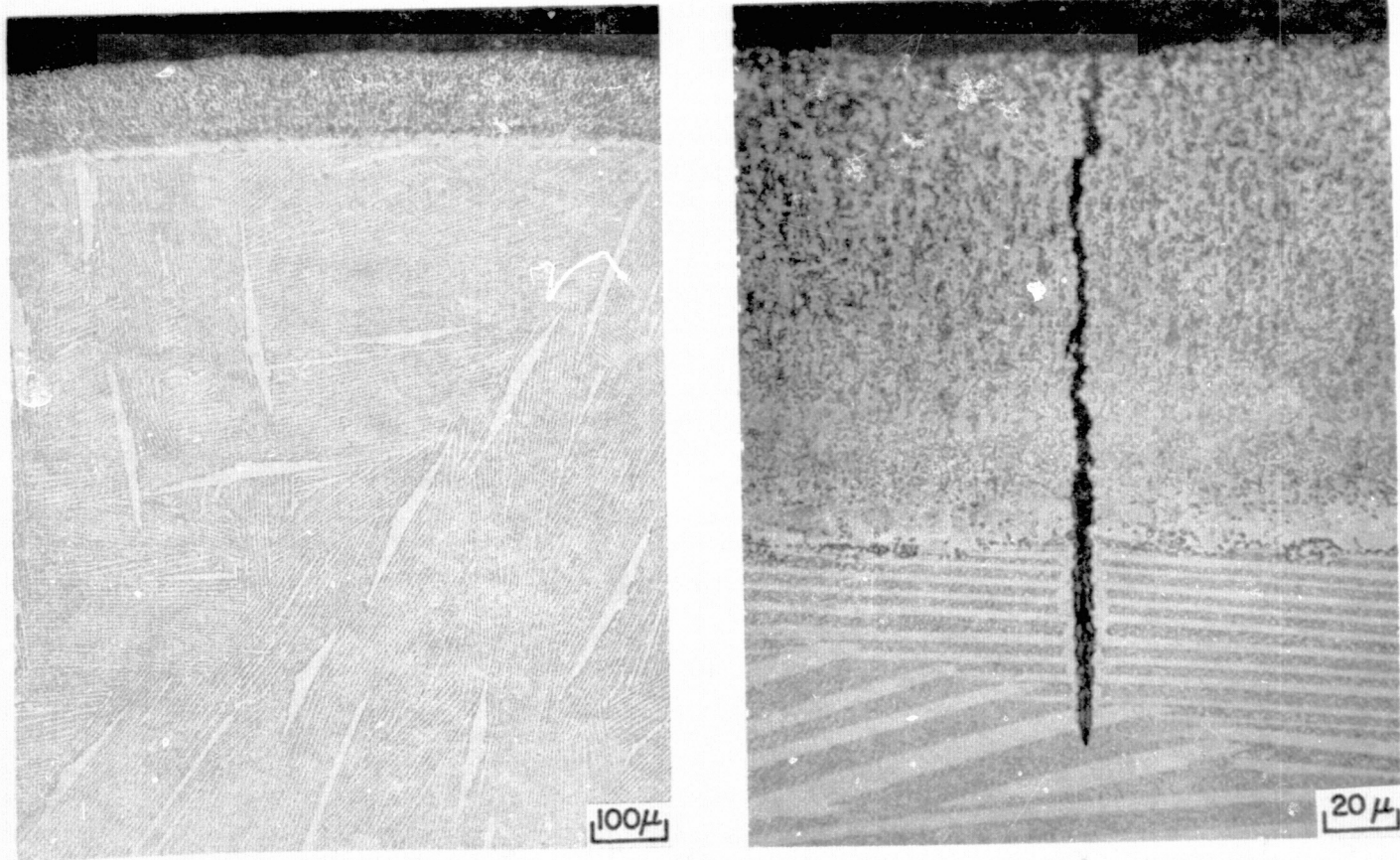


Figure 63 Surface Propagation of Thermal Fatigue Cracks in NiCrAlY Coated  $\gamma/\gamma' - \delta$  Specimen E 300 ( $\Delta\epsilon_{TM} = 0.30\%$ ).



**Figure 64** *Transverse (Left) and Longitudinal (Right) Cross-Section Microstructures of NiCrAlY Coated  $\gamma/\gamma'$ - $\delta$  (6Cr) Specimen (E 487) which was Evaluated for 7286 Cycles in a Cycle I (755 to 1200 K;  $\Delta\epsilon_{TM} = 0.30\%$ ) Thermomechanical Fatigue Test. The Longitudinal Microstructure Shows a Small Thermal Fatigue Crack which has Propagated a Short Distance into the Eutectic Alloy Substrate.*

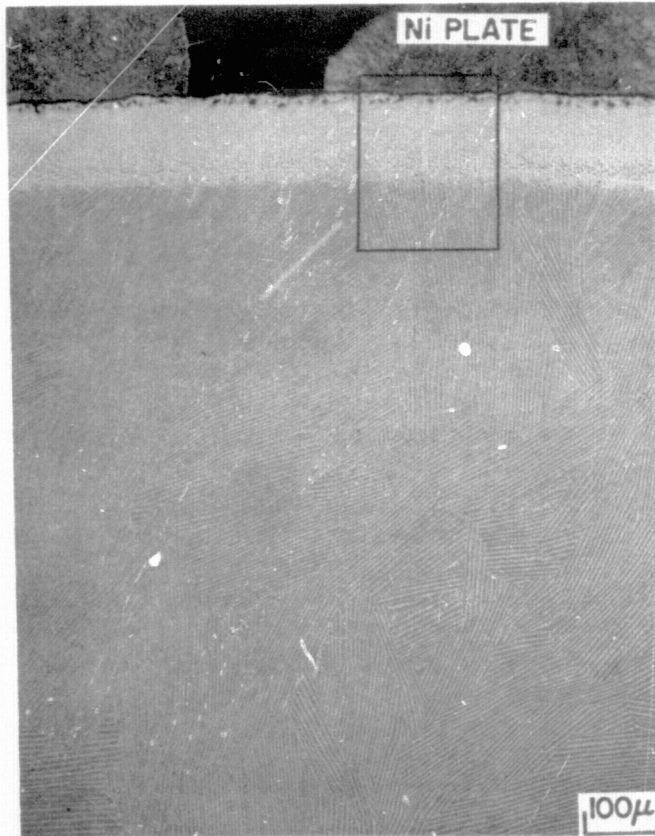


Figure 65 Microstructure of NiCrAlY + Pt Coated  $\gamma/\gamma'$  -  $\delta$  (6Cr) Specimen (E 290) which was Evaluated for 4486 Cycles in a Cycle I (700 to 1311 K;  $\Delta\epsilon_{TM} = 0.30\%$ ) Thermomechanical Fatigue Test.

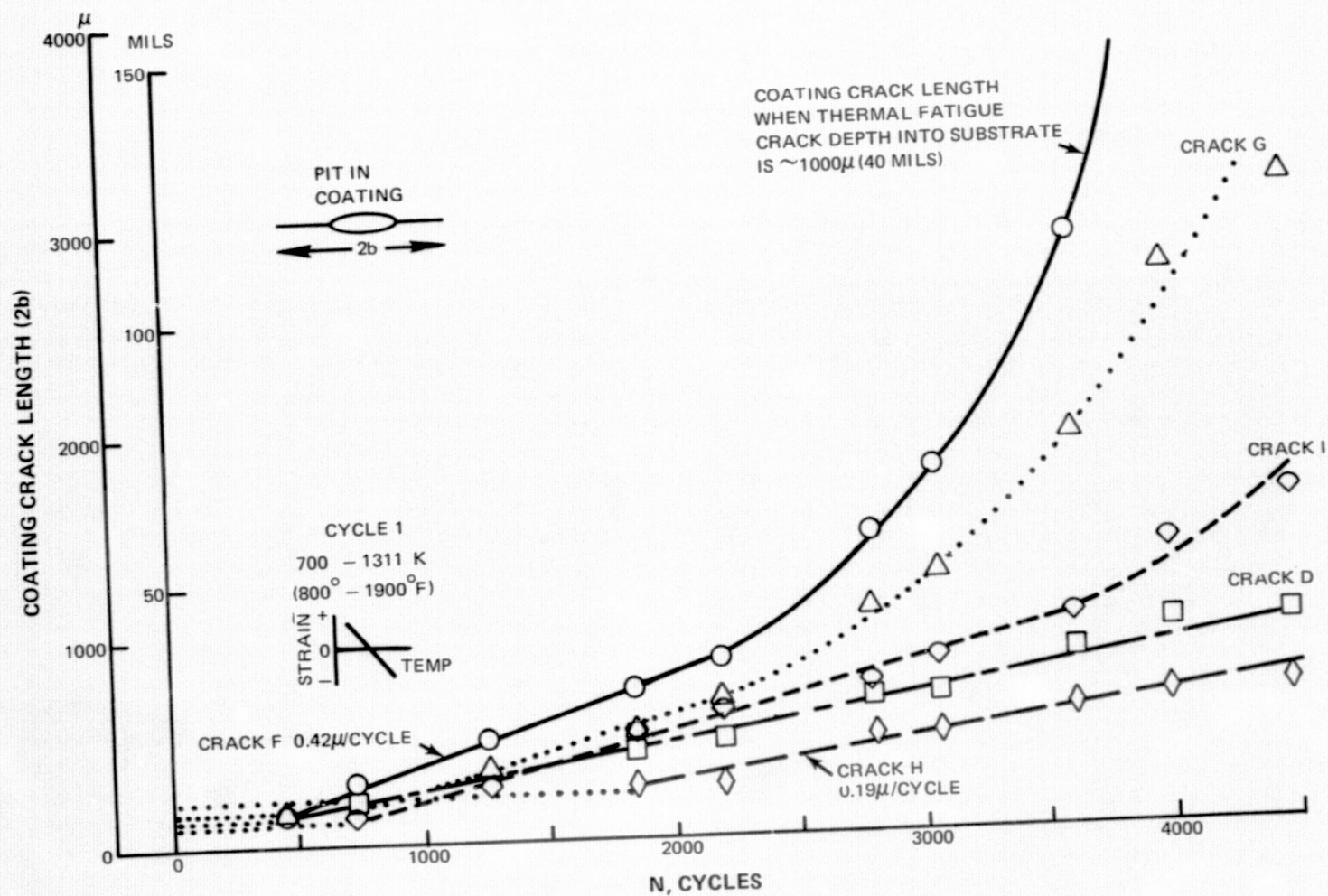


Figure 66 Surface Propagation of Thermal Fatigue Cracks in NiCrAlY + Pt Coated  $\gamma/\gamma'$  -  $\delta$  Specimen E 290 ( $\Delta\epsilon_{TM} = 0.30\%$ ).

ORIGINAL PAGE IS  
OF POOR QUALITY

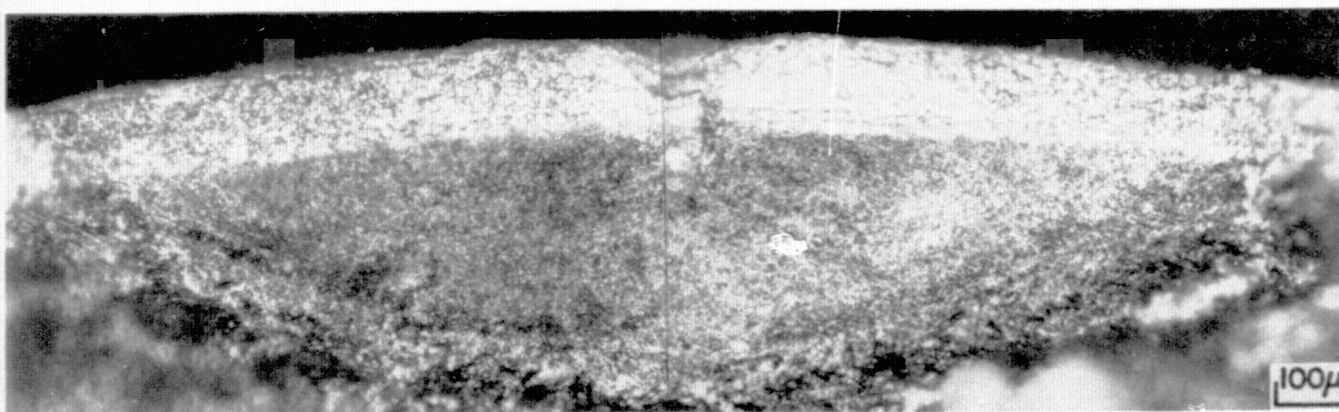
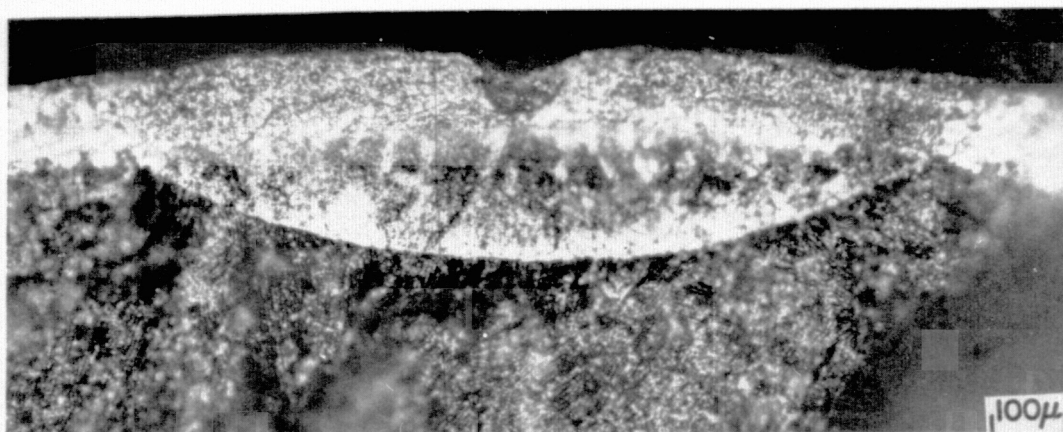


Figure 67    *Optical Fracture Surface Photographs of Secondary Thermal Fatigue Cracks D (top) and E (bottom) in NiCrAlY + Pt Coated  $\gamma/\gamma'$  -  $\delta$  Specimen (E 290) which was Evaluated for 4486 Cycles in a Cycle I (700 to 1311 K;  $\Delta\epsilon_{TM} = 0.30\%$ ) Thermomechanical Fatigue Test. Initiation of Both Coating Cracks was Detected After Approximately 450 Cycles.*  
(K-16737)

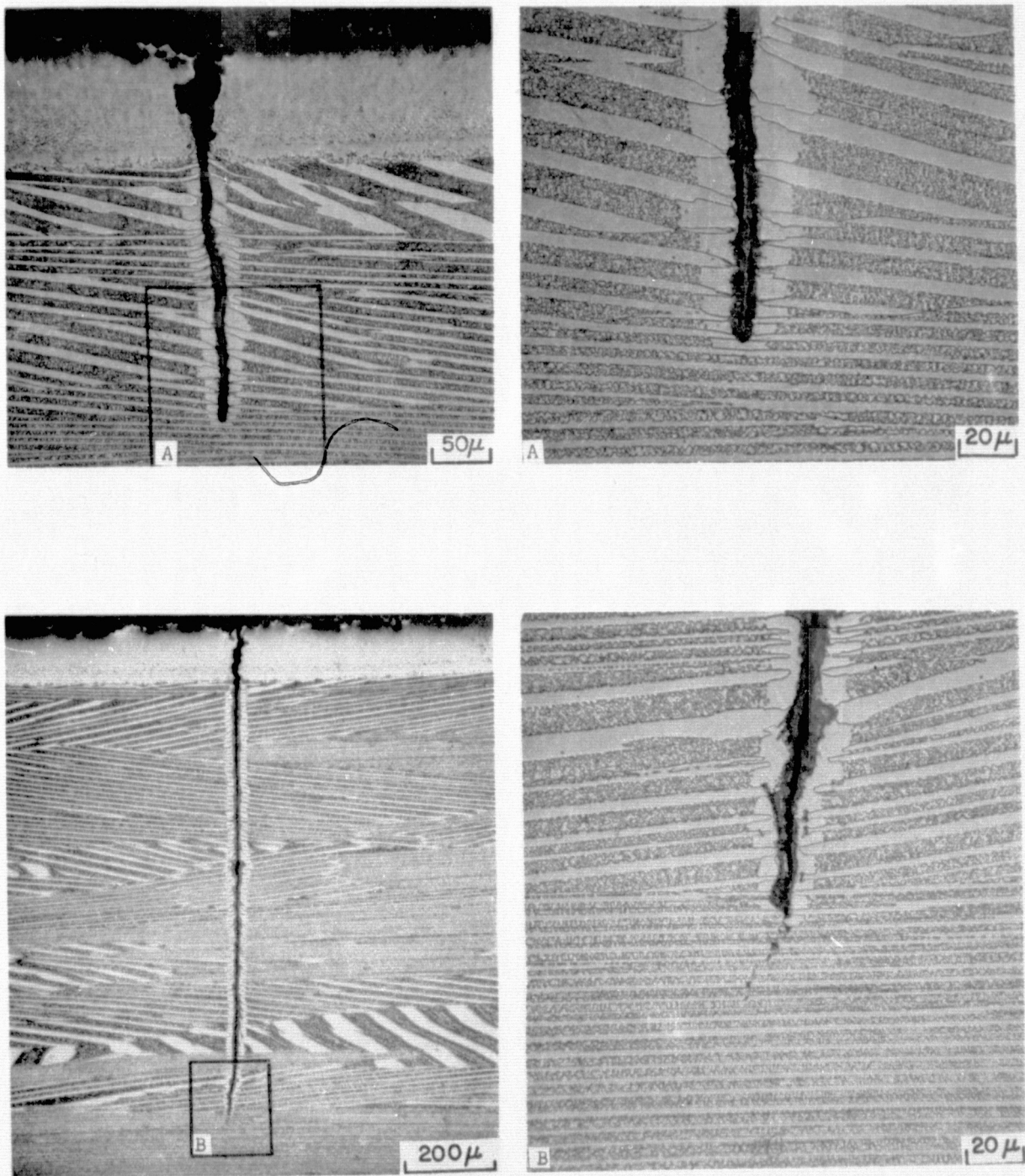
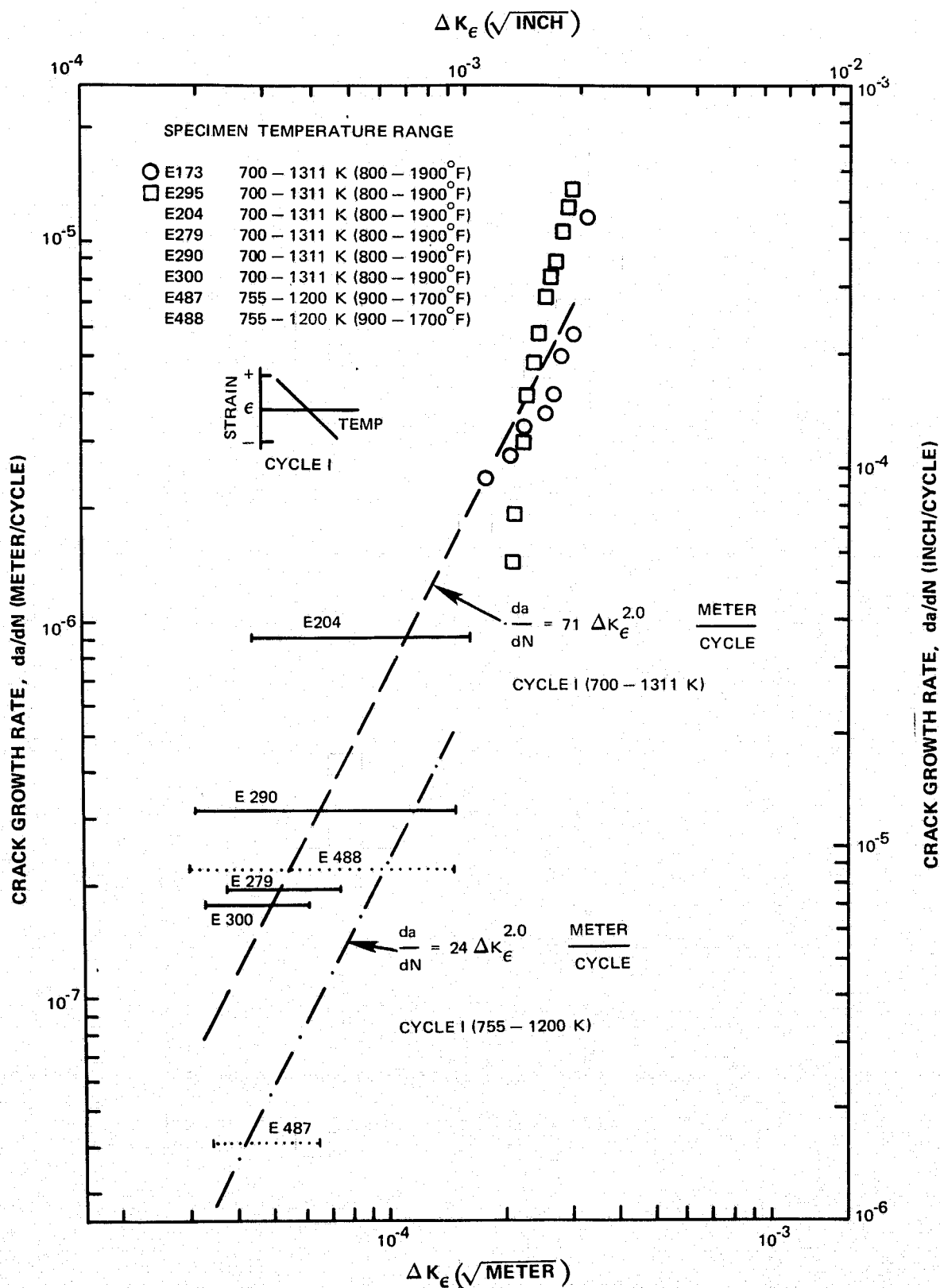


Figure 68 Microstructures of Pit Initiated Thermal Fatigue Cracks in NiCrAlY + Pt Coated  $\gamma/\gamma'$  -  $\delta$  (6Cr) Specimen (E 290) which was Evaluated for 4486 Cycles in a Cycle I (700 to 1311 K;  $\Delta\epsilon_{TM} = 0.30\%$ ) Thermomechanical Fatigue Test. An Oxidation Affected Zone Envelopes both Cracks. In Addition, for the Longer Crack (bottom), the  $\delta$  Phase has Started to Rupture Ahead of the Crack Tip. (K-16738)



Figure 69 Microstructure of NiCrAlY + Pt Coated  $\gamma/\gamma' - \delta$  (6Cr) Specimen (E 488) which was Evaluated for 5270 Cycles in a Cycle I (755 to 1200 K;  $\Delta\epsilon_{TM} = 0.30\%$ ) Thermomechanical Fatigue Test.



**Figure 70** Average Cycle I Thermomechanical Fatigue Crack Propagation Rates in  $\gamma/\gamma'$  -  $\delta$  Eutectic Superalloy Obtained with NiCrAlY (E 300, 487) and NiCrAlY + Pt (E 204, 279, 290, 488) Coated Specimens are Shown with Initial and Final Values of the Strain Intensity Factor Range,  $\Delta K_{\epsilon}$ . Data from Uncoated Specimens (E 173, 295) are Provided for Comparison.

## VIII. ISOTHERMAL FATIGUE TESTING

### A. BACKGROUND

Relatively severe preferential attack of the  $\delta$  phase during oxidation tests at relatively low temperatures (873 to 1073 K) (refs. 1, 2, 3) indicates that root attachment surfaces of turbine blades will require protective coatings. Since blade roots operate at temperatures significantly below airfoil temperatures, diffusion aluminide type coatings are not limited by over-temperature capability considerations. Therefore, aluminizing the blade root while applying the internal surface coating is a viable processing option. Alternatively, applying the airfoil coatings to the root surfaces may provide an acceptable solution to root coating requirements.

Based on the furnace hot corrosion and burner rig test results, the Ni-18Cr-12Al-0.3Y, Ni-18Cr-12Al-0.34 + Pt and Pt + Al candidate blade root coating systems were selected for evaluation in isothermal 977 K (1300°F) low cycle (LCF) and high cycle fatigue (HCF) tests.

### B. SPECIMEN PREPARATION

Forty-two  $\gamma/\gamma' - \delta$  (6Cr) Krouse fatigue specimens (see Figure 71) were machined from investment cast eutectic alloy sheets which were directionally solidified at a rate of 1.25 cm/hour. Thirty-three of these specimens had the solidification axis parallel to the specimen axis. The other nine specimens were machined with a transverse grain orientation; i.e., the solidification direction was perpendicular to the specimen axis. In addition, twelve directionally solidified (D.S.) Mar-M-200 + Hf specimens (eight longitudinal and four transverse) were prepared so that comparative data could be obtained.

Thirty-nine of the above specimens were coated with the NiCrAlY, NiCrAlY + Pt and Pt + Al candidate coating systems for the blade root.

### C. EXPERIMENTAL PROCEDURE

Constant strain range Krouse sheet fatigue specimens were used to assess the fatigue characteristics of the candidate coating systems. These tests were performed in fully reversed bending [stress ratio (R) = minimum stress/maximum stress = -1] with the deflection (strain) controlled by a variable eccentric. The initial strain range which was applied to the specimen was selected such that crack initiation was unlikely during the first  $10^4$  cycles for the LCF test or  $10^6$  cycles for the HCF test. The strain range was increased incrementally and testing of the specimen repeated until the strain range over which coating cracking for each coated alloy, or substrate cracking for the uncoated alloys, was determined. In some instances, the specimens were tested beyond coating crack initiation to specimen failure. The LCF tests were conducted at a frequency of 10 Hertz, and the HCF tests were conducted at a frequency of 60 Hertz. Plastic replicas of the specimen surface were taken after each  $10^4$  cycle increment ( $10^6$  cycle increment for the HCF tests) and examined at a magnification of 100X in order to detect crack initiation.

Post-test analyses of these specimens included both conventional metallographic examination of coating initiated cracks as well as optical examination of the fatigue fracture surface of selected cracks, which were broken open to determine the extent of coating crack penetration into the eutectic alloy substrate.

Both  $\gamma/\gamma' - \delta$  and D.S. MAR-M-200 + Hf longitudinal and transverse (directionally solidified grain orientation) Krouse specimens were evaluated in the coated and uncoated conditions. Longitudinal  $\gamma/\gamma' - \delta$  specimens coated with all three of the candidate coating systems were evaluated in the LCF test. The NiCrAlY and Pt + Al coating systems were also evaluated on longitudinal and transverse  $\gamma/\gamma' - \delta$  specimens in HCF and LCF tests, respectively. For comparative purposes, similar data were obtained for NiCrAlY coated D.S. Mar-M-200 + Hf. Nominal thicknesses of the NiCrAlY and NiCrAlY + Pt coating systems were  $127\mu$ ; in addition, thinner ( $\sim 63\mu$ ) NiCrAlY and NiCrAlY + Pt coating systems were also evaluated in the LCF evaluation of the longitudinal  $\gamma/\gamma' - \delta$  specimens. The Pt + Al diffusion aluminide coatings had average thicknesses in the order of  $80\mu$ .

Of the total of 54 fatigue specimens which were prepared, 42 were tested; the other specimens were retained as spares..

#### D. RESULTS AND DISCUSSION

Data from longitudinal LCF, transverse LCF and longitudinal HCF tests are provided in Tables IX, X and XI, respectively. Baseline data for the uncoated  $\gamma/\gamma' - \delta$  and D. S. Mar-M-200 + Hf alloys are also provided in Figures 72 and 73, respectively. (Metallographic examination of the  $\gamma/\gamma' - \delta$  specimens indicates that, in general, the material had a cellular microstructure. Some of the longitudinal orientation specimens also contained a small volume fraction of  $\delta$  dendrites.)

The comparison of the cyclic lives of these uncoated longitudinal grain orientation directionally solidified alloys is shown in Figures 72 and 73 as a function of the applied strain range; on this basis, the fatigue life at a given strain range is greater for the D.S. Mar-M 200 + Hf alloy than the  $\gamma/\gamma' - \delta$  alloy. However, if the comparison were made on the basis of stress range, instead of strain range, the longitudinal fatigue life of the  $\gamma/\gamma' - \delta$  alloy would exceed that of the D.S. MAR-M-200 + Hf alloy; this reversal in the fatigue life ranking occurs since the elastic modulus of the  $\gamma/\gamma' - \delta$  alloy is approximately twice that of D. S. Mar-M-200 + Hf at 977 K (1300°F).

As expected, the strain range capability of both alloys is relatively low in the transverse orientation. The strain range of the transverse grain D.S. MAR-M-200 + Hf material was approximately 70 percent of that for the longitudinal material for a  $10^4$  cycle LCF life (Figure 73). Test data indicates that the strain range of transverse grain  $\gamma/\gamma' - \delta$  is approximately 50 percent of that for the longitudinal material value for a  $10^4$  cycle LCF life (Figure 72).

Fatigue data for coated longitudinal orientation  $\gamma/\gamma' - \delta$  specimens are provided in Tables IX and XI and shown graphically in Figure 74. These data indicate that the fatigue strength of the coated  $\gamma/\gamma' - \delta$  alloy is less than that of the uncoated alloy. In contrast to the relatively

narrow gap separating crack initiation and specimen failure for the uncoated alloy, failure of the coated specimens can occur at strain ranges which are significantly above that necessary to initiate coating cracks. The data also indicate that coating thickness is an important parameter. Specimens coated with thinner coatings have both a higher strain range for coating crack initiation and specimen failure strains which approach that of uncoated specimens.

Inspection of the NiCrAlY and NiCrAlY + Pt coated  $\gamma/\gamma' - \delta$  specimens indicated that initiation of cracks was associated predominantly with pit defects and, in a few instances, flake defects. (The formation of pit and flake defects in MCrAlY overlay coatings has been discussed in ref. 30.) Fracture surfaces of fatigue cracks initiated by these defects are shown in Figure 75 for a  $127\mu$ -thick NiCrAlY coated  $\gamma/\gamma' - \delta$  LCF specimen. These cracks were initiated at the initial strain range, 0.50 percent, and propagated a short distance in the coating at this strain range. Examination of fatigue fracture surfaces of several cracks indicated that significant penetration into the  $\gamma/\gamma' - \delta$  substrate did not occur until the specimens were loaded to an increased strain range of 0.55 percent. It was also noted that cracking did not initiate at the 0.55 percent strain range level in areas of the specimen where the coating was free of defects. Similar results were achieved with NiCrAlY coated specimens which were evaluated in the HCF test. In the first specimen, coating cracks were detected after  $10^6$  cycles at a strain range of 0.25 percent; post-test examination of several cracks, which were broken open at the end of the test, indicated that the cracking was confined to the coating. Crack initiation in the duplicate HCF specimen was detected after  $10^6$  cycles at a strain range of 0.20 percent. After coating-crack initiation was detected, the specimen was tested for additional  $10^6$  cycle increments with the strain range being increased by 0.05 percent strain at the start of each new increment. Specimen failure did not occur until after the specimen loading was increased to a strain range of 0.40 percent strain for 20,730 cycles; this relatively short failure time, however, indicated that some coating crack penetration into the substrate occurred at 0.35 percent strain. Heat tint patterns on the fracture surface support this observation.

Isothermal LCF, as well as thermomechanical fatigue, crack propagation rates in the  $\gamma/\gamma' - \delta$  alloy are functions of the strain (stress) intensity factor range (ref. 4). If the crack growth rate versus strain intensity factor range,  $\Delta K_{\epsilon}$ , relationship is known, it is possible to integrate the crack growth rate equation between an initial flaw size (e.g., the coating thickness) and final crack size to determine the number of cycles involved in crack propagation. It is also possible to determine values of  $\Delta K_{\epsilon}$  for which a coating crack will not penetrate to a significant depth (e.g.,  $25\mu$ ) into a substrate during the number of cycles (e.g.,  $10^4$  or  $10^6$ ) in the test. To a first approximation, the strain intensity factor range of a coating crack has the following form when the crack tip is at the coating-substrate interface:

$$\Delta K_{\epsilon} = A \Delta \epsilon \sqrt{t}$$

where:  $\Delta \epsilon$  is the applied strain range,  
 $t$  is the coating thickness, and  
 $A$  is a constant.

If a strain range and coating thickness combination which will not result in significant coating crack penetration during the available number of cycles can be calculated or (in this case) determined experimentally, the effect of different coating thicknesses on the failure strength of the  $\gamma/\gamma' - \delta$  alloy can be estimated as shown in Figure 76. It is interesting to note that, based on this relatively simple model, cracks in NiCrAlY coatings less than about  $45\mu$  thick are not predicted to significantly alter the baseline properties of the uncoated  $\gamma/\gamma' - \delta$  alloy. The higher HCF failure strains for the  $\gamma/\gamma' - \delta$  specimen coated with the thinner (approximately  $60\mu$  thick) Pt + Al coating are consistent with this interpretation.

This analysis was developed with the data from the  $\gamma/\gamma' - \delta$  specimens coated with  $\sim 127\mu$  (0.005 inch) thick NiCrAlY coatings. In order to verify the predicted results, additional  $\gamma/\gamma' - \delta$  LCF specimens were coated with thinner ( $\sim 63\mu$ ) NiCrAlY coatings. The results of these tests are in good agreement with the analytical estimates (see Figure 76).

With one exception, the LCF test results of the NiCrAlY + Pt coated  $\gamma/\gamma' - \delta$  specimens were also in excellent agreement with the analysis of the NiCrAlY coated specimens. Examination of the fracture surface of specimen 40 indicated that some propagation into the  $\gamma/\gamma' - \delta$  substrate occurred at a strain range of 0.65 percent; in this particular instance, a small  $\sim 25\mu$  deep pit in the  $\gamma/\gamma' - \delta$  substrate slightly increased the effective size of the coating flaw which initiated the crack. The formation of coating flaws in conjunction with substrate pits has been previously described (ref. 5).

For further comparison, after cracking was initiated in the  $127\mu$  thick NiCrAlY coating on the longitudinal orientation D.S. MAR-M-200 + Hf specimen (No. 14) at a strain range of 0.45 percent, the specimen loading was increased for two additional  $10^4$  cycle increments at strain ranges of 0.50 and 0.55 percent. Two of the cracks were broken open at this point, and examination indicated that the coating cracks had not penetrated into the substrate. In contrast, significant coating crack penetration into the  $\gamma/\gamma' - \delta$  substrate was observed after  $10^4$  cycles at a 0.55 percent strain range.

Propagation data was obtained for several cracks in NiCrAlY coatings from the series of surface replicas which were taken after each  $10^4$  (or  $10^6$ ) cycle increment during the LCF and HCF tests, respectively. Average crack propagation rates (change in coating crack length/cycle increment) obtained from five NiCrAlY coated specimens are shown in Figure 77 as a function of the strain range,  $\Delta\epsilon$ . For the  $127\mu$  coating thickness, the graph implies that the crack growth rate in the coating is constant at a given strain range and has a functional relationship of the form

$$\Delta(2b) / \Delta N = A\Delta\epsilon^B$$

(for the crack growth rates and strain ranges under consideration), where  $\Delta(2b) / \Delta N$  is the crack growth rate in the coating,  $\Delta\epsilon$  is the strain range, and A and B are constants. Similar periods of initially constant crack growth rates have been observed during interrupted (for surface replication) isothermal fatigue tests (at a constant strain range) of CoCrAlY coated D. S. MAR-M-200 + Hf specimens (ref. 33). Further inspection of this figure shows that the isothermal crack growth rate in the  $127\mu$  thick NiCrAlY coating is not strongly dependent on the substrate. It should also be noted that coating thickness (t) is a significant parameter; i.e., the crack propagation rate is significantly slower in the  $66\mu$  thick NiCrAlY coatings.

Similar isothermal fatigue testing with NiCoCrAlY coated specimens (ref. 22) indicated that the coating crack propagation rates in different thickness coatings can be expressed as

$$\Delta (2b)/\Delta N = A_1 (\Delta \epsilon \sqrt{t})^B$$

crack propagation rates of the two thicknesses of NiCrAlY coatings are consistent with this relationship as shown in Figure 78.

If pit type coating defects are the most severe defects present in the coating and if significant substrate defects are absent, then it is possible to estimate the number of cycles to initiate a "detectable" coating crack. In order to determine that the coating is cracked, a small amount of crack propagation must occur in the coating adjacent to the pit. For the purpose of this report, the detectable amount of coating crack propagation is arbitrarily defined to be  $25\mu$ . Integrating the assumed crack growth relationship from an initial coating defect size of  $2b_0$  to a detectable crack size of  $2b_0 + 25\mu$  provides a technique for estimating the number of cycles required to "initiate" a detectable coating crack; i.e.,

$$N = \int_{2b_0}^{2b_0 + 25\mu} \frac{d(2b)}{A_1 (\Delta \epsilon \sqrt{t})^B} = \frac{25\mu}{A_1 (\Delta \epsilon \sqrt{t})^B}$$

Coating crack initiation lives obtained with the above integration for 66 and  $127\mu$  thick NiCrAlY coatings are shown as a function of the strain range in Figure 79. The minimum strain ranges for coating crack propagation into the  $\gamma/\gamma' - \delta$  substrate (from Figure 76) are provided in this figure as a lower limit for coated specimen failure. Crack initiation and specimen failure data for the uncoated  $\gamma/\gamma' - \delta$  alloy are also included for comparison. Thus, the root coating thickness ( $t$ ) can be adjusted to obtain the optimum combination of oxidation/hot corrosion resistance (increased by increasing  $t$ ) and fatigue resistance (increased by decreasing  $t$ ).

It is interesting to note that although the NiCrAlY coatings on the  $\gamma/\gamma' - \delta$  and D.S. MAR-M-200 + Hf alloys had different microstructures, the differences in coating crack propagation rates are small and within the same scatter band (See Figures 77 and 78). The NiCrAlY coatings on both alloys were diffusion heat treated at 1353 K for four hours in hydrogen; following the diffusion heat treatment, the D.S. MAR-M-200 + Hf specimens also received the precipitation heat treatment (1144 K/32 hours/air) which is required for the substrate. As a result, the NiCrAlY coatings on the  $\gamma/\gamma' - \delta$  specimens had a microstructure which was predominantly composed of  $\gamma$  (Ni solid solution) +  $\beta$  (NiAl) phases (Figure 80), while the NiCrAlY coatings on the D.S. MAR-M-200 + Hf specimens transformed to a microstructure which was predominantly  $\gamma'$  ( $\text{Ni}_3\text{Al}$ ) +  $\alpha$  (chromium) during the precipitation heat treatment (Figure 81). The temperature dependence of the NiCrAl microstructure has been described previously (ref. 29). The stability of the  $\gamma + \beta$  NiCrAlY microstructure on the  $\gamma/\gamma' - \delta$  specimens indicates that the kinetics of the phase transformations are relatively slow at 977 K, the test temperature.

Although coating defects (pits) were present in the NiCrAlY coated transverse orientation  $\gamma/\gamma'$  -  $\delta$  specimens, these defects played no role in initiating the primary cracks which resulted in failure; in fact, the coating on the fracture surfaces was free of both pit and flake defects. Very small secondary cracks were initiated at pit defects in the NiCrAlY coated specimen (No. 22) which was tested at the larger (0.40 percent) strain range.

In contrast, coating pits were associated with initiation of the primary cracks in the NiCrAlY coated transverse grain orientation D.S. MAR-M 200 + Hf specimen at a strain range of 0.35 percent. After coating crack initiation was detected, specimen No. 27 was tested for additional  $10^4$  cycle increments with the strain range being increased by 0.05 percent strain at the start of each new increment. The substrate was significantly cracked but not failed (in two pieces) after  $10^4$  cycles at 0.50 percent strain range. Post-test fracture surface analysis indicated that the coating crack started to propagate into the substrate during the  $10^4$  cycles at a strain range of 0.45 percent.

Microstructures of secondary cracks in NiCrAlY + Pt and NiCrAlY coated transverse and longitudinal  $\gamma/\gamma'$  -  $\delta$  specimens are shown in Figure 82. Microstructures of the NiCrAlY and NiCrAlY + Pt coatings were similar to those of virgin coatings; this result indicates that kinetics of the previously mentioned phase transformations in the NiCrAl system are relatively slow at 977 K (1300°F). Oxidation of the fracture surfaces in the NiCrAlY + Pt coated  $\gamma/\gamma'$  -  $\delta$  specimen (Figure 82) shows the low temperature oxidation mode of the  $\gamma/\gamma'$  -  $\delta$  material which is characterized by preferential attack of the  $\delta$  ( $\text{Ni}_3\text{Cb}$ ) phase. Crack propagation in the NiCrAlY coated transverse orientation specimen was transgranular and parallel to the  $\delta$  platelets.

Examination of surface replicas of the Pt + Al coated  $\gamma/\gamma'$  -  $\delta$  specimens indicated that multiple coating cracks initiated at strain ranges above approximately 0.25 to 0.30 percent strain in both the LCF and HCF tests. In most (if not all) cases, the coating cracks propagated across the entire width of the specimens during the test. As expected, the density of coating cracks was greater on those specimens which were tested at the larger strain ranges.

Post-test metallography of a specimen which was tested at a strain range of 0.45 percent for  $10^6$  cycles indicated that most, but not all, of the cracks were confined to the coating; significant penetration of a coating crack into the substrate to a depth of  $330\mu$  (13 mils) was observed in one instance (Figure 83). Similar cracking behavior was also observed in the Pt + Al coated transverse orientation  $\gamma/\gamma'$  -  $\delta$  specimen which was tested at a strain range of 0.30 percent. While most cracking was confined to the coating, one coating crack loaded over a grain boundary propagated a short distance into the eutectic alloy (Figure 83).

In summary, isothermal fatigue testing and furnace hot corrosion testing (Section IV) indicates that  $\gamma/\gamma'$  -  $\delta$  blade roots can be protected by applying either airfoil coatings (NiCrAlY or NiCrAlY + Pt) or the platinum modified diffusion aluminide coating (Pt + Al) to this region. Analysis of the test data indicates that coating thickness can be adjusted to optimize the resistance to hot corrosion and fatigue.

TABLE IX

**977 K (1300°F) 10<sup>4</sup> CYCLE STRAIN-STEPPED LCF TESTS  
OF LONGITUDINAL GRAIN ORIENTATION  $\gamma/\gamma'$  -  $\delta$  (6 Cr) AND  
MAR-M 200 + Hf DIRECTIONALLY SOLIDIFIED SUPERALLOYS**

Specimen Identification	Material	Coating	Coating Thickness, Microns	Initial Strain Range, %	Maximum Strain Range without Crack Initiation, %	Strain Range at Which Cracks Were Detected, %	Final Strain Range, %	Number of Cycles at Final Strain Range
1	$\gamma/\gamma'$ - $\delta$ (6Cr)	Uncoated	—	0.90	— — —	0.90	0.90	6,000
2	$\gamma/\gamma'$ - $\delta$ (6Cr)	Uncoated	—	0.70	0.80	0.85	0.85	7,800
3	$\gamma/\gamma'$ - $\delta$ (6Cr)	Pt + Al	76	0.50	— — —	0.50	0.50	10,000
4	$\gamma/\gamma'$ - $\delta$ (6Cr)	Pt + Al	58	0.40	— — —	0.40	0.40	10,000
5	$\gamma/\gamma'$ - $\delta$ (6Cr)	Pt + Al	90±30	0.20	0.30	0.35	0.35	10,000
6	$\gamma/\gamma'$ - $\delta$ (6Cr)	NiCrAlY + Pt	~127	0.50	— — —	0.50	0.55	7,700
7	$\gamma/\gamma'$ - $\delta$ (6Cr)	NiCrAlY + Pt	~127	0.50	— — —	0.50	0.55	10,000
8	$\gamma/\gamma'$ - $\delta$ (6Cr)	NiCrAlY + Pt	~127	0.30	0.40	0.45	0.45	10,000
39	$\gamma/\gamma'$ - $\delta$ (6Cr)	NiCrAlY + Pt	66	0.35	0.60	0.64	0.75	9,800
40	$\gamma/\gamma'$ - $\delta$ (6Cr)	NiCrAlY + Pt	61	0.60	— — —	0.60	0.70	4,550
9	$\gamma/\gamma'$ - $\delta$ (6Cr)	NiCrAlY	~127	0.50	— — —	0.50	0.55	10,000
10	$\gamma/\gamma'$ - $\delta$ (6Cr)	NiCrAlY	~127	0.50	— — —	0.50	0.55	10,000
11	$\gamma/\gamma'$ - $\delta$ (6Cr)	NiCrAlY	~127	0.35	0.35	0.40	0.50	10,000
41	$\gamma/\gamma'$ - $\delta$ (6Cr)	NiCrAlY	61	0.35	0.65	0.70	0.75	7,500
42	$\gamma/\gamma'$ - $\delta$ (6Cr)	NiCrAlY	66	0.60	0.60	0.65	0.75	8,950
12	D.S.MAR-M 200 + Hf	Uncoated	—	0.85	0.95	1.00	1.05	9,300
13	D.S.MAR-M 200 + Hf	Uncoated	—	0.90	0.95	1.00	1.10	6,700
14	D.S. MAR-M 200 + Hf	NiCrAlY	~127	0.40	0.40	0.45	0.55	10,000
15	D.S. MAR-M 200 + Hf	NiCrAlY	~127	0.40	0.40	0.45	0.45	10,000

ORIGINAL PAGE IS  
OF POOR QUALITY

TABLE X

**977 K (1300°F)  $10^4$  CYCLE STRAIN-STEPPED LCF TESTS  
OF TRANSVERSE GRAIN ORIENTATION  $\gamma/\gamma'$ - $\delta$  (6Cr) AND  
MAR-M 200 + Hf DIRECTIONALLY SOLIDIFIED SUPERALLOYS**

Specimen Identification	Material	Coating	Coating Thickness, Microns	Initial Strain Range, %	Maximum Strain Range without Crack Initiation, %	Strain Range at Which Cracks Were Detected, %	Final Strain Range, %	Number of Cycles at Final Strain Range
16	$\gamma/\gamma'$ - $\delta$ (6Cr)	Uncoated	—	0.30	0.45	0.50	0.50	10,000
17	$\gamma/\gamma'$ - $\delta$ (6Cr)	Uncoated	—	0.40	0.40	0.45	0.45	2,650
18	$\gamma/\gamma'$ - $\delta$ (6Cr)	Uncoated	—	0.40	— — —	0.40	0.40	250
19	$\gamma/\gamma'$ - $\delta$ (6Cr)	Pt + Al	90±30	0.50	— — —	0.50	0.50	50
20	$\gamma/\gamma'$ - $\delta$ (6Cr)	Pt + Al	122	0.30	— — —	0.30	0.30	10,000
21	$\gamma/\gamma'$ - $\delta$ (6Cr)	Pt + Al	90±30	0.20	0.30	0.35	0.35	10,000
22	$\gamma/\gamma'$ - $\delta$ (6Cr)	NiCrAlY	~127	0.20	0.35	0.40	0.40	10,000
23	$\gamma/\gamma'$ - $\delta$ (6Cr)	NiCrAlY	~127	0.20	0.25	0.30	0.30	10,000
24	D.S. MAR-M 200 + Hf	Uncoated	—	0.40	0.60	0.65	0.65	20,000
25	D.S. MAR-M 200 + Hf	Uncoated	—	0.55	0.70	0.75	0.75	10,000
26	D.S. MAR-M 200 + Hf	NiCrAlY	~127	0.35	— — —	0.35	0.45	10,000
27	D.S. MAR-M 200 + Hf	NiCrAlY	~127	0.20	0.30	0.35	0.50	10,000

TABLE XI

977 K (1300°F)  $10^6$  CYCLE STRAIN-STEPPED HCF TESTS  
OF LONGITUDINAL GRAIN ORIENTATION  $\gamma/\gamma'$  -  $\delta$  (6Cr) AND  
MAR-M 200 + Hf DIRECTIONALLY SOLIDIFIED SUPERALLOYS

Specimen Identification	Material	Coating	Coating Thickness, Microns	Initial Strain Range, %	Maximum Strain Range without Crack Initiation, %	Strain Range at Which Cracks Were Detected, %	Final Strain Range, %	Number of Cycles at Final Strain Range
28	$\gamma/\gamma'$ - $\delta$ (6Cr)	Uncoated	—	0.40	0.45	0.50	0.50	1,000,000
29	$\gamma/\gamma'$ - $\delta$ (6Cr)	Uncoated	—	0.40	0.50	0.55	0.55	677,180
30	$\gamma/\gamma'$ - $\delta$ (6Cr)	Pt + Al	56	0.40	—	0.40	0.45	1,000,000
31	$\gamma/\gamma'$ - $\delta$ (6Cr)	Pt + Al	89	0.20	0.25	0.30	0.30	1,000,000
32	$\gamma/\gamma'$ - $\delta$ (6Cr)	Pt + Al	90 $\pm$ 30	0.20	0.30	0.35	0.40	1,000,000
33	$\gamma/\gamma'$ - $\delta$ (6Cr)	NiCrAlY	~127	0.20	0.20	0.25	0.25	1,000,000
34	$\gamma/\gamma'$ - $\delta$ (6Cr)	NiCrAlY	~127	0.15	0.15	0.20	0.40	20,730*
35	D.S. MAR-M 200 + Hf	Uncoated	—	0.45	0.55	0.62	0.62	750,000
36	D.S. MAR-M 200 + Hf	Uncoated	—	0.50	0.50	0.55	0.60	100,000
37	D.S. MAR-M 200 + Hf	NiCrAlY	~127	0.20	0.35	0.40	0.40	300,000
38	D.S. MAR-M 200 + Hf	NiCrAlY	~127	0.20	0.25	0.30	0.35	186,000

\*Some coating crack penetration into substrate probably occurred during  $10^6$  cycles at  $\Delta \epsilon = 0.35\%$ .

ORIGINAL PAGE IS  
OF POOR QUALITY

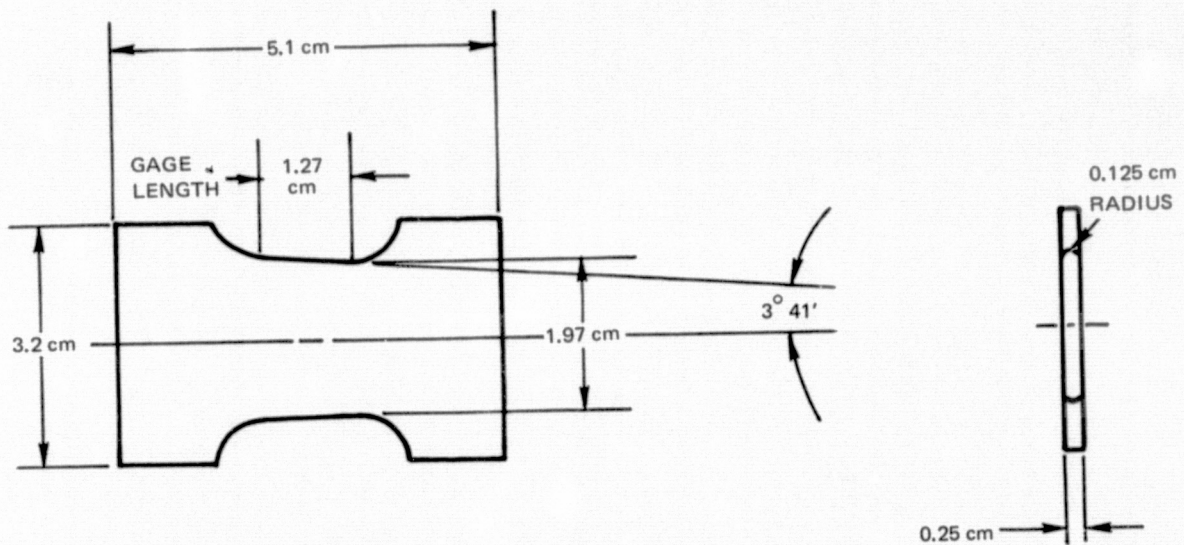


Figure 71 Isothermal Reversed Bending (Krouse) Fatigue Specimen.

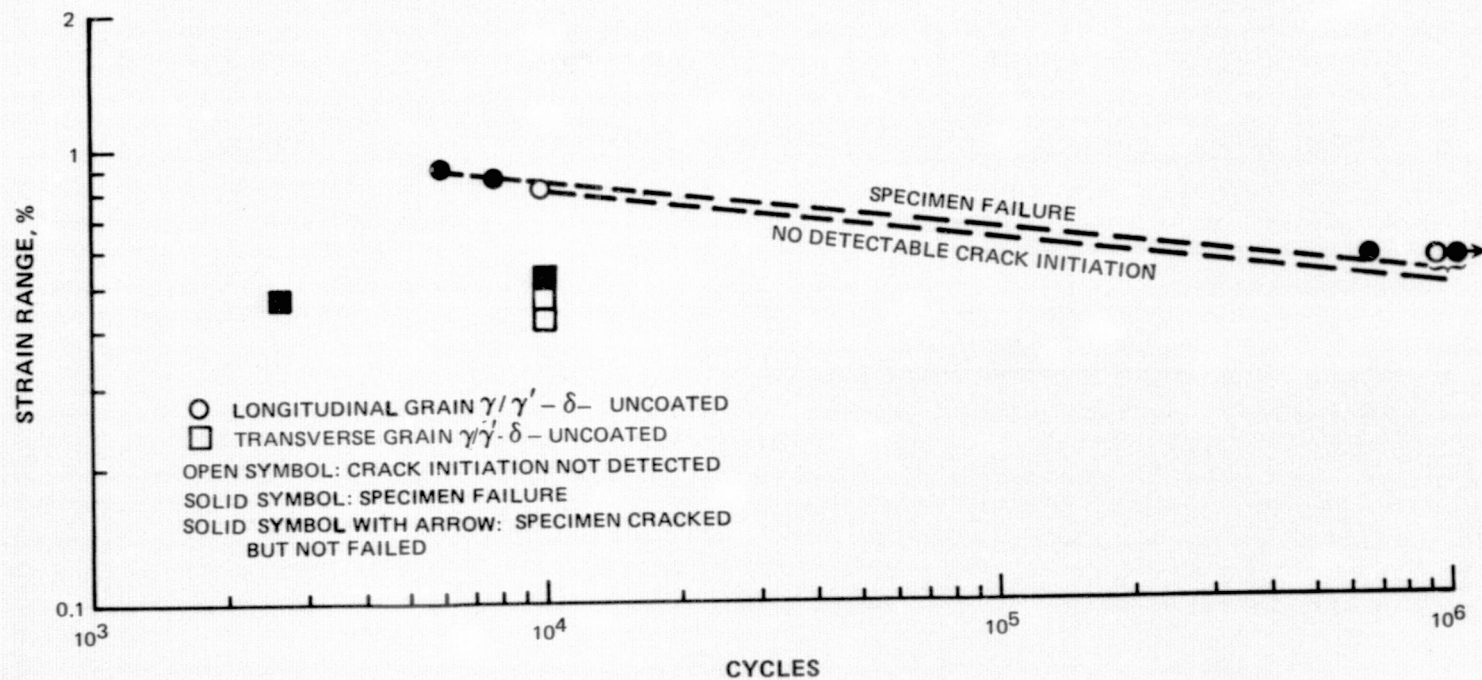


Figure 72 977 K (1300°F) Isothermal Fatigue Data for Directionally Solidified  $\gamma/\gamma' - \delta$  (6Cr) Alloy.

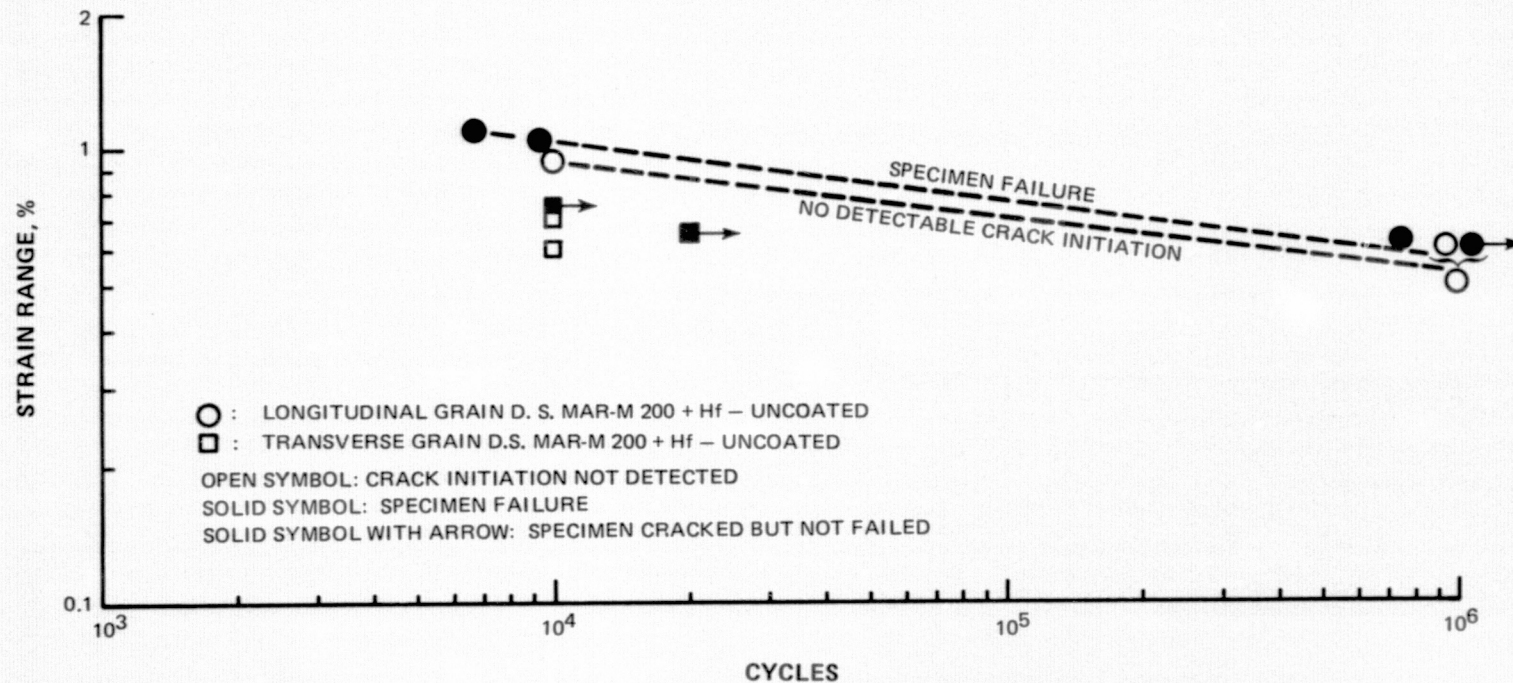


Figure 73 977 K (1300°F) Isothermal Fatigue Data for Directionally Solidified MAR-M 200 + Hf Alloy.

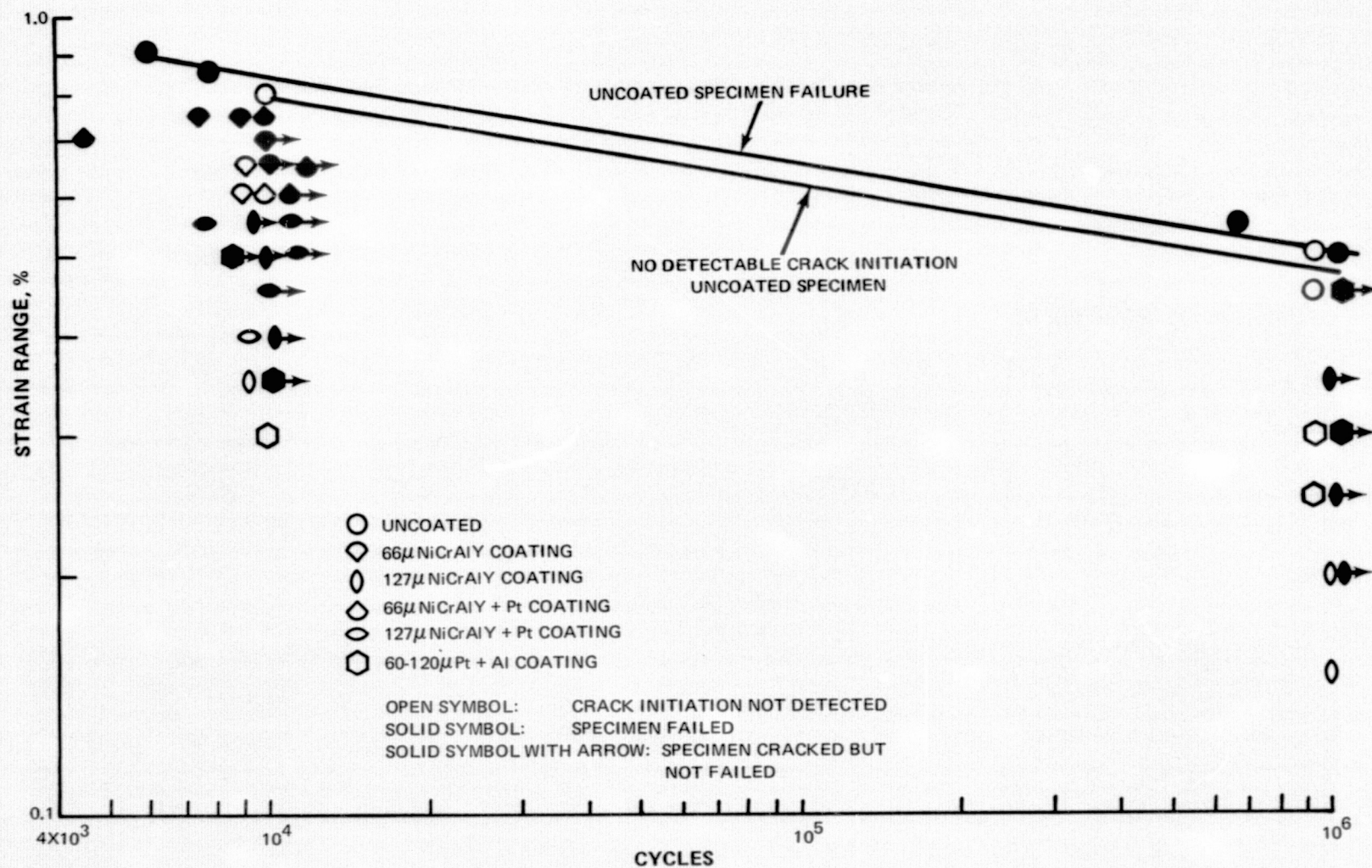


Figure 74 977 K (1300°F) Isothermal Fatigue Data for Coated and Uncoated Longitudinal Grain Orientation  $\gamma/\gamma'$  -  $\delta$  (6Cr) Alloy.

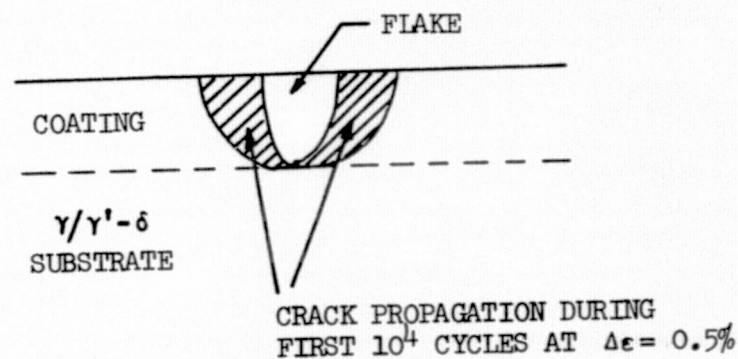
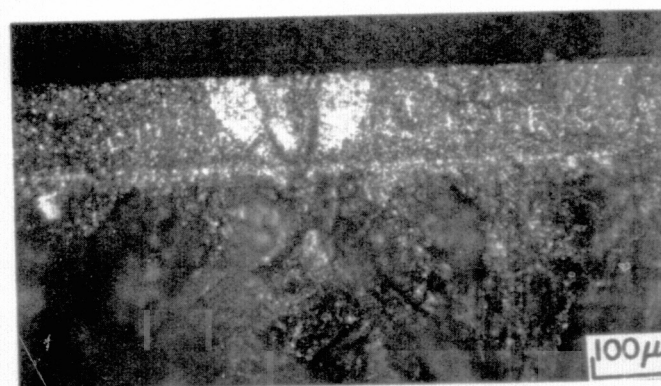
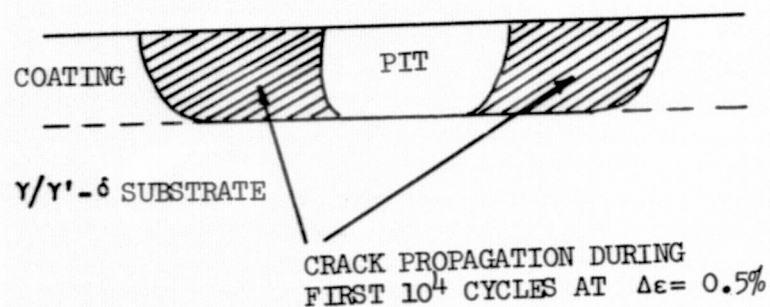
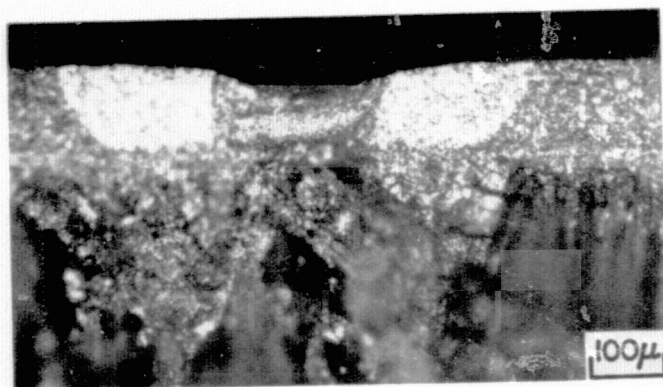


Figure 75 Fracture Surfaces of Pit (Left) and Flake (Right) Initiated Fatigue Cracks in NiCrAlY Coated  $\gamma/\gamma' - \delta$  Specimen (No. 10) Which Was Evaluated in 977 K (1300°F) LCF Test. Cracking was confined to the coating during the first  $10^4$  cycle increment at a strain range of 0.5 percent. Significant crack penetration into the  $\gamma/\gamma' - \delta$  substrate occurred during the next  $10^4$  cycle increment at a strain range of 0.55 percent. (K-16739)

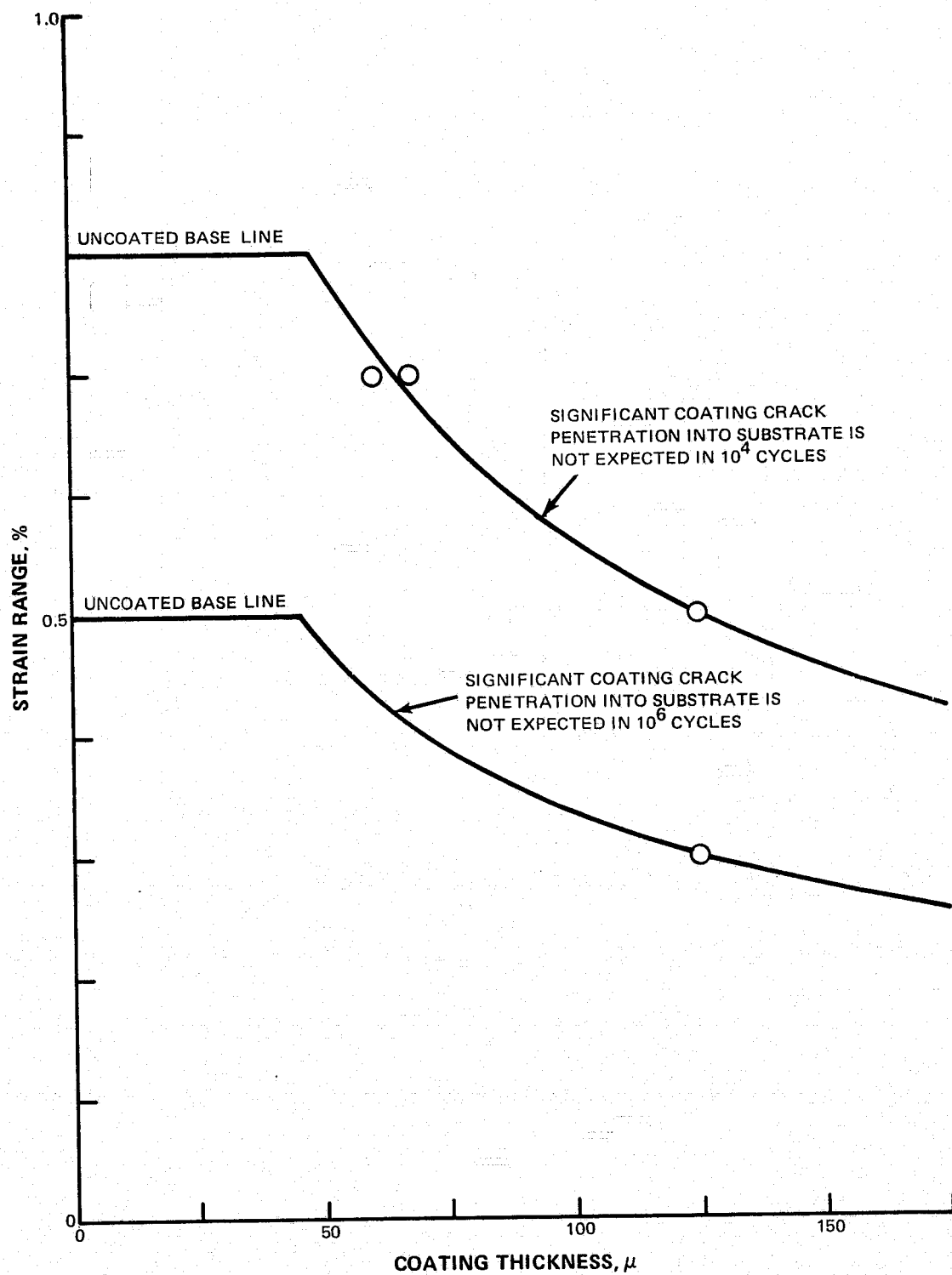
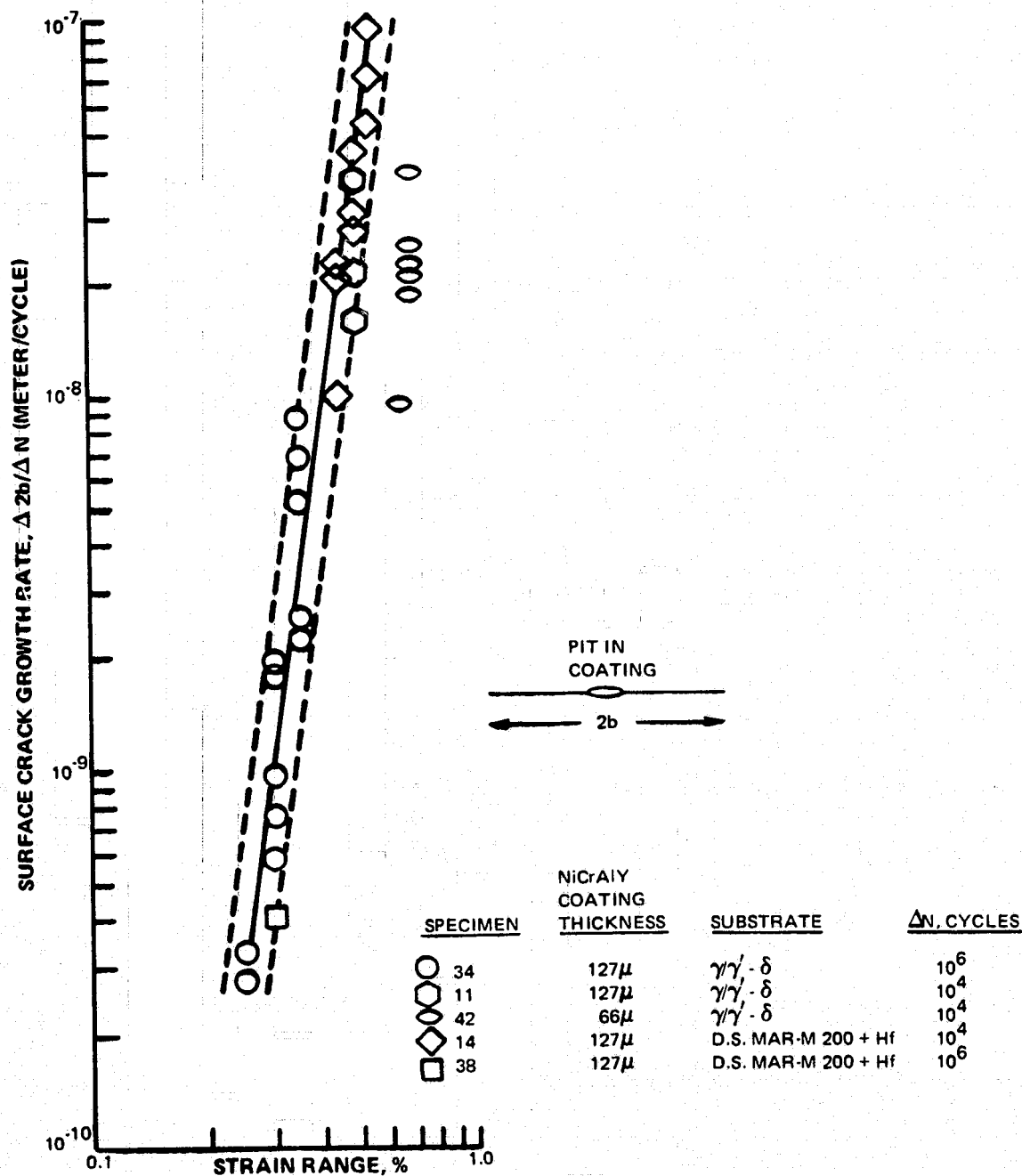


Figure 76 Estimated Effect of NiCrAlY Coating Thickness on 977 K (1300°F) Fatigue Strength of  $\gamma/\gamma' - \delta$  (6Cr) Alloy.



**Figure 77** Coating Crack Propagation Rate Versus Strain Range Data for Several Cracks in NiCrAlY Coated  $\gamma/\gamma' - \delta$  and D.S. MAR-M 200 + Hf Specimens Which Were Fatigue Tested at 977 K (1300°F). Note that the strain range required to achieve a given propagation rate is greater for the thinner coating.

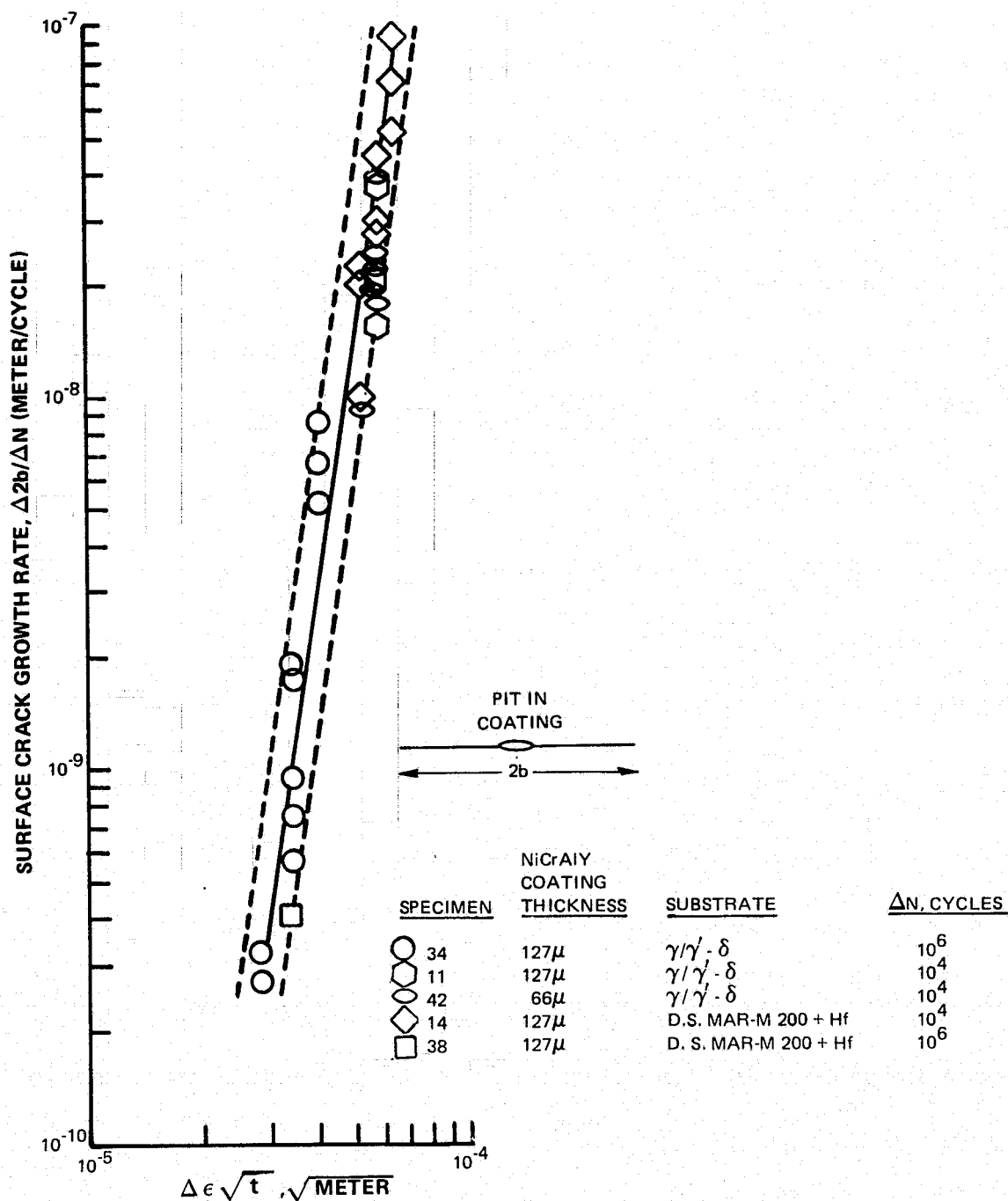


Figure 78 Coating Crack Propagation Rate Data as a Function of the Strain Range ( $\Delta\epsilon$ ) Times the Square Root of the Coating Thickness ( $\sqrt{t}$ ) for NiCrAlY Coated  $\gamma/\gamma' - \delta$  and D.S. MAR-M 200 + Hf Specimens Which Were Fatigue Tested at 977 K (1300°F).

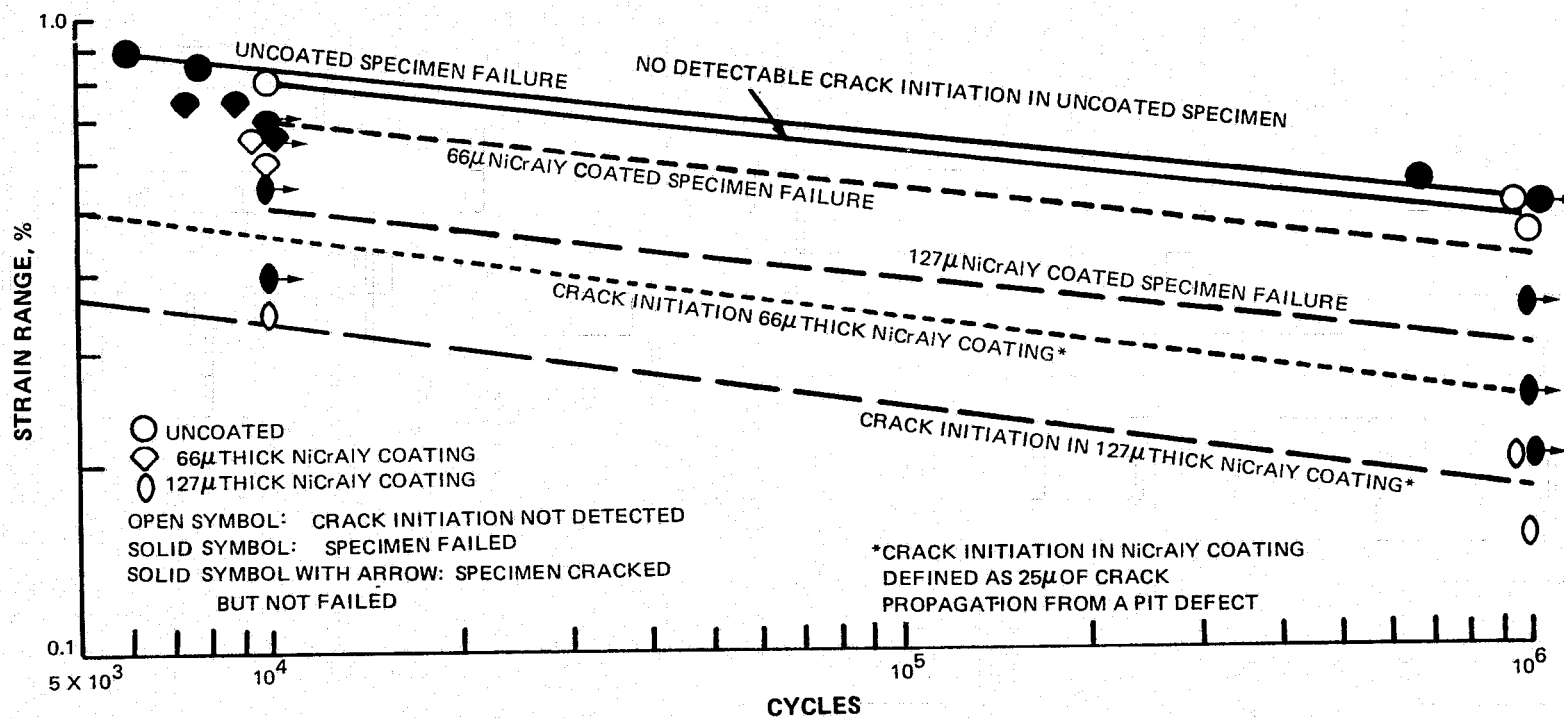
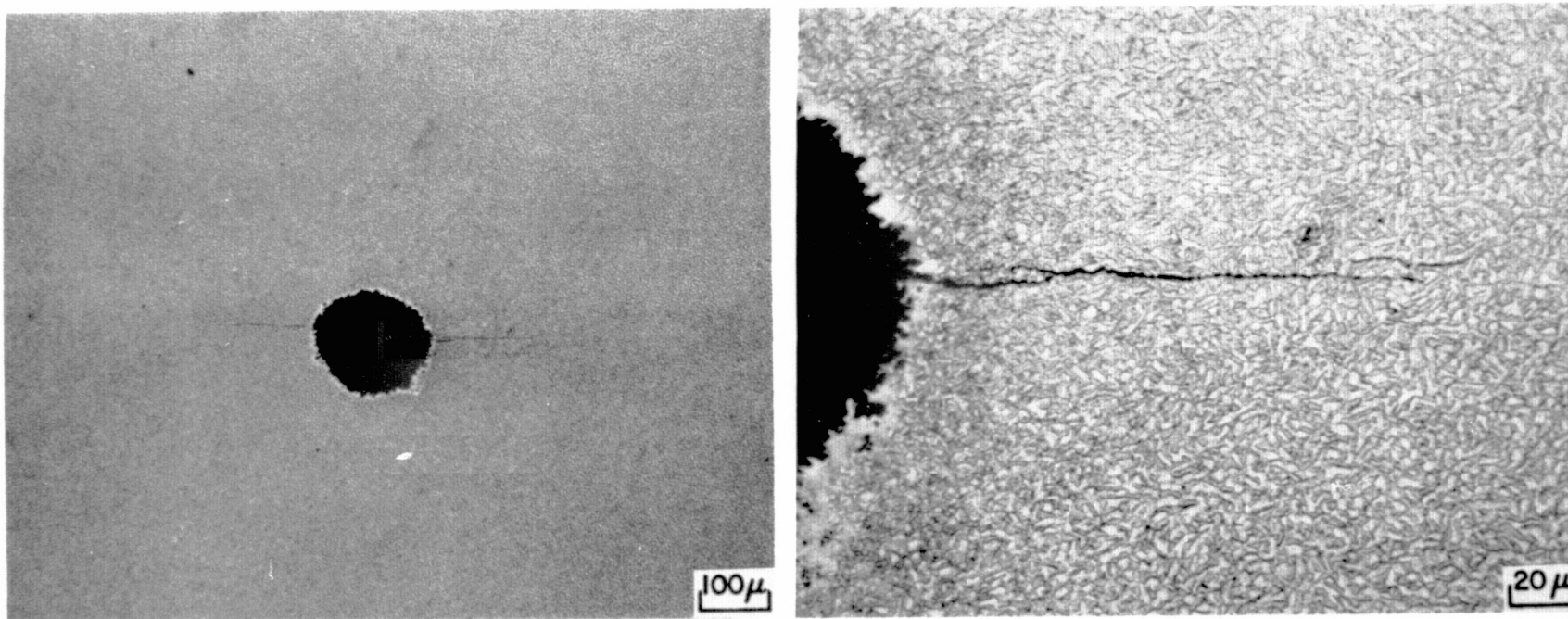
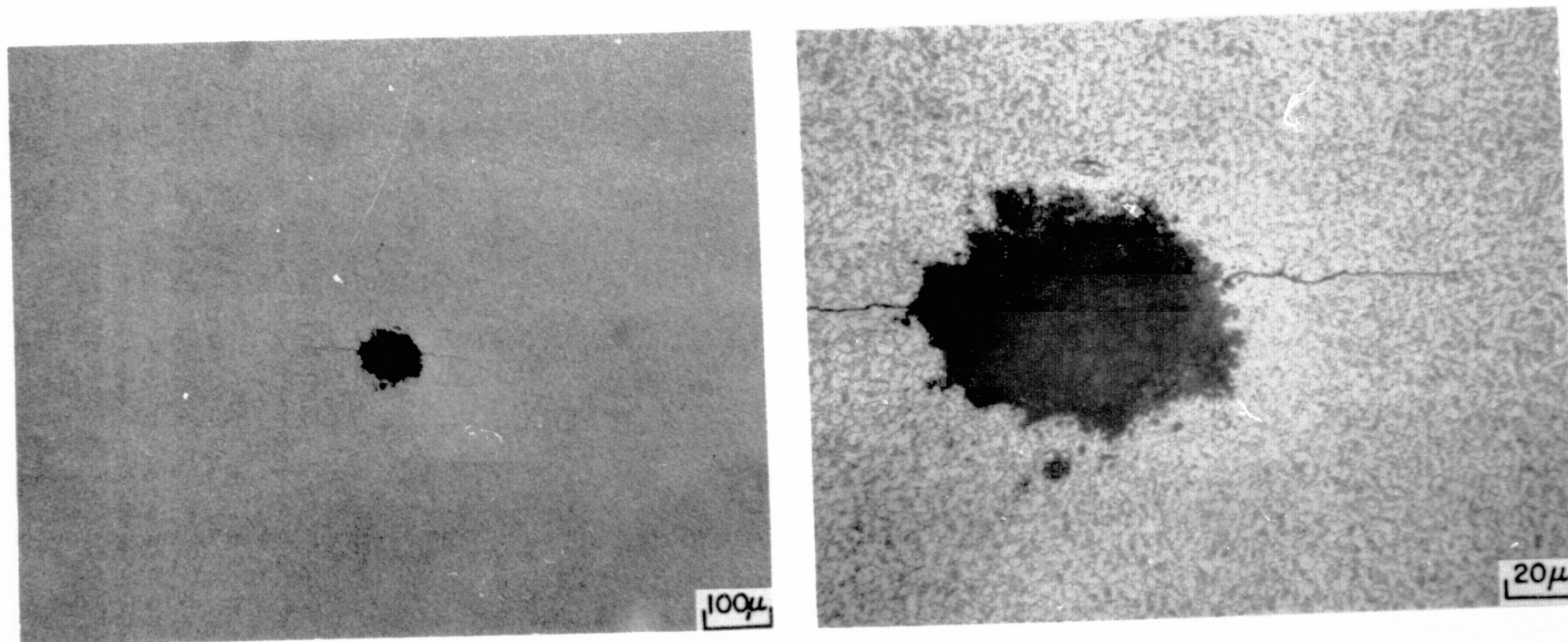


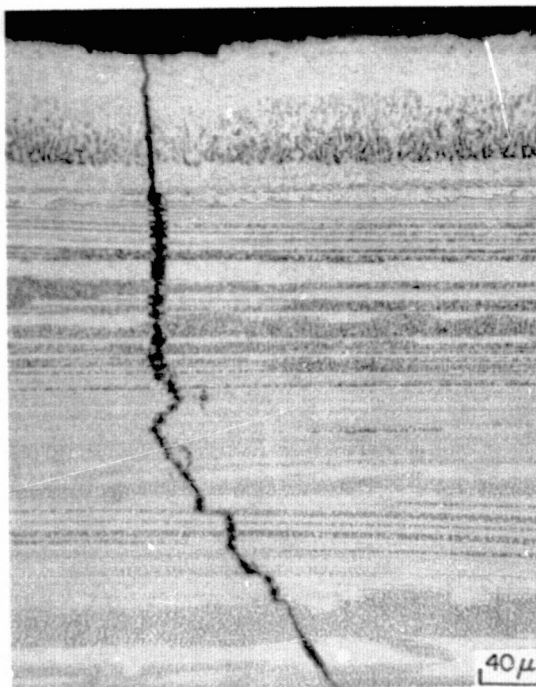
Figure 79 977 K (1300°F) Isothermal Fatigue Data for NiCrAlY Coated Longitudinal Grain Orientation  $\gamma/\gamma' - \delta$  (6Cr) Directionally Solidified Eutectic Alloy Systems.



*Figure 80 Morphology of Pit Initiated Fatigue Crack in Plane of NiCrAlY Coating on  $\gamma/\gamma'$  -  $\delta$  Specimen (No.11) Which Was Evaluated in 977 K (1300°F) LCF Test. (K-17887)*



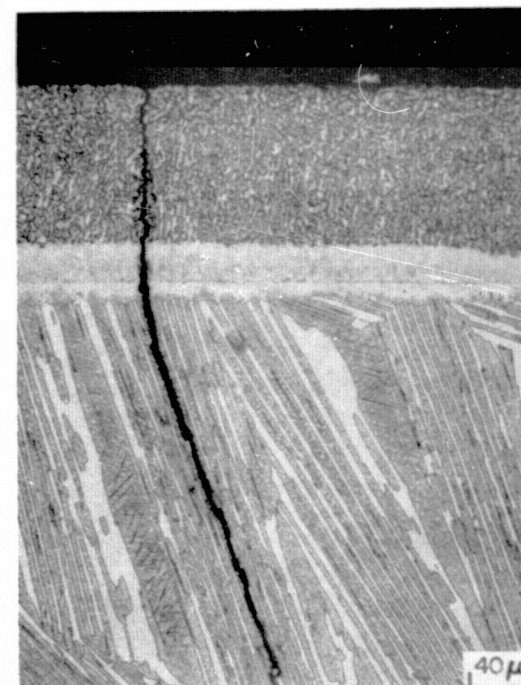
*Figure 81 Morphology of Pit Initiated Fatigue Crack in Plane of NiCrAlY Coating on D.S. MAR-M 200 + Hf Specimen (No. 15) Which Was Evaluated in 977 K (1300°F) LCF Test. (K-17888)*



NiCrAlY + Pt COATING  
LONGITUDINAL  $\gamma/\gamma' - \delta$  SPECIMEN (NO. 6)  
FINAL STRAIN RANGE: 0.55%

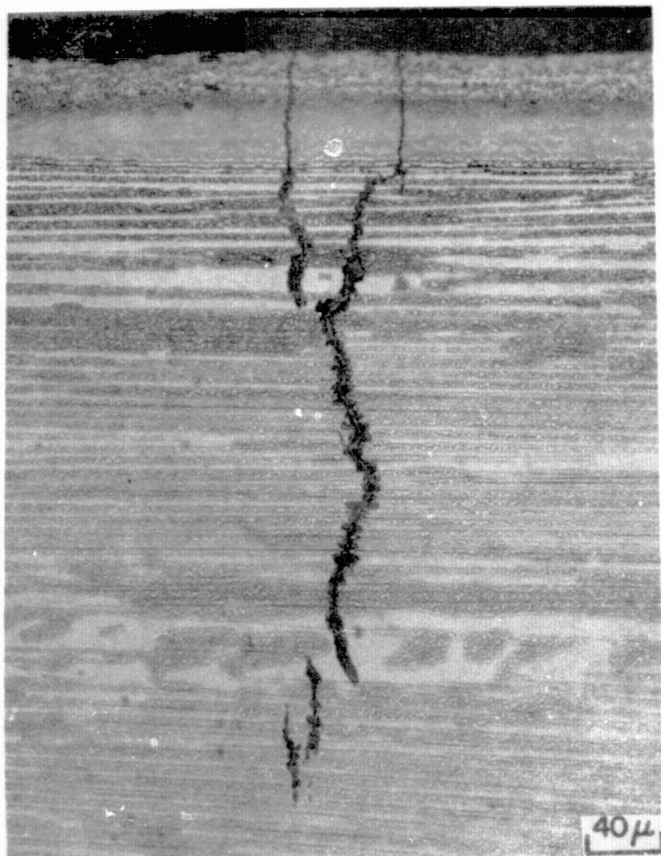


NiCrAlY COATING  
LONGITUDINAL  $\gamma/\gamma' - \delta$  SPECIMEN (NO. 9)  
FINAL STRAIN RANGE: 0.55%



NiCrAlY COATING  
TRANSVERSE  $\gamma/\gamma' - \delta$  SPECIMEN (NO. 23)  
FINAL STRAIN RANGE: 0.30%

Figure 82 Secondary Crack Microstructures in NiCrAlY + Pt and NiCrAlY Coated Longitudinal and Transverse Grain Orientation  $\gamma/\gamma' - \delta$  Specimens Which Formed During  $10^4$  Cycle LCF Tests at 977 K (1300°F). (K-16740)



Pt + Al COATING  
LONGITUDINAL  $\gamma/\gamma'$ - $\delta$  SPECIMEN (NO. 30)  
FINAL STRAIN RANGE: 0.45%



Pt + Al COATING  
TRANSVERSE  $\gamma/\gamma'$ - $\delta$  SPECIMEN (NO. 20)  
FINAL STRAIN RANGE: 0.30%

Figure 83 Secondary Crack Microstructures in Pt + Al Coated Longitudinal and Transverse Grain Orientation  $\gamma/\gamma'$ - $\delta$  Specimens Which Were Formed During 977 K (1300°F)  $10^6$  Cycle HCF and  $10^4$  Cycle LCF Tests, Respectively.  
(K-16741)

## IX. CONCLUSIONS

Burner rig cyclic oxidation, furnace cyclic hot corrosion, ductility and thermal fatigue tests indicated that NiCrAlY + Pt (63 to 127 $\mu$  Ni-18Cr-12Al-0.3Y + 6 $\mu$  Pt) and NiCrAlY (63 to 127 $\mu$  Ni-18Cr-12Al-0.3Y) coatings are capable of protecting the high temperature gas-path surfaces of a  $\gamma/\gamma' - \delta$  airfoil. Burner rig (Mach 0.37) testing indicated that the useful coating life of the 127 $\mu$  thick coatings exceeded 1000 hours at 1366 K (2000°F). NiCrAlY and platinum coating layers were applied by electron beam physical vapor deposition and sputtering techniques, respectively.

Isothermal fatigue and furnace hot corrosion tests indicated that 63 $\mu$  NiCrAlY, NiCrAlY + Pt, and platinum modified diffusion aluminide (Pt + Al) coating systems are capable of protecting the relatively cooler surfaces of the blade root.

Finally, a gas phase coating process was evaluated for diffusion aluminizing internal surfaces and cooling holes of air-cooled eutectic alloy turbine blades.

A brief summary of the principal findings resulting from this program is presented below.

- 127 $\mu$  thick NiCrAlY and NiCrAlY + Pt coating systems were not failed after 1005 hours of Mach 0.37 burner rig cyclic oxidation testing at 1366 K (2000°F).
- 63 $\mu$  thick NiCrAlY and NiCrAlY + Pt coating systems were not failed after 505 hours of Mach 0.37 burner rig cyclic oxidation testing at 1366 K.
- NiCrAlY and NiCrAlY + Pt coatings exhibited the best resistance to thermal fatigue cracking of the coating systems which were evaluated on the  $\gamma/\gamma' - \delta$  alloy in the 1366 K cyclic oxidation burner rig tests.
- Comparative 1366 K cyclic oxidation burner rig testing of the candidate coating systems on  $\gamma/\gamma' - \delta$  and D.S. MAR-M 200 + Hf alloys indicated that thermal fatigue cracking in the NiCoCrAlY, NiCoCrAlY + Pt and NiCrAlY + Al coatings occurred only on the  $\gamma/\gamma' - \delta$  specimens.
- The resistance of a coating to thermal fatigue cracking is dependent on the coating-substrate thermal expansion mismatch strain.
- Ni-18Cr-12Al-4Si-0.3Y and Pt + Al coating systems are limited by incipient melting to use below 1366 K on the  $\gamma/\gamma' - \delta$  alloy.
- The oxidation resistance of NiCrAlY + Pt coated  $\gamma/\gamma' - \delta$  specimens was not noticeably affected by reducing the substrate chromium content from 6 to 1 percent.
- Cyclic furnace hot corrosion tests at 1172 K (1650°F) for 250 hours indicate that NiCrAlY + Pt, NiCrAlY, Pt + Al, NiCoCrAlY + Pt and NiCoCrAlY coatings provided the  $\gamma/\gamma' - \delta$  alloy with significant protection against accelerated oxidation in

the presence of  $\text{Na}_2\text{SO}_4$ . Hot corrosion failures were observed in gas phase aluminide and low aluminum NiCrAlY + diffusion aluminide coated  $\gamma/\gamma' - \delta$  specimens during the course of these tests.

- The gas phase diffusion aluminizing process was evaluated and provided better coating coverage of internal surfaces and small diameter cooling holes of eutectic alloy components that can be obtained with conventional pack aluminizing processes.
- Ductility tests conducted at 578 K (600°F) indicated that fracture strains of all the coating systems evaluated on the  $\gamma/\gamma' - \delta$  alloy exceed the magnitude of anticipated thermal strains (approximately 0.16 percent strain) with the possible exception of the Ni-18Cr-5Al-0.3Y + diffusion aluminide system.
- Thermomechanical fatigue testing of NiCrAlY and NiCrAlY + Pt coated  $\gamma/\gamma' - \delta$  (6 Cr) specimens indicated that reducing the Cycle I temperature range from 700 - 1311 K to 755 - 1200 K decreases the crack propagation rate into the  $\gamma/\gamma' - \delta$  substrate by a factor of about three and also increases the resistance to coating crack initiation.
- The cycles required to initiate thermal fatigue cracking in NiCrAlY and NiCrAlY + Pt coatings is expected to be a significant fraction of the total thermal fatigue life predicted for strain and temperature range conditions of an air-cooled  $\gamma/\gamma' - \delta$  turbine blade.
- Isothermal 977 K fatigue testing of NiCrAlY and NiCrAlY + Pt coated specimens indicates that the root coating thickness can be adjusted to optimize the combination of oxidation/hot corrosion resistance (increased by increasing coating thickness) and fatigue resistance (increased by decreasing coating thickness).
- The platinum modified diffusion aluminide (Pt + Al) coating system is also capable of protecting the blade root region of eutectic alloy turbine blades.

## **X. RECOMMENDATIONS**

Based on the results and conclusions of this program, the following courses of action are recommended.

- Development of ductile overlay coating compositions with improved thermal expansion match between the coating and the eutectic alloy is recommended to improve the thermal fatigue capability of coated eutectic alloy systems.
- To provide improved protection for internal surfaces of air cooled D.S. eutectic alloy turbine airfoils, the development of multi-element gas-phase diffusion coatings is recommended.
- With the identification of the platinum modified NiCrAlY coating composition as a prime candidate for protecting eutectic alloy airfoils, detailed studies of 1) the effects of platinum and other precious metals on the protective mechanism(s) and 2) the impact of processing variables on coating performance are recommended.
- Since design conditions for an advanced air cooled eutectic alloy turbine blade indicate that formation of a coating crack will constitute a significant fraction of the thermal fatigue life, a more detailed study of coating-substrate interactions during thermal fatigue should be conducted.

## REFERENCES

1. E. J. Felten and F. S. Pettit, "High Temperature Oxidation Behavior of Directionally Solidified Eutectic Alloys", Failure Modes in Composites - II, TMS-AIME, 1974, pp. 220 - 246.
2. J. G. Smeggil and M. D. McConnell, "Oxidation Behavior of the Aligned Lamellar Eutectic Alloy  $\text{Ni}_3\text{Al} - \text{Ni}_3\text{Nb}$ ", Oxidation of Metals, 8 (1974) 309-341.
3. J. G. Smeggil, "Research with In-Situ Composites Aligned With Eutectoid and Eutectic Transformations", Air Force Contract F33615-73-C-5083, Report Number AFML-TR-75-133, August 1975.
4. C. W. Hayes and J. J. Jackson, "Applied High Temperature Technology Program", Air Force Contract F33657-71-C-0789, Report Number AFAPL-TR-75-44 (Volume I), October, 1975.
5. E. J. Felten, T. E. Strangman and N. E. Ulion, "Coatings for Directional Eutectics", NASA CR-134735, October 1974.
6. J. K. Tien and F. S. Pettit, "Mechanism of Oxide Adherence on Fe-25Cr-4Al (Y or Sc) Alloys", Metallurgical Transactions, 3 (1972) 1587-1599.
7. I. Kvernes, "The Role of Yttrium in High-Temperature Oxidation Behavior of Ni-Cr-Al Alloys", Oxidation of Metals, 6 (1973) 45.
8. C. S. Giggins, B. H. Kear, F. S. Pettit and J. K. Tien, "Factors Affecting Adhesion of Oxide Scales on Alloys", Metallurgical Transactions, 5 (1974) 1685.
9. C. S. Giggins and F. S. Pettit, "Oxide Scale Adherence Mechanisms and the Effects of Yttrium, Oxide Particles and Externally Applied Loads on the Oxidation of NiCrAl and CoCrAl Alloys", Report Number ARL 75-0234, June 1975.
10. C. S. Giggins and F. S. Pettit, "Oxidation of Ni-Cr-Al Alloys Between 1000° and 1200°C", J. Electrochem. Soc., 118 (1971) 1782-1790.
11. M. A. Gedwill and S. J. Grisaffe, "Oxidation Resistant Claddings for Superalloys", NASA Technical Memorandum X-67925.
12. G. Lehnert and H. Meinhardt, Electrodeposition and Surface Treatment, 1, (1972/73) 71.
13. G. Lehnert and H. Meinhardt, Electrodeposition and Surface Treatment, 1, (1972/73) 189.
14. E. J. Felten and F. S. Pettit, "Development, Growth and Adhesion of  $\text{Al}_2\text{O}_3$  On Platinum - Aluminum Alloys", Oxidation of Metals, To be Published in 1976.

15. S. J. Grisaffe and J. P. Merutka, "Coatings for Aircraft Gas Turbine Engines and Space Shuttle Heat Shields: A Review of Lewis Research Center Programs", NASA Technical Memorandum X-68007.
16. C. E. Lowell and R. V. Miner, "Improvement in Cyclic Oxidation of the Nickel-Base Superalloy B-1900 by Addition of One Percent Silicon", NASA Technical Memorandum X-68191.
17. F. P. Talboom, R. C. Elam and L. W. Wilson, "Evaluation of Advanced Superalloy Protection Systems", NASA CR-72813, December 2, 1970.
18. G. W. Goward, "Coatings and Coating Processing for Gas Turbine Airfoils in a Marine Environment", pp. 277-296 in Proceedings of the 1974 Gas Turbine Materials in the Marine Environment Conference, Castine, Maine, 1974. Edited by J. W. Fairbanks and I. Machlin. Metals and Ceramics Information Center Report MCIC-75-27.
19. K. D. Sheffler, R. H. Barkalow, J. J. Jackson and A. Yuen, "Alloy and Structural Optimization of a Directionally Solidified Lamellar Eutectic Alloy", NASA CR-135000, May 1976.
20. G. W. Goward and D. H. Boone, "Mechanism of Formation of Diffusion Aluminide Coatings on Nickel-Base Superalloys", *Oxidation of Metals*, 3 (1971) 475-495.
21. T. E. Strangman and S. W. Hopkins, "Thermal Fatigue of Coated Superalloys", *Ceramic Bulletin*, 55 (1976) 304-307.
22. T. E. Strangman, Unpublished Research.
23. G. W. Goward, "Current Research on the Surface Protection of Superalloys for Gas Turbine Engines", *J. Metals*, 22 (October 1970) 31-40.
24. G. R. Leverant, T. E. Strangman and B. S. Langer, "Parameters Controlling the Thermal Fatigue of Conventionally-Cast and Directionally-Solidified Turbine Alloys", to be presented at Third International Symposium on Superalloys: Metallurgy and Manufacture, Seven Springs, PA., September 12-15, 1976.
25. F. D. Lemkey, "Eutectic Superalloys Strengthened by  $\delta$ ,  $\text{Ni}_3\text{Cb}$  Lamellae and  $\gamma'$ ,  $\text{Ni}_3\text{Al}$  Precipitates", Final Report for NASA Contract NAS3-15562, January 1973.
26. J. A. Goebel, E. J. Felten and F. S. Pettit, "Concerning the Need for Unification of Hot Corrosion Theories for the Degradation of Materials in Gas Turbines", *Corrosion Problems in Energy Conversion and Generation*, Edited by C. S. Tedmon, Jr., 1974, p. 102.
27. I. Linask and J. Dierberger, "A Fracture Mechanics Approach to Turbine Airfoil Design," ASME Paper No. 75-GT-78, Presented at 20th Annual International Gas Turbine Conference, Houston, Texas, March 1975.

28. K. D. Sheffler, "Stress Analysis, Thermomechanical Fatigue Evaluation, and Root Sub-component Testing of Hollow Blades of Gamma/Gamma Prime - Delta Eutectic Alloy", Monthly Report Under Contracts NAS3-19714 and NAS 3-19732, January 1976.
29. A. Taylor and R. W. Floyd, "The Constitution of Nickel-Rich Alloys of the Nickel-Chromium-Aluminum System", J. Inst. Metals, 81 (1952-3) 451-464.
30. D. H. Boone, T. E. Strangman and L. W. Wilson, "Some Effects of Structure and Composition on the Properties of Electron Beam Vapor Deposited Coatings for Gas Turbine Superalloys", J. Vac. Sci. Technol., 11 (1974) 641-646.
31. P. C. Paris and G. C. Sih, "Stress Analysis of Cracks", Fracture Toughness Testing and Its Applications, ASTM STP 381, 1970.
32. H. Johnson and P. Paris, "Sub-critical Flaw Growth", Engineering Fracture Mechanics, 1 (1968) 3.
33. S. W. Hopkins. K. V. Mattson and T. E. Strangman, Unpublished Research.